université PARIS-SACLAY

New aspects of vascular cyclic nucleotides signalling in pulmonary arterial hypertension and heart failure.

Nouveaux aspects de la signalisation des nucléotides cycliques vasculaires dans l'hypertension artérielle pulmonaire et l'insuffisance cardiaque.

Thèse de doctorat de l'université Paris-Saclay

École doctorale n°569, Innovation thérapeutique : du fondamental à l'appliqué (IFTA)
Spécialité de doctorat : Physiologie, physiopathologie
Graduate School : Health and Drug Scicences.
Référent : Faculté de Pharmacie

Thèse préparée dans l'unité de recherche UMR_S 1180,
sous la co-direction de **Boris MANOURY,** Maître de Conférences, HDR
et la co-direction de **Véronique LEBLAIS**, Professeur des Universités

Thèse soutenue à Paris-Saclay, le 5 octobre 2022, par

Liting WANG

Composition du Jury

David MONTANI PU-PH, Université Paris-Saclay	Président
Jean-François QUIGNARD PU, Université de Bordeaux	Rapporteur & Examinateur
Gervaise LOIRAND DR1 Inserm, Université de Nantes	Rapporteuse & Examinatrice
Alison GURNEY Professor, The University of Manchester	Examinatrice
Liliana CASTRO MCF, Sorbonne Université	Examinatrice
Boris MANOURY MCF, HDR, Université Paris-Saclay	Directeur de thèse
Véronique LEBLAIS PU, Université Paris-Saclay	Co-directrice de thèse

THESE DE DOCTORAT

NNT : 2022UPASQ040

Acknowledgement

Time flies and four years of PhD life has gone so quickly. Recalling all my PhD life, there are so many people giving me help and encouragement, and a lot of touching moments left in my memory. I would like to thank my two mentors, Dr Boris Manoury and Pr Véronique Leblais. I am very grateful that you both accepted me as your PhD student. After I arrived at Paris, especially at the beginning, you helped me prepare every necessary thing for work and life in person, which made me integrate into this lab family very easily and quickly. Then in the subsequent 4 years, Boris taught me to do most of the experiments by himself, and gave me a lot of guidance and help in my projects. I always feel so lucky to work with him, and I greatly appreciate his professional guidance, continuous support and patience in all my PhD research work and thesis writing. And I greatly thank Véronique, since she always gave me timely help and guidance when we needed. Besides, I would like to express my deep appreciation to Dr Rodolphe Fischmeister, for correcting my abstracts, presentations of every conference and manuscripts, and giving me professional suggestions for my projects in team meetings.

I want to thank my thesis committee: Pr David Montani, thank you for accepting to be the president of my thesis committee; I really thank my two reporters Dr Jean-François Quignard and Dr Gervaise Loirand for reviewing my thesis and making insightful comments; I also thank Prof. Alison Gurney and Liliana Castro for examining and evaluating my work.

Then I would like to thank my lab directors Dr Anna-Maria Gomez, and team leader Dr Grégoire Vandecasteele. They are so nice and friendly to every member of lab, and create very good academic atmosphere which make all of us benefit from the lab arrangement and resource. In addition, I want to say "thank you" to our lab secretary Gladys René-Corail for her help in preparing administrative documents, and to Florence Lefebvre and Audrey Varin for their help in ordering agents and teaching me some experiments; to Delphine Mika for helping me do PDE activity assay; and to Patrick Lechêne for helping me install software and repair instruments; to our team members, Drs Guillaume Pidoux and Jérôme Leroy who gave me a lot of useful advices in my projects; to Claudine Deloménie and Emy Ponsardin for their help

in RT-qPCR; to Valérie Nicolas and Séverine Domenichini for their help in immunofluorescence experiments; to Valérie Domergue, Pauline Robert and other staff of animal facility for their help in taking care of PDE9 mice.

In addition, I have to say "thank you" to collaborators from UMR-S 999 and China. Thank you so much, Dr Frédéric Perros, for your helping in right heart catheterization test of mice and other guidance in my projects. And thank you so much, Dr Fabrice Antigny, for helping us with hypoxia-chamber settings; and I still want to thank Yassine Ben Ahmed for helping me doing some cell proliferation experiments, and thank Bahgat Soilih for helps in daily life. I want to thank my supervisor of master degree, Pr Zhicheng Jing, who still is the collaborator of my PhD projects. If without his recommendation and funding of first year, I would not be here today. And I still appreciate China Scholarship Council for their financial support during all my PhD training.

Moreover, I really want to thank all other lab colleagues and PhD students. They helped me a lot in daily life since I can't understand French. They are so enthusiastic and friendly, and always care about my situation and give me helps. Moreover, I want to thank my Chinese friends in this lab, Dawei Liu, Liheng Ying, Jianbin Xue, and Rui Luo. Every time I saw them, just like saw my family members since we shared a lot of happy time together.

At last, I would like to thank my parents for their understanding and encouragement. For 3 years I haven't seen them due to pandemic of Covid-19, they always try to comfort me in video chat even though I know they miss me so much. And I really want to thank my boyfriend, Qinglin Wang, for his love, support, understanding, and accompany in this one more year.

Table of contents

Résumé

Les nucléotides cycliques (CN) adénosine monophosphate cyclique (AMPc) et guanosine monophosphate cyclique (GMPc) sont des seconds messagers intracellulaires clés qui régulent une grande variété de fonctions cellulaires. Dans le système cardiovasculaire, les CNs ont des effets vasodilatateurs, préviennent la prolifération des cellules vasculaires et s'opposent à l'agrégation plaquettaire. La synthèse de l'AMPc est catalysée par les adénylate cyclases (AC), stimulées en aval de l'activation des récepteurs couplés aux protéines Gα(s) (à l'exception des AC solubles) par leur agonistes. Les principaux effecteurs de l'AMPc sont la protéine kinase A (PKA) et les protéines d'échange activées par l'AMPc (EPAC). La génération de GMPc est catalysée par deux types de guanylate cyclase (GC) : i) la forme « particulaire » (pGC), région catalytique intracellulaire des récepteurs des peptides natriurétiques (NP) ; ii) la GC soluble (sGC), directement activée par la liaison du monoxyde d'azote (NO). Le principal effecteur du GMPc est la protéine kinase G (PKG). Les CNs sont dégradés par les phosphodiestérases (PDE), terme englobant les familles d'enzymes classées de PDE1 à PDE11. Ainsi, les PDEs atténuent les voies de signalisations intracellulaires médiées par les CNs. Les familles PDE4, PDE7 et PDE8 hydrolysent exclusivement l'AMPc, alors que les PDE5, PDE6 et PDE9 hydrolysent exclusivement le GMPc. Les autres familles peuvent hydrolyser les deux types de CNs. La variété des propriétés catalytiques, des modes de régulation et des distributions cellulaires ou tissulaires des PDEs leur confère un rôle régulateur de myriades de fonctions cellulaires. Les travaux de Recherche actuels visent à explorer la complexité de cette organisation. Les rôles respectifs des différentes isoformes des PDEs dans le contrôle des dynamiques des CNs dans la cellule restent des aspects importants à clarifier, notamment dans le contexte pathologique des maladies cardiovasculaires.

Le premier projet de ma thèse consistait, en utilisant une lignée de souris déficiente pour la PDE9 (*Pde9a*$^{-/-}$) comparée aux congénères de génotype sauvage (*Pde9a*$^{+/+}$), à élucider le rôle de la PDE9 dans la circulation pulmonaire et à déterminer si la déficience en PDE9 atténue l'hypertension pulmonaire expérimentale. La PDE9, codée par un gène unique *PDE9A*,

hydrolyse exclusivement le GMPc, avec une haute affinité pour ce substrat. Cependant, contrairement à la PDE5, une autre PDE régulatrice du GMPc, sa contribution dans la circulation pulmonaire n'est pas claire. Par ailleurs, la PDE9 est a été récemment décrite comme une contributrice intéressante du remodelage hypertrophique du ventricule gauche dans l'insuffisance cardiaque. Nos résultats ont révélé que la PDE9 est exprimée dans les artères pulmonaires humaines et murines. Par des expériences sur artères isolées, nous montrons que le déficit en PDE9 n'altère pas les réponses contractiles de l'artère pulmonaire en réponse à différents stimuli. Cependant, l'absence de PDE9 est associée à une amélioration des réponses vasorelaxantes des artères pulmonaires en réponse à des stimulations connues pour être médiées par la voie du GMPc : peptide natriurétique auriculaire (ANP), acétylcholine et donneur de NO. Bien que l'expression du transcrit de *Pde9a* soit augmentée dans les poumons et le ventricule droit de souris soumises à l'hypoxie chronique, le déficit en PDE9 ne protège pas contre l'hypertension pulmonaire, ni l'hypertrophie du ventricule droit produites par ce modèle. En outre, l'examen de témoins de l'activité de la PKG, en aval du GMPc, comprenant la phosphorylation de la PDE5 (Ser92) et de la protéine VASP (Ser 239), ne révèle pas d'altération, ni sous hypoxie chronique ni chez les animaux déficients en PDE9. En conclusion, si la PDE9 semble participer à l'atténuation de certains signaux GMPc responsables de la vasorelaxation de l'artère pulmonaire, l'enzyme n'est pas un acteur important participant à la physiopathologie de l'hypertension pulmonaire induite par l'hypoxie chronique chez la souris. D'autres modèles pathologiques plus sévères, ou l'association avec des stimulants des voies des NCs, pourraient permettre de compléter les données quant à la pertinence de la PDE9 comme cible thérapeutique dans l'hypertension artérielle pulmonaire, une maladie grave dont la prise en charge reste instisfaisante.

Par ailleurs, j'ai réalisé une étude portant sur les contributions des PDEs de l'AMPc dans les artères de rats soumis à un modèle d'insuffisance cardiaque chronique (IC) induite par une sténose aortique proximale. Nous nous sommes concentrés sur l'artère mésentérique (AM), un exemple de lit vasculaire de résistance ayant un impact direct sur la postcharge cardiaque. En réalisant des études de réactivité vasculaire sur AM isolées, nous avons montré que les

contributions des PDE3 et PDE4 subissent des altérations subtiles dans l'IC par rapport aux animaux contrôles. Contrairement aux observations précédentes dans l'aorte, l'influence de la PDE3 est plus limitée dans chez les animaux contrôles que dans l'IC, tandis que la contribution de la PDE4 est évidente à la fois dans les contextes normaux et pathologiques, faisant de cette famille d'enzymes une cible potentielle chez les patients atteints d'IC. Pour la première fois, nous avons mis en évidence que l'activité PDE2 apparaît comme un promoteur de la réponse contractile induite par U46619 (analogue du thromboxane), via un mécanisme dépendant du NO, à la fois chez les animaux IC et contrôles. Nous avons démontré que la PDE2 est exprimée dans les cellules musculaires lisses et les cellules endothéliales d'AM de rat. Ce projet ouvre de nouvelles perspectives sur la manière dont les activités spécifiques des PDEs ajustent le contrôle des lits vasculaires périphériques par les NCs.

Enfin, dans le cadre d'un projet mené en parallèle, j'ai étudié le rôle de la sous-unité régulatrice de la protéine-kinase A de type 1α (PKA-R1α) dans l'aorte de souris. Pour cela, j'ai profité d'une lignée de souris knock-in portant une mutation dans le gène codant pour PKA-R1α (R368X), récapitulant certaines caractéristiques d'une maladie humaine, l'acrodysostose de type-1. Les résultats préliminaires suggèrent que la PKA-R1α est exprimée et fonctionnelle dans l'aorte de souris. L'expression générale de l'ARNm des sous-unités PKA-R1α, PKA-R2α, Cα et Cβ sont diminuées dans l'aorte de la souris mutante, tandis que l'expression de la protéine PKA-R1α ne montre pas de diminution et que l'expression de la protéine Cα est augmentée. Le dosage de l'activité PKA a montré une activité basale de la PKA plus élevée et une altération de la capacité d'un analogue de l'AMPc sélectif R1 à stimuler l'enzyme dans les homogénats d'aorte de souris mutantes. La réactivité vasculaire de cette dernière en réponse à l'U46619 est augmentée, tandis que la réponse relaxante à la stimulation de l'adénylate cyclase avec le L858051 est moins puissante. Globalement, ces résultats préliminaires suggèrent que PKA-R1α pourrait être un acteur important dans les vaisseaux sanguins.

Ainsi, mes travaux contribuent à la compréhension générale de la façon dont des éléments importants de la signalisation CN, à savoir les isoformes des PDEs et de la PKA, se distribuent

dans le système vasculaire et contribuent à l'homéostasie cardiovasculaire et à ses dérèglements pathologiques.

Abstract

Cyclic nucleotides (CNs), namely, cAMP and cGMP, are important second messengers that regulate a wide variety of cellular functions. In cardiovascular system, CNs have vasodilating, anti-proliferative, and anti-platelet aggregative effects. Synthesis of cAMP is catalyzed by adenylyl cyclases(ACs), which are activated by Gs protein-coupled receptors (except soluble AC) once binding with their ligands. The main effectors of cAMP are protein kinase A(PKA) and exchange proteins activated by cAMP(EPAC). Generation of cGMP is catalyzed by two types of guanylyl cyclase(GC), particulate GC(pGC), a subfamily of catalytic receptors represented by natriuretic peptide(NP) receptors, as well as soluble GC (sGC), which is directly activated by nitric oxide (NO). The main effector of cGMP is protein kinase G(PKG). The CNs are degraded by phosphodiesterases (PDEs), which encompass a large group of different families from PDE1 to PDE11, display various catalytic properties to CNs and different cellular or tissue distribution so as to precise control myriads of cellular actions. Among of which, PDE4, PDE7 and PDE8 mainly hydrolyze cAMP, and PDE5, PDE6 and PDE9 mainly hydrolyze cGMP, others hydrolyze both CNs. The respective roles of various PDE isoforms in controlling CN dynamics remain important challenges to define, especially in the pathological context of cardiovascular diseases.

The first project of my thesis was, by using PDE9-deficient mouse (*Pde9a*$^{-/-}$) and its wide-type littermates (*Pde9*$^{+/+}$), to elucidate the role of PDE9 in pulmonary circulation, and to investigate whether PDE9 deficiency ameliorates experimental pulmonary hypertension. PDE9, encoded by a unique gene *PDE9A*, is a potent cGMP-hydrolyzing PDE. By contrast to PDE5, however, its contribution in pulmonary vasculature is unclear. Besides, PDE9 has emerged as an interesting regulator of hypertrophic remodeling of the left ventricle in heart failure. Our results revealed that PDE9 is expressed in human and mouse pulmonary arteries. PDE9 deficiency does not alter contractile properties of pulmonary artery in response to different stimuli, however, it does enhance relaxant vascular reactivity of pulmonary arteries in response to both the NO- and the natriuretic peptide-mediated cGMP signaling pathways. Despite PDE9

transcript expression is increased in lung and right ventricle from mice challenged by chronic hypoxia, PDE9 deficiency fails to protect against pulmonary hypertension and right ventricle hypertrophy in this model. Besides, the downstream of cGMP-PKG pathway, which includes phosphorylation of PDE5(Ser92) and VASP(Ser 239), is neither altered by chronic hypoxia nor by PDE9 deficiency.

Besides, I completed a study addressing the contributions of cAMP-PDEs in arteries from rats submitted to a proximal aortic stenosis induced chronic heart failure (HF) model. We focused on mesenteric artery (MA), an example of resistance vascular bed that directly impact cardiac afterload. We showed that the contributions of PDE2, PDE3 and PDE4 to vascular tone of rat MA undergo subtle alterations in HF compared to sham animals by using isometric tension assays of myography experiment and enzymatic test. We demonstrated that PDE2 is expressed both in endothelial and smooth muscle cells of rat MA. PDE2 activity emerges as a discrete, NO-dependent promoter of U46619 (thromboxane analogue) induced contractile response, and this effect is preserved in HF. By contrast with previous observations in aorta, PDE4 participates equally as PDE3 in controlling reactivity of MA. The influence of PDE3 is more limited in Sham than in HF MA, while the role of PDE4 is prominent in both normal and pathological contexts, making this family of enzyme as a potential target in patients with HF. This project opens new perspectives on how specific PDE activities fine tune the control of peripheral vascular beds by CNs.

Eventually, as part of a side project, I studied the role of protein-kinase A regulatory subunit type 1α (PKA-R1α) in mouse aorta. For this purpose, I took advantage of a knock-in mouse lineage carrying a mutation in the gene coding PKA-R1α, recapitulating some features of a human disease of Acrodysostosis type-1. Preliminary results suggest that PKA RIα is expressed and functional in mouse aorta. The general mRNA expression of PKA subunits is decreased in aorta from mutant mouse, while the protein expression does not show decrease. Conversely, Cα expression is increased. PKA activity assay showed higher basal activity and impairment of RI selective cAMP analogue-stimulated PKA activity in aorta of mutant mouse. Vascular

reactivity is altered in response to U46619 and L858051. Overall, this suggests that PKA-R1α is an important player in blood vessels.

So all of my work contributes to the general understanding on how important elements of CN signalling, namely, PDE and PKA isoforms, distribute in the vasculature and contribute to the control of vascular tone, as well as participate in health and diseases.

List of abbreviations

AC: adenylyl cyclase

ACEI: angiotensin-converting-enzyme inhibitors

Ach: acetylcholine

AKAPs: A-kinase anchoring proteins

ANP: atrial natriuretic peptide

ARBs: angiotensin-receptor blockers

ARNI: angiotensin receptor–neprilysin inhibitor

ATP: adenosine-tri-phosphate

BH4: tetrahydrobiopterin

BNP: brain natriuretic peptide

cAMP: cyclic adenosine monophosphate

cGMP: cyclic guanosine monophosphate

CCBs: calcium-channel blockers

CNs: Cyclic nucleotides

CNG: cyclic nucleotide gated ion channels

CNP: C type natriuretic peptide

COPD: Chronic obstructive pulmonary disease

CPI-17:17KDa PKC-potentiated protein phosphatase 1 inhibitor protein

CTEPH: chronic thromboembolic pulmonary hypertension

DAG: diacylglcerol

ECs: endothelial cells

ED: endothelial dysfunction

EDHF: endothelium-derived hyperpolarization factor

EF: ejection fraction

eNOS: endothelial NOS

EPAC: exchange protein activated by cAMP

ERA: endothelin receptor antagonists

ET-1: endothelin-1

HF: heart failure

HFmrEF: heart failure with mildly reduced ejection fraction

HFpEF: heart failure with preserved ejection fraction

HFrEF: heart failure with reduced ejection fraction

GC: guanylyl cyclase

GEFs: guanine nucleotide exchange factors

GPCRs: G protein coupled receptors

ILK: integrin-linked kinase

iNOS: inducible NOS

iPAH: idiopathic PAH

IRAG: IP3R-associated cGMP kinase substrate

IP3: inositol 1,4,5-trisphosphate

IP3R: IP3 receptor

ISO: isoprenaline

KI : knock-in

KO : Knockout

LTCC: L-type Ca channels

LV: left ventricle

MA: mesenteric artery

MCT: monocrotaline

MLC20: 20-kDa subunit of myosin light chain

MLCK: myosin light chain kinase

MLCP: myosin light chain phosphatase

MRA: mineralocorticoid-receptor antagonists

mPAP: mean pulmonary artery pressure

NE: norepinephrine

nNOS: neuronal NOS

NO: nitric oxide

NOS:NO synthetases

NPs: Natriuretic peptides

NPRs: natriuretic peptides receptors

PA: pulmonary artery

PAH: pulmonary arterial hypertension

PAAT: pulmonary artery acceleration time

PASMC: pulmonary artery smooth muscle cell

PDEs: phosphodiesterases

PET: pulmonary ejection time

pGC: particulate guanylate cyclase

PGF2α: Prostaglandin F2α

PGH2: prostaglandin H2

PIP2: phosphatidylinositol 4,5-bisphosphate

PGI2: prostacyclin

PLB: phospholamban;

PLC: phospholipase C

PLCβ: phospholipase C-β

PMCA: plasma membrane Ca^{2+}-ATPase

PKA: cAMP-dependent protein kinase

PKC: protein kinase C

PKG: cGMP-dependent protein kinase

Popdc: Popeye domain containing

RAAS: renin-angiotensin-aldosterone system

RGS2: regulator of G protein signaling-2

ROS: reactive oxygen species

ROK: Rho-associated kinase

RVFWT: right ventricular free wall thickness

RVH: right ventricle hypertrophy

RVSP: right ventricle systolic pressure

RyR2: ryanodine receptor 2

SERCA: sarcoplasmic reticulum Ca^{2+}-ATPase

sGC: soluble guanylate cyclase

SMCs: smooth muscle cells

SNS: sympathetic nervous system

SOCE: store-operated Ca^{2+}entry

SR: sarcoplasmic reticulum

TAPSE: tricuspid annular plane systolic excursion

TTE: trans-thoracic echocardiography

TXA_2: thromboxane A_2

UCRs: upstream conserved regions

VEGF: Vascular endothelial growth factor

VOCC: voltage-operated Ca^{2+} channels

vWF: von Willebrand factor

WT: wide-type

ZIPK: zipper-interacting protein kinase

List of figures

List of tables

1. Introduction

1.1 Overview of cardiovascular system

1.1.1 Physiology of cardiovascular system and pulmonary circulation

Cardiovascular system is generally consisted of heart, which is a muscular pumping device, and circulatory system. Its vital role is to maintain homeostasis and ensure continuous and controlled distribution of blood to perfuse every tissue according to their specific needs. Blood flow supplies oxygen, nutrients, and other necessary things, and carry carbon dioxide and waste products away from the body.

The heart is structured in 4 chambers. The two top chambers are the right and left atria, which are separated by interatrial septum. The two bottom chambers are the right and left ventricle, which are separated by interventricular septum. The atria mainly receive the venous blood and participates in filling the ventricles during diastole, whereas ventricles mainly pump blood out of the heart. Right and left ventricles feed two circulatory system in series, namely pulmonary and systemic circulation, respectively (Figure 1).

Specifically, right ventricle receives blood from systemic venous through right atrium and then pump blood to the lung through pulmonary artery in order to proceed gas exchange. Next, oxygenated blood comes back to the left atrium via pulmonary vein. Then left ventricle receives oxygenated blood from left atrium and in turn launches systemic circulation by push blood to all the rest of body by artery. And next, blood substances work into the cells through capillary due to its thin wall, finally vein carries blood back to right heart. Among entire circulatory system, some valves, mainly in heart and veins, ensure the blood flows in unidirectional.

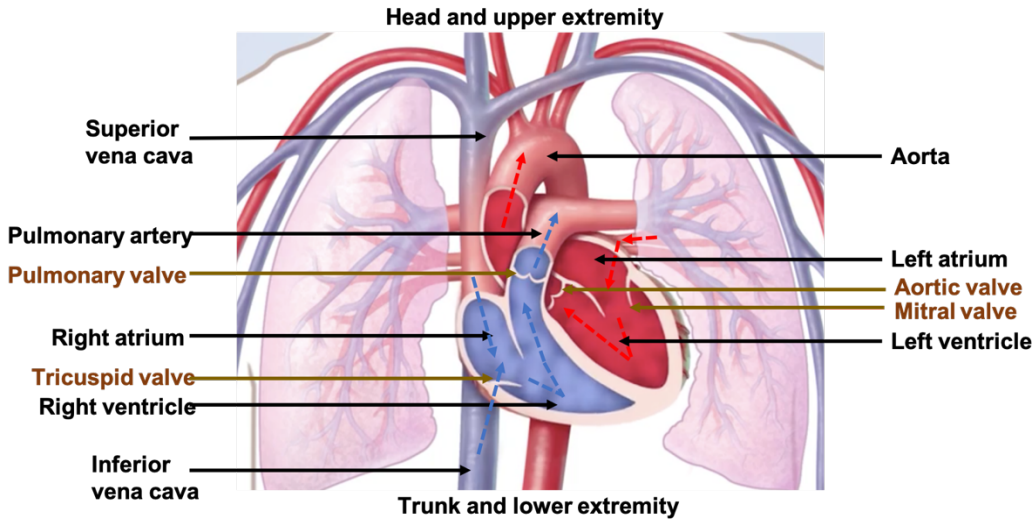

Figure 1. Structure of cardiovascular and pulmonary circulation system (Adapted from https://www.mayoclinic.org)

1.1.2 Differences between pulmonary circulation and systemic circulations

There are some differences between pulmonary circulation and systemic circulation. Hemodynamically, normal adult pulmonary circulation is a low-pressure (normal pulmonary artery systolic pressure at rest is 15 to 30 mm Hg, with a mean pulmonary pressure ranging from 8 to 20 mm Hg) and low-resistance circuit[1], while systemic circulation is conversely a high-pressure and high-resistance system with normal systolic pressure at rest is 90 to 120 mm Hg and mean blood pressure ranging from 65 to 110 mm Hg, as well as the systemic vascular resistance is 10 times higher of pulmonary vascular resistance[2,3]. Anatomically, pulmonary artery wall encompasses much thinner layer of smooth muscle cells in physiological condition compared with systemic arteries. Functionally, the pulmonary artery is maximally dilated at all times, whereas systemic artery is always keeping constricted to hold resistance arteries by different regulating mechanisms. These characteristics confer upon high compliance for pulmonary circulation to accommodate to gas exchanging surface, and high pressure for systemic circulation to ensure tissue perfusion.

1.1.3 Structure of artery

1.1.3.1 General structure of an artery

The archetypal wall of an artery is made up of three layers. The innermost layer is tunica intima, which is made of a monolayer of endothelial cells (ECs) supported by an elastic membrane made of extracellular matrix. The middle layer is tunica media, which predominately includes smooth muscle cells (SMCs) and is usually the thickest layer. It not only provides support for the vessel but also changes vessel diameter thanks to contractile activity of SMCs. Importantly, this participates in blood flow and blood pressure regulation. The outermost layer is the tunica externa, also called tunica adventitia, which attaches the vessel to the surrounding tissue. Although it is common knowledge that arteries throughout the body generally function in similar manners, there are important fundamental differences among vasomotor properties in different tissues[4], and there are diverse SMC subtypes even in the same tissue[5]. Among these components, ECs and SMCs are most important ingredients to regulate vascular tone and guarantee blood distribution. The systemic circulation comprises of several types or ranks of artery (Figure 2). The largest vessel is aorta, which origins from left ventricle and is main vessel to distribute blood to the arterial system. Aorta is then branched off into large arteries which distribute the blood flow to specific organs. In turn, they branches into smaller arteries to distribute blood flow into the organ. These vessels continue to branch and become arterioles which could be observed only under microscope with dimeter 0.01-0.2mm. Together, the small arteries and arterioles are referred to as resistance vessels since they are involved in the regulation of arterial blood pressure as well as blood flow within the organ. These resistance vessels are highly innervated by autonomic nerves, especially sympathetic adrenergic, and respond to nerve activity and circulating hormones by modulating vascular tone to constrict or dilate vessels. The vascular tone, meaning the contractile activity of vascular smooth muscle cells in the walls of small arteries and arterioles, is the major determinant of the resistance to blood flow through the circulation. As arterioles become smaller in diameter, they gradually lose their smooth muscle and contain only endothelial cells and a basement membrane, which

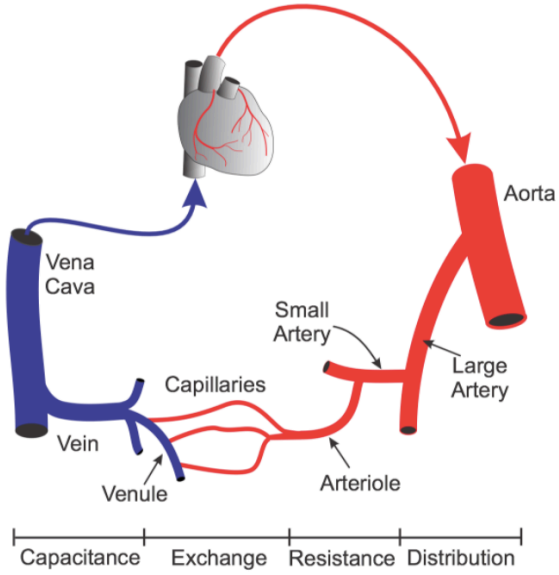

Figure 2. The illustration of different vessel types and their function. (Adapted from www.cvphysiology.com)

are termed capillaries. The capillaries are smallest vessels within the microcirculation and is responsible for substances exchange within the body.

1.1.3.2 Endothelial cells (ECs)

ECs form only one layer and line the inner vessel wall. Commonly, they have vital roles in healthy condition[6]. First, they keep integrity and maintain barrier function to safeguard transportation system. Once this integrity has been broken, they lose their basal anticoagulant features and initiate coagulation by exposure of procoagulant molecules, like von Willebrand factor (vWF), and thus are involved in hemostasis. Second, they control vascular permeability which allows to mediate immune responses at places of injury or infection. Third, they can sense the shear stress and respond to mediators to regulate vascular tone via generating and/or sending paracrine or circulating signals to underlying vascular SMCs to maintain balance of vasodilatory and vasoconstrictive signals. Vasodilatory factors include NO, PGI_2, endothelium-derived hyperpolarization factor (EDHF), CNP and others. The vasoconstrictive molecules

include endothelin-1(ET-1), thromboxane A_2 (TXA_2) , prostaglandin H_2 (PGH_2), and reactive oxygen species (ROS) and others[7]. Upon EC dysfunction, the balance will be disrupted and cline to generate more constrictive and pro-inflammatory products, and produce less vasodilatory molecules[8]. So in lots of vascular diseases, no matter primary or secondary, the dysfunction of endothelial cells play a key role to initiate impairment in vessels.

1.1.3.3 Vascular smooth muscle cells (VSMCs)

The VSMCs are final integrator of all incoming vascular control signals to exert contraction or relaxation by responding to various hormonal and hemodynamic stimuli so as to regulate blood pressure and blood flow distribution. However, they display considerable plasticity in their phenotype. Generally speaking, in healthy and young blood vessels, VSMCs possess mainly contractile property due to high density of contractile filaments inside SMCs, so called contractile phenotype. However, they can change their phenotype into a synthetic phenotype under adverse condition, such as aging, pro-inflammatory stimuli, gene mutation, atherosclerosis, stent restenosis and so on that results in vessel remodeling. This process is called “phenotypic modulation/switching”, and is at least partly reversible after removing the risk or adverse factors[9]. This two states of SMCs possess not only different morphology but also different functional properties, as the latter is more proliferative, has quicker migration rate, synthesizes more extracellular matrix. This phenotypic switching mechanism is very important for SMCs to fit various stimulus in short term and adapt to changing environment in long term[10]. Both the ECs dysfunction and synthetic SMCs phenotype are involved in pathological manifestation of a large variety of vascular diseases. Smooth muscle type II myosin is the motor protein accepted to be responsible for force generation in VSMCs (Figure 3).

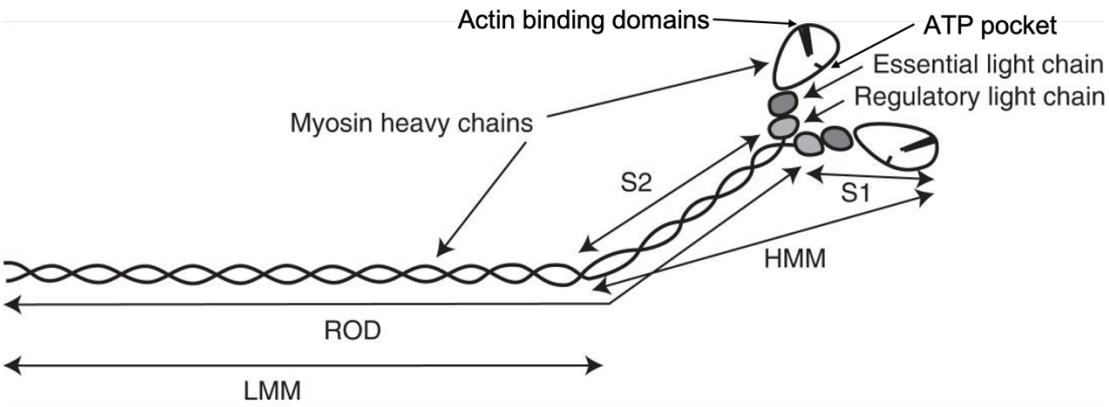

Figure 3. The smooth muscle myosin II and its proteolytic fragments. Smooth muscle myosin consists of two heavy chains (MHC) with intertwined tail domains and globular, catalytic heads that possess an actin binding domain and ATP pocket. Pairs of essential and regulatory light chains are bound to the neck region of each MHC. Myosin II is activated by phosphorylation of one regulatory light chain with molecular weight 20kDa (LC20). The S1 fragment comprising of catalytic heads and light chains is commonly referred to as the "myosin head." The remainder of the myosin molecule comprising the amino-terminal portion (S2) and light meromyosin (LMM) fragments, forms an α-helical coiled coil. LMM forms the backbone of myosin filaments. Whereas the heavy meromyosin (HMM) including S1 and S2 segment does not form filaments.(Adapted from Sweeney et al, 2018[11])

1.2 Mechanism of vascular tone regulation

1.2.1 General principle of vascular tone regulation

According to a core paradigm, phosphorylation of a key residue of regulatory light chain(LC20) of myosin II, namely Ser-19, is vital for actomyosin cross-bridging and subsequent vessel contraction. The amount of phosphorylated ser19 is dependent on 2 major mechanisms: (1) intracellular Ca^{2+} concentration; (2) Ca^{2+} sensitivity to the contractile proteins[12]. All vasoactive factors signaling converge to these pathways. Specifically, force development is initiated by

increased cytosolic free Ca^{2+} concentration ($[Ca^{2+}]_i$) that combines with calmodulin protein, forming $(Ca^{2+})_4$CaM. This complex then activates the enzyme myosin light chain kinase (MLCK), resulting in LC20 phosphorylation. However, constitutive myosin light chain phosphatase (MLCP) activity dephosphorylates LC20, which counteract the magnitude of contraction owing to MLCK activation and evokes relaxation. So factors which influence MLCP activity are regarded as modulators of Ca^{2+} sensitivity, since they either potentiate or impair contraction at a given $[Ca^{2+}]_i$[13]. Hence, any stimulus which can raise intracellular Ca^{2+} concentration or decrease MLCP activity will result in vasocontraction. Conversely, it will cause vasodilation.

1.2.2 Vasocontraction

In general, the stimulus that induce vessel contraction can be classified into 2 groups according to their different mechanisms. Abundant research results support that both $[Ca^{2+}]_i$ increase and Ca^{2+} sensitivity alteration are involved in even one given stimuli.

First, some factors such as physical stretch following increase in intravascular pressure, or under experimental conditions, for instance high concentration KCl stimulation, can produce VSMC depolarization. Such pathway is regarded as electromechanical coupling pathway, which mainly activates voltage-operated Ca^{2+} channels(VOCC) that leads to increases in $[Ca^{2+}]_i$, thereby induces vasocontraction[14]. In addition, there are some studies pointed out that contraction induced by KCl or increased stretch is in some extent involving Ca^{2+} sensitization which related to activation of RhoA kinase[14-16].

Second, contractile agonists stimulate specific cell surface receptors, normally G protein coupled receptors(GPCRs), to induce vasocontraction, this mechanism being regarded as pharmaco-mechanical coupling (shown in Figure 4). GPCRs form a family sharing a conserved structure of seven transmembrane α-helices. Once binding to their ligands, GPCRs change into an active conformation and stimulate heterotrimeric GTP-binding regulatory proteins (namely G proteins) which locate in intracellular domains. This stimulation promotes the dissociation of the Gα from the Gβγ subunits to mediate downstream signaling. Gα subunit family mainly

comprehend 4 types: G_i, G_s, $G_{q/11}$ and $G_{12/13}$[17-19]. There are two well-known kinds of agonists inducing vasocontraction pathway. Firstly, agonists such as norepinephrine, angiotensin II, serotonin, endothelin, mainly activate receptors coupled to $G_{q/11.}$ This subsequently stimulates phospholipase C-β (PLCβ) mediating conversion of phosphatidylinositol 4,5-bisphosphate (PIP2) into inositol 1,4,5-trisphosphate (IP3) and diacylglcerol (DAG). The IP3 diffuses into cytosol, then stimulates the sarcoplasmic reticulum (SR) IP3 receptor (IP3R) open to release Ca^{2+}. The resulting elevated $[Ca^{2+}]_i$ activates contractile proteins and initiates contraction. DAG, along with Ca^{2+}, activates PKC, which subsequently phosphorylates 17 kDa PKC-potentiated protein phosphatase 1 inhibitor protein (CPI-17) at Thr-38 and thereby increases the inhibitory effect of CPI-17 on MLCP catalytic activity (PP1c-δ) by around 1000-fold[20], thus eventually inducing contraction[21-23]. Secondly, ligands like TXA_2, PGF2α and lysophosphatidic acid, binding to $G_{12/13}$ coupled GPCRs, lead to RhoA activation via RhoGEF, and RhoA activates Rho-associated kinase (ROK), which inhibits MLCP activity to induce vasocontraction either by phosphorylating MYPT1 at Thr-696 or by Thr-855, with a preference for Thr855[13,24]. Besides, the activation of Rho kinase has been demonstrated to phosphorylate CPI-17 at Thr-38[23].

Furthermore, other kinases like zipper-interacting protein kinase (ZIPK), integrin-linked kinase (ILK) are also demonstrated to be involved in modulating MLCP actvity[24]. However, it is important to note that changes in membrane potential may occur secondary in the pharmaco-mechanical coupling[25].

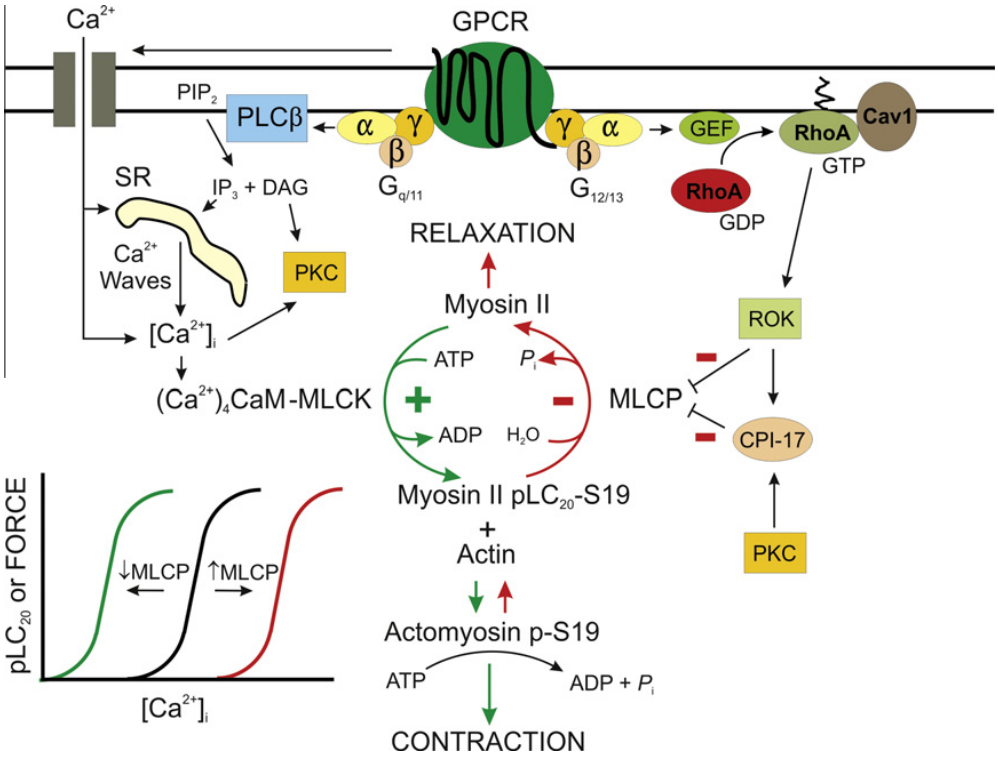

Figure 4. Signaling pathways of agonist-evoked contraction. Agonists binding to GPCR that interact with $G_{q/11}$ stimulate PLCβ mediated conversion of PIP2 into IP3 and DAG, then IP3 induces Ca^{2+} release from SR stores after binding to its receptor (IP3-R). DAG stimulates PKC activity directly along with Ca^{2+}. In contrast, agonists binding to $G_{12/13}$ coupled GPCRs lead to RhoA activation via RhoGEF, and subsequently activates ROK activity, along with alteration of membrane potential. Both the activation of PKC and ROK can inhibit MLCP activity by indirectly interaction with MLCP catalytic subunit (PP1c-δ) mediated by phosphorylation of CPI-17 or directly phosphorylates MLCP regulatory subunit-MYPT1 (and possibly CPI-17). The inhibition of MLCP reserves LC_{20} phosphorylation levels, leading to contraction. The lower-left corner shows the relationship between $[Ca^{2+}]_i$ and MLCP activity. The more MLCP activity is inhibited (green curve), the more force will be generated under same $[Ca^{2+}]_i$ concentration or MLCK activity. Conversely, the more MLCP activity is activated (red curve), the less force will be generated at similar calcium condition. Abbreviations: DAG: diacylglcerol; GPCRs: G protein coupled receptors; IP3: inositol 1,4,5-trisphosphate; MLCP: myosin light chain phosphatase; MLCK: myosin light chain kinase; PIP2: 4,5-bisphosphate; PLCβ: phospholipase C-β; ROC: Rho-associated kinase. (Adapted from Cole et al, 2011[13])

1.2.3 Vasorelaxation

1.2.3.1 Role of cyclic nucleotides (CNs) in vasculature

Cyclic nucleotides (CNs), which include 3', 5'-cyclic adenosine monophosphate (cAMP) and 3', 5'-cyclic guanosine monophosphate (cGMP), are pivotal intracellular second messengers existing in large variety of systems. Here we will mainly focus on their role in vasculature. Generally speaking, CNs vasodilate vessels, modulates endothelial permeability, exert antiproliferative and pro-apoptotic effect and inhibit platelet[26-29]. Thus, elevation of their intracellular concentration represents useful strategies in many cardiovascular pathological conditions. Importantly, the intracellular level of CNs are the result of the balance between the rate of their synthesis and the rate of their degradation. Cyclic AMP and cGMP are produced by distinct enzymes, the adenylyl cyclases (AC) and the guanylyl cyclases (GC), respectively, and act via different effectors to modulate cellular function. The concentration of cAMP is around 5 times higher than cGMP in systemic arteries tissue[30]. Intracellular concentrations of CNs are degraded by cyclic nucleotide phosphodiesterases (PDEs), among which the GAF domain of some PDEs are still the effectors of CNs. Here we will mainly focus on their role and pathway to relax vascular tone.

1.2.3.2 Role of cGMP in vascular tone

1.2.3.2.1 Generation of cGMP

Synthesis of cGMP in VSMCs is catalyzed by two classes of GCs, which hydrolyze GTP into cGMP either by the soluble guanylate cyclase (sGC) or particulate guanylate cyclase (pGC), the latter including two isoforms, namely GC-A and GC-B[26,31]. Therefore, there are two pathways of cGMP signaling stimulated by two kinds of independent mediators.

1.2.3.2.2 Nitric oxide(NO)-sGC-cGMP pathway

A free radical, NO is an autacoid gaseous mediator able to initiate vasorelaxation, inhibit VSMC proliferation, platelet aggregation[32]. In addition to participating in cardiovascular

system regulation, NO also mediates neurologic, immune and inflammatory systems. Thus either deficit or even excess of NO is involved in a variety of pathological and physiological processes including most of vascular diseases, neurodegeneration and sepsis, tumors and so on[33-35].

NO is synthesized from the substrate L-arginine by NO synthetases (NOS). There are 3 isoforms of NOS encoded by 3 distinct genes: neuronal NOS (NOS1, nNOS), inducible NOS (NOS2, iNOS) and endothelial NOS (NOS3, eNOS). Structurally, all NOS proteins are oxidoreductases associated in homodimers. The C-terminal of NOS is reductase domain, associating with electron-providing cofactors (NADPH), while the N-terminal of NOS is oxygenase domain, allowing association with the substrates, cofactor tetrahydrobiopterin (BH4), and a ferric heme group, that eventually generate NO[36]. Both nNOS and eNOS are expressed constitutively and are stimulated by Ca^{2+} /CaM, whereas iNOS is Ca^{2+}-independent and induced by inflammatory stimuli[37]. All three isoforms have been detected in vessels[36,38], while eNOS is the main contributor to the production of NO following stimulation of the endothelium[39]. Inhibition of NOS is sufficient to potentiate the vasoconstrictor response of an isolated vessel, indicating the existence of a constitutive production of NO at basal state[40]. The activity of eNOS can be stimulated by $[Ca^{2+}]_i$ elevation and subsequent Ca^{2+} /CaM binding. This process can be enhanced by agonists such as acetylcholine (Ach), bradykinin and histamine binding to Gq-coupled membrane receptors which leads to an influx of cacium[34,41]. Eventually, it accelerates NO production by facilitating electron flux from the reductase to the oxygenase domains of the enzyme[42]. Moreover, the activity of eNOS are modulated by several mechanisms, including phosphorylation, nitrosylation, interaction with other proteins, cofactor/substrate availability, and changes in transcription[32,42,]. Furthermore, pharmacological agents such as Sodium Nitroprusside, Diethylamine NONOate, can release NO in vitro or in vivo independent from its endogenous sources, so are regarded as NO donor. Some prodrugs that release NO such as Nitroglycerin and Sodium Nitroprusside had been used for acute coronary syndrome before NO was recognized[43].

The main target of NO is sGC, which mediates a large proportion of vasorelaxant effects. sGC, localizing in cytosol, is a heterodimeric α/β-heme protein (shown in Figure 5). The enzyme is classically stimulated by the binding of NO to N-heme-nitric oxide binding domain (H-NOX) in β subunit of sGC[44]. Except for NO, there are two kinds of pharmacological agents that can increase sGC activity. One is sGC stimulators which bind directly to reduced, heme-containing sGC, and results in an increase in cGMP production[45]. Another is sGC activators, which binds to oxidized, heme-free sGC, which results in sGC activation and cGMP generation[46]. The action of sGC stimulators is independent of NO but is enhanced in the presence of NO whereas the action of sGC activators is not influenced by NO. The representative agent of sGC stimulators is Riociguat, which has been approved to treat pulmonary artery hypertension (PAH)[47] and chronic thromboembolic pulmonary hypertension (CTEPH)[48] diseases by FDA. The representative agent of sGC activators is Cinaciguat (BAY 58-2667). Multiple sGC activator projects aiming at treating cardiovascular disease have been terminated in Phase 2 due to lack of significant beneficial effects or occurrence of unwanted effect such as hypotension. This has hampered the further development of sGC activitors toward larger clinical trials and approval[44].

In addition, NO reacts with the thiol groups of protein cysteine residues, forming a covalent modification called S-nitrosylation and can thus modify the activity of targets, ion channels involved in the control of vascular tone[49].

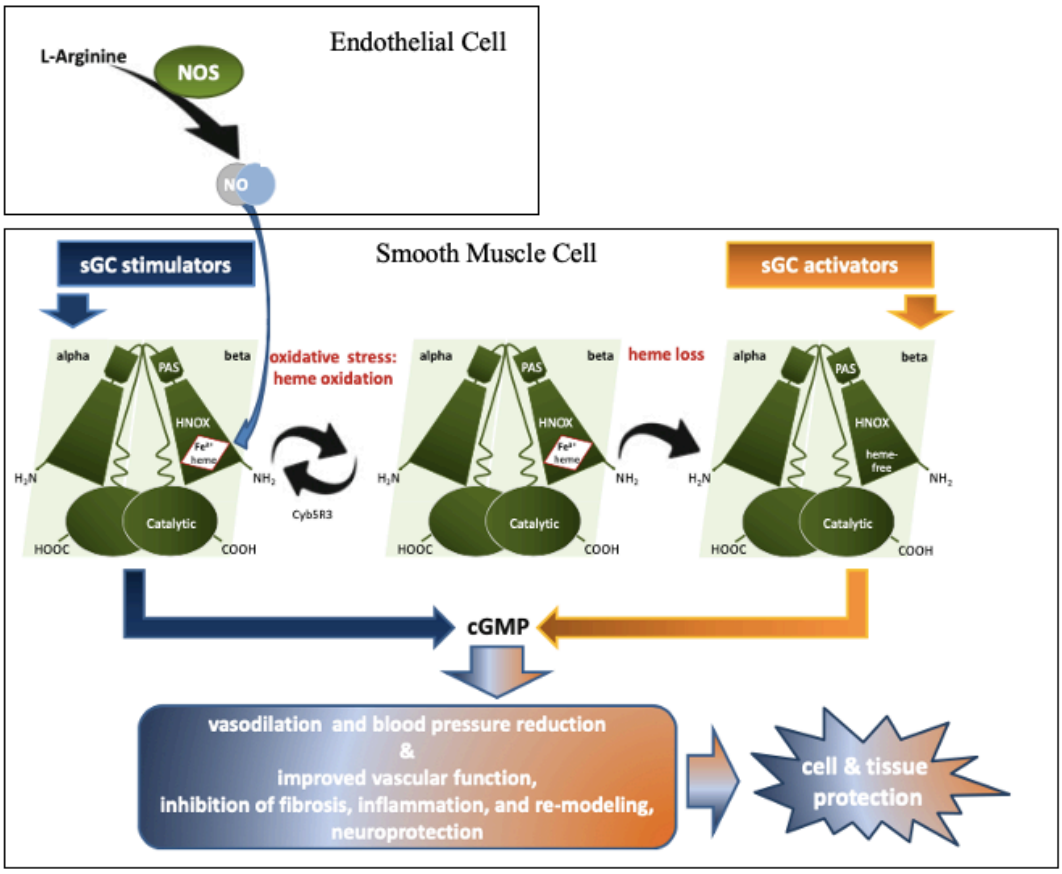

Figure 5. Schematic representation of the sGC structure and its pharmacological intervention. Native sGC is heme-containing. It can be oxidized by oxidative stress, and loses heme group, thus turning into a dysfunctional, heme-free sGC that is unresponsive to NO. This balance can be repaired by Cyb5R3, a heme iron reductase, which is ubiquitously expressed in vascular smooth muscle cells, and can reduce the sGC heme iron and thereby re-sensitize sGC to NO. The sGC stimulators and sGC activators act on heme-containing sGC and the heme-free sGC, respectively, to enhance sGC/cGMP pathway which mediates the beneficial effects in vasculature. (Adapted from Sandner et al., 2021[44])

1.2.3.2.3 Natriuretic peptides (NPs)-pGC-cGMP pathway

There are some circulating or paracrine peptides which can stimulate receptors coupled to an intracellular GC enzymatic activity, which constitutes an additional pathway for cGMP synthesis. These peptides are natriuretic peptides (NP_S), and the receptors coupled GC is therefore pGC.

There are 3 types of NPs that can lead to cGMP generation and involve in maintaining cardiovascular homeostasis. Atrial natriuretic peptides (ANP) and brain natriuretic peptides (BNP) are expressed in the heart [50-52] and are released in response to a volume-induced stretch of the atria and ventricles, respectively[53,54]. These peptides act as endocrine hormones and contribute to the regulation of blood pressure and blood volume[55]. CNP is mainly expressed in chondrocytes, whereas within cardiovascular system, it is mainly expressed in ECs[56,57], but also expressed in cardiomyocytes[58] and fibroblasts[59]. CNP tissue expression and plasma levels are relatively low, suggesting that this peptide most likely acts as a local paracrine/autocrine mediator in the heart and blood vessels.

All these NPs classically exert vasorelaxant effect via binding to natriuretic peptides receptors (NPRs). The structure of NPRs is shown in Figure 6. There are 3 kinds of NPRs: NPR-A, NPR-B and NPR-C. All of them are homodimeric proteins, whereas the NPR-C lacks the intracellular kinases domain and guanylyl cyclase domain, displaying instead a 37 amino acid domain. The binding potency of ligands to NPR-A is ANP ≥ BNP >> CNP, to NPR-B is CNP >> ANP ≥ BNP, and to NPR-C is ANP > CNP ≥ BNP[55]. All of NPs can bind to NPR-C, which mediates internalization of NPs followed by lysosomal degradation[55]. Another way to degrade NPs is by neutral endopeptidase or neprilysin (NEP), a zinc-dependent enzyme expressed on the plasma membrane that has broad substrate specificity and tissue distribution.

The resulting elevation of intracellular cGMP levels from either NO-sGC pathway or NPs-pGC pathway mainly activates cGMP-dependent protein kinase (PKG) to modify downstream effectors in vasculature.

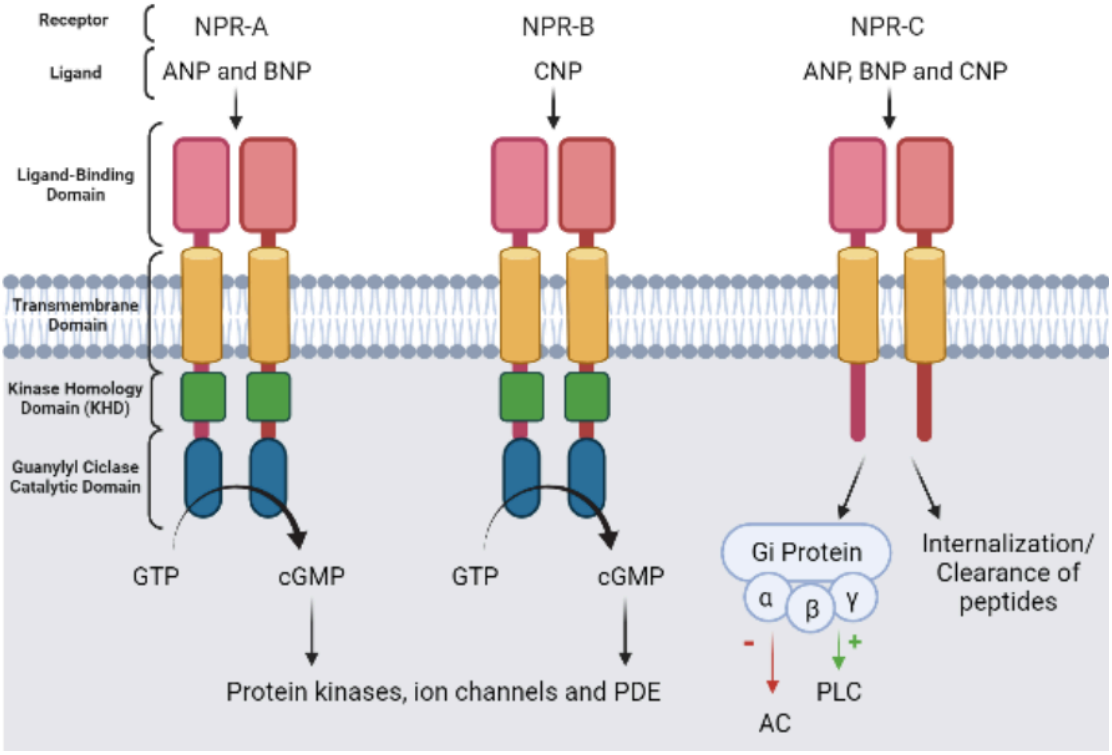

Figure 6. Structure and pathway of the natriuretic peptide receptors (NPR). ANP and BNP mainly bind to NPR-A, and CNP mainly binds to NPR-B. All of them can bind to NPR-C, which is involving in clearance of NPs. NPR-A and NPR-B have similar structure, which comprises of extracellular N-terminal domain, transmembrane domain, kinase homology domain (KHD), and intracellular GC catalytic domain. Whereas NPR-C lacks the GC catalytic domain.(adapted from Lorigo et al., 2021[60])

1.2.3.2.4 Protein Kinase G(PKG)

There are two isoforms of PKG: PKGI and PKGII, but PKGI is predominantly expressed in cardiovascular system, which in turn phosphorylate substrates[26]. PKGI include 2 subtypes, namely PKGIα and PKGIβ. Both are soluble enzymes and equivalently expressed in arterial tissue and exhibit similar affinity for cGMP (half activation constant of 0.29 and 0.44 μM, respectively)[61-63]. Both PKG-I and PKG-II exist as homodimers and kept in inactive state by interactions with the N-terminal regulatory (R) domain which covers active sites in C-terminal catalytic domain (C). Selective binding of cGMP to cyclic nucleotide binding (CNB) domains within the R-domain disrupts the inhibitory R-C interaction by conformational change, leading

to the release and activation of the C-domain, which in turn catalyzes the phosphorylation of a serine/threonine residue of the target substrate with sequence of Arg-Lys-Arg-Ser/Thr-Arg-Lys-Glu, and not restricted to this sequence but overlaps with that of PKA (Arg-Arg-X-Ser/Thr-X)[64,65]. The use of mice deficient for the PKGI highlighted the role of this kinase in the vasodilating properties of the NO-cGMP signaling[66,67]. Besides, these pathways are also involved in regulation of endothelial permeability[31]. Stimulation of PKGI inhibits vasocontraction by both lowering $[Ca^{2+}]_i$ and decreasing Ca^{2+}sensitivity. Manoury et al's article[68] reviews various mechanisms by which PKG promotes vasorelaxation that mainly comprises of three aspects (Figure 7): I. PKG reduces intracellular calcium levels via inhibiting PLCβ activation and Ca^{2+} release from the SR stores (pathway 1and 2) [69-72], activating Ca^{2+} uptake by the SR (pathway 3)[73-75], activating intracellular Ca^{2+} efflux channels (pathway 4 and 5)[76-83], as well as inactivating extracellular Ca^{2+} influx channels (pathway 6) [28,68]; II. PKG induces hyperpolarization of the membrane potential through activation of outward potassium channels (pathway 6)[28,68]; III. PKG decreases Ca^{2+} sensitivity by activation MLCP activity and inhibiting RhoA (pathway 8 and 9)[84-87].

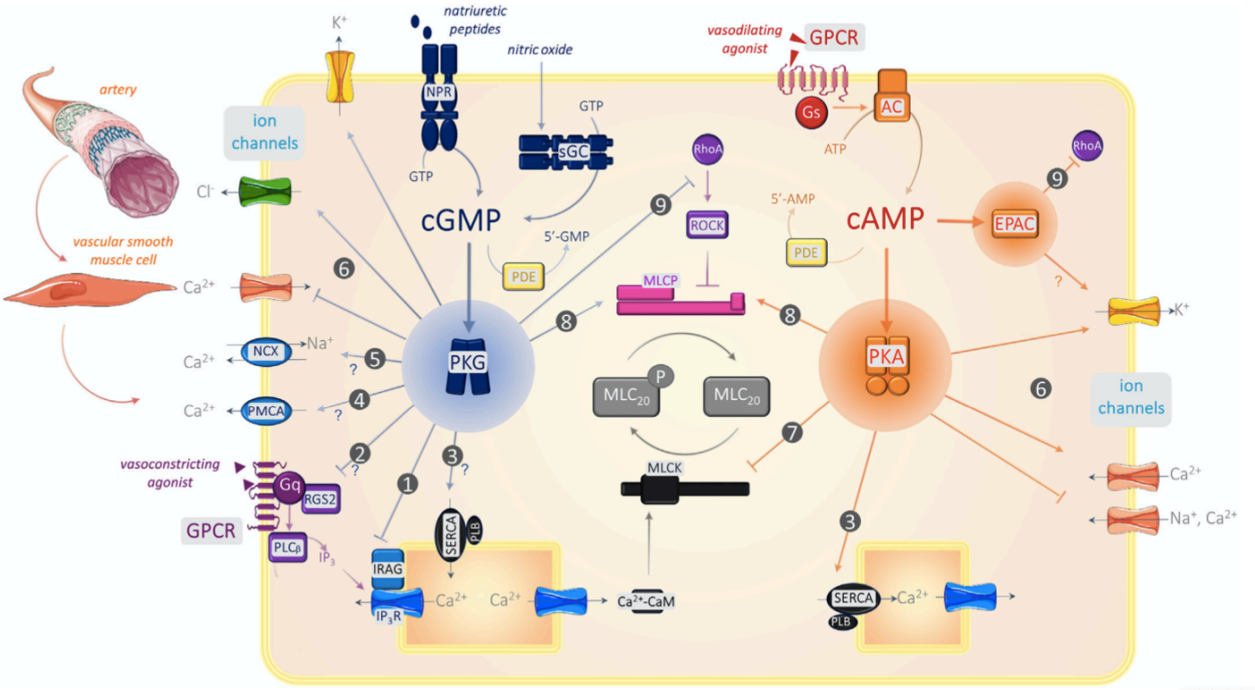

Figure 7. Summary of vasorelaxant mechanisms mediated by cAMP and cGMP (see next page for legend).

Figure 7 (continued) . Categories numbered 1 to 9 indicate targets of PKA, EPAC or PKG and associated pathways. Pointed arrows indicate stimulation, truncated arrows indicate inhibition. Number 1 to 6 means mechanisms of $[Ca^{2+}]_i$ decrease. 1. IP3R, IRAG: PKG reduces the Ca^{2+} efflux from SR by phosphorylating IP3R and the regulatory protein IRAG. 2. PLC: The cGMP/PKG pathway inhibits PLCβ via the RGS2 protein. 3. SERCA, PLB: Inhibition of SERCA reduces relaxation induced by cGMP and cAMP pathways. Phosphorylation of the ser-16 residue of PLB by PKA or PKG is associated with vasorelaxation. 4. PMCA: the cGMP-PKG pathway, but not PKA, would activate the PMCA pump by uncertain mechanism. 5. NCX: the cGMP analogue 8-Br-cGMP activates the NCX exchanger of cultured VSMCs. However, the importance of PMCA and NCX is not major in the physiological control of $[Ca^{2+}]_i$ by cGMP. 6. Ion channels: cAMP and cGMP pathways act on many ion channels with consequences on membrane potential and $[Ca^{2+}]_i$. Number 7-9 means mechanisms acting on sensitivity to $[Ca^{2+}]_i$. 7: MLCK: phosphorylation of MLCK by PKA at ser-1760 reduces activity of MLCK and its affinity for calmodulin. 8: MLCP: PKGIα and PKA phosphorylate the MYPT1 regulatory subunit of MLCP. Phosphorylation by PKG at ser-695 interferes with phosphorylation at thr-696 by Rho-kinase. 9: RhoA: PKG inhibits RhoA by phosphorylating it on ser-188. EPAC inhibits the RhoA pathway. The abbreviations are defined in the list at the opening of the thesis. Abbreviations: EPAC: exchange protein activated by cAMP; IP3R: IP3 receptor; IRAG: IP3R-associated cGMP kinase substrate; MLCK: myosin light chain kinase; MLC20: 20-kDa subunit of myosin light chain; MLCP: myosin light chain phosphatase; NCX: Na^+ , Ca^{2+} exchanger; NO: nitric oxide; NOS: nitric oxide synthase; NPR: natriuretic peptide receptor; PDE: phosphodiesterase; PKA: cAMP-activated protein kinase; PKG: cGMP-activated protein kinase; PKC: protein kinase C; PLB: phospholamban; PLC: phospholipase C; PMCA: plasma membrane Ca^{2+}-ATPase; RGS2: regulator of G protein signaling-2; SERCA: sarcoplasmic reticulum Ca^{2+}-ATPase; SMC: smooth muscle cell; SOCE: store-operated Ca^{2+}entry. (Adapted from Manoury et al., 2020[68]）

1.2.3.3 Role of cAMP in vascular tone

1.2.3.3.1 cAMP generation

Synthesis of cAMP in VSMCs is achieved by adenylyl cyclases (ACs) which use adenosine-tri-phosphate (ATP) as a substrate. There are nine membrane-bound ACs isoforms and one soluble (sAC) isoenzymes, each with distinct expression and regulatory profiles[88]. In common with most other cell types, VSMCs express multiple AC isoenzymes, with strongest evidence for ACs 3, 5, and 6[89,90]. AC6 was proposed as the most relevant contributor to cAMP production and recruitment of downstream effectors[91]. Expressions of AC2 and AC8 are increased in cultured VSMCs that have adopted a proliferative and dedifferentiated phenotype[91-93]. In VSMCs, ACs are classically stimulated following activation of Gs protein-coupled receptors by their respective agonists, which mainly includes β_2-adrenoreceptors (stimulated by endogenous catecholamines adrenaline/epinephrine, noradrenaline/norepinephrine, or isoproterenol), A_2 receptors (bind to adenosine), and IP receptors (stimulated by prostacyclin, PGI_2)[94]. In addition, ACs can be directly stimulated by chemical drugs, such as forskolin and L858051(a water-soluble forskolin derivative). Several cAMP effectors are described, including protein kinase A (PKA), exchange protein activated by cAMP -1 and -2 (EPAC1/2), cyclic nucleotide gated ion channels (CNG) and the Popeye domain containing (Popdc) family of proteins, whereas only PKA and EPAC1 are reported expressed and functioned in vasculature.

1.2.3.3.2 Protein Kinase A (PKA)

The main effector for cAMP is PKA, which is another serine/threonine protein kinase. PKA holoenzyme exists as a tetramer with two regulatory subunits locking two catalytic subunits in inactive state. Once cAMP binding to regulatory (R) subunits, the enzyme is activated by releasing of the catalytic (C) subunits (Figure 8). Each R subunit has two cAMP binding sites, site A and site B respectively. When a molecule of cAMP binds to B site, it stimulates cooperative binding of a second molecule to A site, hence, site B has been regarded as ‘‘gatekeeper’’ for PKA activation[95-97].

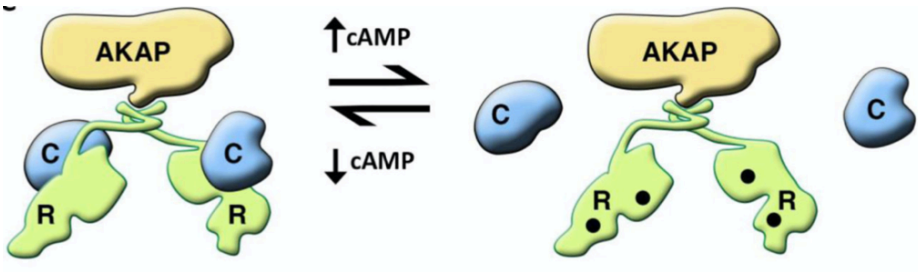

Figure 8. The anchored PKA holoenzyme and activation by cAMP. PKA holoenzyme contains 2 C subunits (blue) and 2 R subunit dimer (green), and anchored by AKAP (yellow) at N-terminal dimerization and docking(D/D) domain. Following stimulation of cAMP synthesis, the cAMP (black) binds to the regulatory subunits, which induces the release the catalytic subunits. Then the catalytic subunits is activated to phosphorylate target substrates on serine or threonine residues presented in a sequence context of Arg/Lys-Arg/Lys-X-(X)-Ser/Thr-X[65], (with X as hydrophobic residues).(Adapted from Turnham et al., 2016[98])

There are 2 forms of PKA holoenzyme, type I and type II, containing either an RI dimer or RII dimer, and each type of R subunit has 2 isoforms, RIα and RIβ, RIIα and RIIβ respectively. Type I PKA is more sensitive to cAMP with an activation constant (Kact) of 50–100 nM of cAMP, and is classically know to be preferentially cytosolic; whereas most of type II PKA presents a Kact of 200-400 nM of cAMP, and is mainly associated with the particulate fraction of cell lysates and compartmentalized to subcellular organelles via specific A-kinase anchoring proteins(AKAPs)[99], which act as scaffolds and engage in direct protein-protein interactions[100]. Furthermore, more and more evidence support PKA RI is more readily dissociated by cAMP than RII, even though all R subunits share 75% identity in their cAMP binding pockets[95,98].

One important mechanism to maintain high specificity of cAMP signaling pathway is subcellular compartmentalization. Compartmentalization is formed by AKAPs working as scaffolding proteins that assemble PKA, together with PDEs, to specific substrates and distinct subcellular compartments, thus providing spatial and temporal specificity in the mediation of biological effects controlled by the cAMP–PKA pathway[100-103].

The PKA subunits expressions in vasculature are not well documented. However it has been reported that the RIα, RIIα/β, Cα/β forms are expressed in rat mesenteric artery[104], and RIα and

RIIβ are predominant in cultured aortic VSMCs[105]. PKA functionally regulates vascular tone by several ways which has been well-described in Manoury et al's review[68] (summarized in Figure 7). Briefly: I. PKA reduces intracellular calcium levels mainly through activation of Ca^{2+} uptake by the SR (pathway 3)[75] and inhibition of extracellular Ca^{2+} influx (pathway 6)[28,68]; II. PKA induces hyperpolarization of the membrane potential through activation of outward potassium channels (pathway 6)[28,68]; III. PKA decreases Ca^{2+} sensitivity by activation MLCP activity(pathway 8)[85,106] or inhibition of MLCK activity (pathway 7)[107-110]. In addition, high concentrations of cAMP can bind to PKG, so certain effects of stimulating cAMP pathway have thus been attributed to the activity of PKG[111].

1.2.3.3.3 Exchange protein activated by cAMP (EPAC)

EPAC is another effector of cAMP, which was discovered three decades later than PKA in 1998. EPAC proteins, including EPAC1 and EPAC2 isoforms, are directly activated by cAMP (K_d 2.8 μM) via binding to their regulatory domain CNBD-B[112], and act as guanine nucleotide exchange factors (GEFs) for the small Ras-like GTPases, Rap1 and Rap2 (Figure 9). EPAC1 is the form that is predominantly expressed in the vascular system[113]. Activation of EPAC/Rap1 is involved in the regulation of vascular tone. It is reported that activation of EPAC induces vasorelaxation by inhibition of RhoA-ROCK via Rap-1 dependent manner in phenylephrine-contracted rat portal veins [114]. Activation of EPAC promotes intracellular Ca^{2+} release from SR through ryanodine receptors and thus activates of large conductance Ca^{2+}-sensitive K^+(BKCa) channels in phenylephrine-contracted rat mesenteric arteries[115]. Interestingly, another study points out that EPAC activation inhibits K_{ATP} channel in a Ca^{2+}-dependent manner through Ca^{2+}-sensitive protein phosphatase 2B (calcineurin)-dependent mechanism and is only happened when PKA inactivation in isolated rat aortic smooth muscle cells[116]. However, the role of EPAC in vascular tone appears to be vascular bed-specific. It is reported that activation of EPAC/Rap1 is associated with vasoconstriction in microvasculature by promoting transcription and mobilization of α_{2C}- adrenoceptors to the plasma membrane and Rho-ROCK-mediated stabilization of filamentous actin[117]. Besides, activation of EPAC/Rap1 can enhance eNOS activity and thus mediates cAMP-induced vasorelaxation[118,119]. Consistently, knockout

of Rap1 inhibits NO-dependent vasorelaxation and thus results in increased vasoconstriction and hypertension[120]. EPAC is also involved in modulation of VSMC proliferation and migration which is reviewed by Wehbe et al.[121].

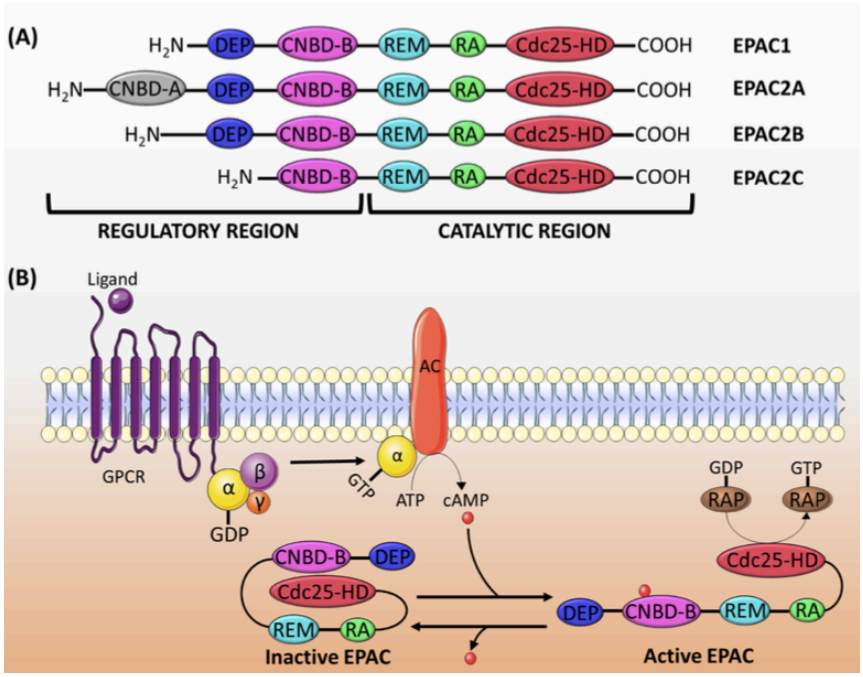

Figure 9. Structure and mechanism of EPAC activation. (A) EPAC consists of one regulatory region in N-terminal and one catalytic region in C-terminal, then each of them is divided into several sub-domains. (B) Following stimulation of cAMP synthesis, the cAMP (red) binds to the regulatory domain of CNBD-B, which triggers conformational change releasing the auto-inhibitory effect. It permits the binding of Rap1/2 to the catalytic domain (Cdc25-HD) and subsequently activated by the GEF activity of EPAC. (Adapted from Wehbe et al., 2020[121])

1.2.3.4 Other Targets of CNs

PDEs present GAF domain which can stimulate their catalytic activity once binding cGMP or cAMP[122-125] (see following chapter). Thus, cGMP stimulates its own elimination through the activation of PDE5[126], and stimulates the elimination of cAMP through the activation of PDE2[127]. Conversely, the GAF-B domain of PDE10 only binds to cAMP and can be activated in vitro with high concentration of cAMP, whereas its function is still not clear in vivo[128]. Besides, binding of cGMP to GAF-A of PDE6 increases affinity for the PDE6γ subunit. Less

is known about the GAF domain-dependent regulatory mechanisms of PDE11, although a cyanobacterial adenylyl cyclase fused with PDE11A4 GAF domains is activated by cGMP[128].

Cyclic nucleotide-gated (CNG) channels are non-selective cation channels first identified in retinal photoreceptors and olfactory sensory neurons[129]. Six different genes encoding CNG channels, four A subunits (A1 to A4) and two B subunits (B1 and B3), give rise to different channels. CNGA1 is found to be strong expressed in the endothelium layer and lower in VSMC[130]. Whereas CNGA2 has been found in both the endothelium and media of human arteries with strong expression[131]. CNG contributes to thromboxaneA2-induced contraction of rat small mesenteric arteries[132]. CNGA2 plays an important role in endothelium dependent vascular dilatation to a number of cAMP-elevating agents including adenosine, adrenaline and ATP[133-135]. CNGA2 also mediates membrane depolarization in in pulmonary artery endothelial cells[136].

1.3 Overview of Phosphodiesterases (PDEs)

As CNs effectors and hydrolase, PDEs have an influence on vascular tone. Hence, hemodynamics, ingeniously regulated by intracellular CNs levels, are still influenced by activity of PDEs. These PDEs selectively catalyze the hydrolysis of the cAMP and/or cGMP into their biologically inactive metabolites 5'-AMP and 5'-GMP, respectively, thereby limiting the activity of these molecules on their effectors[122,123].There are totally 11 structurally related but functionally distinct gene families (PDE1 to PDE11). Each PDE family encompasses one to four distinct genes, giving rise to 21 genes in mammals that encode more than 100 different PDE proteins that are all probably expressed in mammalian cells[122,123]. PDE isozymes generally exist as dimers. Structurally, each PDE family mainly comprises of one divergent N-terminal regulatory regions and one conserved C-terminal catalytic core[101,137] (Figure 10).

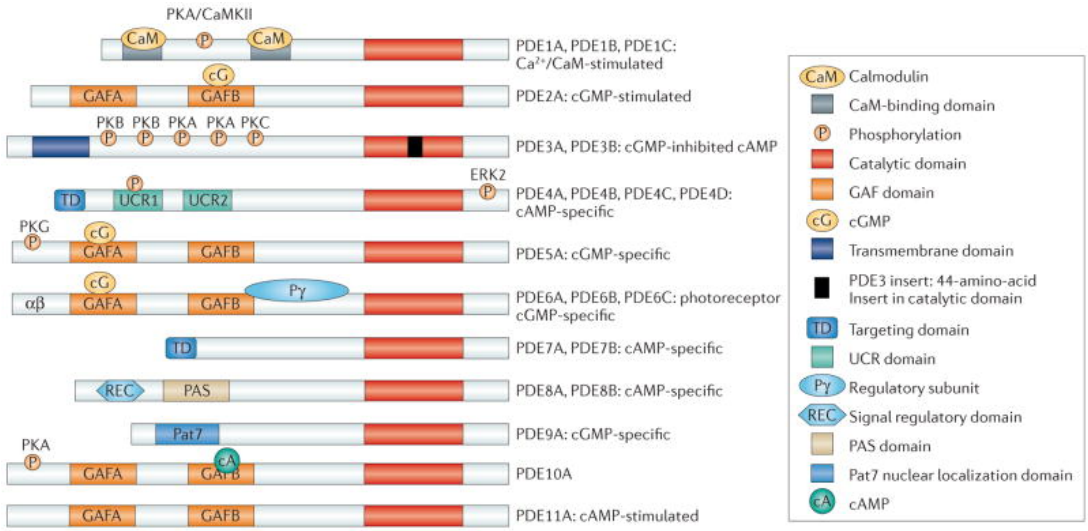

Figure 10. Structure and domain organization of 11 mammalian PDE families. The conserved catalytic domain of PDEs is shown in red and locates in C-terminal region. All PDEs exhibit similar sequence of catalytic domain except PDE3, which contains a 44-amino-acid insert. N-terminal regulatory regions contain structural determinants that permit different PDEs to respond to specific regulatory signals, including binding sites for effectors (CaM domain for PDE1) and allosteric modulators (GAF domains for PDE2, PDE5, PDE6, PDE10 and PDE11), phosphorylation site. PDE3 contains transmembrane domain; PDE4 contains upstream conserved regions (UCRs); and PDE8 contains Per-Arnt-Sim (PAS) domains and receiver (REC) domains. Some PDE9 splice variance contains a pat7 motif responsible for nuclear localization signaling[138]. (Adapted from Maurice et al. 2014[101])

Different PDEs differ in their primary structures, properties of their catalytic site (Km, Vmax) for cGMP and cAMP, and responses to specific activators and inhibitors, cellular function as well as in their mechanisms of regulation[101,122-124]. Among these PDEs families, PDE4, PDE7 and PDE8 specifically hydrolyze cAMP, whereas PDE5, PDE6 and PDE9 specifically hydrolyze cGMP. Others, including PDE1, PDE2, PDE3, PDE10, PDE11, hydrolyze both CNs. The characteristics of human PDEs families are shown in **Table 1**. Besides, the role of PDEs has been extensively studied both in pulmonary artery and systemic arteries (**Table 2**).

Table 1: fundamental biochemical characteristics of PDEs family and their inhibitors

PDE	Gene	Km (μM)	Selectivity	Inhibitors (IC_{50}, nM)
PDE1	PDE1A PDE1B PDE1C	cAMP:73-120 cGMP:2.6-5 cAMP:10-24 cGMP:1.2-5.9 cAMP:0.3-1.2 cGMP:0.6-2.2	Ca^{2+}/calmodulin regulated	8MM-IBMX (NS) Vinpocetine :14000 IC224 :80
PDE2	PDE2A	cAMP:30-50 cGMP:10-30	cGMP stimulated	EHNA:800 BAY60-7550:4.7
PDE3	PDE3A PDE3B	cAMP:0.02-0.15 cGMP:0.18	cGMP inhibited	Cilostamide: 20 Cilostazol:200 Milrinone: 150
PDE4	PDE4A PDE4B PDE4C PDE4D	cAMP:2.9-10	cAMP specific	Rolipram:1000; Cilomilast: 120 Roflumilast: 0.8 Ro20-1724:2000
PDE5	PDE5A	cGMP:1-6.2	cGMP binding, cGMP specific	Zaprinast: 130 Sildenafil:10 Vardenafil:1 Tadalafil:10
PDE6	PDE6A	cGMP:15-17	Photoreceptor	ND
PDE7	PDE7A PDE7B	cAMP:0.1-0.2	Rolipram insensitive	IC242 :370
PDE8	PDE8A PDE8B	cAMP:0.04-0.06	cAMP specific	ND
PDE9	PDE9A	cGMP:0.17-0.39	cGMP specific	BAY73-6691:55 PF-04447943:2.8
PDE10	PDE10A	cAMP:0.26 cGMP:7.2	cAMP inhibited, dual substrate	Papaverine:36
PDE11	PDE11A	cAMP:1.04-5.7 cGMP:0.52-4.2	dual substrate	ND

NS:non-selective;

Table 2: PDEs families expressed in pulmonary artery and systemic artery

PDE	Pulmonary artery Activity/expression	Systemic vessels Activity/expression
PDE1	Vessel:+[139-142] VSMC:+[143-145] PDE1C:+++(proliferative phenotype)[143] EC:ND	Vessel:+[30,142,146,147] VSMC:+[148] PDE1C:+++(proliferative phenotype)[149] EC:±[150]
PDE2	Vessel:+[139,140,142,151,152] VSMC:+[145] EC:+[153]	Vessel:+[142,154] VSMC:±[155] EC:+[150,156-159](+ in vein, cap; +/- in arteries)[160]
PDE3	Vessel:++[139,140,142] VSMC:+[145,161] EC:+[153]	Vessel:+[142,146,147,159,162-164] VSMC:+[165] EC:+[150,157,166]
PDE4	Vessel:++[139,140,142] VSMC:++[145] EC:+[153]	Vessel:+[30,142,146,147,162,163] VSMC:+[167] EC:+[150,156,157,168]
PDE5	Vessel:+++[139,140,142] VSMC:+++[143,161,169] EC: ND	Vessel:+[30,142,146,147] VSMC:+[170] EC:+[150,157,171]
PDE6	not expressed[123]	not expressed
PDE7	VSMC:+(mRNA)[172,173] EC : ND	VSMC:+(mRNA)[155,172] EC : ND
PDE8	VSMC : +(human mRNA)[173]; -(rat mRNA)[172]; EC : ND	VSMC : +(rat mRNA)[155] ; -(rat mRNA)[172]; EC : ND
PDE9	VSMC:±(mRNA)[172,173] EC : ND	VSMC:±(mRNA)[172] EC : ND
PDE10	VSMC : +(mRNA)[173], -(rat mRNA)[172]; (immunoreactivity)[174] EC : ND	VSMC :-(rat mRNA)[172]; EC : ND
PDE11	VSMC : + (mRNA)[173] EC : ND	VSMC : +(human mRNA)[173] EC : ND

VSMC: vascular smooth muscle cell; EC: endothelial cell; ND: not documented

Generally, PDE1-6 were discovered earlier before 1990s, and are regarded as “classic PDEs”. PDE7-11 were found later thanks to the increasing knowledge of the genome, thus are documented less and referred to as “novel PDEs”. Chromatography is major method used to separate different cellular fractions containing differential PDE activity for classic PDEs. The contributions of PDE1 to PDE5 have been demonstrated in the various vessels, VSMCs as well as ECs (Table 2). The existence of relatively selective inhibitors for different PDE families[101,124], such as BAY60-7550 for PDE2[175], Cilostamide for PDE3[176], Ro-20-1724[177] or Rolipram[178] for PDE4, and Sildenafil[179] for PDE5, helped dissect the PDE activities in different tissues in vitro and explore therapeutic potential of PDE inhibition in multiple diseases in vivo. Regarding vascular tone regulation, inhibition of these predominantly expressed enzymes increases the levels of CNs and causes vasorelaxation[140,152,172]. By contrast, until now, understanding the role of PDE1 has remained more challenging because lack of selective inhibitors. Of note, PDE1C, which is absent in normal vessels and contractile SMCs, is reported abundant in human proliferative SMCs or fetal aorta[143,180], thus offering a target for therapeutic intervention aimed at anti-remodeling effect. Currently, with advent of more and more selective and potent inhibitors[181,182], we expected promising therapeutic role of PDE1 in various diseases, including cardiovascular diseases.

The main knowledge about PDEs expressed in ECs was characterized in the primary cultures. ECs have been shown to primarily express PDE2, PDE3, PDE4, and PDE5[150,183,156,158]. PDE2 and PDE4 are reported to be involved in angiogenesis[29,157,184]. Elevation of cAMP by PDE inhibition can decrease endothelial permeability[153]. Moreover, endothelial permeability is influenced by cGMP levels via relative activity PDE2A and PDE3A in endothelial cells[159]. Specifically, low concentration of cGMP inhibits PDE3A and thereby increases a local pool of cAMP to decrease permeability, whereas higher concentrations cGMP activates PDE2A, thus increase permeability[159].

Until now, the therapeutic potential of PDE inhibitors has been explored in many diseases[185]. More than 20 PDEs non-selective or selective inhibitors have been approved to use in clinic for various diseases[185], which includes, e.g., non-selective inhibitors, Theophylline and

Aminophylline for treatment of asthma and bronchoconstriction; PDE3 inhibitor, Cilostazol, to treat intermittent claudication[186]; another PDE3 inhibitor, Milrinone, to treat refractory heart failure with a narrow window[187]; PDE4 inhibitors, for instance Roflumilast to treat COPD[188]; PDE5 inhibitors, Sildenafil, Tadalafil, Vardenafil to treat pulmonary arterial hypertension[189-191] and erectile dysfunction[101,192], and so on. Nevertheless, this field may be still in its infancy due to the complexity of this superfamily enzymes, multiple means to regulate PDE expression and activity, and differential spatial distribution and specificity of action in different cell types. However, with the growing exploration of these proteins and development of selective inhibitors targeting specific PDE or PDE variants, we expect to elucidate a more refined appreciation of the intramolecular mechanisms regulating PDE function and trafficking, and aim at discovering novel strategies to therapeutically target PDE function. The basic research of PDE has been expanded into a lot of diseases, and in particular in cardiovascular diseases, such as heart failure, hypertension, erectile dysfunction, post-angioplasty restenosis/atherosclerosis, ischemia/reperfusion injury, angiogenesis and PAH[102]. Next, we mainly focus on the therapeutic role of PDE inhibition in PAH.

1.4 Pulmonary Arterial Hypertension (PAH)

1.4.1 PAH definition and classification

Pulmonary hypertension (PH) is a syndrome hemodynamically characterized by a mean pulmonary arterial pressure (mPAP) higher than 20 mmHg at rest, which is standardly measured by right heart catheterization[1]. PH may result from a myriad of etiologies and thus possess different manifestations. Hence, the World Health Organization (WHO) has classified PH into five major groups according to clinical and pathological findings and treatment responses[1] (shown in table 3), namely: Group 1, PAH; Group 2, PH due to left-sided heart

disease; Group 3, PH due to lung disease, hypoxia, or both; Group 4, PH due to pulmonary-artery obstructions; and Group 5, PH with multifactorial or unclear mechanisms. In addition, every group is further classified by their different etiology. Here we will mainly focus on the Group 1 (PAH).

Table 3. Clinical Classification of Pulmonary Hypertension (PH)

1. Pulmonary arterial hypertension (PAH)
    - 1.1 Idiopathic PAH
    - 1.2 Heritable PAH
    - 1.3 Drug- and toxin-induced PAH
    - 1.4 PAH associated with:
        - 1.4.1 Connective-tissue disease
        - 1.4.2 HIV infection
        - 1.4.3 Portal hypertension
        - 1.4.4 Congenital heart disease
        - 1.4.5 Schistosomiasis
    - 1.5 PAH long-term responders to calcium-channel blockers
    - 1.6 PAH with overt features of venous or capillary involvement (PVOD or PCH)
    - 1.7 Persistent PH of the newborn
2. PH due to left-sided heart disease
3. PH due to lung disease, hypoxia, or both
4. PH due to pulmonary-artery obstructions
5. PH with multifactorial or unclear mechanisms

PAH is a disease due to primarily involvement of the pulmonary vasculature, and contains patients with similar pathophysiological, histological, and prognostic features even though caused by multiple reasons. PAH is further classified according to etiology as listed in **Table 1**. The disease with absence of any specific etiology is termed idiopathic PAH (iPAH). When PAH patients have an identified mutation in genes which are strongly associated with PAH,

such as *BMPR-II, ACVRL1, ENG* and so on, the disease is referred to as "heritable PAH" (hPAH); other PAH subgroups are termed based on their specific etiology or some particular characteristics of histological pattern or hemodynamics. Precisely, diagnosis of PAH is defined hemodynamically by mPAP>20 mmHg, together with a normal pulmonary artery wedge pressure (PAWP) ≤15 mmHg and elevated pulmonary vascular resistance (PVR) >3 Wood Units. In addition, other causes of pulmonary hypertension, such as lung disease and chronic thromboembolic disease, must be excluded before PAH is diagnosed.

1.4.2 Epidemiology

PAH is a rare disease with an estimated prevalence around 15-50 cases per million population in western countries and with an annual incidence of 2 to 5 cases per million[193-196]. In general, iPAH (30-50%) and connective tissue disease-associated PAH (CTD-PAH, 15-30%) are the most common subtypes, then followed by congenital heart disease-associated PAH (CHD-PAH, 10-23%)[193,197,198]. However, it should note that PAH subgroup distribution is related to economic development, where high prevalence of CHD, HIV infection and schistosomiasis-associated PAH are more frequent in low or medium income countries[199-201]. This disease afflicts people of all races and cultures, but more affected in woman than man[193,202], the ratio of woman to man is 2.3:1 in younger patients before menopause (median 54 years), and this ratio decreases in older patients (1.2:1 in 75-year-old patients) as reported in COMPERA registry[203]. However, man is associated with worse survival[203-205]. Besides, PAH was originally regarded as affecting young-to-middle-aged people with mean age 36±15 years at diagnosis[202]. Over past 3 decades, however, one of the most striking changes is increasing proportion of older patients diagnosed with iPAH[206,207].

Before the era of PAH-specific therapies in 1990's, the prognosis of PAH was very poor, with a 1- , 3- and 5-year survival of 68%, 48% and 34% respectively, and the median survival is 2.8 years[208]. After 2 decades development of PAH targeted therapies until to 2012, PAH survival has shown large improvement, increasing 1-,3- and 5-year survival rates from time of diagnosis of 85%, 68% and 57%, respectively[209]. Now another decade has gone, with the improvement

of clinical experience, refined treatment algorithm, and decreased drug price, it is expected that the prognosis of PAH continues to improve. To date, there is no clear data of survival rate of all population of PAH, however, it has been reported that the 1-, 3-year survival rates are 97% and 83% in patients accepted up-front dual oral combination therapy (PDE5 inhibitors plus endothelin receptor antagonists)[210].

1.4.3 Pathological features and pathogenesis

The shared vascular pathology of PAH is progressive remodeling of the distal pulmonary arteries (PA), which results in increase in pulmonary vascular resistance and thereby overload of the right ventricle, eventually leading to right ventricular failure and premature death. The histopathological features of PAH[211,212] include (1) intima thickening, which results from ECs hyperproliferation, hypercoagulation or in site thrombosis; (2) media hypertrophy and muscularization of distal pulmonary arteries, which is mainly caused by SMC hyperplasia and hypertrophy and migration; (3) adventitia remodeling, which involves fibrosis and inflammatory cells infiltration, and collagen disruption; (4) plexiform lesions, that are present in advanced and severe stages of PAH, are constituted by cells originating within the vessel wall (mainly endothelial cells, but also including fibroblasts and smooth muscle cells), and possibly cells from the circulation. The most accepted hypothesis of plexiform lesion formation is that vascular injury initiates endothelial apoptosis that leads to selection of apoptosis-resistant and hyperproliferative endothelial population, and along with other types of cells assemble in a “plexiform” or “glomeruloid-like” lesions and thus obliterate small distal pulmonary artery lumen[213]. All of these changes result in luminal narrowing or complete obliteration of small vessels, as shown in Figure 11. Some of these histological features are also present in other groups of PH, but to a lesser extent.

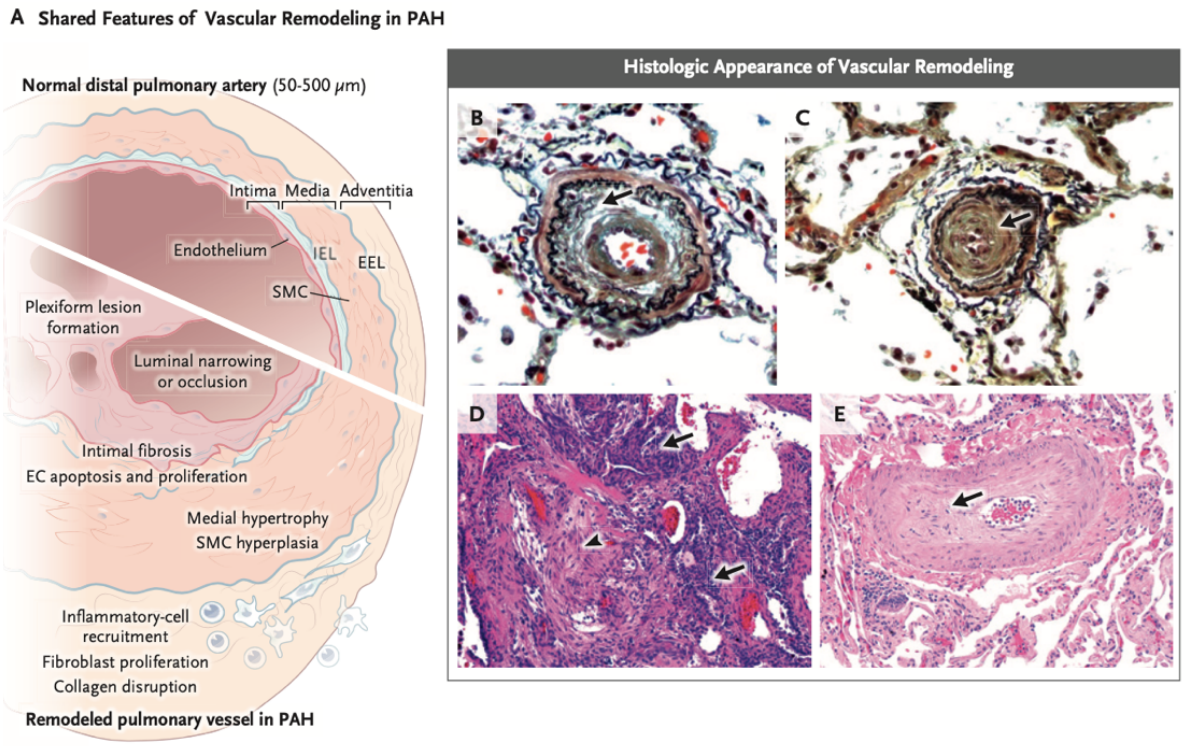

Figure 11. Pathological features of pulmonary arterial hypertension. Panel A shows normal distal PA and PA from PAH subjects characterized by remodeling of the three layers of vessel wall. EC apoptosis and proliferation cause intimal thickening, more serious, plexiform lesion formation; SMC hyperplasia causes medial thickening; infiltration of inflammatory cells such as monocytes, B and T lymphocytes, and dendritic cells, along with collagen disruption fibroblast proliferation result in adventitial remodeling. Panel B shows obvious narrowing of the PA lumen, with concentric intimal proliferation and fibrosis, together with destruction of the internal elastic lamina (arrow). Panel C shows total occlusion of a small PA(arrow). Panel D shows a plexiform lesion with an occlusive lesion (arrowhead) and excessive, poorly formed capillaries and large clusters of endothelial-like cells (arrows). Panel E shows PVOD, with intimal fibrosis (arrow) and evident obliteration of the vessel lumen (adapted from Hassuon, 2021[214])

The exact mechanisms are still partially unknown and are the subject of intensive research efforts. Vascular lesion may be in part initiated by dysfunction of ECs induced by shear stress, hypoxia, autoimmune phenomena, viral infections, drugs and toxins, or genetic alterations and

so on, which subsequently leads to chronically impaired production of vasodilators such as nitric oxide (NO), prostacyclin (PGI_2), and endothelium-derived hyperpolarizing factor (EDHF) along with overexpression of vasoconstrictors such as ET-1, angiotensin II (AngII) so that triggers PASMC contraction and proliferation[215,216], and therefore have been identified as logical pharmacological targets. Besides, the remodeling is recognized in relation to disturbed crosstalk between cells within the vascular wall, and inhibited death processes, as well as enhanced proliferative signaling by various machenisms[217]. Among which, the dysfunction of bone morphogenetic protein (BMP) pathway caused by BMP receptor 2 (BMPR2) mutation is the most studied and important pathway since it induces endothelial dysfunction, increased cellular proliferation, and pulmonary vascular remodeling[218]. The heterozygous mutation of BMPR2 is found in approximately 70%-80% of hPAH and up to 20% of sporadic cases[214]. BMPR2 encodes a transmembrane type II receptor with an intrinsic serine/threonine kinase domain that is expressed on pulmonary vascular endothelial and smooth muscle cells and different inflammatory cell types. BMP ligands can form homo- or heterodimers, and their receptors are tetrameric complex, comprising 2 type I and 2 type II receptors. Binding of BMP dimers to the receptors triggers a phosphorylation cascade that results in phosphorylation of Smad 1/5/8 and players of various non-SMAD pathways to initiate SMAD and non-SMAD signaling cascades. Phosphorylated Smads are able to form complexes with Smad4 and translocate to the nucleus to maintain physiological function in pulmonary arteries[218]. The majority of BMPR2 heterozygous genetic mutations lead to degradation of the mutant transcript via nonsense-mediated mRNA decay, thus results in haploinsufficiency and is the primary molecular mechanism to trigger proliferation in pulmonary vasculature. Besides, mutations inactivate protein function are also common, such as deletions or duplications involving ≥1 exons of BMPR2, which would overtly disrupt protein structure, and amino acid substitutions occurring in functionally important domains, likes kinase domain.

Furthermore, recent findings highlight the role of inflammation in the PAH pathogenesis, since reports indicate that an accumulation of inflammatory cells, including macrophages, dendritic cells, T and B lymphocytes in vascular lesions[219] and circulating inflammatory markers

correlate with disease severity[220] combined with the fact that PAH often complicates autoimmune or inflammatory diseases[221,222].

1.4.4 Therapies

Prior to 1995, there were no specific treatment for PAH, so we called this time as "traditional therapy time", which mainly use calcium-channel blockers (CCBs), anticoagulation therapy, digitalis and diuretics to relieve symptoms of right ventricle failure. Since then, there has been growing development of new specific therapies for PAH as listed in **Table 4**. Currently, there are 10 kinds of PAH specific medications approved by the US Food and Drug Administration (FDA) to treat PAH[223]. These medications target three classical pathways as showed in Figure 12. These medicines have demonstrated efficacy mainly in group 1 PAH rather than other PH groups. However, Riociguat is also approved for Group 4 PH, CTEPH[48]. Besides, another drug, named Sotatercept (a first-in-class fusion protein), targeting dysfunctional BMP pathway signaling has been tested in phase 2 clinical trials and showed beneficial hemodynamic effect with reduction of pulmonary vascular resistance and serum N-terminal pro–BNP levels and improved functional capacity in patients with PAH who were receiving background therapy[218]. The mechanism of Sotatercept is to sequester excess ligands of activin receptor type IIA (ActRIIA), thereby reducing ActRIIA–Smad2/3 signaling which in turn can mitigate its inhibitory effect of BMPR2–Smad1/5/8 pathway by inhibiting expression of the endogenous BMP antagonists gremlin-1 and noggin, thus achieving the effect of enhancing BMPR2–Smad1/5/8 pathway. On the basis of this promising data, Phase 3 trials of Sotatercept in PAH are performed now: a study of Sotatercept for the Treatment of Pulmonary Arterial Hypertension (STELLAR; NCT04576988), a study of Sotatercept in Newly Diagnosed Intermediate- and High-risk PAH Patients (HYPERION; NCT04811092), and a study of Sotatercept in Participants With PAH WHO FC III or FC IV at High Risk of Mortality (ZENITH; NCT04896008). However, there is still a significant unmet medical need, because these advanced therapies can relieve PAH symptoms or impede progression of the disease, yet

they could not reverse the remodeling and the mortality remains high. Hence, lung transplantation is the only way to cure this disease[209].

Table 4: PAH-specific therapies approved by FDA

Prostanoids-Prostacyclin Analogs & IP receptor agonist	**Endothelin Receptor Antagonists (ERA)**	**PDE5 inhibitors & sGC stimulator**
Epoprostenol (Flolan), IV, 1995 (Veletri), IV, 2008 Treprostinil, SC, 2002 IV, 2004 inhaled, 2009 po, 2013 Iloprost, inhaled, 2004 Selexipag, po, 2015 IV, 2021	Bosentan, po, 2003 Ambrisentan, po, 2009 Macitentan, po, 2013	Sildenafil, po, 2005 Tadalafil, po, 2011 Rociguat, po, 2013

IV: intravenous; SC, Subcutaneous

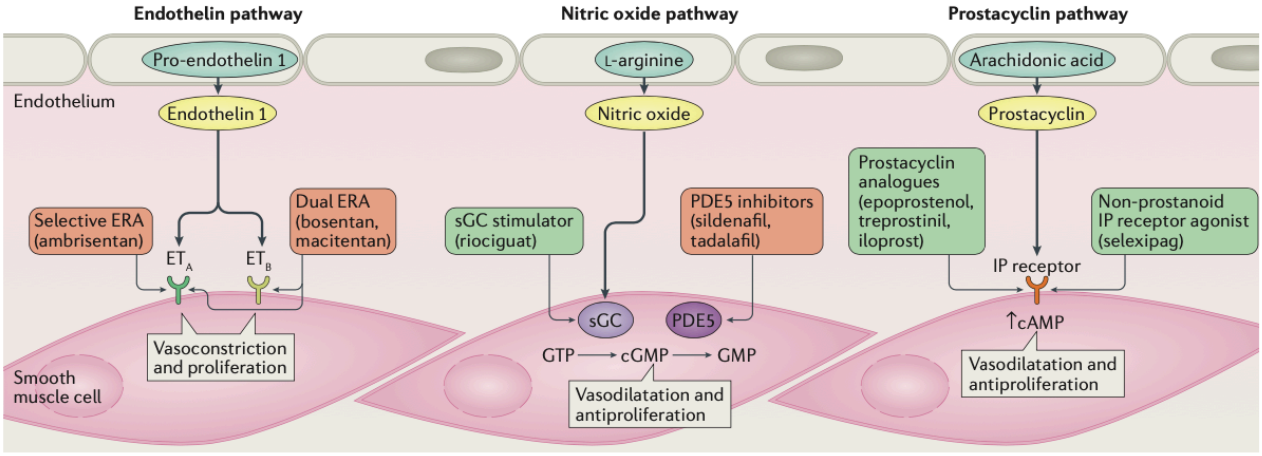

Figure 12. Three classical pathways for targeted therapy of PAH. Molecular targets of approved PAH drug therapies. The endothelin-1 (ET-1) pathway can be blocked by selective or non-selective ET-1 receptor antagonists (ERAs), Ambrisentan or Bosentan, Macitentan respectively; the nitric oxide (NO) pathway can be enhanced by either phosphodiesterase 5 (PDE5) inhibitor or soluble guanylate cyclase (sGC) stimulator, Sildenafil, Tadalafil and Riociguat respectively; the prostacyclin pathway can be enhanced by prostanoid analogues or

non-prostanoid IP receptor agonists, Epoprostenol, Treprostinil, Iloprost and Selexipag, respectively. ET_A, endothelin A; ET_B, endothelin B. (adapted from Lau et al, 2017[224])

1.4.5 Animal models for PAH

Before introducing animal models used to study PAH, it is important to note that such models do not fully recapitulate the feature of PAH in human. Some of them may only represent global PH, such as chronic hypoxia-induced PH models in mice or rats, which should be ascribed to 3rd group of PH (PH due to lung disease, hypoxia, or both), but have frequently been used to explore PAH due to lack of ideal model for PAH. Each model has its own limitations in mimicking the pathophysiology of PAH that takes place in human (Figure 13). Currently, classical rat models include chronic hypoxia-induced PAH (CHx), monocrotaline-induced PAH (MCT), and combination of Sugen-5416 and chronic hypoxia (Su-Hx)-induced PAH models. Even though mouse models have been considered as less relevant than rats, this species has been often used for research via CHx induced PH models.

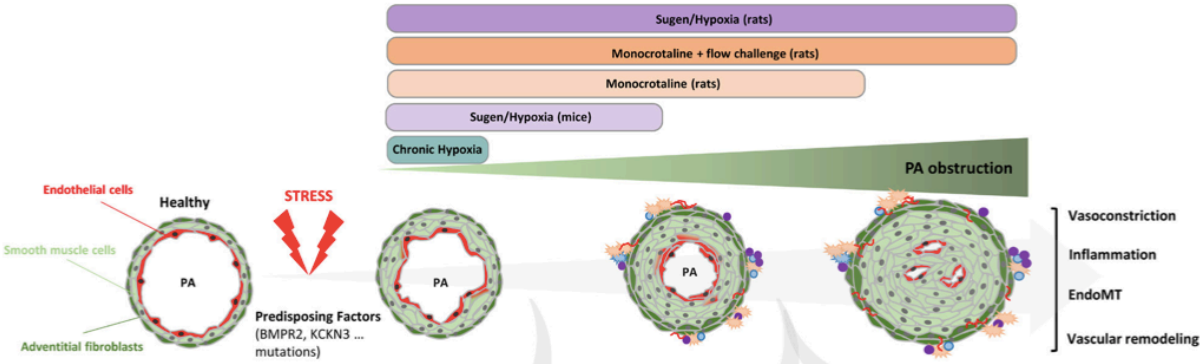

Figure 13. Classical rodent models of pulmonary arterial hypertension. BMPR2: bone morphogenetic protein receptor 2; EndoMT, endothelial-to-mesenchymal transition; KCNK3, potassium two pore domain channel subfamily K member 3.(Adapted from Boucherat et al, 2022[225])

1.4.5.1 Chronic hypoxia (CHx) model

Exposure animals to chronic hypoxia is largely regarded as a model mimic the pulmonary vascular changes observed in PH patients induced by long-term exposure to high altitude. This model is easily established by exposure animals to a chamber containing 10% oxygen at least 3 weeks. This model is widely used as it is predictable and reproducible in a given selected animal strain, even though there is variability among different species, strains, age. It is reported that, for instance, newborn calves develop more severe phenotype of PH compared with rodents under same challenge of chronic hypoxia[226], and the fawn-hooded (FH) rats is more severe than Sprague-Dawley (SD) rats[227], as well as all rats are more susceptible than C57BL/6 mice[228]. In addition, the younger age is more susceptible to develop severe phenotype[229].

Hypoxia-induced PH in almost all mammals is associated with similar structural changes but different magnitude, which is featured by muscularization of small, non-muscular arteries and increased thickening of the previously muscularized precapillary pulmonary arteries in layer of medial and adventitia. In addition, large proximal pulmonary arteries are afflicted with significant thickening and fibrosis, as well as significant stiffening[229]. Inflammation mediated by monocytes appears to play a significant role in the hypoxia-induced remodeling process in rats[230]. RV hypertrophy occurs, but there is little evidence of RV failure. The mechanisms are multifactorial, such as ECs dysfunction induced release of vasoconstrictors, growth factors, matrix proteins and adhesion molecules, and alteration of Ca^{2+} homeostasis in PASMCs and stimulation of the vasoconstrictive and proliferative effects[229]. Particularly, the impaired prolyl hydroxylase domain protein 2 (PHD2)/hypoxia-inducible factor 2α (HIF-2α) signaling axis[231,232], enhanced TGF-β1 (transforming growth factor-beta) and HIF-1α expression[233], are all reported involved in development of PAH. Moreover, microRNAs (miRs) play important role in chronic hypoxia induced PAH, it was reported that inhibition of miRs, such as miR-17 and miR-20a prevent development of pulmonary vasculopathy in mouse model[234,235].

However, compared with PAH in human, the main disadvantages are (1) lack of key pathologic features observed in human PAH, such as angio-obliterative plexiform lesions and neointima proliferation; (2) reversibility of changes upon return to normoxia conditions. This is contrast

with PAH process but consistent with high-altitude induced PH, which can be markedly improved when returned to sea level conditions[236].

Exposure of mice to chronic hypoxia, causes an elevation in RVSP and remodeling of PA, but less extent than rat models[237]. Furthermore, a transcriptomic approach revealed that the expression of a number of genes was increased in the rat lungs but decreased in the mouse lungs in this model[228]. However, this model remains an essential tool to appreciate the susceptibility of genetically modified mice to PH development.

1.4.5.2 Sugen-5416 and chronic hypoxia (Su-Hx) model

Vascular endothelial growth factor (VEGF) and its receptor-2 (VEGFR-2) are involved in proper maintenance, differentiation, and function of ECs. Sugen-5416 is synthetic inhibitor of VEGFR-2. Combination of treatment by Sugen-5416 with chronic hypoxia exposure in rats can cause a severe PAH phenotype associated with precapillary arterial endothelial proliferation, concentric laminar intima thickening and plexiform lesions[238,239]. Normally, this model is established by single injection of Sugen-5416 (20 mg/kg) before exposure to chronic hypoxia (10% oxygen) for 3 weeks. Of note, Sugen-5416 alone can induce mild PAH, yet it is insufficient to induce right ventricle hypertrophy (RVH)[238]. However, Su-Hx model increases right ventricle systolic pressure (RVSP) and RVH more prominently than Sugen-5416 or hypoxia solely[238,240]. It was reported that blockade of VEGF receptor causes EC apoptosis, then chronic hypoxia possibly triggers a subset of apoptosis-resistant endothelial cells and adjacent PASMCs proliferation, thus results in obliterative arterial remodeling and PAH[238]. Some studies revealed that after Su-Hx stimulation, lesions continued to develop even upon return to normoxia. Thus progression of the deleterious tissue remodeling was irreversible and similar to that observed in patients[239,241,242]. By contrast, another group reported that this model was partly reversible for RVSP and RVH, whereas intima obstruction was progressively developed[243]. Additionally, it is reported that Sugen-5416 only affects the lung rather than influencing other organs[238]. Taken together, the Su-Hx(or-Nx) rat model is among one of the strongest preclinical rodent models used to study PAH because of its extremely severe phenotype.

In Su-Hx model in mouse, which is established by Sugen-5416 (20 mg/ kg once a week) over 3-week period of chronic hypoxia, displays a more profound PH phenotype than hypoxia alone, but the phenotype is not severe compared to rat models[244]. The main disadvantage of this model is that, the vascular remodeling, pulmonary hypertension and RV hypertrophy are largely relieved upon return to normoxia[244]. Besides, this model seems to lack reproducibility, as another group couldn't repeat the same results yet by using a similar protocol and background of mice[245]. The difference between mouse and rat models may be partly due to the clearance and metabolism of Sugen-5416, as it is reported that the systemic clearance and liver metabolism are higher in mouse than rat[246]. However, this mouse model is useful in evaluating transgenic mice to see genotype-phenotype consequences.

1.4.5.3 Monocrotaline (MCT) injury induced model

MCT is a toxic pyrrolizidine alkaloid derived from the plant *Crotalaria spectabilis*. After ingestion of MCT, it will be activated into the reactive pyrrole metabolite dehydromonocrotaline (MCTP) in the liver via cytochrome *P*-450 (CYP3A4). Subsequently, MCTP induces a syndrome characterized by marked raise of PA pressure, pulmonary mononuclear vasculitis, and RV hypertrophy and death within 4-6 weeks[247-249].The rat MCT model is easily achieved by subcutaneous or intraperitoneal injection of a single dose of MCT 60 mg/kg, making it a technically simple, and reproducible, low cost animal model.

However other manifestations, not related to PAH, are also present, such as myocarditis, hepatic veno-oclusive disease and acute lung injury and interstitial pulmonary fibrosis[250]. It has been widely used, as it represents 76% of PAH animal interventions[251]. However, the response to MCT is variable among species, strains, and even animals because of differences in the hepatic metabolism by cytochrome *P*-450, the rat being currently the preferred species[236].

The clear mechanism of this pathology is unknown. It is speculated that MCTP directly cause EC damage, interstitial edema, vasoconstriction, perivascular inflammatory infiltrate, and cytokine secretion followed by progressive medial hypertrophy and adventitial fibrosis. There are some traits similar to PAH patients, such as a glycolytic switch with enhanced expression

of pyruvate dehydrogenase kinase[252,253], reduced BMPR2 expression[254], increased growth factor signaling (PDGF [platelet-derived growth factor][255], TGF [trans- forming growth factor][256]), as well as sustained activation of the DNA damage response[257,258] and so on.

With regard to the relevance to PAH patients, the disadvantages of the rat MCT model are (1) the absence of any obstructive intimal plexiform lesion in pulmonary arteries [247]; (2) occurrence of acute/subacute damage of the peripheral vasculature, not only affecting lung and arteries, but also other organs and veins[250]; (3) mild severity, as the model is reported to be cured easily by almost every intervention tried[236]. This may be due to its acute/subacute toxic damage, which is very unlike the human with PAH, and thus limits translation from basic research to clinic. However, it is reported that, regarding the cellular inflammation, the MCT model may recapitulate human PAH better than Su-Hx model[259]. In addition, based on the idea of two-hit model to generate more severe PAH phenotype, combination of MCT and chronic hypoxia model in rat was tested and reported to induce the plexiform-like lesions[260]. And another rat model involving pneumonectomy with MCT administration is reported and can recapitulate many aspect of human PAH, including plexiform-like lesions, but is invasive and not commonly used[261,262].

Of note, however, MCT is ineffective in mice, probably because of the inability of mice to metabolize MCT to its active metabolite, which requires a CYP3A isoenzyme but lacks in the mouse liver[263,264]. There may be some unknown mechanisms since a single injection of bioactive MCTP mice failed to reproduce the MCT-induced PH in mice[265].

1.4.5.4 Other models of PAH.

Transgenic animals have been largely used to study the susceptibility of mutant gene in pulmonary vessels remodeling spontaneously or in response to different stimulus such as chronic hypoxia, inflammation stress. Currently, the genetic mutations of several genes have been identified in associated with heritable PAH[266]. As aforementioned, BMPR2 is most frequent one and been extensively studied. Therefore, many transgenic rodents targeting BMPR2 have been generated and explored. Since the global knockout of BMPR2 is embryonic

lethality in mice[267], heterozygous mice (BMPR2$^{+/-}$) were widely studied and showed contradictory results regarding whether or not this kind of mice can develop PAH spontaneously[268,269]. However, heterozygous mice are more susceptible to develop PAH phenotype once given another stimuli, such as chronic hypoxia[269,270], pro-inflammation mediators and factors such as serotonin infusion[271], Interleukin-1[272], 5-lipoxygenase[268], lipopolysaccharide (LPS)[273]. Besides, smooth muscle–specific transgenic mice expressing a dominant-negative BMPR2[274] or cytoplasmic tail mutation (R899X) of the BMPR2[275], as well as endothelial cell–specific BMPR2 inactivation[276], all of which display PA remodeling and elevation of RVSP to some extent. In addition, by taking benefit of CRISPR/Cas9 system to edit gene, BMPR2 mutant rats have been generated and characterized. In one study, exon 1 was targeted and 71 bp was deleted including loss of translation initial codon. This kind of heterozygous BMPR2 mutant rats exhibited age-dependent spontaneous PAH phenotype with low penetrance (16-27%), and IL-6 was significantly overexpressed in PAH rats[277]. However, another study reported that 2 strains of rats with frameshift mutations of exon 1 did not present sign of PAH after follow-up more than 1 year[278]. Only 5-lipoxygenase was shown to generate additive/synergistic effects on PAH development in this kind of heterozygous mutation of BMPR2, but another hit such as MCT, Su-5416, chronic hypoxia, and Su-Hx failed to see any additive effects based on BMPR2 mutation[278]. Thus, due to incomplete penetrance and variable expressivity of BMPR2 mutant phenotypes, a 2-hit model is necessary to establish PAH successfully.

Except for BMPR2, other gene modified mice have been generated corresponding to mutations identified in PAH patients, such as ALK-1(activin receptor-like kinase 1) heterozygous mice[279], ENG(endoglin) heterozygous mice[280], CAV-1(caveolin-1) knock out mice[281], KCNK3 heterozygous or homogenous mutant rat[282], these mutant rodent were showed to develop PAH phenotype spontaneously including RVSP elevation, PA remodeling or musculation, with or without RV hypertrophy. In addition, there are a few genetic modified mice showing plexogenic arteriopathy. It is reported that IL-6-overexpresing mice, with or without hypoxia, can exhibit moderate or severe features of PAH, respectively, as observed in human[283]; Prolyl-

4 Hydroxylase 2 (PHD2) deficiency in endothelial cells and hematopoietic cells can induce obliterative vascular remodeling and severe PAH[232]. EH-KO$^{ITSN+/-}$ [intersectin (ITSN) knockout heterozygous (KO $^{ITSN+/-}$) mice transduced with Epsin15-homology domain fragment of ITSN (EH_{ITSN})] mouse model displays plexogenic arteriopathy similar to that observed in human PAH lung samples[284]. Whereas these genetic models are useful for a better understanding of PAH mechanisms, such as cell-to-cell interactions, immune dysregulation and abnormal cell phenotype, they have been less used to evaluate therapeutic effect of potential pharmacological agents.

1.4.6 Role of CNs in PAH

Both cAMP and cGMP are very important intracellular second messengers in pulmonary circulation to maintain its low pressure and high output properties by mechanisms that dilate PA as previous introduced[285-287]. Compartmentalization of cAMP signaling is important for pulmonary ECs barrier function, and it is demonstrated that sub-plasma membrane cAMP protects the endothelial barrier whereas cytosol cAMP disrupts the barrier[288]. In addition, although the cAMP levels are around 5 times higher than cGMP in systemic artery[68], it is reported that in rat PA under normal condition, the cGMP concentration is around 2 times higher than cAMP[289].

Interestingly, the PAs from rat models of PAH and the PASMCs isolated from PAH patients have decreased CNs levels[173,289]. Many agents or products which possess potential to increase CNs levels have been explored, mainly by means of stimulating CNs generation or decreasing CNs degradation. For instance, NO or natriuretic peptides (ANP or BNP) to induce cGMP generation can reduce mPAP and PVR in experimental models of PAH[290]. Because they require continuous delivery, however, such agents are difficult to use clinically. Hence, other compounds such as sGC stimulators and PDE inhibitors were gradually investigated and are now indicated for the management PAH. Besides, targeting cAMP pathway by using stable prostacyclin analogues, such as Epoprostenol, Treprostinil, and Iloprost, and its receptor (IP) agonist, Selexipag, that can all stimulate cAMP generation, are also approved to treat PAH.

Nevertheless, in general, the therapeutic potential of prostacyclin analogues is hampered by issues related to their delivery and tolerance[291], so that this kind of therapy is mainly used for inpatients in severe condition, despite efforts to develop new forms of drugs.

1.4.7 Targeting PDEs in PAH

The rationale for targeting PDEs to treat PAH ascribes to the beneficial effects achieved by increasing intracellular CNs levels together with the fact that amplitude and duration of their concentration can be enhanced by suppressing their degradation via inhibition of PDEs activity. In addition, several PDE isoenzymes perform special role in PAH, which makes them interesting candidates to target. First, the expression and/or activity of both cAMP and cGMP related PDEs are overall increased in PA from PAH patients and animal models compared normal control[139,173] . The increased PDE activity is detrimental to CNs accumulation and could not be counteracted by stimulation of CNs generation in some reports, so a PDE inhibitor is necessary to reverse this phenomenon. For example, it was reported that under stimulation by forskolin or prostacyclin analogue Beraprost, cAMP accumulation was attenuated in PASMCs from PAH patients compared with control patients, whereas it can be rescued by the presence of PDE inhibitor[173]. Secondly, tissue-specific distribution of PDEs make them good pharmacological targets for PAH treatment. For example, since PDE5 are abundant in the lung, this helps to explain success of PDE5 inhibitors as PAH treatments. Furthermore, nearly all PDEs are reported to be variably expressed in PA and lung altogether. Some have higher proportion of expression, such as PDE5, while other PDEs are believed not functionally redundant but may still exert a special role in PAH, like PDE2.

The general pattern of PDEs expression in human PASMCs has been reported. Using Real-time quantitative polymerase chain reaction (RT-qPCR), it was reported that human PASMC express mRNA for multiple PDE isoforms: 1A, 1C, 2A, 3A, 3B, 4A, 4B, 4C, 4D, 5A, 7A, 7B, 8A, 9A, 9B, 10A, and 11A, while neither PDE1B nor PDE8B were detected[173,292]. And among this, PDE3A, PDE4 and PDE5A are most abundant in PA of human and animals[140,142]. Whereas in iPAH patients, this pattern is altered, the transcription of PDE1A, PDE1C, PDE2A, PDE3A,

PDE3B, PDE5A, and PDE7A were upregulated, whereas the increase in protein levels for PDE1A, PDE1C, PDE3B, PDE5A were confirmed by western blot[173]. Besides, total cAMP- and cGMP-PDE activity were increased in PASMC from iPAH patients, 3-fold and 2-fold respectively compare with control, however the total cGMP-PDEs activity is much higher than cAMP-PDEs activity[173,293]. In control patients, cAMP PDEs activity ranked as follows : PDE4> PDE3>PDE1>PDE2; Whereas in PAH patients, the PDE1 and PDE3 activity were upregulated, consistent with their expression, so that the proportion was altered into PDE3> PDE1≥PDE4>PDE2[173,292,293]. It is reported that most of cGMP-PDE activity ascribes to PDE5, and in a smaller extent to PDE1, in human PASMCs[293]. We will review next the basic research and clinical data about the respective contributions of PDEs families in PAH. A summary of available data is provided in **Table 5**.

Table 5: Summary of non-clinical explorations on PDEs as therapeutic targets for the treatment of PAH.

PDE	Expression alteration in PA from PAH patients	Efficacy of pharmacological inhibition in experimental PAH
PDE1	↑ PDE1A (+)[143#], [173#], [144#] ↑ PDE1C (++)[143], [173#]	The PDE1 inhibitor 8MM-IBMX improves hemodynamic parameters and remodeling in rat MCT or CH mouse models[143].
PDE2	↓ mRNA[152#] ↑ moderately[173 #]	PDE2 inhibitor Bay 60-7550 improves hemodynamic parameters and remodeling in mouse CH model[152].
PDE3	↑ [173#]	PDE3 inhibition by Cilostamide improves hemodynamic parameters and remodeling in the rat CH model, only when combined with Iloprost[172]
PDE4	Unchanged[173#]	PDE4 inhibition by Rolipram improves hemodynamic parameters and remodeling in the rat CH model, only when combined with iloprost[172]. Roflumilast, a selective inhibitor, attenuates severity in CH and MCT models[294].
R	↑ [173#, 293#]	PDE5 inhibitors improve hemodynamic parameters and remodeling in the rat MCT model[295] or CH mouse model[296,297] and rat[169.290]
PDE6	PDE "γ" subtype is increased under hypoxia [298#]	Not documented
PDE7	↑ moderately[173#]	Not documented
PDE8	Unchanged[173#]	Not documented
PDE9	Unchanged[173#]	Not documented
PDE10	Unchanged[173#]	Papaverine, a non-selective inhibitor, improves hemodynamic parameters and remodeling in the rat MCT model[174].
PDE11	Unchanged[173#]	Not documented

1.4.7.1 Phosphodiesterase 1 (PDE1)

PDE1 is the unique PDE family that is activated by Ca^{2+}-calmodulin (CaM, a 16 kDa Ca^{2+}-binding protein) complex, and is therefore often referred to as the "Ca^{2+}/ CaM-stimulated PDE"[299] (**Table 1**). Thus, this family potentially represents an interesting regulatory link between CNs and intracellular Ca^{2+} signalling/handling, especially with respect to vascular tone. The PDE1 family is coded by 3 genes, *PDE1A*, *PDE1B* and *PDE1C*. In humans, PDE1A and PDE1B shows high affinity for cGMP, the latter being more selective for cGMP than the former.

Also, PDE1B hydrolyzes cGMP with a higher V_{max} value than for cAMP. High affinity for both cAMP and cGMP is observed with PDE1C[299].

Transcripts of *PDE1A* and *PDE1C* are detected in human lung homogenate, PA and isolated PASMC[143], as well as PDE1 activity is detected in cytosolic and microsomal fraction of human PA[140]. An upregulation of PDE1A and PDE1C expressions are noted in PASMCs from iPAH patients compared with healthy donors, both at the mRNA and proteins levels. Besides, a stronger immunolabelling for PDE1C in PA of iPAH patients suggests that the PDE1C is a major isoform[143,173].

Similarly, PDE1 activity is detected in rat cultured PASMC[172] and cytosolic and microsomal fraction of bovine PA[142]. PDE1A and PDE1C proteins are detected in rat PA[141]. Among PDE1 isoforms, PDE1B is less documented both in human and animal PA. In general, PDE1 is not a main PDE in PA compared to PDE3, PDE4, and PDE5, although PDE1 hydrolyzes both cGMP and cAMP, its contribution for cGMP-hydrolysis is far less than PDE5 and cAMP-hydrolysis is less than PDE3 and PDE4 in pulmonary circulation[139,142]. However, no upregulation of PDE1C is observed in MCT-treated rats nor in CHx-induced mice models, examining either lung, PA or PASMCs, whereas only *PDE1A* mRNA expression is increased in PASMC from both models[143]. Interestingly, another study showed that in a cold-induced PAH model in rats, protein expression of PDE1C in PAs is increased, whereas PDE1A expression is unaffected[141]. In addition, in CHx-induced rat models, it is observed that increased cGMP-PDE and cAMP-PDE activity in pathological model is associated with an increase in PDE1 activity in main PA[300].

It is reported that treatment with PDE1C-targeted siRNA enhances cAMP accumulation and inhibits cellular proliferation to a greater extent in PAH PASMC than in controls[173]. Consistently, PDE1 inhibitor (PI79) dose-dependently inhibits the DNA synthesis in proliferating human PASMCs[143]. PDE1 inhibitor (Vinpocetine) shows anti-proliferative effect in rat cultured PASMC[172]. Preclinical therapeutic assessment of another PDE1 inhibitor (8-methoxymethyl 3-isobutyl-1-methylxanthine, 8MM-IBMX) was performed in 3 animal models of PAH, namely MCT-treated rats, cold-induced PAH rats, and chronically hypoxic mice[141,143].

Long-term PDE1 inhibitor treatment in these experimental models results in reduced PAP, reversed remodeling of the lung vasculature, and reduction in RVH. In addition, inhibition of PDE1 by 8MM-IBMX is reported to suppress macrophage infiltration and superoxide production in cold-induced pulmonary hypertension rat models[141]. Besides, PDE1 inhibitors have been reported to exert a vasorelaxant effect on mouse PA, rat lung and lamb PA[143,172,301]. Taken together, these findings indicate that upregulation of PDE1, especially PDE 1C, plays a role in the structural remodeling process underlying PAH and, thus, offers a novel therapeutic target.

Even though the vinpocetine[302] and 8MM-IBMX[303] are commonly used PDE1 inhibitors, these compounds are not selective for PDE1. Vinpocetine inhibits several sodium channels[304] and inhibits NF-κB-dependent inflammation *via* an IκB-dependent but PDE-independent mechanism[305]. Besides, there are variable data on the expression of PDE1 isoforms in different species and models, the PAH rodent models are not able to replicate the pathological change in PDE1C expression in human. Even though the PDE1 inhibitors showed beneficial effects in PAH models, until now there is no clinical trials for PDE1 inhibitors to treat PAH[181]. However, there are some promising PDE1 selective inhibitors reported, such as Lu AF41228 and Lu AF58027, which can induce vasodilation of mesenteric artery and lower blood pressure[182], and ITI-214, that can enhance cardiac function acutely. ITI-214 entered recently in clinical trials (phase 1/2, NCT03387215) for heart failure treatment, providing an interesting opportunity to evaluate the safety and efficacy of this class of inhibitors[306]. Besides, the vinpocetine is approved for cerebral vascular disorders and memory impairment[185].

1.4.7.2 Phosphodiesterase 2 (PDE2)

PDE2 hydrolyzes both cGMP and cAMP with similar maximal rates and relatively high K_m values[122] (**Table 1**). PDE2 contains two homologous GAF domains (domains found in certain proteins, i.e., c**G**MP binding PDEs, **A**nabena adenylyl cyclase, and **F**h1A, an *Escherichia coli transcriptional regulator*) tandemly arranged in their regulatory regions. GAF-A domain of PDE2 is involved in dimerization and GAF-B domain in cGMP-binding. The latter triggers conformational changes, resulting in a catalytic activity increase up to 30-fold[127]. Thus PDE2 is referred to as

"cGMP-activated, cAMP-hydrolyzing PDE". PDE2A GAF B is moderately selective with around 20-fold preference for cGMP(K_D < 10 nM) over cAMP[307]. PDE2 isozymes are encoded by a single gene (*PDE2A*) containing three known variations (*PDE2A1*, *PDE2A2*, *PDE2A3*), distinguished from each other by changes in their N-terminal domain and likely mediated different localizations of the proteins. Specifically, PDE2A1 is more soluble and PDE2A2/3 are preferentially membrane-associated[299].

PDE2 mRNA and activity can be detected in PA from various species, but demonstrating lower levels compared to PDE3, PDE4 and PDE5. First, PDE2 mRNA is detected in human PASMCs, even though an upregulation of mRNA is observed in PAH patient , the PDE2 activity is not significantly altered[173]. Besides, inhibition of PDE2 by ENHA 10μM (IC50 1μM, a non-selective inhibitor, also potently inhibits adenosine deaminase) in presence of excess cGMP can increase Forskolin-induced cAMP accumulation in PASMCs[173]. At the same time, several reports showed that PDE2 exists in PA from different species of animals by using pharmacological method. First, the PDE2 inhibitor EHNA can reverse hypoxic vasoconstriction ex vivo in perfused rat lung[151] and PDE2 activity can be detected in rat PA[139]. Next, PDE2 activity is reported high in EC from porcine PA, and PDE2 localizes predominantly in the cytosol[153], whereas the role of PDE2 in PASMC is not clear. Moreover, again based on the detection of an EHNA-sensitive PDE activity, PDE2 was reported to be present in the media layer of PA from bovine, but at a low level[142]. ENHA has a vasorelaxant effect in EC-denuded rat PA, but far less than inhibitors of PDE3, PDE4 or PDE5[142].

The comprehensive role of PDE2A in PAH is reported in a study by Bubb et al. in 2014[152]. Interestingly, this study shows PDE2A expression is down-regulated in PASMC from iPAH patients and in isolated PA tissue from CHx induced rat models. This is contrast to another report as previous mentioned did by Murray et al.[173], even though the PDE2 activity do not display any significant reduction[152]. The relatively selective PDE2 inhibitor, BAY 60-7550 (IC50 4.7nM)[308], was used to reveal participation of PDE2 activity in influencing vascular tone in rat PA and aorta[152]. BAY 60-7550 produced a dose-dependent relaxation in PA isolated from chronically hypoxic rats with an EC50 around 1μM. Furthermore, BAY 60-7550 (0.1 μM)

potentiated ANP evoked pulmonary vascular relaxation in both normal and hypoxia condition, whereas it amplified the Spermine-NONOate(NO donor) induced relaxation only in normal condition and the Treprostinil induced relaxation only in hypoxia condition . Most importantly, the BAY 60-7550 prevents the develop of both hypoxia- and bleomycin-induced PH in mouse without influencing the systemic arterial pressure, whereas the PDE2 inhibitor can't cure established PH models. When given in combination with a neutral endopeptidase inhibitor (enhances endogenous natriuretic peptides), Treprostinil, Inorganic Nitrate (NO donor), or a PDE5 inhibitor, this strategy produced a significantly greater reduction in the salient features of the model, compared with monotherapy of each drug mentioned above. In addition, proliferation of PASMCs from PAH patients was reduced by BAY 60-7550, an effect further enhanced in the presence of ANP, NO or Treprostinil. By considering these amplified effects of PDE2 inhibitor in combination treatment, one may hypothesizes that PDE2 inhibition can bolster both cGMP and cAMP signaling in pulmonary circulation. Interestingly, the beneficial effect of PDE2 inhibition is dependent on endogenous NP bioactivity rather than intact NO-pathway since the salutary effect was absent in natriuretic peptide receptor A(NPR-A) KO mice whereas maintained in animals treated with the NO synthase inhibitor L-NAME. Notably, in this study, the inhibition of PDE1 and PDE3 did not alter ANP- nor Spermine-NONOate-induced relaxation[152], which highlights the importance of PDE2 in CNs signaling. An additive effect of PDE2 inhibition on top of PDE5 inhibition was observed either by inhibiting proliferation of PASMCs or by in vivo preventing development of PAH. This is of potent interest because this may explain why some PAH patients are resistant to PDE5 inhibitor therapy in the beginning or along with time, and provides the hint that inhibition of both enzymes may optimize the cGMP signaling pathway. The underlying reason for that is, possibly, PDE5 inhibition may exacerbate PDE2 activity.

Therefore, the role and mechanism of action of PDE2A in pulmonary circulation demands to be furthered explored using different animal models. New PDE2 inhibitors, PF 05180999(Pfizer) and TAK-915 are currently investigated in healthy volunteers in Phase I trial, which may be helpful for clinical trials of PAH patients.

1.4.7.3 Phosphodiesterase 3 (PDE3)

The PDE3 family is coded by 2 genes, namely *PDE3A* and *PDE3B*, which shows high affinity for both cAMP and cGMP[299]. A low *Vmax* value for cGMP compared to cAMP makes cGMP a competitive inhibitor for cAMP hydrolysis[309]. Therefore, PDE3 is often referred to as the "cGMP-inhibited, cAMP-hydrolyzing PDE (**Table 1**).

In human PA tissue, PDE3 activity can be tested using PDE3 inhibitor (Motapizone). Motapizone inhibits 60% of total cAMP-PDE activity and 13% of cGMP-PDE activity[140]. Combination of PDE3 and PDE4 inhibitors, Motapizone and Rolipram, or using Zardaverine (dual PDE3 and PDE4 inhibitor) almost completely inhibits total cAMP-PDE activity (82%). PDE3 inhibitor effectively relaxes human PA precontracted by $PGF_{2\alpha}$ ex vivo, and this relaxant effect can be amplified by inhibiting PDE4 altogether using Zardaverine, whereas PDE4 inhibitor alone almost ineffective[140]. Another study using PASMCs from human patients shows that both PDE3A and PDE3B are expressed in human PASMCs, and both mRNA levels are upregulated in iPAH patients, whereas only PDE3B protein is increased in PASMCs from iPAH patients[173]. Consistently, PDE3 activity is increased in PASMCs from iPAH patients, which can partly explain the total cAMP-related PDE activity increase in patients. PDE3 activity contributes to the largest portion of cAMP hydrolysis in PASMCs of PAH patients, occupying around 40-50%, whereas in control PASMCs occupying around 30%. Under Forskolin (10μM) stimulation and PDE3 inhibition (Milrinone 10 μM), there are more cAMP generated in PASMCs from iPAH patients compared to control patient. Besides, as PASMCs from iPAH have a more proliferative phenotype compared to control cells, PDE3 inhibitor (Milrinone 10 μM) shows much higher anti-proliferative effect in iPAH patients compared with control patients[173]. This therapeutic effect of PDE3 inhibition may largely ascribe to cAMP elevation. Taken together, this two studies shows the pivotal role of PDE3 in regulating human pulmonary arteries under physiological or pathological conditions.

Consistently, in bovine media layer of PA, PDE3 inhibitor mainly hydrolyzes cAMP (50%), and this effect is even more potent than PDE4 inhibitors (30%). PDE3 inhibitor, Cilostamide, can effectively relax rat PA in a concentration-dependent manner[142]. PDE3 inhibition

(Motapizone) can protect PA EC against H_2O_2-induced increase in endothelial permeability in Suttorp et al.'s report[153]. The activity and expression of PDE3 are increased in PA from CH-induced PAH rats [139,161]. PDE3 inhibitors also reverse the reduced responsiveness of pulmonary vessels to Isoprenaline and Forskolin in rats with PAH[310].

Furthermore, many in vivo animal experiments were performed to test the efficacy and safety of PDE3 inhibitor in treating PAH. Some studies show that Cilostazol therapy attenuates RVSP and RVH in the MCT-induced PAH model in rat, but not in CH-induced models[311,312]. Another PDE3 inhibitor, Cilostamide, also does not attenuate CH-induced PAH rats neither, but combination treatment with Iloprost or Rolipram can relieve the PAH phenotype[172]. In addition, it is reported that combination treatment with low-dose of PDE3 inhibitor Motapizone can amplify the pulmonary vasodilatory response to inhaled PGI_2 in rabbit experimental PAH[313]. Similarly, PDE3 inhibitor, Milrinone, reduces the elevated pulmonary vascular resistance induced by U46619, and showed a synergistical effect when combined with a PDE5 inhibitor[314]. Another in vivo study suggests that Milrinone produces dose-related decreases in mean systemic arterial pressure when used to treat acute pulmonary hypertension, with the vasodilatory effect being much lower than that of a PDE5 inhibitor[315]. Hence, even though PDE3 inhibitor alone has a little favorable effect in experimental PAH treatment, considering its major role in regulating cAMP hydrolysis in PAH pathological condition, and a beneficial effect once combining with other products, such as PGI_2, PDE5 and PDE4 inhibitor, it may be promising to use low-dose PDE3 inhibitor to improve other drugs efficacy in combination treatments.

Two PDE3 inhibitors have been approved in clinic to treat cardiovascular diseases. First, Milrinone has been approved for acute treatment for patients with decompensated and refractory heart failure. However, since chronic administration of the this drug increases mobility and mortality, clinical application window is limited and narrow[316]. Moreover, Milrinone is reported comparable to Dobutamine in cardiogenic shock treatment[317]. Another PDE3 inhibitor, Cilostazol, is approved to treat intermittent claudication[318] and is considered

for several repurposing applications. So far there has been no clinical trials for PDE3 inhibitors in treating PAH.

1.4.7.4 Phosphodiesterase 4 (PDE4)

PDE4 is well characterized by its substrate selectivity for cAMP and its sensitivity to inhibitors such as rolipram. PDE4 isozymes consist of four subfamilies (4A, 4B, 4C and 4D) encoded by distinct genes, which produce over than 25 PDE4 isoforms in human[319] (**Table 1**). Based on the presence and size of domain-upstream conserved regions 1 and 2 (UCR1 and UCR2), PDE4 isoforms can be divided into 4 categories, that are, long isoforms have both UCR1 and 2, short isoforms have only UCR2, super-short have a truncated UCR2, and dead-short isoforms lack both UCR domains and have a truncated catalytic domain[319]. UCR1 contains a PKA phosphorylation site that upon phosphorylation activates PDE4 activity[320]. The catalytic region contains an ERK phosphorylation site, phosphorylation of which induces the activation of PDE4 short forms and the inhibition of PDE4 long forms[321]. Besides, the UCR modules mediate dimerization, only long-form PDE4 splice variants containing UCR1 and UCR2 are dimerized[322]. PDE4 isoforms show unique intracellular distribution patterns characterized by interaction with several anchoring or targeting proteins such as immunophilin XAP2, DISC1, SH3 domain–containing proteins, β-arrestin, receptor for activated C-kinase (RACK1), and AKAPs.

In human PA from control patients, PDE4 activity is detected by using selective inhibitors such as Rolipram(IC50 0.05-2μM) or Ro 20-1724(1-2 μM)[323]. However, PDE4 inhibitor alone does not exert vasorelaxant effect to regulate PA tone, but should rely on combination inhibition of PDE3[140]. In cultured cells, PDE4A-D transcripts are expressed in PASMCs from human, but none of them are altered in PAH patients compared with control patients[173]. Although cAMP-PDE activity is increased in PASMCs from PAH patients, the PDE4 activity does not contribute for this, because PDE4 activity is decreased from control (around 45%) to PAH patients (30%)[173]. Consistently, PDE4 inhibitor (Rolipram) has anti-proliferative effect in PASMCs, but less in PASMCs from PAH patients compared with control[145,173].

PDE4 is demonstrated high activity in EC from porcine PA. PDE4 inhibition by Rolipram can protect PA endothelial cells against H_2O_2-induced increase in endothelial permeability in Suttorp et al.'s report[153], and this effect can be amplified 100 fold by another AC receptor-operated stimulus, Prostaglandin E1 (PGE1) with 1μM. In bovine media layer of PA, PDE4 is a quantitatively important cAMP hydrolyzing PDE, even though slightly weaker than PDE3[142]. Vascular reactivity from endothelium-denuded rings of rat PA showed that the PDE4 inhibitor Rolipram can relax precontracted preparations in a concentration-dependent manner which is different from in human[142]. Rolipram can relax rat PA which induced by acute hypoxia in vivo[172]. This PDE4 inhibitor has anti-proliferative effect in rat PASMC, and this effect can be synergized with prostacyclin analogs[172].

In addition, some animal experiments were conducted to test the efficacy of PDE4 inhibition in treating PAH. These studies showed that chronic Rolipram monotherapy could not attenuate mPAP, RVH nor distal vessel muscularization in the CH-induced rat PAH model, except for combination treatment with Iloprost or a PDE3 inhibitor[172]. Whereas another PDE4 inhibitor, Roflumilast, used at high dose (1,5 mg/kg) can not only prevent both MCT-induced and CH-induced rat PAH phenotype, but also partly reverse established PAH phenotype induced by MCT[294], whereas a lower dose (0,5 mg/kg) only can prevent MCT rather than CH-induced PAH phenotype[294]. Similarly, dual-selective PDE3/PDE4 inhibitor can attenuate MCT-induced rat PAH development, and combination with Iloprost can reverse established MCT-induced rat PAH model phenotype[324].

So taken together, even though PDE4 is an important cAMP-hydrolyzing PDE in pulmonary circulation, it seems mildly involved in PAH development. PDE4 expression, activity are not increased in PAH condition, PDE4 inhibitors have minor effect in tuning the human PA tone. Nevertheless, some preclinical studies indicate antiproliferative and protective effects of PDE4 inhibition, that is potentiated by other cAMP-elevating agents. Further development of more selective compounds, targeting either discrete PDE4 isoforms or variants, may pave the way for refining the therapeutic assessment of PDE4 enzymes in PAH.

1.4.7.5 Phosphodiesterase 5 (PDE5)

PDE5 is a cGMP-specific hydrolyzing PDE, and coded only by one gene, *PDE5A*, while including 3 variants (PDE5A1, PDE5A2 and PDE5A3). Structurally, PDE5 N-terminal region contains 2 allosteric cGMP-binding sites (GAF-A and GAF-B) and one phosphorylation site (Ser92 in bovine and Ser102 in human)[325,326]. High-affinity cGMP binding occurs only to the GAF-A domain, which stimulates the enzyme activity 9 to 11 fold. GAF A has higher affinity for cGMP (K_D < 40 nM) [327]. The role of GAF-B is currently unclear. The major kinase responsible for this phosphorylation site is PKG, whereas PKA can also phosphorylate this site. The phosphorylation of this site not only activates the catalytic function but also further increases cGMP-binding affinity, thus form a positive feedback to control cGMP levels[299,325].

PDE5 has been most studied in PAH and this target has been successfully used to treat PAH[285]. Compared to other PDEs, PDE5 has the highest expression and occupies majority of cGMP hydrolysis in the lungs, pulmonary arterial vessels and PASMCs both from animal[142,328,329] and human[140,173]. Many studies addressed the role of PDE5 in PAH , giving compelling basis for the treatment of pulmonary hypertension. Results can be summarized into 4 aspects. First, the increase in PDE5 expression and activity in lung and/or pulmonary artery from animal models or PAH patients[161,169,293] suggests that PDE5 may represent a marker of vascular remodeling in PAH development. Second, ex vivo studies show that PDE5 inhibitors can effectively relax PA either in in human[140,330] and in animals models of PAH[290,329,331]. Furthermore, PDE5 inhibitor increases cGMP levels in an concentration-dependent manner, and has anti-proliferative and pro-apoptosis effect in PASMCs from PAH patients. This effect can be augmented synergistically or additively by NO donor or NP analogs[293,330]. Third, in vivo studies suggest that PDE5 inhibitor can not only prevent the development of various PAH models in animals[290,332-334], but also is able to partially reverse the remodeling of PA from established PAH models[169,333]. This translates into a decrease in mPAP or RVSP, reduction in RVH, and or a lowering of PA remodeling extent or distal vascular muscularization, while without decreasing of systemic blood pressure. Fourth, PDE5 has been reported to be upregulated in RVH compared to normal RV both in PAH patients and MCT-induced PAH rat models.

Interestingly, acute inhibition of PDE5 in isolated hypertrophied RV or myocardium exerts positive inotropism which is mediated by increased cAMP levels resulting from inhibition of PDE3 activity by increasing cGMP[335]. Based on and consistent with these beneficial effects of PDE5 inhibition in ex vivo and animals models, 3 kinds of PDE5 inhibitors, Sildenafil, Tadalafil, Vardenafil, have been tested in clinical trials, showing chronic efficacy in treating PAH[189,336-338]. Hence two of them (Sildenafil, Tadalafil) are approved to treat PAH by the FDA. In more details, PDE5 inhibitors show definite clinical benefit only in group 1 PH, that is PAH, compared to placebo, with regard of direct improvement of hemodynamics, following gradually improvement in WHO functional class, six-minute walk distance (6MWD), quality of life including dyspnea, and can in the long term improve time to clinical worsening, and mortality[190]. It should be noted that although the PDE5 inhibitors are generally well tolerated, there are some common side effects due to off-targets effect and PDE5 inhibition in other tissues, which include headache, flushing, vision problems, gastrointestinal discomfort, and muscle and joint pain[191,339].

Besides, even though the PDE5 inhibitors can prevent cGMP degradation, their efficacy is dependent on cGMP synthesis and the generation of NO from PA ECs in vivo. Although some NO donor such as sodium nitroprusside (SNP) have been used in clinic, they mainly decreases the systemic blood pressure, hence are limited for PAH treatment. Riociguat, as stimulator of sGC which can directly stimulate the native sGC independently of NO and is also able to sensitize sGC to low levels of NO by stabilizing NO-sGC binding[44], is reported to be favorable in PAH treatment. Combination of PDE5 inhibitor with this drug is however contraindicated due to hypotension and other relevant side effects[340]. PDE5 inhibition in combination with other treatments initially or sequentially has been recommended to manage moderate to serious PAH as showed in clinical guidelines[341].

1.4.7.6 Phosphodiesterase 10 (PDE 10)

PDE10 is coded by one gene, *PDE10A*. PDE10 hydrolyzes both cAMP and cGMP, the affinity for cAMP is higher than for cGMP, but a 2–5-fold lower Vmax for cAMP compared with cGMP. Therefore cAMP inhibits cGMP hydrolysis thus making this enzyme a cAMP-inhibited

cGMP PDE[122], which is opposite to PDE3 family. There are two GAF domains in the N-terminal region. In contrast to other PDEs, the GAF domain apparently binds only cAMP and thus actives PDE10[128,342]. Papaverine is known as the first potent inhibitor of PDE10A[174].

Since PDE7-11 are more novel PDEs, therefore relative less researches are reported in PAH. PDE10 is reported to be expressed in human PASMCs but no significant increase in iPAH from RNA levels in PASMCs [173]. Nevertheless immunostaining experiments confirms that there are stronger PDE10 signal in remodeled medial layer of PA from PAH patients compared with control patients[174], whereas the thorough quantification of protein from human lung and PA are unknown from both groups. However, PDE10 transcripts and protein levels are upregulated in PASMCs, PA and lung from MCT-induced rat models, and inhibition of PDE10 has been reported to increase cAMP levels and to activate downstream phosphorylation of the transcription factor CREB and exert anti-proliferative effect[174].

The MCT-induced PAH models has been used to evaluate the effect of PDE10 inhibitor. Studies using papaverine and other novel synthetic PDE10 inhibitors (compound 2b, 14·3HCl) showed that PDE10 inhibition can prevent the development of MCT-induced PAH by decreasing mPAP or RVSP, RVH and PA thickness or distal vascular muscularization[174,343,344]. However, the effect of PDE10 in ex vivo systems aiming at studying vascular tone or cell proliferation is not reported. Therefore, additional studies on other PAH animal models should be performed in order to verify the effect of PDE10 inhibitor, since MCT-induced rat model is more curable than other models. Besides, the PDE10 is reported to be upregulated in mouse and human failing hearts, and PDE10A inhibition is beneficial in pathological cardiac remodeling and dysfunction[345].

There are several PDE10 selective inhibitors has been developed until now. MP-10 has been tested in several clinical trials in schizophrenia and Huntington's disease, but failed mainly due to lack of efficacy or safety concerns[185]. And other inhibitors, such as [18F]MNI-659, PBF-999 and EVP-6308, RO5545965, and TAK-063 have been tested in clinical trials for schizophrenia and Huntington's disease, and cancer[185]. Moreover, TP-10, has been investigated in preclinical

study for the treatment of schizophrenia[346]. So such growing PDE10 selective inhibitors provide promising pharmacological approaches to treat PAH.

1.4.7.7 Other PDEs

In contrast to other PDEs, the PDE6 family is reported to be restricted to retina and work as photoreceptor. Whereas PDEγ, an inhibitory subtype of PDE6, has been found outside the eye[347,348], and seems to have a critical role in regulating p42/p44 mitogen-activated protein kinase (MAPK) signaling[349]. PDEγ is also found in rat pulmonary artery and cultured human PASMCs, and is upregulated in chronic hypoxic conditions, which is as well as correlated with an enhanced activation of p42/p44 MAPK[298]. Transcripts of PDE7A are reported overexpressed in PASMCs from PAH patients[173] and rat models[174], whereas PDE7B, PDE8A, PDE8B and PDE9A, PDE11A show no significant changes in PASMCs from iPAH patients[173]. Even though there are increasing amount of more selective PDE inhibitors, these PDEs are for now mostly studied in diseases of central never systems[101].

1.4.7.8 Phosphodiesterase 9 (PDE9): a potential target to in PAH?

PDE9 was discovered in the late 1990s and is coded by a single gene, *PDE9A*[350-352]. *PDE9A* was reported to encompass more than 21 splice variants possibly displaying differential subcellular localizations and properties [353,354]. PDE9 lacks "GAF" in structure. PDE9 is highly specific for cGMP hydrolysis with Km about 70-170 nM for cGMP and only 230 μM for cAMP. Importantly, the affinity of PDE9 for cGMP is 40–170 times higher than two other cGMP-specific-PDEs, PDE5 and PDE6, respectively. Maximum velocity of the catalytic site is similar to PDE5. All these properties make PDE9 a potential sensitive tuner of cellular cGMP signaling. Tissue distribution of PDE9 is ubiquitous and PDE9 mRNA was detected in many organs. The highest levels are in brain, kidney, spleen, and relative lower levels are found in the lung [350-352] and heart [351,352,355]. However, reports accounting for expression of PDE9 in vasculature are scarce. PDE9 was only mentioned to be expressed at the mRNA level in fetal rat and human pulmonary artery smooth muscle cells (PASMC) in a couple of reports [173,356]. As a report

mentioned that PDE9 inhibition decreased leucocyte adhesion in arterioles[357], expression of PDE9 by endothelial cells (EC) cannot be ruled out, although molecular evidence was not supplied.

To date, several selective PDE9 inhibitors have been characterized (Table 6) and studies mainly focused on their ability to rescue cognitive function[358-361]. In recent years, the role of PDE9 in the cardiovascular system has been emphasized by use of PDE9 selective inhibitors associated with the study of *Pde9a*$^{-/-}$ mice. PF-04449613 and, more recently, CRD-733 have shown curative efficacy on hypertrophy and HF induced by a pressure overload model (TAC) in mice[355,362]. The group of David Kass has also shown that PDE9 is specialized in the control of cGMP produced in the heart by NPs[355]. In addition, it was reported that PDE9 pharmacological inhibition is able to improve hemodynamic and renal functions in experimental heart failure models[363]. By contrast, by following a pharmacological approach combined with real time cGMP measurement by means of an intracellular FRET-based biosensor, data by Zhang et al. suggests that PDE9 selectively regulates NO-related cGMP levels in rat aorta smooth muscle cells[170]. PF-047499982 administered intravenous produces a dose-dependent decrease (30-100-300 mg) in blood pressure and peripheral vascular resistance in control sheep or sheep subjected to an HF model[363], which suggests a vascular effect of the PDE9 inhibitor, although the hypothesis of a non-selective effect on other PDEs cannot be ruled out. PDE9 is reported highly expressed in hematopoietic cells and upregulated in neutrophil cells of sickle cell disease (SCD)[364]. Consistently, PDE9 inhibitor (BAY-736691), combination with hydroxyurea, has shown immediate benefits on acute vaso-occlusive events in sickle cell disease of mice[357]. PDE9 inhibitor (PF-04447943) is well-tolerated in patients with stable SCD and has protective effect against vaso-occlusion in early clinical trial (Ib)[365]. Recently, it was also reported that PDE9 inhibition (PF-04447943) reduces obesity and cardiometabolic syndrome in mice[366].

Nevertheless, the roles of PDE9 in the pulmonary circulation and right heart in particular, have so far less been documented. Recently, a report concluded that *Pde9a* deficiency did not protect from experimental PAH[367]. Despite these data, physiological role of PDE9 in regulating

vascular tone and right ventricle (RV) function remain largely unexplored. So encouraged by its beneficial effect in left heart failure[355,363], we hypothesized that PDE9 play a relevant role in pulmonary circulation and participate in the progressive development of PAH. Therefore, our aim for this part of my thesis was to shed light on the specific contribution of PDE9 in pulmonary circulation, and to assess whether interventions that inhibit their function are amenable to being used as a new therapeutic strategy to treat PAH by using both pharmacological approach and Pde9a-deficient mouse (*Pde9a*$^{-/-}$).

Table 6: Pharmacological properties of PDE9 inhibitors.

Compound	Reference	IC_{50} for PDE9 (species)	Ratio of selectivity($IC_{50(PDE X)}$ /$IC_{50(PDE9)}$)	**increase cGMP levels in vivo?**
Bay73-6691	Wunder et al., 2005[361]	55 nM (human)	PDE1C: 25 PDE11 : 47 Other PDEs : > 73	Yes (hippocampus)[368]
PF-04449613	Claffey et al., 2012[369] Kleiman et al., 2012[359]	24 nM (human)	PDE1C : 35 Other PDEs : > 41	Yes (heart, cerebrospinal fluid(CSF))[355]
PF-04447943	Hutson et al., 2011[360] Kleiman et al., 2012[359]	12 nM (human)	PDE1C : 78 Other PDEs : > 83	Yes (CSF, plasma and brain) [360]
PF-04749982	Claffey et al., 2012[369]	32 nM (human)	PDE1C : 30 Other PDEs : > 312	Yes (CSF, plasma, urine)[363]
BI 409,306	Moschetti et al.,2016[370] Rosenbrock et al.,2019 [371]	52 nM (human)	Not available	Yes (rat CSF rat and cortex)[371]
CRD-733	Richard et al., 2021[362]	Not available	Not available	Yes (plasma) [362]

1.5 Heart Failure (HF)

HF, a major public health issue, is defined by the inability of the heart to maintain sufficient blood flow at rest or during exercise to meet the metabolic needs of the body. It is a complex clinical syndrome, manifested by typical signs and symptoms (fatigue, dyspnea, edema) resulting from structural and/or functional abnormality of the heart[372]. HF can be categorized according to acute (new onset or sudden worsening) or chronic forms, or according to the ejection fraction (EF) (reduced (≤40%, HFrEF) , preserved (≥ 50%, HFpEF) or mildly reduced (between 41and 49, HFmrEF)[373].The distinction between systolic and diastolic dysfunction no longer seems relevant, since these two characteristics can coexist in both HFrEF and HFpEF[374].

HF has a prevalence of approximately 1 to 2% of the population in developed countries, rising to more than 10% for subjects over 70 years old. The risk of suffering HF at age of 55 is 33% and 28% for the male and female populations respectively, even though the incidence seems to decrease, in particular for HFrEF[374]. The proportion of HFpEF is very variable according to the studies (22-73%), and seems more common in older people, in female and in those who have a history of atrial fibrillation or arterial hypertension, metabolic comorbidities (diabetes, obesity) whereas a history of myocardial infarction is more common in HFrEF patients[374].

1.5.1 Pathophysiology of heart failure

The etiologies of HF are very diverse, and can generally be classified into 3 groups: (1) diseased myocardium: ischemia, immune or inflammatory reaction, toxic, infiltration, metabolic disorders or genetic anomalies affecting sarcomere proteins; (2) abnormal loading conditions: valvopathies, myocardium structural defects, pericardial or endomyocardial pathologies, hypertension, renal insufficiency; (3) arrhythmias[374].

The pathophysiology of HFpEF or HFmrEF is heterogeneous due to their diverse concomitant diseases[375]. The hospitalization and death of this group patients is more likely to be non-cardiovascular[376,377]. Moreover, unlike HFrEF, no treatment is favorable to reduce morbidity and mortality.

The pathophysiology of HFrEF is relatively well-recognized, and long-term activation of neurohormonal responses is thought to a most important mechanism (Figure 14). Neurohormonal activation mainly refers to as sympathetic nervous system (SNS) and renin-angiotensin-aldosterone system (RAAS). Acute action of both systems improves or compensated the dysfunction of heart to maintain blood supply for important organs. When chronically activated, however, they are proved to be deleterious to the myocardium, hence resulting in fueling the deleterious processes that promote pathophysiology of HF[378]. On one side, the vasopressor effects of norepinephrine (NE) and angiotensin II on the systemic vasculature results in an increased afterload. On the other side, an increased cardiac preload is generated by sodium and fluid retention and increase of venous return. The latter leads to an increase in cardiac filling pressures as Frank-Starling effect is ineffective in HF[379]. Although stimulation of neuroendocrine factors can increase heart rate and ventricle contractility in the short term, long term response, combined with inappropriate mechanical stretch and increased wall tension of heart, the cardiomyocyte biology undergoes a series of changes and eventually contributes to remodeling of the left ventricle: (1) stimulation of cellular hypertrophic response via well-identified transcriptional pathways, such as calcineurin-NFAT, MEF2, HDAC signaling [380]; (2) desensitization of β-adrenergic receptors caused by high level of catecholaminergic stimulation[381]; (3) alteration of excitation-contraction coupling by reduction of calcium transients due to calcium leakage via ryanodine receptor 2 (RyR2) and decrease in the expression and activity of the sarcoplasmic/ endoplasmic reticulum Ca^{2+} ATPase 2a (SERCA2a) pump[382]; (4) alteration of energy metabolism, such as resistance to insulin, increased use of the glucose rather than fatty acids[383]; (5) alterations in cytoskeleton and related proteins, e.g. qualitative switch of myosin heavy chain gene expression (from MYH-6 to MYH-7), which results in loss of contractile property[384]. Consequently, apoptosis, necrosis, autophagic cell death happens in end-stage heart failure [385], accompanying by the formation of extracellular matrix and myocardial fibrosis which further worsens heart function by stiffening the cardiac wall and impairing electrical propagation.

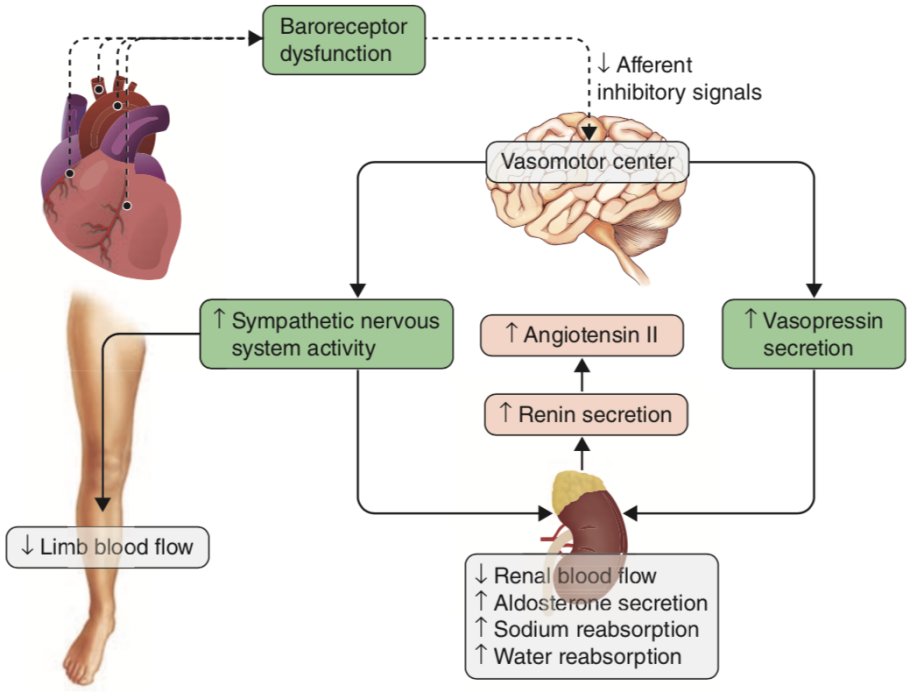

Figure 14. Activation of neurohormonal systems in heart failure with reduced ejection fraction (HFrEF). Decreased cardiac output following various anomalies or injuries results in reduced pressure which is sensed by baroceptors (black circles) in the left ventricle, carotid sinus, and aortic arch. This unloading signal is sent to central nervous system (CNS), which in turn, on the one hand, activates efferent sympathetic nervous system pathways that innervate the heart, kidney, peripheral vasculature, and skeletal muscles, and on the another hand, stimulates cardioregulatory centers in the brain that stimulate the release of arginine vasopressin from the posterior pituitary (Adapted from Volpeet al., 2016)

1.5.2 Current treatments for chronic heart failure

Current treatments of HFrEF are mainly based on the understanding of the above mentioned pathophysiology, and aim at antagonizing neurohormonal systems (Figure 15). This includes three classic classes of drugs, namely angiotensin-converting-enzyme inhibitors (ACEI)（if intolerant, using angiotensin-receptor type 1 blockers/antagonists (ARBs) to inhibit RAAS）; beta-adrenergic receptor antagonists (to inhibit the SNS); and mineralocorticoid-receptor antagonists (MRA) as diuretics. Recently, a new therapeutic class of drug, angiotensin

receptor–neprilysin inhibitor (ARNI, LCZ696)[374], has been approved to treat HFrEF. This drug combines valsartan, an angiotensin-receptor type 1 blockers(ARB), with sacubitril, a prodrug that eventually limit the degradation of NPs therefore increases the cGMP pathway. It is contraindicated to combine with other ACEIs and ARBs. More recently, large randomized clinical trials revealed that the sodium-glucose co-transporter 2 (SGLT2) inhibitors dapagliflozin[386] and empagliflozin[387] added to therapy with ACE-I/ARNI/beta blocker/MRA reduced the risk of cardiovascular death and worsening HF in regardless of whether they have diabetes or not, thus were recommended for HFrEF therapy. Moreover, vericiguat, an oral soluble guanylate cyclase stimulator may be considered in patients with HFrEF based on its beneficial effect of reduction of the risk of cardiovascular mortality or HF hospitalization[388] but not yet recommended in new guidelines[373]. HFrEF has benefited from significant progress in such therapeutic management over the past 30 years, with a huge reduction in mortality and hospitalizations[389]. Still, the all-cause mortality rate at 1 and 5 years remains high, respectively from 17.4%[390] to 52%[391] in developed countries from Europe.

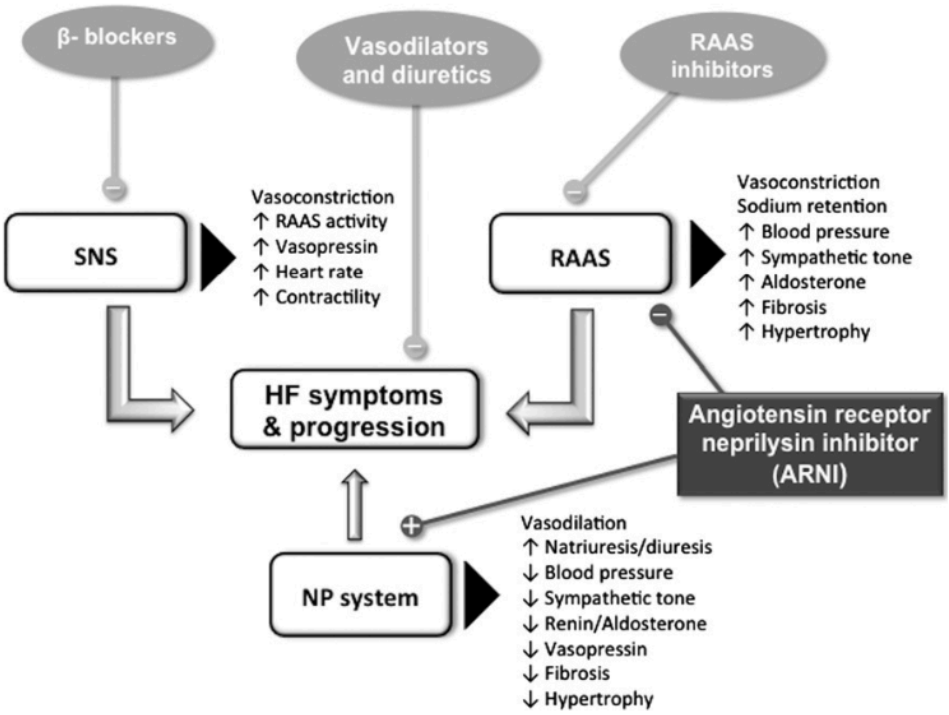

Figure 15. Current treatment of heart failure with induced ejection fraction (HFrEF). (adapted from Volpe et al., 2016[392])

1.5.3 The role of CN and PDEs in heart

Because of its chronotropic, inotropic and lusitropic responses, stimulation of the AMP - PKA axis by the β-adrenergic pathway resulting from SNS stimulation is thought to be beneficial in the early stages of heart failure. Nevertheless, chronic stimulation of these compensatory mechanisms eventually lead to a vicious cycle leading to worsening of heart failure[378,393-395].

Conversely, cGMP - PKG pathway induced by NPs or NO alleviates this adverse effects of cardiac sympathetic activation, hampering the hypertrophy and fibrosis caused by norepinephrine and angiotensin II[396,31]. Yet, both NO bioavailability and NPs signaling are impaired in HF patients due to endothelial dysfunction and downregulation of NP receptors in a condition of overstimulation of RAAS[397,398,399,400]. Despite upregulated circulating NP concentrations in HF which is manifested by elevated pro-BNP and BNP in clinical test[392], this response is apparently insufficient to counteract the activation of vasoconstriction and sodium retention of RAAS and SNS.

The CNs pathways have revealed to be relevant targets to treat HF. The strategy of inhibiting cAMP hydrolysis by a PDE3 inhibitor, milrinone, whereas it can improve contractility in short-time application of treating acute HF, is deleterious in long-term therapy[316]. And another drug, levosimendan, non selective PDE3 inhibitor and ca2+ sensitizer, Conversely, another study showed that increasing the activity of PDE4 prevents the deleterious effects of exacerbated sympathetic activation, a strategy that may serve as an alternative to β-blockers[401]. The cGMP accumulation is considered to be beneficial, antihypertrophic and antifibrotic, as suggested by non-clinical studies of the inhibition of neprilysin[402,403]. Inhibitors of cGMP PDEs (PDE1, PDE2, PDE5, PDE9) also demonstrated preclinical approaches that demonstrated protective action in pre-clinical models [355,363,404-406]. Besides, PDE10 inhibitors, that enhance both cAMP and cGMP, exert protective effects in mouse models of hypertrophy and heart failure[345]. However, the clinical efficacy of these approaches remains to be established[407], and current clinical trails are mainly focus on PDE5 selective inhibitors and nesiritide , a recombinant NP (clinical trial.gov)

1.5.4 Vascular alterations in HF

HF is accompanied by histological and functional changes in peripheral circulation, including an increase in vascular resistance and a decrease in vascular compliance[408,409]. The common vascular pathophysiology of peripheral artery in HF includes: endothelial dysfunction (ED), abnormalities of vasomotor tone, remodeling of arterial vascular wall.

Endothelial dysfunction (ED), a functional anomaly present in diseases of the cardiovascular system or other diseases probably causing cardiovascular disease, is generally associated with a deficit in the bioavailability of NO and an excess production of endothelial vasoconstrictor factors, such as endothelin-1[410,411]. The presence of ED in chronic HF is a well-established fact, usually documented by a decrease in the vasodilator response to endothelial stimulation (by using acetylcholine or flow mediated vasodilation in most cases). ED is more important when the HF is severe, and is a predictive factor for the occurrence of clinical events and death[412]. ED is not only present in HFrEF but also HFpEF[413]. ED affects both the coronary network (often documented by invasive measurement)[411,414-417], and peripheral vessels[418-421] in patients with chronic HF and in vivo animal models [422-424]. Yet the severity of ED in chronic congestive HF is not uniform among vascular beds. It is reported that the ED is substantial in PA and femoral arteries and minimal in mesenteric resistance vessels in coronary artery ligation induced chronic HF models[425,426].

The vascular tone is influenced by many factors in vivo, which include not only SNS and RAAS stimulation, but also other circulating hormones, endothelial or neuronal release of vasoactive agents, changes in hemodynamics (intraluminal pressure, shear stress), and regional modulation, alteration of structure [408]. In respect to vessels itself, the abnormalities of vasomotor tone cannot be completely explained by a deficit in endothelial function, but also by a defect in the mechanisms located downstream, in underlying smooth muscle. The following aspects indicate that the properties of vascular smooth muscle are altered in HF. Firstly, an altered response to nitrates or “NO donors” is often demonstrated in the peripheral beds[409,419-421,427-429]. Similarly, animal experiments indicate a vulnerability of the NO-induced relaxant pathway in the

coronary bed in HF, while this is relatively preserved at the periphery[424,430,431]. Secondly, it is observed that the density of β-adrenergic receptor is significantly reduced in vessels from HF animals[431,432]. Consistently, the peripheral vasodilator response in vivo and ex vivo to isoprenaline (ISO, β-adrenergic agonist) is attenuated in HF models compared to control animals[424,431,433,434]. In several studies, the response to forskolin, a direct AC activator, was unchanged, suggesting that the downstream cascade of β-adrenergic was preserved[424,432,434]. Regarding the coronary bed, vasodilator responses attributed to cAMP signaling are more markedly reduced both in HF patients[417,435] and in experimental models[424]. However, the results obtained in the aorta differ according to the models and studies, reporting a reduction in the effect of ISO [162,432] or not[424,433]. It is reported in patients, there is no β-adrenoceptor desensitization in limb vessels[428]. Thirdly, changes to vasoconstrictor in some vascular beds in patients or in animal models of HF have been observed, indicating that the pathology also affects contractile responses. For instance, studies reported that the contractile properties are undermined in peripheral vessels and coronary artery[163,427]. Conversely other studies account for an increased contractile response in mesenteric arteries[436-439] and aorta[162]. Interestingly, some studies reveals that the PDEs functional alteration contributes to change of vascular tone in coronary artery[163] and aorta[162].

Besides, remodeling of arterial vascular wall is speculated to occur due to chronically exposure to neurohormones, impaired NO production and increased ET-1 generation, whereas this only reported in coronary artery[163,440]. There is scant evidence that support this hypothesis in peripheral vasculature. Some studies pointed out that thickness of capillary basement membrane are increased in peripheral vessels of chronic HF patients[441,442]. Another study reported increase in hyalinosis in basement membrane of terminal arterioles in peripheral vessels from HF patients[443]. Whereas in animal models, the structural alterations of both femoral arteries and mesenteric arteries have not been observed[426].

1.5.5 Contribution of PDEs to alterations of vascular reactivity in heart failure models

1.5.5.1 The role of PDE in alteration of the tone in aorta from HF rats.

Hubert et al. first described the role of PDE3 and PDE4 in aorta isolated from rats with HF induced by aortic stenosis [162]. This model was characterized by reduced fractional shortening, cardiac hypertrophy and dilation, lung congestion, and systolic blood pressure[162]. In this study, PDE3A and PDE4B protein expression are increased in aorta lysates of HF compared to vessels from the control, sham animals. Yet, the activities of both PDE3 and PDE4 families shows no significant increase.

Vascular reactivity experiments were conducted by using isolated aortic rings mounted on an isometric myograph. The endothelial dysfunction (ED) is obvious in aorta of HF models, which may partly explain the hyperreactive response to vasoconstrictor KCl and $PGF_{2\alpha}$ in the HF group compared to sham group. Relative contributions of PDE3 and PDE4 were inferred from the vasorelaxant properties of their pharmacological inhibition with Cilostamide (1 μM) and Ro-20-1124 (10 μM), respectively. PDE4 is only functional in presence of intact ECs, and, PDE4 inhibition is ineffective in HF models, consistent with the presence of ED in this group. By contrast, PDE3 function is partially inhibited by the presence of intact endothelium in sham group, probably due to constitutive NO and cGMP generation. Accordingly, PDE3 contribution can be enhanced by endothelium disruption, and is preserved in HF aorta. Interestingly, PDE4 function can be restored by PDE3 inhibition, suggesting that PDE activities in SMC are somewhat redundant. Furthermore, β-adrenoceptor stimulation by ISO induces relaxation in sham aorta, but is abolished in the absence of intact EC, so as in HF aortas, but can be restored after PDE3 inhibition in all unresponsive arteries. So in summary, this study reveals that PDE4 may be redundant in controlling aortic tone in HF, due to exacerbated PDE3 activity, probably caused by endothelial dysfunction and lack of repressing action of cGMP on the enzyme. Thus PDE3 plays a major effect in modulating aorta tone of HF, and PDE3 inhibition can help to restore functional relaxation to β-adrenoceptor stimulation.

1.5.5.2 The role of PDE in alteration of vascular tone of coronary artery from HF

In another study from the laboratory, Idres et al. described the role of PDE3 and PDE4 in coronary artery isolated from the same HF model as in Hubert et al. [163]. In this report, the protein expression of PDE3A and PDE4D is decreased, whereas PDE4B expression is increased in coronary artery from the HF group. Even though there is an ED in HF group, the contractile response to K60 and U46619 is decreased in HF group, which is opposite with aorta. The role of BK_{Ca} channels in mediating the vasorelaxant effect of PDE3 and PDE4 inhibition is lost in coronary artery from heart failure.

1.5.5.3 Rationale for exploring PDE contribution in mesenteric artery of HF

As introduced above, changes in vascular tone are not homogeneous, so that certain vascular beds may respond to a stimulus quite differently from other vascular beds. Hence, although PDE alterations are documented in aorta and coronary artery of HF[162,163], whether such changes are happening in mesenteric artery (MA) in HF has never been documented. Since MA are important resistance artery in the cardiovascular system, the impact of HF on vascular PDEs may be divergent from those observed in coronary artery or other conduit vessels. One could hypothesize that PDEs alteration may partly contribute to the increased vascular reactivity of MA which has been observed in HF models[436,438,439].

Besides, PDEs are “hot” targets in cardiovascular disease[102,292,306]. Their role in modulating vessels has been emphasized in recent years, whereas their research in MA is less documented except for PDE1[148,182,444] (Table 7). The expression and activity of PDE in MA is reported similar to aorta, among which, PDE3 and PDE4 are the main cAMP-PDEs, whereas PDE1 and PDE5 are main cGMP-hydrolysis PDEs[146]. The role of PDE2 in MA is not clear in animals, whereas the PDE2 activity can be clearly detected in human[445].

So exploring the contributions of PDEs in MA from an HF model may help us to better understand how it may participate in HF pathophysiology and to anticipate how interventions aiming at modulating CN signaling in the whole cardiovascular system may impact peripheral vascular resistance and organ perfusion.

Table 7. Summary of PDEs expression and function in tissue of MA.

PDE	Expression and ativity	Vasorelaxant effect of PDEs inhibitor
PDE1	mRNA of PDE1A&1B: rat[182], PDE1A>PDE1B[148] protein of PDE1: rat[444], mainly PDE1A[148] activity: human√[445] activity: rat√[146]	√ rat MA: BTTQ[444] √ rat MA: Lu AF41228 and Lu AF58027[182] √ rat MA : Lu AF58027 (potent for PDE1A)[148] √ rat MA : Vinpocetine[446]
PDE2	activity: human√[445]	not documented
PDE3	mRNA and protein of PDE3A&3B: rat,√[447] activity: human√[445] activity: rat√[146]	√ rat MA : Cilostamide[447] and cilostazol[448] (enhance Ach relaxant response) √ human MA : Milrinone[449]
PDE4	mRNA and protein of PDE4D: rat,√[447] activity: human√[445] activity: rat√[146]	√ cat MA: Ro 20-1724[450]
PDE5	activity: human√[445] activity: rat√[146]	√ rat MA : Sildenafil[446]
PDE9	mRNA: rat, √[451]	not documented
PDE10	mRNA: rat,√[451]	not documented
PDE11	mRNA and protein: rat,√[451]	not documented

2. Objectives

2.1 Project 1: The role of PDE9 in pulmonary artery hypertension

Pulmonary arterial hypertension is a rare and fatal disease with no cure. Based on previous introduced background, now we proposed a hypothesis that inhibition of PDE9 may work as new therapeutic strategy to treat this disease.

Thus the global aim of this project is to shed light on:

- First, the exact expression of PDE9 in the pulmonary artery, lung and RV from control and pathological conditions of human and animal models by western blot or RT-qPCR;
- Second, the physiological role of PDE9 in pulmonary artery and the selectivity of PDE9 inhibitors (PF-04447941 and Bay73-6691) in pulmonary artery by comparing *Pde9a*$^{+/+}$ and *Pde9a*$^{-/-}$ mice and by using myograph experiment;
- Third, whether PDE9 deficiency is amenable to ameliorate experimental PAH induced by chronic hypoxia mouse models by comparing *Pde9a*$^{+/+}$ and *Pde9a*$^{-/-}$ mice;
- At last, whether PDE9 inhibitors can exert anti-proliferative effect in human PASMCs.

2.2 Project 2: The role of cAMP-related PDEs in mesentery artery from both normal and heart failure rats

Our team has studied the role of PDE3 and PDE4 in aorta from both sham and aortic stenosis induced rat HF models. Whereas the contribution of these PDEs in mesenteric artery under same condition of heart failure is never documented. Considering the mesenteric artery represents a typical resistance vascular bed which differs from aorta, thus as a complementary study to previous study, we want to explore a physiological role of PDE2, PDE3 and PDE4 in regulating MA, and the possible pathological alteration in context of heart failure.

Thus the global aim of this project is to elucidate:

- First, the exact expression and activity of PDE2, PDE3, PDE4 in isolated rat mesenteric artery both from Sham and heart failure models;
- Second, the functional role of these PDEs on isolated vessels both from Sham and heart failure models by using a pharmacological approach.
- Third, how PDE contribution correlates with possible endothelial dysfunction in these arteries.

2.3 Project 3: The role of PKA RI in aorta

Protein kinase A (PKA) is a key enzyme activated by binding of cAMP. PKA induces smooth muscle relaxation and vasodilatation. The PKA-RIα knock-in heterozygous mice, [R368X]/[+] (KI), leading to the generation of a truncated RIα and the repression of PKA activation (Le Stunff et *al.*, 2017 *J Bone Miner Res*) may help decipher the contribution of PKA-RIα in vascular system which has remained elusive.

Thus the global aim of this project is to explore:

- First, the expression of PKA subunits and activity of PKA both in wide-type (WT, $RI\alpha^{+/+}$) and heterozygous mutant (KI, $RI\alpha^{R368X/+}$) mouse.
- Second, function of PKA-R1α in mouse aorta and its role in modulating arterial tone.
- Third, the special compartmentalization of PKA type I may be involved.

3. Materials and Methods

3.1 Drugs and reagents for all projects

Table 8. Stock solutions and suppliers of drugs and reagents.

Name	Stock Conc.(M)	Solvent	Pharmacological property	Supplier
Phenylephrine (PE)	10^{-2}	H_2O	alpha-1 adrenergic receptor agonist	Sigma Aldrich
U46619	10^{-3}	methyl acetate	Analog of thromboxane A_2: TP receptor agonist	Cayman Chemical
Acetylcholine (Ach)	10^{-2}	H_2O	cholinergic agonist with muscarinic and nicotinic actions	Sigma Aldrich
L-NAME	10^{-1}	H_2O	NOS inhibitor	Enzo life science (Villeurbanne, France)
Diethylamine NONOate (DEA-NO)	10^{-2}	H_2O	NO donor	Enzo life science (Villeurbanne, France)
Rat atrial natriuretic peptide (rANP)	10^{-3}	H_2O	agonist of natriuretic peptide receptor-A	Sigma Aldrich
C-type natriuretic peptide (NP)	10^{-5}	H_2O	agonist of natriuretic peptide receptor-B	Sigma Aldrich
Sildenafil (Sild)	10^{-2}	DMSO	PDE5 inhibitor	Sigma Aldrich
PF-04447943	10^{-2}	DMSO	PDE9 inhibitor	Sigma Aldrich
BAY-73 6691	10^{-2}	DMSO	PDE9 inhibitor	Sigma Aldrich
BAY 60-7750	10^{-2}	DMSO	PDE2 inhibitor	Sigma Aldrich
Cilostamide (Cil)	10^{-2}	DMSO	PDE3 inhibitor	Tocris Bioscience
Ro-20-1724(Ro)	10^{-2}	DMSO	PDE4 inhibitor	Calbiochem
3-isobutyl-1-methylxanthinec(IBMX)	10^{-2}	DMSO	Non-selective PDEs inhibitor	Sigma Aldrich
Isoprenaline(ISO)	10^{-2}	0.1% ascorbic acid	agonist of β-adrenergic receptors	Sigma Aldrich
L-858051(L85)	10^{-2}	H_2O	A water-soluble forskolin derivative	Enzo life science (Villeurbanne, France)
8-AHA-2-Cl-cAMP	$3{\cdot}10^{-3}$	H_2O	PKA RI site B Activator	Biolog

All salts for solutions were from Sigma-Aldrich or Euromedex (Souffelweyersheim, France).

3.2 Project 1: The role of PDE9 in pulmonary artery hypertension

3.2.1 Human samples

Biological resources from patients were obtained through a collaboration with U999 (Frederic Perros, Fabrice Antigny). Patients are part of the French Network on Pulmonary Hypertension, a program approved by our institutional Ethics Committee (2008), and give written informed consent (Protocol N8CO-08- 003, ID RCB: 2008-A00485-50, approved June 18, 2008). Human PA were obtained during lung transplantation from patients with PAH and, for control tissue, during lobectomy or pneumonectomy for localized lung cancer from non-PAH subjects.

3.2.2 Animals and genotyping

3.2.2.1 PDE9 linage mouse

All protocols involving animals followed the European Community guiding principles in the care and use of animals (2010/63/EU) and complied with French institution's application decrees for animal care and handling. PDE9A global knockout (*Pde9a* $^{-/-}$, KO) mice were developed by Pfizer Inc from the C57BL6/J background, which was described in Lee et al [355]. Specifically, this model replaced exon 12 in the catalytic domain of Pde9a with a lacZ-neomycin cassette (Figure 1), and all PDE9 variants of mice share this sequence. Two heterozygote couples kindly provided by Pr. David Kass' laboratory (Johns Hopkins University School of Medicine, Baltimore, MD, USA) were received by our laboratory in January 2019. So animals were housed, mated, breed in "AnimEX" platform of IPSIT (Faculté de Pharmacie, Châtenay-Malabry).

To avoid potential confounding effects due to hormonal variations, only males were used in this study. Expression of alternative cGMP- targeting PDEs (*Pde1a, Pde1b, and Pde1c, Pde2a,*

Pde3a, Pde3b, Pde5a) are not significantly altered in *Pde9a*$^{-/-}$ versus wide-type(WT) littermates lungs, RV and pulmonary artery (Figure 16).

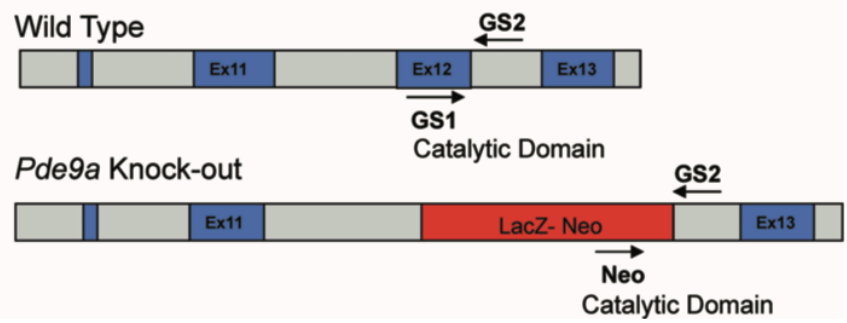

Figure 16. Development of Pde9a knockout (*Pde9a*$^{-/-}$) mice. (Adapted from Lee et al, 2015[355])

3.2.2.2 Genotyping

The mice tails were cut for genotyping. The DNA was extracted by NaOH 50mM 300µl for heating 45min, then mixed with Tris-HCl(PH 8.0) 25µl. After centrifuge, the supernatant containing DNA was used for genotyping. The specific primers were designed between exons 11 and 13 including neomycin as following:

GS1 (5'-CACAGATGATGTACAGTATGGTCTGG-3');

GS2 (5'-TGCAGTCATCAGGACCAAGATGTCC-3');

Neo (5'-GACGAGTTCTTCTGAGGGGATCGATC -3').

Then prepare the PCR reaction condition as following:

Table 9: PCR reaction mix for genotyping.

	stock concentration (µM)	Volume (µl)	final concentration (µM)
GS1 10µM	10	0,2	0.1
GS2 10µM	10	0,2	0.1
Neo 10µM	10	0,2	0.1
DTmix (2X)	2X	10	1X
DNase free water	-	9,4	-
DNA		1 µl	

Next running PCR as below condition:

94 ℃	3min	
94 ℃	30s	×40 circles
60.8 ℃	30s	
72 ℃	60s	
72 ℃	10min	

The typical genotyping pattern of *Pde9*$^{-/-}$ mice was shown on 2% agarose gel, 250 bp for wild type(WT, *Pde9*$^{+/+}$) and 600 bp for knock out (KO, *Pde9*$^{-/-}$) mice as shown in Figure 17.

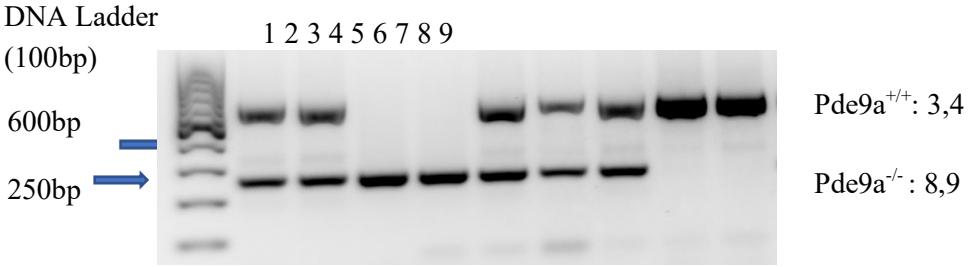

Figure 17. Example of genotyping PCR result of PDE9 linage mouse.

3.2.3 Mouse tissue preparation

The mice were sacrificed by cervical dislocation. The chest cavity contents were quickly isolated and placed in an ice-cold "Krebs" solution of following composition (in mM): NaCl 119, KCl 4.7, $CaCl_2$ 2.5, $MgSO_4$ 1.2, KH_2PO_4 1.2, glucose 11, $NaHCO_3$ 25, bubbled with 95% O_2 and 5% CO_2 to maintain pH at 7.4. The left ventricle(LV), right ventricle (RV) were dissected and frozen in liquid nitrogen quickly. Then aorta (Ao) was pinned on a Sylgard®-coated dish filled with cold Krebs solution, the connective tissue was removed under microscope, then cleaned Ao was frozen in liquid nitrogen. The lung was fixed in same way as Ao, and the intra-pulmonary bronchi looked relative white and thick was dissected carefully first, and the intra-pulmonary artery looked relative transparent and under bronchi was dissected subsequently (Figure 18). All dissected bronchi and a part of PA was frozen in liquid nitrogen, and reminding part of PA was used for vascular reactivity assay. Finally, part of outer

edge of lung was cut and frozen. Dissecting solution was renewed every 10-15 min with cold, bubbled solution. All the tissues frozen in liquid nitrogen were used for biochemical experiments, and stored in -80°C.

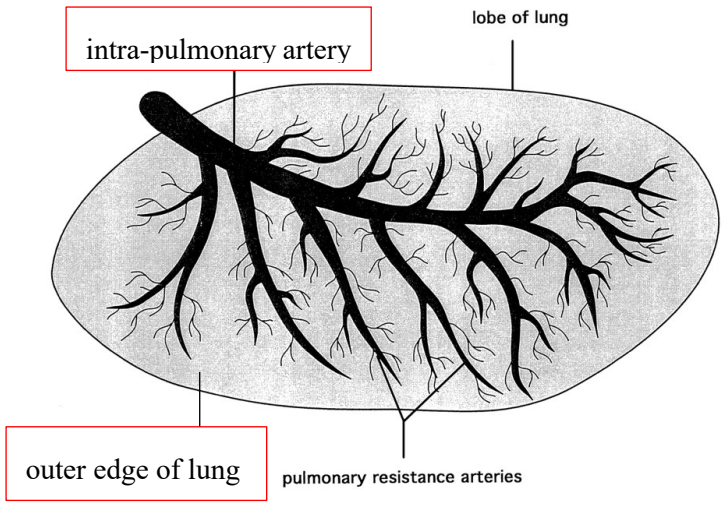

Figure 18. The diagram of intra-pulmonary artery used in this study. (adapted from Maclean et al., 1997[139])

3.2.4 Measurement of vascular reactivity

Most experiments were performed in adult male PDE9A KO and WT mice, around 8-17 weeks. Some experiments were also conducted on female mice. PAs were cut into around 2mm segments for isometric tension measurement. The vessels were mounted in the chamber of a small vessel myograph (620 M, Danish Myo Technology A/S, Aarhus, Denmark) (Shown in Figure 19) using 25 µm tungsten wire, as previously described [163,452]. Chambers were filled with Krebs solution, bubbled with 95% O^2 - 5% CO^2 mixture and warmed at 37°C. Data were digitized using a Powerlab 8/30 (AD Instruments, Paris, France) and acquired using the Labchart7 software (AD Instruments).

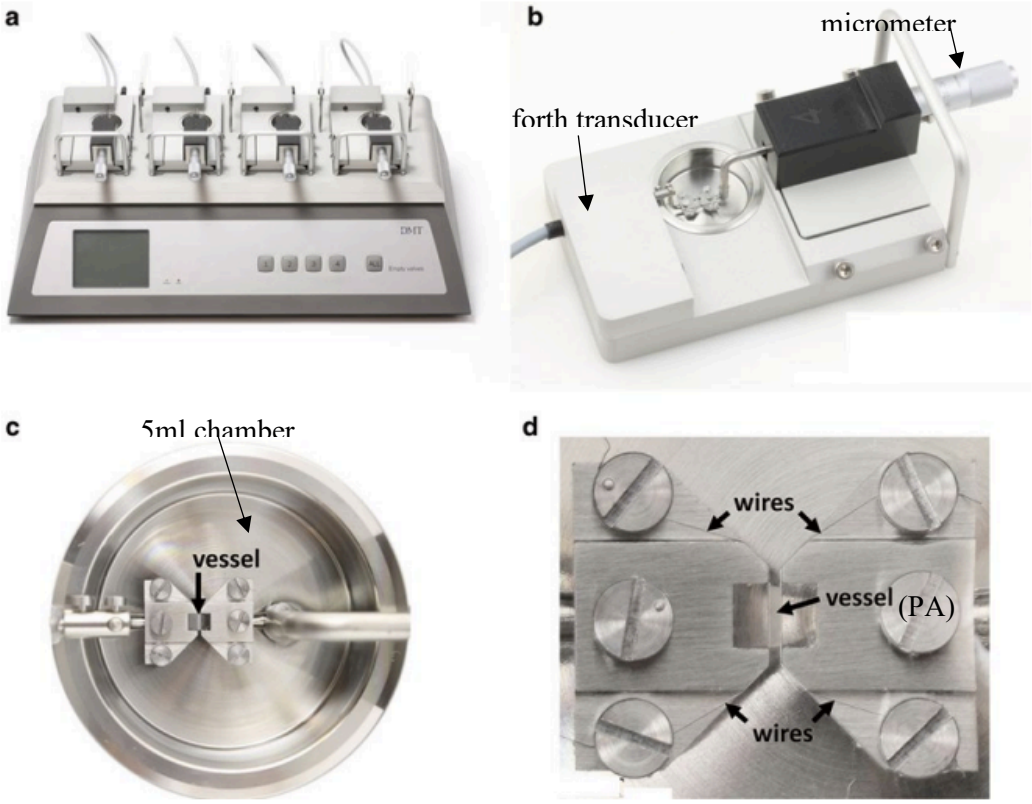

Figure 19. Essential components of the myograph. (a) DMT multi-chamber 620M Wire Myograph. (b) Each myograph unit contains a force transducer (left) and a micrometer (right), which are both connected to corresponding jaws to support the vessel inside the chamber. (c) Detail of the chamber with the jaws and a mounted vessel segment. The left and right jaws are connected to the force transducer and micrometer screw, respectively. (d) Detail of the jaws, screws, wires, and a mounted vessel segment (PA). (Adapted from www.dmt.dk)

Vessels underwent a normalization procedure by stretching the vessels stepwise to construct tension-circumference relationship. Rings were eventually set as 90% internal circumference when they were submitted to a transmural pressure of 25 mmHg (3.33 kPa). After an equilibration period of 20-30 min, contractile capacity of the vessels was evaluated by a challenge with a modified Krebs solution containing 60 mM KCl (K60) with equimolar substitution of NaCl, as shown in **Table 10**. This depolarizing solution (K60) normally evoked robust contraction, and was left for 5 min. Chambers were then washed with control Krebs

solution, until the vessel was fully relaxed and tension was stabilized. The vessels were challenged again with K60. Vessels with response less than 0.5 mN/mm were excluded from analysis. Endothelial function was evaluated in all vessels by measurement of the relaxant effect induced by 10 μM ACh. After an additional series of washes, the vessels were bathed in control Krebs solution and used for various pharmacological protocols.

Table 10: Composition of solutions for vascular reactivity.

	Concentration(mM)		
	Krebs	KCl 60mM (K60)	KCl 120mM (K120)
NaCl	119	63.7	3.7
KCL	4.7	60	120
$CaCl_2 \cdot 2H_2O$	2.5		
$MgSO_4 \cdot 7H_2O$	1.17		
KH_2PO_4	1.18		
$NaHCO_3$	25		
D-Glucose	11		

3.2.4.1 The contractile cumulative dose response of mouse PA

All the contractile response were explored both in male and female mice. The contractile stimuli include KCl solutions (depolarizing), U46619 (thromboxane A2 mimetic) and phenylephrine (PE, α_1-adrenergic receptor agonist). The series of KCl gradient concentration was prepared using mixture of Krebs and K120 following the concentration of KCl needed. Contractile responses were expressed in mN/mm or contractile amplitude in percentage of the contraction evoked by K60.

3.2.4.2 The relaxant cumulative dose response of mouse PA to cGMP-mediated vasodilators

To explore the possible pathway for PDE9 to regulate the vascular tone, both the NO and natriuretic peptides (NP) mediated relaxing pathway have been explored. Specifically, both the Ach and DEANO (NO donor) were measured to explore NO-soluble guanylate cyclase (sGC)-cGMP pathway since the former relaxes vessels mainly via stimulating NO generation from ECs, whereas the latter is a NO donor. Whereas the rat atrial natriuretic peptide (r-ANP) and

CNP was performed to assess NP-particulate guanylate cyclase (pGC)-cGMP pathway. The Ach dose response was carried out on vessels precontracted by PE used at EC_{80} (130 nM). The DEANO, rANP and CNP dose response were tested after pretreatment with L-NAME 300 μM for 20 minutes to inhibit endogenous cGMP generation, and precontraction by PE (50 nM). Relaxant responses were expressed as percentage of relaxant amplitude relative to the amplitude of the contraction obtained with PE.

3.2.4.3 The cumulative dose response of mouse PA to selective PDE5A or PDE9A inhibitors

To evaluate the selectivity of PDE9 pharmacological inhibitors, 2 well-known PDE9 inhibitors, PF-04447943 and BAY-73-6691 were used to perform relaxant dose response of PA from both WT and KO mice. And PDE5 selective inhibitor, sildenafil, was used to assess the relaxant response from both WT and KO mice. Relaxant responses were expressed as percentage of relaxant amplitude to the amplitude of the contraction obtained with PE.

3.2.4.4 Data analysis

For each analysis, the results are expressed as the mean ± SEM. The number of data for each group was denoted by N, corresponding to number of mice. For each vessel, the concentration-response curves(CRC) were obtained using Hill's equation using Prism9 software. Then the concentration producing 50% of the maximum response (EC50) as well as the maximum effect (Emax) were estimated for each curve. The EC50 is then converted into a negative logarithmic value, pD2 (pD2=-LogEC50). The comparation of 2 groups used student-t test, and the CRC was compared using 2-way ANOVA of repeated measurements followed by Sidak's post hoc test. $P<0.05$ was regarded as significance.

3.2.5 Real-time quantitative PCR

3.2.5.1 RNA extraction

Total RNA was extracted from mouse PA, aorta, bronchi, LV, RV, lung. First, add 1ml TRIzol to the "Bertin" tubes under hood, and quickly add the samples to the "Bertin" tubes. Then launch Bertin rotor for homogenate: for lung, RV, and LV, running 2*8s with one circle; For PA, aorta, and bronchi, running 2*8s with two circles. Leave these tubes containing tissue homogenate at room temperature for 5 minutes to permit the complete dissociation of nucleoprotein complexes, during this time transfer each homogenate by pipet into another 2ml tube without beats. Then add chloroform 200µl (per ml TRIzol reagent) into each tubes under hood, and shake tubes very hard by hand for 15 seconds. Wait for 3 min at room temperature, then centrifuge at + 4 ° C, 10,000G for 15 min to separate mixture. Carefully transfer the upper aqueous phase which containing the RNA into another 1.5ml tube, and add 250µl of cooled isopropanol, then shake for 15 seconds very hard by hand. Put at -20 °C overnight to precipitate the RNA. On second day,centrifuge tubes at 4 °C, 12000 G for 15 min, and empty the isopropanol by inverting the tube over a beaker. Add 1ml of 75% ethanol to wash the RNA pellets 2 times. Centrifuge the tubes at + 4 ° C, 12,000 G 5 minutes between washing 2 times. Finally, carefully pour off the solution of tubes, and install the tubes in an inverted position upon absorbent paper, then let the pellets dry 30 min at room temperature. Add RNase-free water to each RNA pellet, 16µl for PA, aorta and bronchi, and 20-30 µl for LV,RV, lung. Leave these tubes in ice for 1 hour, and shake gently 1-2 times to promote rehydration of the RNA. Freeze RNA at –80 ° C for storage. The RNA concentration was measured by Nanodrop, DO260nm / DO280nm more between 1.7 to 2.0 was used for following experiments.

3.2.5.2 Reverse transcription from RNA into cDNA.

cDNA was synthesized using 1µg total RNA for most tissue, whereas the 0.75µg total RNA for PA. Total volume is 20ul prepared. The iSCRIPT cDNA Synthesis Kit (Bio-Rad, Marnes-la-Coquette, France) was used according to manufacturer's instructions. Negative RT controls were prepared by using no reverse transcriptase reagent to assess the amount of DNA contamination present in an RNA preparation. Additional negative controls included non-

template controls, performed without template to check for exogenous contamination and serve as an important control for primer dimer formation. Then incubate the complete reaction mix in a thermal cycler using the following protocol for reaction (**Table 11**):

Table 11: Reverse transcription condition.

Priming	5 min at 25°C
Reverse transcription	20 min at 46°C
RT inactivation	1 min at 95°C
Optional step	Hold at 4°C

3.2.5.3 Running qPCR

Real-time quantitative PCR (RT-qPCR) was performed using the SYBR-Green method on a CFX384 TouchTM Real-Time PCR Detection System (Bio-Rad, Marnes-la-Coquette, France). SsoAdvanced^{TM} Universal SYBR Green Supermix (Sso Mix, Bio-Rad) was used all genes detection in mouse and most genes of rat. Only *Pde2a* and *Pde4c* genes for rat were carried out using SYBR Premix (Takara Bio Europe, Saint-Germain-en-Laye, France). For each target gene, a standard curve was constructed from the analysis of serial dilution of cDNA and was used to determine efficiency (E). *Ywhaz*, *TBP* and *Rplp2* were generally used as reference genes. The reaction mix of each well for RT-qPCR is listed in **Table 1**2. The protocol for running RT-qPCR is listed in **Table 13**, and sequences for primers in **Table 14**.

Table 12: The reaction mix of each well for RT-qPCR.

	Concentration	Volume/well (µL)
Sso Mix	2X	5
primer-F	10 µM	0.5
primer-R	10 µM	0.5
cDNA template	2,5ng/µL	4

Table 13: RT-PCR protocol

94,0 °C	30s	
95,0 °C	5s	×40 circles
60,0 °C	20s	
Plate read		
Melt curve 65, 0 °C to 95,0 °C		Increment 0,5°C 5s

Table 14: Sequences of the primers used in PDE9 mouse project.

Target	**Forward 5'→3', Reverse 5'→3';**	**Product size (bp)**	**Annealing temperature (°C)**	**Accession number**
Pde1a	GCAGGGAGACAAAGAAGCTG CAATCATGGTGGACGAGCTG	224	60,0°C 20s	NM_001355142.2
Pde1b	GTCCACAACTGTCTCAAGAACC TAAAGCGGCTGATGAGGCTAT	133	60,0°C 20s	NM_001357980.1
Pde1c	CTGAACAAGGCACAACCAGC ACCGTCTTTCAAGTCACCGT	155	60,0°C 20s	NM_001355475.1
Pde2a	TGGGGAACTCTTTGACTTGG ATGACCTTGCAGGAAAGCTG	135	60,0°C 20s	NM_001243758.1
Pde3a	CAGCATAAAGCCGCACGAAG GTGAGAGTCGTCAACCCTGG	81	60,0°C 20s	NM_018779.2
Pde3b	ATGTTCAGGAGACCGTCGTT TTGGGTCAATCAGCAGGTCT	175	60,0°C 20s	NM_011055.2
Pde5a	ATCTGGAGACCCTTGCGTTG GGTTGCCTGGGCTGTTTAGA	177	60,0°C 20s	NM_153422.2
Pde9a	CACAGATGATGTACAGTATGGTCTGG ATGTGATCATCCCCTGCCTG	294	60,0°C 20s	NM_001163748.1
Nppa	AGGCCATATTGGAGCAAATC CTCCTCCAGGTGGTCTAGCA	88	60,0°C 20s	NM_008725.3

Nppb	CTGGGAAGTCCTAGCCAGTC TTTTCTCTTATCAGCTCCAGCA	132	60,0°C	20s	NM_013684.3
Myh7	AATGCACTCAATGCCAGGAT GTCAGAGCGCAGCTTCTCC	153	60,0°C	20s	NM_080728.3
Ywhaz	AGACGGAAGGTGCTGAGAAA GAA GCATTGGGGATCAAGAA	127	60,0°C	20s	NM_001356569.1
TBP	AAAGACCATTGCACTTCGTG GCTCCTGTGCACACCATTTT	132	60,0°C	20s	NM_013684.3
Rplp2	GCTGTGGCTGTTTCTGCTG ATGTCGTCATCCGACTCCTC	119	60,0°C	20s	NM_026020.7

3.2.5.4 RT-qPCR analysis

Each target gene has a distinct E, marked as E1. Threshold cycle (Ct) of each sample subtracts the Ct of geometric mean obtained from control samples to get the ΔCt, so the formula of ΔCt1= Ct (test sample- mean of control sample). The relative quantity(RQ) or fold change of target gene is expressed as $RQ1=(1+E1)^{-\Delta Ct1}$. Then for normalization, the Ct of each sample is calculated by mean of Ct for 3 reference genes, and the E of reference gene, marked as E2, is calculated by mean of E for 3 reference genes. In similar way as target gene, the ΔCt2= Ct (test sample- average of control sample), and $RQ2=(1+E2)^{-\Delta Ct2}$. Normally the RQ2 should be close to 1 due to these genes will not influenced by intervention of experiment. Each data point was obtained from one single animal following below formula:

$$R=(1+E1)^{-\Delta Ct1(\text{test sample-average of control sample})}/(1+E2)^{-\Delta Ct2(\text{test sample-average of control sample})}$$

E1: efficacy of target gene; E2: efficacy of reference gene; ΔCt1: the difference of Ct value of the target gene in each test sample compared to average of control sample; ΔCt2: the difference of Ct value of the reference gene in each test sample compared to average of control sample.

So we can get an individual R from each sample, then compare experimental group and control group by student t-test or welch t-test if unequal variances.

3.2.6 Immunoblot

3.2.6.1 Protein extraction

The tissue from lung and RV were placed in a tube containing ceramic beads (Ozyme, Montigny le Bretonneux, France) and 100 to 200µL cold Lysis buffer (**Table 15**). The tissue was homogenized using a tissue homogenizer (Bertin Technologies) according to the following procedure: 2*8s with one circle. Then, the lysate was left on ice for 30 min and centrifuged for 10 min at 12,000 g at 4 °C. The supernatant was stored at -80 °C before determined the protein concentration by bicinchoninic acid (BCA) protein assay according to the manufacturer's instructions.

Table 15: the components of RIPA lysis buffer.

	Stock	Final	3ml lysis buffer(µl)
Tris-HCl pH8	1 M	50 mM	150
NaCl	3 M	150 mM	150
EDTA	0,5M	2 mM	12
NP40	100	1%	30
DOC	10%	0.50%	150
SDS	10%	0.10%	30
Anti-protease	100X	1X	30
Anti-phosphatases	50X	1X	60
H2O			2388

3.2.6.2 Measure the concentration of protein

The concentration of extracted proteins are assayed by a colorimetric technique using the bicinchonicic acid (BCA) contained in the Smart™ Micro BCA Protein Assay kit (iNtRON biotechnologies, France). Proteins reduce copper Cu^{2+} to Cu^{+}. The latter has a strong affinity for BCA and forms an intensive purple complex in an alkaline environment and exerted a maximum optical absorption at 532 nm. The absorbance is directly proportional to the concentration of protein contained in the sample. The concentration is determined graphically using a standard curve produced from a known concentration range of BSA. Certain samples are diluted if necessary in order to be in the linear part of the range. The preparation of this dilution was carried out with the same proportions of lysis buffer used for the sample preparation. This therefore generates a straight line establishing a linear relationship between

the concentration and the measured absorbance. The latter will allow to calculate the concentration of protein from samples using the absorbances from BCA reaction. On average, 300µg of protein is obtained from one lung and 200µg of protein from the RV.

3.2.6.3 Principle of western blot

Western blotting uses specific antibodies to identify and quantify proteins that have been separated based on size by gel electrophoresis. The immunoassay uses a membrane made of nitrocellulose or PVDF (polyvinylidene fluoride). The gel is placed next to the membrane and application of an electrical current induces the proteins to migrate from the gel to the membrane. The membrane can then be further processed with antibodies specific for the target of interest, and visualized using secondary antibodies and detection reagents.

3.2.6.4 Protocol of western blot

3.2.6.4.1 Prepare the samples for loading into gels:

After protein extraction, the loading samples were prepared containing following composition and eventually containing protein 1µg/µl, so we directly took 30µl of samples to load. Hence the quantity of 30µg protein was used to test protein expression.

i. Tissue lysate: to supply protein;
ii. RIPA lysis buffer(the same as extraction): to adjust protein concentration;
iii. Bolt™ 10X Sample Reducing Agent (Invitrogen™): containing 500 mM dithiothreitol(DTT) to reduce disulphide bridges;
iv. Loading buffer 4X: containing 40% (v/v) glycerol, 0.004% (m/v) bromophenol blue, 0.25M Tris-HC1 (pH = 6.8) and 10% (m/v) β-mercaptoethanol, 4% SDS.

The samples are then heated at 70°C for 10 min to denature.

3.2.6.4.2 Loading samples and electrophoresis

The commercial gel of Novex™ WedgeWell™ 4-20%, Tris-Glycine, 1.0mm, Mini Protein Gel, 15 well or 10 well (Invitrogen) was used to do this experiment. The gels were placed into a migration tank and submerged in migration buffer which normally contains 25 mM Tris Base, 190 mM glycine and 0.1% SDS. Then the first well was loaded with molecular weight marker

(Thermo Scientific), and other wells were loaded with samples. A electric voltage of 120 V was applied for 1h 30 minutes, which allowed the separation of the proteins in gel. When the dye molecule (the "migration front") reached the bottom of the gel, the power was turned off.

3.2.6.4.3 Transfer of proteins

The gels were equilibrated in 20% ethanol for 5–10 minutes prior to transfer. The iBlot™ 2 Transfer Stacks, PVDF(Invitrogen) was installed into iBlot 2 Gel Transfer Device using method of semi-dry to transfer. Then the gel was carefully transferred on PVDF membrane. The sandwich composed of paper/PVDF membrane/gel/paper from bottom to top was placed directly between positive and negative electrodes (cathode and anode respectively) following the manuals. Since method P0 (20 V for 1 min, 23 V for 4 min, 25 V for remainder) for 7 minutes is recommended for transferring most proteins (30–150 kDa) with PVDF stacks, so we used this mode to transfer the membrane.

3.2.6.4.4 Blocking the membrane

The membrane was incubated in 5% (m/v) non-fat milk solution dissolved in a "TBS-Tween (TBST)" buffer consisting of 0.153M Trizma-HCl, 1.36M NaCl, 0.1% (v/v) Tween 20, for 1h in room temperature with a slow speed agitation. This step prevents non-specific background binding of the primary and/or secondary antibodies to the membrane.

3.2.6.4.5 Incubation with the primary antibody and secondary antibody

The antibody was prepared in blocking solution- 5% (m/v) milk solution in TBST. The membrane was incubated with the primary antibody, overnight, at +4°C with slight agitation.

Table 16: antibody information used in pulmonary arterial hypertension project.

Antibody	Company	Dilution	Species	Molecular Weight (KDa)
Target Proteins				
PDE9A	Millipore, ABN32	1:1000	rabbit	60-65
PDE9A	L. Jaffe, U Con Health, (gift)	1:5000	rabbit	60-65
PDE5A	J. Beavo, University of Washington (gift)	1:1000	rabbit	100
PDE5A-phospho	J. Beavo University of Washington (gift)	1:1000	rabbit	100
VASP	Cell signalling, 3112	1:1000	rabbit	46-50
VASP-S239	Cell signalling, 3114	1:1000	rabbit	46-50
Reference Protein				
GAPDH	Cell signalling, 2118	1:1000	rabbit	37

After 3 washes of 10 minutes with TBST on second day, the membranes were incubated for 1 hour at room temperature with the secondary antibody (anti-rabbit, 1:10000) coupled to horseradish peroxidase (horseradish peroxidase, HRP). And wash 3 times of 10 minutes with TBST, the membrane was well prepared to reveal.

3.2.6.4.6 Revealing the membranes

The revelation was done by chemistry-luminescence after incubation of the membranes with the reagent, substrate of the peroxidase. We use different SuperSignal® West Substrates with different sensitivity, the sensitivity from lower to higher is PICO<PICO plus<Dura<Femto (Thermo Scientific). The reagents used for revelation depending on the type of protein to be revealed. The signal emitted is analyzed using a CCD ChemiDoc™ camera (BioRad).

7.5 Data analysis

The intensity of the different bands was quantified by densitometry using Imagel software. The ratio of the values of the target protein to the GAPDH was calculated for each sample. This percentage of the intensity makes it possible to determine the relative level of the protein of interest in the 4 groups of animals. The results are expressed as the mean ± SEM, the 2-way ANOVA was used to analyze 4 groups with 2 variables (WT vs KO, Normoxia vs Hypoxia),

and student t-test was used to analyze 2 groups comparison. The number of data for each of the groups is denoted by N corresponding to the number of mice.

3.2.7 Establishment of PAH models

For chronic hypoxia (CH) mice PAH model, PDE9 linage WT and KO littermates, between 8-14 weeks, only male, were age-matched arranged and placed in hypoxia chamber (10 % O_2) for 3 weeks. Other PDE9 mice were placed in the same room during 3 weeks in normoxia condition.

3.2.8 Echocardiographic measurement

Trans-thoracic echocardiography (TTE) was performed using a high-frequency, high-resolution digital imaging platform with linear array technology and color Doppler mode (Vevo 3100, FUJIFILM VisualSonics, Toronto, Canada). By using a ultra-high frequency linear array transducer (MS550D, frequency range 25-55MHz, FUJIFILM VisualSonics, Toronto, Canada), the in vivo parameters of mice cardiovascular function can be assessed.

Mice were performed TTE the day before establishment of CH-models (Day 0) and the day before terminating the CH-models (Day 20). Mice body weight were measured before start the Echo.

3.2.8.1 Preparation

Mice were induced to anesthesia by relative high concentration of isoflurane 3% with an Isoflurane Rodent Anesthesia System (Minerve, Esternay, France). After reaching an adequate anesthesia, the mice were placed onto a pre-warmed imaging animal platform which can detect electrocardiogram and respiratory rhythm once adhered the paws of mice to the 4 electrodes. Then using around 1ml electrode gel connects them to electrodes. The ocry-gel was applied for eye protection. Rectal body temperature was monitored by insert the temperature probe into rectal. Hairs were shaved by the use of commercially available hair removal cream(Veet, Minima Pure^{TM}, France). Echocardiographic (Echo) evaluation procedure was performed under a continuous isoflurane 1-1.5% at room air. Mice body temperature was controlled between 36-

38°C during experiments by using heat lamp. And by adjusting the body temperature and anesthesia level, the HR was controlled in most of time in the range of 400-450 bpm, a very small portion of mice were difficult to keep in this range. HR less than 300 bpm means severe respiratory and cardiac depression, so the anesthesia should be decreased. HR more than 500 bpm may indicate anesthesia is inadequate. The transducer probe (MX550D) was set up in Vevo imaging station, which allows quick adjustment of ultrasound probe. And combined with animal platform, which realize stable and flexible positioning of the anesthetized animal.

3.2.8.2 Parasternal Long Axis (PLAX) to obtain LV parameters and ejection fraction(EF)

Adjust the mouse position by put the foot side of the animal platform down 30° to keep the apex and the root of aorta in the same horizontal level. Squeeze ultrasound gels on mice chest of area without hair. Adjust the ultrasound probe with the notch pointing cephalic direction, and put on animal with about 30° angle counterclockwise to the left parasternal line.

First, use B-Mode setting to obtain a full parasternal long axis view. Then adjust the probe angle by tilting slightly along Y-axis 30-45° of the probe to obtain a full LV chamber view in the center of the screen. Once aorta and apex are in horizontal levels, and LV is visualized, save this B-mode image and switch to M-Mode. An indicator line will show up on the screen in the M- Mode setting. The line should be positioned to go through the widest portion of LV chamber and avoid artifacts of papillary muscle, then save this M-mode information and image (Figure 20). Ejection fraction (EF), and HR can analyzed from this mode.

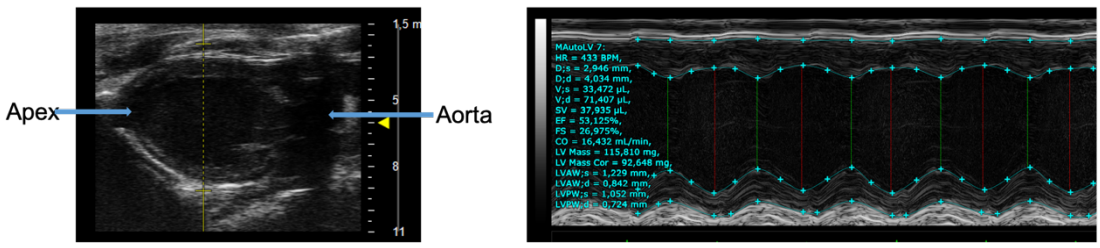

Figure 20. The view of Parasternal Long Axis (PLAX) and measurement of ejection fraction(EF).

3.2.8.3 Modified Parasternal Long-axis View of RV and PA to obtain PA peak velocity

Continue on B-Mode setting, move the probe parallelly to right parasternal line of mice to clearly visualize the PA crossing over aorta as illustrated in Figure 21. Then switch to Color Doppler Mode to check the blood flow (blue). Click Pulse-Wave(PW) Doppler, and position the dashed line parallel to the direction of flow in the vessel. Place the PW cursor at the tip of the pulmonary valve leaflets and around 1cm from upper aorta wall in this image. The image was saved, pulmonary artery acceleration time(PAAT) and pulmonary ejection time(PET) can be measured from this view (Figure 21).

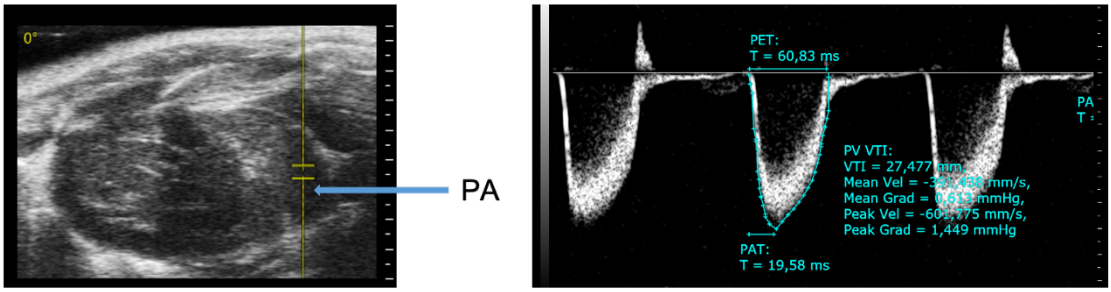

Figure 21. The view of modified Parasternal Long Axis(mPLAX) and measurements of pulmonary artery accelerating time(PAAT) and pulmonary ejection time(PET).

3.2.8.4 Apical 4-chamber view to obtain Tricuspid Annular Plane Systolic Excursion (TAPSE)

Rotate the probe 90° clockwise and make the notch directly toward right. Adjust the angle between probe and abdomen of the mouse around 45°, you can see the 4-chamber heart, and make fine adjustments to get the best picture. TAPSE was measured in M-mode from this view (Figure 22) by positioning the cursor on the lateral tricuspid annulus near the free RV wall and aligning it as close as possible to the apex of the heart.

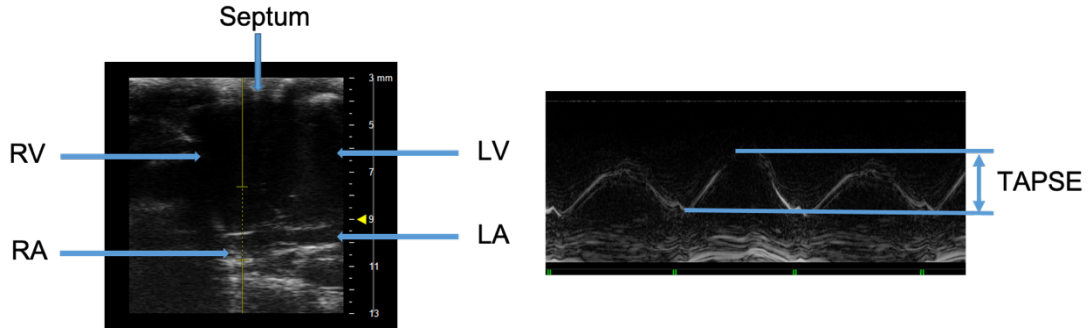

Figure 22. The view of Apical 4-chamber and measurement of tricuspid annular plane systolic excursion (TAPSE).

3.2.8.5 Parasternal Long-axis of RV outflow tract to obtain right ventricular free wall thickness (RVFWT)

Put the probe back to the PLAX position, and tilt the animal plate clockwise around 30°. Then move plate slowly to right heart side, using B-Mode to see the RV chamber and outflow tract. And once RV free wall can be seen clearly, switch to M-Mode and position the line in the middle of ventricular septum to collect data (Figure 23). At last save the image, and RVFWT was measured during end-diastole will be analyzed.

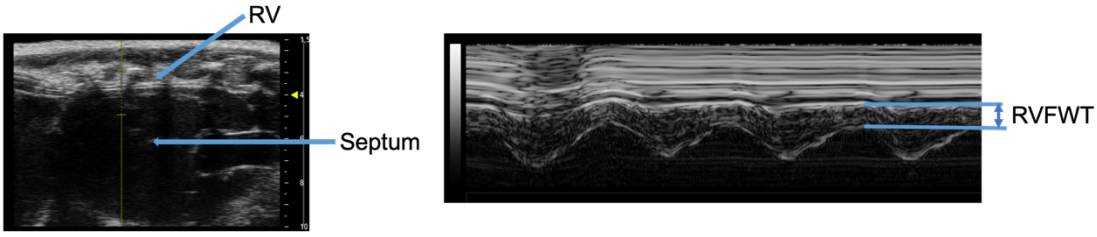

Figure 23. The view of parasternal long-axis of RV outflow tract and measurement of right ventricular free wall thickness (RVFWT).

3.2.8.6 Measurements, calculations, and statistical analysis

All measurements and calculations were made using the Vevo lab software (FUJIFILM VisualSonics Inc., Toronto, Canada). The EF of left ventricle was obtained by auto-LV in M-mode from continuous several heart rate and calculated by the software automatically. The PAAT is the time measured from start of PA ejection to the maximum velocity; the PET is time

from start of ejection to end of ejection. The TAPSE is distance of systolic annular RV excursion along a longitudinal line. RVFWT is the thickness of RV during end-diastole.

3.2.9 Hemodynamic measurements and tissue harvesting

3.2.9.1 Hemodynamic measurement of right ventricle systolic pressure (RVSP)

Mice were placed under general anesthesia and spontaneous breathing with an Isoflurane Rodent Anesthesia System (Minerve, Esternay, France) (maintenance: isoflurane 2%-3% at room air) in the supine position. The upper abdomen was opened, and the xiphoid was lifted with forceps, and the mouse heart could be clearly seen. The left and right ventricles are white, and the interventricular septum is slightly dark, so the right ventricle can be distinguished easily (Figure 24). The needle 21G x1 (BD microlance^{TM}) connected to right heart catheterization (RHC), containing a Millar pressure transducer, as flow probe was inserted directly into the RV to assess the right ventricular systolic pressure (RVSP) and heart rate (HR). Hemodynamic measurements were recorded with a PowerLab 4/35 data-acquisition system and analyzed with LabChart software (AD-Instruments, Oxford, UK).

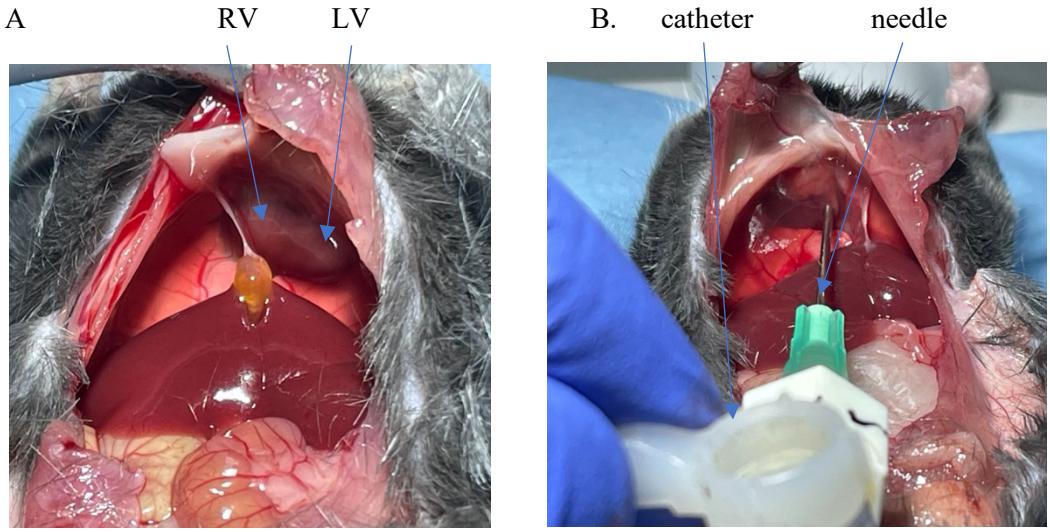

Figure 24. The way to test RVSP by right heart catheterization.

3.2.9.2 Right ventricular weight measurement and tissue harvesting

The heart was harvested. Atria and connecting vessels were removed and discarded. Then RV was separated from left ventricular(LV) and septum under microscope, and both were weighed. For Fulton's index to evaluate RV hypertrophy, the ratio of RV weight to LV plus septal (S) weight (RV/LV+S) was calculated. Then the LV was dissected from septum, and RV and LV were collected and put in liquid nitrogen, long-term stored at -80°C freezer.

3.2.9.3 Lung harvesting

The left lung was ligated from the root with a thread, and then excised and frozen in liquid nitrogen. Then insert a small needle tubing adaptor from the trachea directly into the right bronchus, and inject 1 mL of the OCT suspension (OCT:PBS 1:1) into the right lung. The right lung was fully inflated, then the small tube was withdrawn and the trachea was quickly ligated to avoid OCT overflow. This lung was then put into a disposable embedding mould (Simport™ Scientific, fisher Scientific) and filled with OCT suspension to solid by dry ice.

3.3 Project 2: The role of cAMP-related PDEs in mesentery artery from both normal and heart failure rats

Here I will present the methods related to the experiments I carried out myself during my thesis. Other methods, including those related to the heart failure model and myography experiments that were performed previously by co-authors, are presented in the article inserted below.

3.3.1 Animals

Adult male Wistar rats were purchased from Elevage JanvierLabs (Le Genest St Isle, France). All animal care and experimental procedures conformed to the European Community guiding principles in the Care and Use of Animals (Directive 2010/63/EU of the European Parliament),

the local Ethics Committee (CREEA Ile-de-France Sud) guidelines, and the French law (decret no. 2013-118 of February 1st, 2013) on the protection of animals used for scientific purposes. Authorizations to perform animal experiments were obtained from the French Ministry of Agriculture, Fisheries and Food (No. C92-019-01, 3rd August 2016). Rats were anesthetized by intraperitoneal injection of pentobarbital (0.1 mg/g) and subjected to isolate the gut and dissect the mesenteric artery under microscope within cold Krebs solution.

3.3.2 Immunocytochemistry

3.3.2.1 Principle

Immunocytochemistry is a technique used to assess the presence of a specific protein or antigen in cells by use of a specific antibody that binds to it. The antibody allows visualization of the protein under a microscope. Hence, this technique can reveal presence and sub-cellular localization of proteins.

3.3.2.2 Protocol to isolate endothelial cells from MA

Rat MA EC sheets were isolated by using a modified Hank's balanced salt solution (HBSS) solution (**Table 17**) of following composition (in mM):

Table 17: The composition of HBSS for ECs isolation.

	Final conc. (mM)
$CaCl_2 \cdot 2H_2O$	1.26
$MgCl_2 \cdot 6H_2O$	0.49
$MgSO_4 \cdot 7H_2O$	0.41
KCl	5.33
KH_2PO4	0.44
NaCl	137.9
$Na_2HPO_4 \cdot 7H_2O$	0.34
NaHCO3	4.16
D-Glucose	5.55

After MAs were dissected under microscope, they were cut into 2-3 mm segments. These MA segments were transferred into enzymatic HBSS solution containing papain (0.2 mg/ml) and DTT (0.2 mg/ml) and incubated for 60 min at 37 °C. Then the vessels were gently triturated

using a fire-polished glass pipette to release the ECs in HBSS solution with BSA (2 mg/ml). The EC-containing solution was centrifuged for 3 min at 800 rpm, 4°C. The supernatant was removed and the ECs were resuspended in control HBSS buffer for immunocytochemistry.

3.3.2.3 Protocol to isolate endothelial cells from MA

The MAs were dissected in the same way of EC isolation. The SMCs were isolated using a dissociation medium (DM) as previously described (**Table 18**) [163]. The composition is as below:

Table 18: The composition of dissociation medium for SMCs isolation.

Salt (pH=7)	Final conc. (mM)
NaCl	110
KCl	5
$CaCl_2$	0.16
$MgCl_2$	2
HEPES	10
KH_2PO4	0.5
NaH_2PO_4	0.5
NaHCO3	10
Taurine	10
EDTA	0.5
D-Glucose	10
Phenol Red	0.03

The segments of MA were transferred into enzymatic DM containing 1.5 mg/mL papain. They were first incubated in ice for 0.5-1 h, then at 37°C for 6 min after addition of 1 mg/mL DTT. The vessels were then gently transferred into another tube containing 1.6 mg/ml collagenase and 1.6 mg/ml trypsin inhibitor in DM and incubated at 37°C for 4 min. Vessel segments were washed 3 times in DM containing 1 mg/mL BSA and gently triturated by pipette to release the SMCs. The SMC-containing solution was collected and centrifuged for 3 min at 800 rpm at 4°C. The supernatant was removed and the SMCs were resuspended in control DM for immunocytochemistry.

3.3.2.4 Isolation of ventricular myocytes from PDE2-transgenic mice

Mice were anesthetized by intraperitoneal injection of pentothal (150 mg/kg), then the heart was quickly removed and put into a cold Ca^{2+}-free Tyrode's solution as following **Table 19**:

Table 19: The composition of Ca^{2+}-free Tyrode's solution for ventricular myocytes isolation.

Salt (pH=7.4)	Final conc. (mM)
NaCl	113
KCl	4.7
$MgSO_4 \cdot 7H_2O$	1.2
HEPES	10
KH_2PO4	0.6
NaH_2PO_4	0.6
NaHCO3	1.6
Taurine	30
D-Glucose	20

The ascending aorta was cannulated, and the heart was subsequently perfused with oxygenated Ca^{2+}-free Tyrode's solution at 37°C for 4 minutes using retrograde Langendorff perfusion system. Then dissociate the myocytes by enzymatic dissociation. First, the heart was perfused with Ca^{2+}-free Tyrode's solution containing LiberaseTM Research Grade (Roche Diagnostics) for 10 minutes at 37°C. Then the heart was took off and placed into a dish containing Tyrode's solution with 0.2 mmol/L $CaCl_2$ and 5 mg/ml BSA. The atria was removed and the ventricle was cut into small pieces, and triturated by a pipette to disperse the myocytes. Ventricular myocytes were filtered on gauze and sedimented by gravity for 10 minutes. The supernatant was removed, and cells were suspended in Tyrode's solution with 0.5 mmol/L $CaCl_2$ and 5 mg/ml BSA. Then freshly isolated ventricular myocytes were plated in a 12-well plate, where a coverslip was in the bottom of well and was coated with laminin (10 μg/ml), and cultured in 37°C for 2 hours before using.

3.3.2.5 Protocol of Immunocytochemistry

The coverslips for ECs were incubated with Corning@ Cell-Tak adhesive (Sigma) to improve cell adhesion. Single drops around 50 μl of the cell suspension (ECs and SMCs) were added on glass coverslips. All of these cells, ECs, SMCs, and ventricular myocytes, were fixed with

paraformaldehyde 4% for 20 minutes. After washing with PBS for 3 times, the cells were permeabilized with Triton X-100 0.3% in PBS containing 0.2% BSA for 10 minutes, and quenched with NH_4Cl 50 mM in PBS for 30 minutes, and subsequently blocked with BSA 5% in PBS for 1h. Coverslips were then incubated overnight at 4°C with the following primary antibodies(**Table 20**).

Table 20: The primary antibody for immunocytochemistry experiment.

antibody	Company	host	dilution	For coverslip
PDE2A (101AP)	Fabgennix	rabbit	1/150	EC & SMC& ventricular myocytes
CD-31	Abcam	rabbit	1/50	EC & SMC
Calponin	Santa Cruz Biotechnology	rabbit	1/300	EC & SMC
Negative control	-	-	-	EC & SMC& ventricular myocytes

I removed the primary antibody and then incubated with secondary antibodies(anti-rabbit) for 1 h at room temperature (1:500, Alexa Fluor 488- or Alexa Fluor 647-conjugated; Invitrogen, Thermofisher Scientific, Les Ulis, France). The cells were viewed under a fluorescent microscope in inverted confocal laser scanning microscope Leica TCS SP8 (Leica Microsystems, Germany) with an HC PL APO CS2 63x/1.40 oil immersion objective. Sections stained by immunofluorescence were visualized using Leica SP8 LAS X software (Version 3.5.5; Leica Microsystems, Germany) and processed using the FIJI/ ImageJ software. Furthermore, Bright Field (BF) images were present to show relevant cell shape. Cells incubated with secondary antibody, without primary antibody, were included as negative controls.

3.3.3 cAMP -PDE activity assays

3.3.3.1 Principle of the radioenzymatic assay

Cyclic AMP/cGMP-PDE activity was measured according to a modification of the method described by Thompson and Appleman (Thompson and Appleman 1971[453]). In brief, [^{3}H]-

cAMP/[^{3}H]-cGMP is hydrolyzed into [^{3}H]5'AMP/[^{3}H]-5'GMP in the presence of PDEs. The exceed 5'-nucleotidase (snake venom from Crotalus atrox) catalyzes the hydrolysis of [^{3}H]-5'AMP/[^{3}H]-5'GMP into [^{3}H]-adenosine/[^{3}H]-guanosine, respectively. [^{3}H]-adenosine/[^{3}H] guanosine is then separated from [^{3}H]-cAMP/[^{3}H]-cGMP by an anion-exchange resin column which retains [^{3}H]-cAMP/[^{3}H]-cGMP but releases [^{3}H]-adenosine/[^{3}H]-guanosine. Therefore, the quantified [^{3}H]-adenosine/[^{3}H]-guanosine in the eluate reflects the hydrolytic activity of PDEs in the cell or tissue lysate.

3.3.3.2 Preparation of the proteins for PDE activity assays

The protocols of protein extraction and concentration assay(BCA) are the same as previous described for western blot. But the lysis buffer (Table 20) is different from western blot, here we used the buffer as following illustrated.

Table 21: The lysis buffer for PDE activity assay.

Reagents	**Final conc.**
NaCl	150 mM
Hepes (PH 7.4)	20 mM
EDTA	2 mM
Glycerol	10%
NP40	0.5%
Protease and Phosphatase Inhibitor Cocktail (100X) (Thermo Scientific™)	1X
H_2O	Add to target volume

3.3.3.3 Preparation of other necessary buffers or products

Table 22: Incubation Mix for PDE activity assay.

Reagents	**Final concentration**
Tris-HCl (PH=8)	40 mM
β-mercaptoethanol (β-ME)	20 mM
$MgCl_2$	40 mM
cAMP	4μM
[^{3}H]-cAMP(Perkin Elmer, Waltham, MA, USA)	420 cpm
H_2O	Add to target volume

Table 23: Tris-BSA for PDE activity assay.

Reagents	Final concentration
Tris-HCl (PH=8)	40 mM
BSA	0,1%
H_2O	Add to target volume

(1) Snake Venom: 1mg/ml in H_2O (store at -20°C)

(2) Resin:

- Add 100g resin into 300ml distilled H_2O ;
- Stir for 100 min, allow resin to settle, take off the water, and repeat more than 2 times;
- Finally for 100g resin, add 400ml distilled H_2O, and store at 4°C.

(3) PDE inhibitors:

Table 24: PDEs inhibitors used for PDE activity assay.

Reagents	solvent	Stock concentration
BAY-60-7750	DMSO	10^{-2} M
Cilostamide	DMSO	10^{-2} M
Ro-20-1724	DMSO	$5*10^{-2}$ M
IBMX	DMSO	10^{-2} M

3.3.3.3 PDE activity assay

Keep everything in ice, and prepare following tubes, each condition in duplicate:

Table 25: Prepare samples for PDE activity assay.

Blank condition	Sample condition
100 µL Tris-BSA	100 µL samples in Tris-BSA
50 µL Ctrl (0.1% DMSO in H_2O)	50 µL Ctrl or PDE inhibitors
50 µL Incubation mix	50 µL Incubation mix

Table 26: The concentrations of PDE inhibitors in cAMP-PDE activity assay.

BAY-60-7750	0.1 µM
Cilostamide	1 µM
Ro-20-1724	10 µM
IBMX	1 mM

Vortex these tubes immediately and incubate for 20min in 33 °C water bath to reaction and put back the tubes in ice immediately after reaction. This step allows PDEs hydrolyse cAMP into 5'-cAMP. Then stop the reaction by denaturing the enzymes using boiling water for 1 min. The reaction product, 5'-AMP, was then hydrolysed into adenosine by incubating the reaction mixture with 50 µg of snake venom (Crotalus atrox, Sigma Aldrich, Saint-Quentin Fallavier, France) for 20 min at 33°C. Then the resulting adenosine was separated by anion exchange chromatography using AG1-X8 resin (BioRad, Hercules, CA, USA) which makes non-hydrolyzed 5′-AMP retain in the resin. The adenosine was then eluted in vials and the activity assay was carried out in the presence of a scintillation liquid using a scintillation β-counter. Another series of tubes was prepared, which were the same as blank tubes but not went through the anion exchange resin columns. These tubes will be used to calculate the "total radioactivity".

The blank value is subtracted from each measurement performed since it's not produced by the hydrolysis of PDE, and theoretically this value is close to zero. The amount of protein used in this assay was determined by the percentage of hydrolysis of the nucleotide in the absence of PDE inhibitor, which should be less than 15% according to the calculation: % hydrolysis = [(X-blank) / Total radioactivity - blank) × 100], and the X indicates radioactivity of the eluent of the control sample. This percentage of hydrolysis makes it possible to ensure that the reaction takes place under optimum conditions and exerts the linearity of the reaction. The original data of percentage of hydrolysis from different tubes uses the same formula as here. The X indicates radioactivity of the eluent of the experimental or control sample.

3.3.3.4 Results analysis

Each experimental condition was performed in duplicate during the same experiment to limit variability. The enzymatic activity is calculated according to the following formula:

Enzyme activity (pmol/min/mg)= [(% hydrolysis x amount of cAMP) / (time of incubation x amount of protein].

The results are expressed as % of residual hydrolysis activity observed in the presence of PDEs inhibitor. The hydrolytic activity of PDEs in different conditions are expressed as a percentage

of the total cAMP-PDE activity in the absence of any pharmacological drug. The results are expressed as the mean ± SEM. The number of data for each of the groups is denoted by N, indicating the number of experiments animals, therefore 5 rats in every group.

3.3.4 Real-time quantitative PCR

Most of protocols are same as previously described, except for that detection of *Pde2a* and *Pde4c* were carried out using SYBR Premix (Takara Bio Europe, Saint-Germain-en-Laye, France) and detection of other genes using SYBR Supermix (Bio-Rad), which include *Pde3a*, *Pde3b*, *Pde4a*, *Pde4b* and *Pde4d* detection. *Ywhaz*, *Rpl32* and *Rplp2* were generally used as reference genes, except for *Pde2a* and *Pde4c* where *Tbp* substituted for *Rplp2.* Sequences of the primers are listed in **Table 27**.

Table 27: Sequences of the primers used in MA project.

Target	Forward 5'→3', Reverse 5'→3'	Product size (bp)	Annealing temperature	Accession number
Pde2a	CTGTGCTGGCTGCACTCTAC GAGGATAGCAATGGCCTGAG	77	60,0°C 20s	NM_001143847
Pde3a	ACCTCCCTGCCCTGCATAC CCTCTCTTGTGGTCCCATTC	65	60,0°C 20s	NM_017337
Pde3b	GTGGCTACAAATGCACCTCA GTGGCTACAAATGCACCTCA	100	60,0°C 20s	NM_017229
Pde4a	CGTCAGTGCTGCGACAGTC CCAGCGTACTCCGACACACA	190	60,0°C 20s	NM_ 013101
Pde4b	GATGAGCAGATCAGGGAACC GATGGGATTTCCACATCGTT	81	60,0°C 20s	NM_017031
Pde4c	GACCCTGTCCTTCCTGTTGA AACCGTCTCAGGATCACACC	99	60,0°C 20s	XM_214325
Pde4c	GCCAGCCTTCGAACTGTAAG ATGGATGGTTGGTTGCACAT	98	60,0°C 20s	NM_001113328

Ywhaz	AGACGGAAGGTGCTGAGAAA GAA GCATTGGGGATCAAGAA	127	60,0°C	20s	NM_013011
Tbp	AAAGACCATTGCACTTCGTG GCTCCTGTGCACACCATTTT	132	60,0°C	20s	NM_001004198
Rplp2	GCTGTGGCTGTTTCTGCTG ATGTCGTCATCCGACTCCTC	119	60,0°C	20s	NM_001030021
Rpl32 *Rpl32*	GCTGCTGATGTGCAACAAA GGGATTGGTGACTCTGATGG	115	60,0°C	20s	NM_013226

3.4 Project 3: The role of PKA RI in aorta

3.4.1 Animals

All protocols involving animals followed the European Community guiding principles in the care and use of animals (2010/63/EU) and complied with French institution's application decrees for animal care and handling. The *PRKAR1A* point mutation (translating in R368X) knock-in (KI) mice were generated on a C57Bl/6J genetic background by GenOway (Lyon, France) and kept on same genetic background as described in Le Stunff et al[454]. All experiments were performed in adult wide-type(WT, $RI\alpha^{+/+}$) and heterozygous mutant mice (KI, $RI\alpha^{R368X/+}$) mice aged 10-20 weeks. Genotype of mouse pups was confirmed by PCR assay. To avoid potential confounding effects due to hormonal variations, only males were used in this study.

3.4.2 Real-time quantitative PCR

All protocols are same as previous mentioned. The average Ct obtained in WT mice was used as a calibrator, and *Ywhaz*, *TBP* and *Rplp2* housekeeping gene were used as the reference for normalization. Sequences of the primers are provided in **Table 28**.

Table 28: Sequences of primers for PKA subunits, housekeeping genes as well as genotyping.

Target	Forward 5'→3', Reverse 5'→3';	Product size (bp)	Annealing temperature (°C)	Accession number
mouse primers				
Prkar1a	TGGAGAAGGAGGAGGCAAG	178	60,0°C 20s	NM_021880.2
	TTTCTAACGTAGGAGGCAGCA			
Prkar2a	GGGGAGAGTGACTCGGACT	155	60,0°C 20s	NM_008924.2
	TGCTCATCAGTTTTGGGATG			
Prkar1b	CGGTGTGAGTGCTGAAGTCT	134	60,0°C 20s	NM_001253890.1
	CGTCCAGGTGAGAAAAGAGC			
Prkar2b	AGAGGTTTCTGAACGCCTGA	181	60,0°C 20s	NM_011158.3
	TTCCACAGCTCCGTTCTCTT			
Prkaca	AGCACAAGGAGAGTGGGAAC	103	60,0°C 20s	NM_008854.5
	AGGATGCGCTTCTCATTCAG			
Prkacb	TCTGACAAAGCGATTCGGGA	113	60,0°C 20s	NM_011100.4
	ATGGAGCCTCAACCTTTCTCT			
Ywhaz	AGACGGAAGGTGCTGAGAAA	127	60,0°C 20s	NM_001356569.1
	GAAGCATTGGGGATCAAGAA			
Tbp	AAAGACCATTGCACTTCGTG	132	60,0°C 20s	NM_013684.3
	GCTCCTGTGCACACCATTTT			
Rplp2	GCTGTGGCTGTTTCTGCTG	119	60,0°C 20s	NM_026020.7
	ATGTCGTCATCCGACTCCTC			
genotyping primers				
73294cof-SHM1	ACTTTATTCAGTTAATAGATGAGCACAGACCAAGC			
73295cof-SHM1	AAAGAGACAGTAACGACTATCACCTATGGAAGC			

3.4.3 Immunoblot

Protocols are same with previous described. Here 20 μg protein was loaded, and separated in Novex™ WedgeWell™ 10% or 12%, Tris-Glycine (Invitrogen) polyacrylamide gels. The primary antibodies used were: RIα (Proteintech Europe), RIIα (BD Biosciences 612242), Cα(BD Biosciences 610981); rabbit anti-VASP (Cell signalling, 3112); rabbit anti-VASP-S157 (Cell signalling, 3111) and rabbit anti-GAPDH (Cell signalling) as internal reference.

3.4.4 PKA activity assay

Aorta tissue was lysed using the cell lysis buffer from PKA activity kit (Arbor Assays), and the protein concentration was determined by BCA method. 100 ng of protein was used to test PKA activity after stimulation by serial dilutions of 8-AHA-2-Cl-cAMP from 100 pM to 10 μM. This ligand is highly selective to the B domain of PKA RIα[455]. Assays were conducted in the presence of 300 μM IBMX and was performed following manufacturers' instructions by ELISA method. Absorbance was measured at 450 nm using a Microplate reader (BioRad). PKA activity (U/L) was calculated with an internal calibration curve. The basal state in the absence of 8-AHA-2-Cl-cAMP stimulation was added to evaluate basal PKA activity of aorta. Another condition with PKA inhibitor (PKI 10 μM, fragment 6-22 amide, Sigma) and 100 μM 8-AHA-2-Cl-cAMP was added to validate that signal could be ascribed to endogenous PKA activity.

3.4.5 Vascular reactivity

The protocol of this experiment is same as previous described. Since aorta is larger than pulmonary artery, so in this project aorta rings were mounted using 40 μm tungsten wire, and vessel rings were eventually set as 90% internal circumference (IC90) when vessels were submitted to 100 mmHg (13.3 kPa) transmural pressure. Contractile response to KCl, PE and U46619 were tested and were expressed in percent of the contraction evoked by K60. Various vasorelaxant responses were studied, namely to Ach (muscarinic receptor agonist, endothelial-dependent relaxation), ISO (β-adrenergic receptor agonist) and L858051 (direct broad AC activation). All vessels relaxant responses were studied upon precontraction produced by PE.

Relaxant responses were expressed as percentage of relaxant amplitude relative to the amplitude of the contraction obtained with PE.

3.5 Statistics

All results are expressed as mean ± SEM and were analyzed using the GraphPad Prism software (GraphPad software, Inc., La Jolla, CA, USA). Normal distribution was tested by the Shapiro-Wilk normality test. For simple two-group comparison, we used an unpaired Student t-test or Welch t-test when the data did not follow a normal distribution. Two-way ANOVA (ordinary or repeated measurements) with Holm Sidak's post-hoc test was used in vascular reactivity and comparing 4 groups data with 2 variables. N represents number of mice or number of samples. P-value<0.05 was considered statistically significant.

4. Results

4.1 Project 1: The role of PDE9 in pulmonary artery hypertension

4.1.1 Original Research article

The results of this work will be presented as a "ready-to-submit" manuscript (**ARTICLE #1**), entitled:

"**PDE9 controls pulmonary arterial tone but does not influence chronic hypoxia-induced pulmonary hypertension in mouse**",

by the following authors:

Liting Wang[1], Liang Zhang[1], Audrey Varin[1], Zhi-Cheng Jing[2], Rodolphe Fischmeister[1], Fabrice Antigny[3], Frédéric Perros[3], Véronique Leblais[1], Boris Manoury[1].

[1]Université Paris-Saclay, Inserm, UMR-S 1180, 17, avenue des Sciences 91400 Orsay, France.

[2]Key Lab of Pulmonary Vascular Medicine, Peking Union Medical College Hospital

Chinese Academy Medical Sciences and Peking Union Medical college, Beijing, China

[3]Université Paris-Saclay, Inserm, UMR-S 999, 92350, Le Plessis-Robinson, France.

PDE9 controls pulmonary arterial tone but does not influence chronic hypoxia-induced pulmonary hypertension in mouse.

Authors: Liting Wang[1], Liang Zhang[1], Audrey Varin[1], Zhi-Cheng Jing[2], Rodolphe Fischmeister[1], Fabrice Antigny[3], Frédéric Perros[3], Véronique Leblais[1], Boris Manoury[1].

[1]Université Paris-Saclay, Inserm, UMR-S 1180, 17, avenue des Sciences 91400 Orsay, France.

[2]Key Lab of Pulmonary Vascular Medicine, Peking Union Medical College Hospital Chinese Academy Medical Sciences and Peking Union Medical college, Beijing, China

[3]Université Paris-Saclay, Inserm, UMR-S 999, 92350, Le Plessis-Robinson, France.

Correspondence to: Boris Manoury, Université Paris-Saclay, Inserm, UMR-S 1180, 17, avenue des Sciences 91400 Orsay, France.

E-mail: boris.manoury@universite-paris-saclay.fr;

Tel: +33-1-80-00-62-90

Data availability statement

Data available on request from the authors. The data that support the findings of this study are available from the corresponding author upon reasonable request. Some data may not be made available because of privacy or ethical restrictions.

Acknowledgements

We thank Pauline Robert and the staff from animal core facility for efficient animal care (IPSIT, Université Paris-Saclay, Châtenay-Malabry, France). This work was funded by the Grant ANR-10-LABX-33 as member of the Laboratory of Excellence LERMIT and ANR13BSV10003-02. L.W was supported by the China Scholarship Council (PhD fellowship) and by a grant from Pr Zhi-Cheng Jing (Peking Union Medical College Hospital, Chinese Academy of Medical Sciences and Peking Union Medical College, Beijing, China). A travel grant was allowed to B.M. by the Xu Guangqi program 2019 (Campus France).

Abstract

Introduction:

PDE9 is a phosphodiesterase which has recently emerged as a regulator of cGMP in cardiac and vascular myocytes. By contrast with PDE5, however, its contribution in vasculature is unclear.

Objective:

We sought to investigate PDE9 expression and function in mouse pulmonary artery by comparing wild type (WT) and PDE9-deficient (*Pde9a*$^{-/-}$) mice. We also addressed the hypothesis that PDE9 could represent a new therapeutic target to treat pulmonary arterial hypertension, a severe, deadly disease.

Methods and Results:

Immunoblots and RT-PCR showed that PDE9 is expressed in human and mouse pulmonary arteries, respectively. Pulmonary artery segments isolated from *Pde9a*$^{-/-}$ mice, mounted on a wire myograph and contracted with phenylephrine displayed more potent relaxant responses to acetylcholine, the NO donor diethylamine NONOate and to atrial natriuretic peptide than vessels from WT animals. Following a challenge with 21-day, 10% O_2-hypoxia, *Pde9a* expression was increased in lung and right ventricle from WT mice. In this model, PDE9 deficiency failed to ameliorate pulmonary hypertension criteria, namely invasive right ventricular systolic pressure and echocardiographic pulmonary arterial acceleration time. Right ventricle hypertrophy and dysfunction, reflected by the Fulton index, echocardiographic TAPSE, right ventricle free wall thickness and increase in fetal gene expression, were similar between *Pde9a*$^{-/-}$ and WT groups.

Conclusion:

We show that PDE9 is expressed in PA and intervenes in relaxant responses mediated by the cGMP pathway. The ablation of *Pde9a* in mouse, however, does not prevent the development of pulmonary hypertension in a chronic hypoxia model, nor does it attenuate right ventricle deleterious remodeling.

Key words

Phosphodiesterase type-9 (PDE9), vascular reactivity, pulmonary arterial hypertension (PAH), right ventricle hypertrophy (RVH)

Abbreviations

PAH: Pulmonary arterial hypertension; PA: pulmonary artery; NO: nitric oxide; CN: cyclic nucleotides; cGMP: cyclic guanosine-3', 5'- monophosphate; cAMP: cyclic adenosine-3', 5'-monophosphate; sGC: soluble guanylate cyclase; PDEs: Phosphodiesterases; PASMCs: pulmonary artery smooth muscle cells; NOS: Nitric oxide synthase; PE: Phenylephrine; Ach: Acetylcholine; rANP: rat atrial natriuretic peptide; CNP: C-type natriuretic peptide; EC: endothelial cells; WT: wide-type; KO: Knockout; NP: natriuretic peptides; CH: chronic hypoxia; TTE: Trans-thoracic echocardiography; EF: ejection fraction; PAAT: pulmonary artery acceleration time; PET: pulmonary ejection time; TAPSE: tricuspid annular plane systolic excursion; RVFWT: right ventricular free wall thickness; RV: right ventricle; LV: left ventricle; RVSP: right ventricular systolic pressure; PH: pulmonary hypertension; RVH: right ventricle hypertrophy.

1. Introduction

Pulmonary arterial hypertension (PAH) is a chronic, fatal disease characterized by increased mean pulmonary artery pressure (mPAP) >20 mmHg, pulmonary artery wedge pressure ⩽15 mmHg and elevated pulmonary vascular resistance >3 Wood Units[1]. The main pathological feature of PAH is progressive remodeling of the pulmonary vasculature[2, 3] which increases the pulmonary vascular resistance and ultimately results in right ventricular failure and premature death[4-6]. Current therapies aiming at rescuing some of the abnormal vascular signaling associated with PAH, despite relieving the symptoms, remain insufficient to tackle this disorder[7, 8].

Medications that enhance the signaling pathways mediated by the intracellular second messenger guanosine-3',5'-monophosphate (cGMP) are currently pivotal to PAH management. Stimulated either by nitric oxide (NO) or natriuretic peptides (NP), cGMP launches vasodilation action and also have salutary actions on pulmonary vascular remodeling, fibrosis, and right ventricular function[9, 10]. Enhancing cGMP signaling can be achieved by soluble guanylate cyclase (sGC) stimulators[11] or via the reduction of cGMP degradation by inhibitors[12]. Phosphodiesterases (PDEs) represent the main route to rapidly decrease intracellular cGMP concentrations[13, 14]. As such, several cGMP-PDEs have been subjected to preclinical examination for their implication in PAH pathophysiology[15-17], although only inhibitors against the PDE type-5 (PDE5) isoenzyme have been clinically approved[18, 19]. Nevertheless, the PDE type-9 enzyme (PDE9) has received little attention in the setting of PAH, despite being a cGMP-specific PDE displaying a 40-time higher affinity for cGMP than PDE5[20-22]. PDE9 is coded by a single gene, *PDE9A*, which was reported to encompass more than 21 splice variants possibly displaying differential subcellular localizations and properties[23, 24]. PDE9 is ubiquitously distributed and highly expressed in brain, kidney, spleen, and relative lower levels are found in the lung[20-22] and the heart[21, 22, 25]. While and important role for PDE9 as a regulator of cardiac left ventricle deleterious remodeling in heart failure has emerged[25, 26], reports accounting for expression of PDE9 invasculature are scarce. PDE9 was only mentioned to be expressed at the mRNA level in fetal rat and human PA smooth muscle cells (PASMC)[16, 27]. PDE9 inhibition was also proposed to decrease leucocyte adhesion in arterioles[28].

To date, several selective PDE9 inhibitors have been well characterized and mainly under investigation for the rescue of cognitive function[29-32]. Pharmacological intervention has help decipher the contribution of PDE9 to compartmentalization of cGMP signaling in the cardiovascular system. In the cardiac myocyte, PDE9 was shown to selectively mitigate natriuretic peptide-triggered cGMP antihypertrophic signaling, as opposed to PDE5 that segregates to NO-dependent signaling[25] . This paradigm seems to be at odds with data obtained in the vascular system, as Zhang et al. suggested that PDE9 selectively regulates NO-related cGMP levels in cultured rat aorta smooth muscle cells[33].

Until recently, roles of PDE9 in the pulmonary circulation and in the right heart had not been documented. Therefore, we hypothesize that PDE9 family may play a relevant role in tuning pulmonary vascular tone and participate in the progressive development of PAH. Recently, a report concluded that *Pde9a* deficiency did not protect from experimental PAH[34]. Despite these data, physiological role of PDE9 in regulating vascular tone and right ventricle (RV) function remain largely unexplored.

In this study, both pharmacological and *Pde9a*-deficient mouse ($Pde9a^{-/-}$) were used to explore the specific contribution of PDE9 in normal pulmonary vascular reactivity. Furthermore, we conducted an independent exploration of the PAH phenotype of $Pde9a^{-/-}$ and $Pde9a^{+/+}$ mice search for any hint linked to cardiopulmonary pathophysiology.

2. Materials and methods

2.1 Materials

Phenylephrine (PE), Acetylcholine (Ach), rat atrial natriuretic peptide (rANP), C-type natriuretic peptide (CNP), PDE5 inhibitor-Sildenafil, and PDE9 inhibitors-BAY-73 6691[32] and PF-04447943[31] were purchased from Sigma Aldrich. Nitric oxide synthase (NOS) inhibitor, L-NAME and NO donor, diethylamine NONOate (DEA-NO) were bought from Enzo life science (Villeurbanne, France). U46619 was obtained from Cayman Chemical.

2.2 Animals and PAH model

All protocols involving animals followed the European Community guiding principles in the

care and use of animals (2010/63/EU) and complied with French institution's application decrees for animal care and handling (APAFIS authorization No. C9201901). Animal housing and procedures were carried out in our animal facility and laboratory at *Université Paris-Saclay, Faculté de Pharmacie*, (Authorizations No. C92-019-01, 03 August 2016).

Pde9a global knockout (*Pde9a*$^{-/-}$, KO) mice were generated by Pfizer Inc. with C57BL6/J background as described in Lee et al [25]. A colony was bred in our animal facility, starting from 2 heterozygote couples that were kindly provided by Pr. David Kass' group (Johns Hopkins University School of Medicine, Baltimore, MD, USA). Homozygous animals (*Pde9a*$^{+/+}$ and *Pde9a*$^{-/-}$) animals were littermates obtained after breeding heterozygous *Pde9a*$^{+/-}$ male and females. The strain was maintained in C57BL/J background by backcrossing with wild-type animals obtained from Janvier Labs (Le Genêst St-Isle, France).

For induction of the PAH model, 8-14 week-old male *Pde9*$^{-/-}$ and *Pde9*$^{+/+}$ mice were placed in a normobaric, hypoxic (10 % O_2) chamber for 21 days[35]. Age-matched normoxia-exposed control mice were placed in the same room for 3 weeks with room air. Mice were killed by exsanguination under deep anesthesia under isoflurane (5 % - 3L/min).

Other 8-17-week-old mice that had not been submitted to any specific constraints were sacrificed by cerebral dislocation.

2.3 Human samples

Biological resources from patients were obtained from patients part of the French Network on Pulmonary Hypertension, a program approved by our institutional Ethics Committee (2008), and gave written informed consent (Protocol N8CO-08- 003, ID RCB: 2008-A00485-50). Human pulmonary arteries were obtained during lung transplantation from patients with PAH and during lobectomy or pneumonectomy for localized lung cancer from non-PAH subjects as control samples.

2.4 Echocardiographic measurement

Trans-thoracic echocardiography was performed using a high-frequency, high-resolution digital imaging platform (Vevo 3100, FUJIFILM VisualSonics, Toronto, Canada). By using a

ultra-high frequency linear array transducer (MS550D, frequency range 25-55MHz), some parameters of mice cardiovascular function can be assessed. Ejection fraction (EF) was assessed by using the parasternal long axis view with M-mode. Then the transducer position was adjusted to modified parasternal long-axis view of RV and PA to obtain pulmonary artery acceleration time (PAAT) and pulmonary ejection time (PET) data by using the pulse-wave (PW) doppler mode. Right ventricular free wall thickness (RVFWT) was also assessed in this view in end diastole. To evaluate the RV function, the tricuspid annular plane systolic excursion (TAPSE) was measured in the apical 4-chamber view with M mode.

2.5 Hemodynamic measurements

Mice were placed under general anesthesia and spontaneous breathing with an isoflurane rodent anesthesia system (Minerve, Esternay, France) (maintenance: isoflurane 2%-3% in room air at 1,5 L/min) in the supine position. The upper abdomen was opened to expose the diaphragm. A needle (gauge 21G) , connected to a Millar pressure transducer as a probe was inserted through the diaphragm and into the RV to assess the right ventricular systolic pressure (RVSP). Hemodynamic measurements were recorded with a PowerLab 4/35 data-acquisition system and analyzed with LabChart software (AD Instruments, Oxford, UK).

2.6 Right ventricular weight measurement and tissue harvest

Following sacrifice of mice , the lungs and heart were quickly isolated and used for various procedures or frozen in liquid nitrogen and stored at -80°C for further biochemical analysis.

Lung to be dissected for PA isolation were placed in an ice-cold “Krebs” solution of following composition (in mM): NaCl 119, KCl 4.7, $CaCl_2$ 2.5, $MgSO_4$ 1.2, KH_2PO_4 1.2, glucose 11, $NaHCO_3$ 25, bubbled with 95% O_2 and 5% CO_2 to maintain pH at 7.4.

Mouse heart was harvested, then RV wall was dissected out from the left ventricle (LV) and septum (S). The weight ratio of RV over (LV+ S) (RV / LV+S) was calculated as the Fulton’s index to evaluate RV hypertrophy (RVH).

2.7 Vascular reactivity

Following lung isolation, PA were carefully dissected out in cold Krebs solution, cut into 2 mm segments and used for isometric tension measurement. Each vessel was mounted in a one of

the chamber of a small vessel myograph (DMT620M, Danish Myo Technology A/S, Aarhus, Denmark) using a 25 µm tungsten wire, as previously described [36, 37]. Chambers were filled with Krebs solution, bubbled with 95% O_2 - 5% CO_2 mixture and maintained at 37 ± 0.2 °C. Data were digitized using a Powerlab 8/30 (AD Instruments, Paris, France) and acquired using the Labchart7 software (AD Instruments). Vessels underwent a normalization procedure by stepwise stretch increments to construct tension-circumference relationship. Vessel segments were eventually set at a transmural pressure of 25 mmHg (3.33 kPa). After an equilibration period of 20-30 min, contractile capacity of the vessels was evaluated by a challenge with a modified Krebs solution containing 60 mM KCl (K60) with equimolar substitution of NaCl. Vessels with a response less than 0.5 mN/mm were excluded from analysis due to potential damage. Relaxant effect induced by 10 µM Acetylcholine (Ach) was tested after K60 induced-contraction. After a series of 3 washes with Krebs solution, vessels were submitted to various pharmacological protocols.

The contractile stimuli included various solutions with various KCl amounts (depolarizing solution), U46619 (thromboxane A2 mimetic, TP receptor agonist) and phenylephrine (PE, α_1-adrenergic receptor agonist). Contractile responses were expressed as percent, relative to the amplitude of the contraction obtained with K60. Concentration-response relationship was obtained by adding increasing amount of agent in a cumulative manner.

Relaxant responses to cGMP-elevating agents, namely Ach, DEANO, rANP and CNP, were studied. Ach was added on vessels precontracted by PE used at EC_{80} (130 nM). The responses to DEANO, rANP and CNP were tested in the presence of L-NAME (NO synthase inhibitor, 300 µM), in order to inhibit any endogenous cGMP generation stimulated by constitutive NO production. L-NAME was added 20 minutes before treatment with PE (50 nM) to evoke contraction.

The relaxant effects of PDE5 inhibitor Sildenafil and to PDE9 pharmacological inhibitors PF-04447943 and BAY-73-6691 were studied on PE-contracted PA. Relaxant responses were expressed as percentage relative to the amplitude of the contraction obtained with PE.

2.8 Real-time quantitative PCR

Total RNA was extracted using Trizol reagent (MRCgene). Reverse transcription of RNA samples was carried out by using iScript cDNA synthesis kit (Bio-Rad) according to manufacturer's instructions. Real-time quantitative PCR (RT-qPCR) was performed using the SsoAdvanced™ Universal SYBR Green Supermix (Sso Mix, Bio-Rad) on a CFX384 TouchTM Real-Time PCR Detection System (Bio-Rad, Marnes-la-Coquette, France). A standard curve was constructed according to serial dilution of cDNA to determine efficiency (E). *Ywhaz*, *TBP* and *Rplp2* were used as reference genes for normalization. Sequences of the primers are provided in Supplemental Table 1.

2.9 Western blot

Proteins were extracted from human or mouse tissue lysates and concentration was measured by the BCA method. 30 μg protein were loaded, and separated in Novex™ WedgeWell™ 4-20%, Tris-Glycine (Invitrogen) gel and subsequently transferred onto PVDF membranes. After blocking the membranes with 5% milk buffer for 1 h, the incubation with one of the following primary antibodies was carried out over night at 4°C : custom rabbit anti-PDE9A polyclonal antibody (13128-5, a kind gift from L. Jaffe, UConn Health)[38]; rabbit anti-PDE5A and rabbit anti-PDE5A-phospho (kind gifts from J. Beavo, University of Washington)[39]; rabbit anti-VASP (Cell signalling, #3112); rabbit anti-VASP-S239 (Cell signalling, #3114) and rabbit anti-GAPDH (Cell signalling) as internal reference. After incubation with appropriate secondary antibodies for 1 h, proteins were visualized by enhanced chemiluminescence and quantified with Quantity One software.

2.10 Statistics

Statistical analyses were performed using the GraphPad Prism 9.0 software (GraphPad software, Inc., La Jolla, CA, USA). All the data are expressed as mean ± SEM, and the N stands for the number of animals used in each group unless otherwise specified. For *Pde9* mRNA expressed in pulmonary artery and airway, each sample contains tissues at least from 3 mice. For two-group analysis, unpaired student t-test or Mann-Whitney were used if the data were or were not normally distributed, respectively. For vascular concentration-response relationships (CRC), 2-way ANOVA with repeated measures followed by Holm Sidak's post hoc test were performed. For each vessel, the CRCs obtained for each vessel were individually fitted with the Hill

equation and pharmacological parameters, namely pD2 (equal to -LogEC_{50}) and maximal effect (Emax), were obtained. Data obtained from PAH models were analysed by using 2-way ANOVA with genotype (*Pde9a*$^{+/+}$ vs. *Pde9a*$^{-/-}$) and intervention (chronic hypoxia vs normoxia) as variables to analyze among 4 groups. $P<0.05$ was regarded to be statistically significant.

3. Results

3.1 PDE9 is expressed in human pulmonary arteries (hPA) and multiple mouse tissues

Because data on vascular expression was scarce, we searched for PDE9 expression in hPA. Immunoblot against PDE9 protein yielded a signal at ≈ 60 kDa, matching the expected size for PDE9A6/13 proteins[23, 24]. *Pde9a* transcripts were also detected in hPA samples and showed no significant alteration between PAH patients and control patients (Figure 1, A and B). In addition, PDE9 protein was expressed in lung tissues of rodents (Figure 1A). *Pde9a* mRNA was detected in intralobar PA and other tissues from mouse. *Pde9a* was highly expressed in mouse lung (Figures 1C, 1D), and in a minor extent in left ventricle, RV, and intralobar PA, while expression in airway was poor. Selectivity of the RT-PCR amplification was indicated by the absence of robust signal in samples from *Pde9a*$^{-/-}$ mice (Figures 1C, 1D). Also, a sharp reduction of the signal at ≈ 60 kDa for PDE9 protein was observed in lung samples from *Pde9a*$^{-/-}$ mice compared to *Pde9a*$^{+/+}$, residual signal being caused by the presence of one among many non-specific band obtained with this antibody[38]. Transcripts for other cGMP-hydrolyzing PDEs, including *Pde1a*, *Pde1b*, *Pde1c*, *Pde3a*, *Pde3b* and *Pde5a*, were not significantly altered in lung, PA and RV from *Pde9a*$^{-/-}$ mice compared with that of PDE9 WT mice. Transcript for *Pde2a* was not detected in mouse pulmonary arteries and did not show any difference in lung or RV (Supplementary Figure 1).

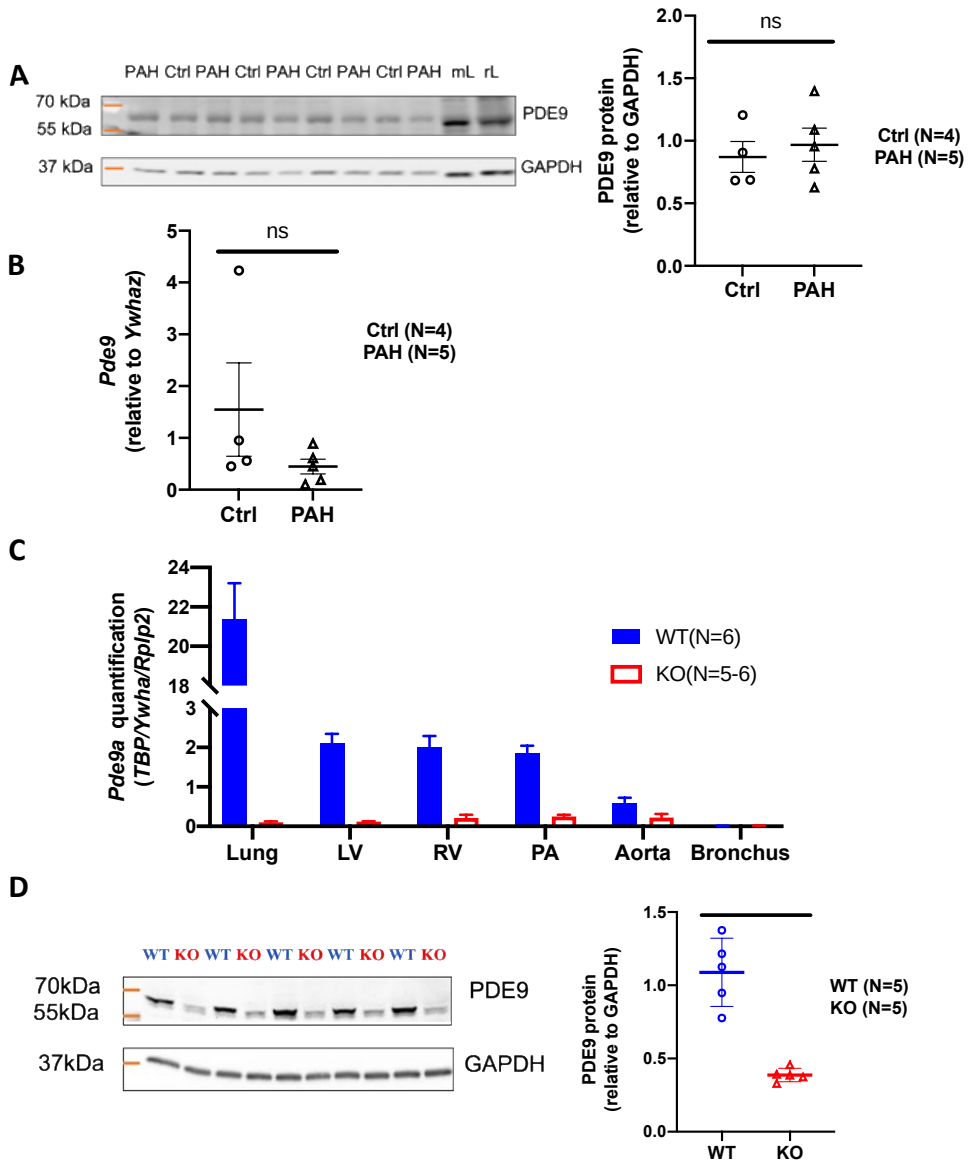

Figure 1. PDE9 expression in human pulmonary artery (hPA) and rodent tissues. **A, B**: PDE9 protein (**A**) and transcripts (**B**) expression was tested in hPA from control or PAH patients, and in mouse lung (mL) or rat lung (rL). **C:** *Pde9a* transcript level was tested in tissues from *Pde9*$^{+/+}$ (WT) and *Pde9*$^{-/-}$ (KO) mice. **D:** PDE9 protein expression in lung was detected in whole-lung homogenates from *Pde9*$^{+/+}$ (WT) and *Pde9*$^{-/-}$ (KO) mice. Left : immunoblot showing robust signal only in WT samples while a non-specific band with slightly lower molecular weight is present. Right : Quantification of the immunoblot signal.

Data are expressed as means ± SEM from N independent experiments. One PA sample includes tissues from at least 3 animals. Statistical analysis was performed by using t-test (**A**) and Mann Whitney test (**B, D**). NS, non-significant. ***P < 0.001.

3.2 Relaxant responses to cGMP-elevating stimuli are potentiated in PAs isolated from *Pde9a*$^{-/-}$ mice.

Mouse PA mounted on the myograph displayed ≈1 mN/mm contraction in response to a challenge with a depolarizing solution containing 60 mM [K^+] (Figure 2A). Basic endothelial functionality was assessed by addition of 10 µM Ach on vessels precontracted with K60, which produced a ≈ 10% relaxation (Figure 2B). No difference was observed between vessels isolated from *Pde9a*$^{-/-}$ or *Pde9a*$^{+/+}$ mice. Furthermore, responses to cumulative addition of [K^+], PE or U46619 were similar in both genotypes (Figure 2A, C, D and E).

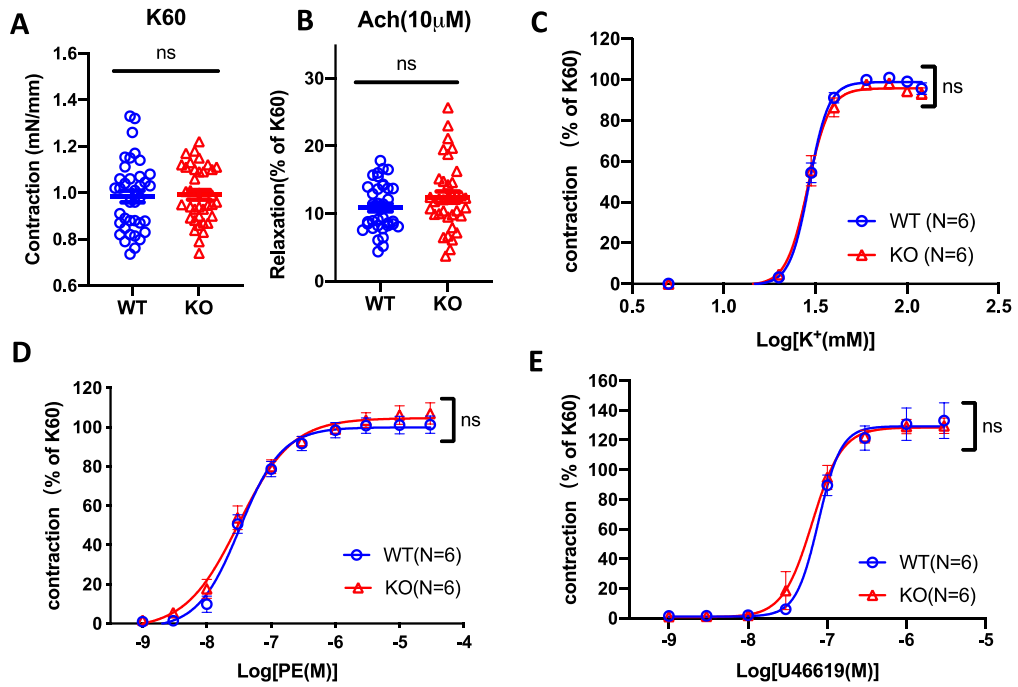

Figure 2. Evaluation of basic vascular reactivity and contractile concentration response in pulmonary artery isolated from *Pde9*$^{+/+}$ (WT) and *Pde9*$^{-/-}$ (KO) mice. **A:** Basic contractile response to 60 mM KCl (K60). **B:** Relaxant response to acetylcholine (Ach, 10 µM) in K60-contracted PA. **C-E:** Contractile-response curves to increasing concentrations of K^+ (**C**), phenylephrine (PE, α_1-adrenergic receptor agonist, **D**) and U46619 (thromboxane A2 mimetic, **E**). Data are expressed as mean ± SEM from N animals. Statistical analysis was performed using t-test (A-B) or 2-way-ANOVA with repeated measures (C-E). NS: not significant.

Because relaxant responses are generally attenuated when using a high K^+ solution as a precontraction stimulus[40], Ach response was further examined after contracting PAs with a submaximal concentration of the α1-adrenergic receptor agonist PE. Ach produced a concentration-dependent relaxation that was significantly stronger in *Pde9a*$^{-/-}$ PAs compared with PAs from *Pde9a*$^{+/+}$ littermates (P<0.0001, Figure 3A). Accordingly, the corresponding

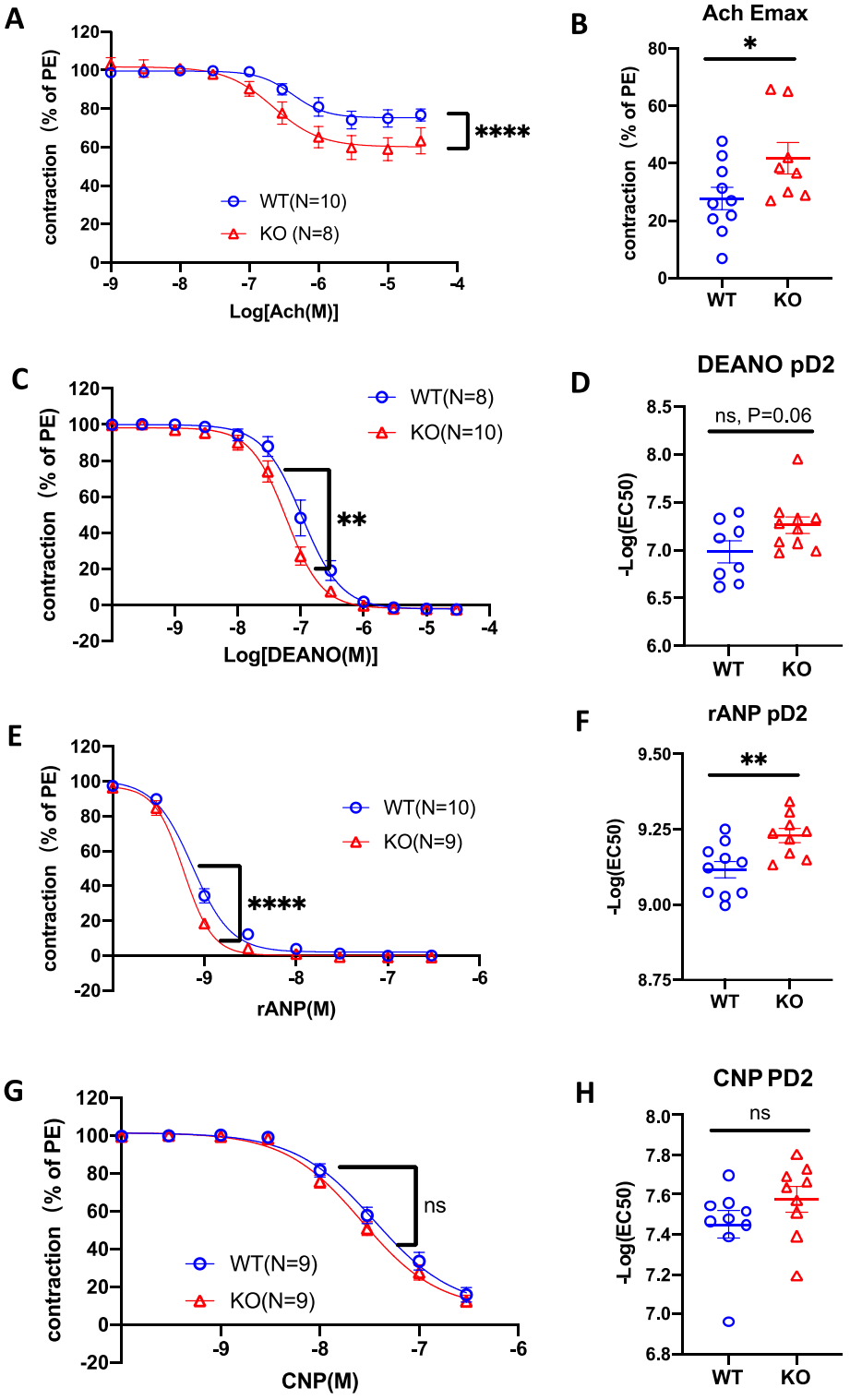

Figure 3. (caption is presented in next page).

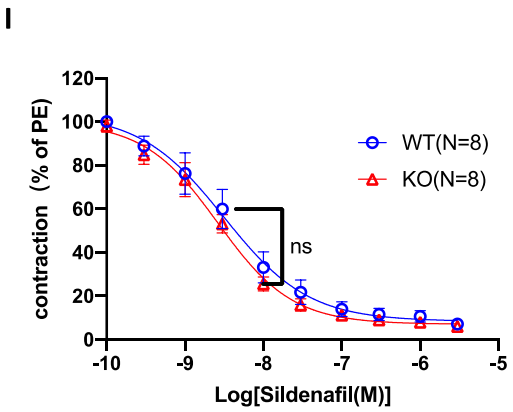

Figure 3 (continued). Relaxant responses to cGMP-elevating stimuli are potentiated in pulmonary artery isolated from *Pde9a*$^{-/-}$ mice. A, C, E, G, I: Concentration-relaxant response curves to acetylcholine (Ach, **A**), NO donor DEANO (**C**), rat atrial natriuretic peptide (rANP, **E**), C-type natriuretic peptide (CNP, **G**) and PDE5 inhibitor sildenafil (I) in pulmonary artery rings isolated from *Pde9*$^{+/+}$ (WT) and *Pde9*$^{-/-}$ (KO) mice. Vasodilators were added on vessels precontracted with phenylephrine. **B**: Maximum effect (Emax) of Ach responses in *Pde9*$^{+/+}$ (WT) and *Pde9*$^{-/-}$ (KO) mice. **D, F, H** show pD2 (-LogEC$_{50}$) values for DEANO, rANP and CNP responses, respectively. Data are expressed as mean ± SEM from N mice. Statistical analysis was performed using t-test with (**D**) or without (**F**, **H**) Welch's correction for 2-group comparisons, and using 2-way-ANOVA with repeated measures concentration response curves (**A**, **C**, **E** and **G**). NS: not-significant. * P < 0.05, **P < 0.01, ****P < 0.0001.

Emax was a higher in *Pde9a*$^{-/-}$ PAs (P<0.05, Figure 3B).

Main relaxant action of Ach is mediated by generation of endothelial NO that stimulates cGMP production in the underlying smooth muscle. To further confirm the role of PDE9 in NO-cGMP-dependent relaxant pathway, PE-precontracted PAs were stimulated by an exogenous NO donor, DEANO. These experiments were conducted in the presence of L-NAME, in order to rule out any influence of constitutive NO release by the endothelium. The results showed that relaxant effect of DEANO was more potent in *Pde9a*$^{-/-}$ PAs compared to *Pde9a*$^{+/+}$ PA (P<0.01, Figure 3C). pD2was slightly higher in *Pde9a*$^{-/-}$ PAs although not significantly different (P=0.056, Figure 3D).

Because cGMP can also be synthetized by particulate guanylate cyclases upon stimulation by endogenous, vasodilating, natriuretic peptides, we examined the responses to rANP and CNP, selective agonists for GC-A and GC-B receptors, respectively. We observed that rANP was a more potent vasodilator in *Pde9a*$^{-/-}$ PA compared to wild-type controls (P<0.001, Figure 3E), with a smaller higher pD2 (Figure 3F). Responses to CNP displayed a similar trend, although showed no significant difference (Figure 3G, 3H).

As PDE9 may compete with broadly expressed PDE5 for cGMP hydrolysis, we examined whether the relaxant action of PDE5 inhibitor sildenafil was potentiated by the absence of PDE9 in knockout animals. Sildenafil showed potent concentration-dependent relaxation that was similar in both genotypes (Figure 3I).

Taken together, these results indicate that deficiency in PDE9 potentiates both NO- and ANP-mediated vasodilating responses in mouse PA, indicating that the enzyme participates in hampering these tone-regulating pathways.

3.3 Vasorelaxant properties of PDE9 inhibitors

Because PAs isolated from PDE9-deficient mice are more prone to cGMP-mediated vasodilation, one would expect that PDE9 pharmacological inhibition oppose vascular tone. Therefore the relaxant effects of two PDE9 inhibitors, namely BAY 73-6691[32] and PF-04447943[30] were examined in isolated PAs precontracted with PE. Both BAY 73-6691 and PF-04447943 produced concentration-dependent relaxation in *Pde9a*$^{+/+}$ PAs at concentration > 30 nM and 100 nM, respectively (Figure 4, A and B). Yet, similar responses where observed in *Pde9a*$^{-/-}$. This indicates that vasorelaxant of both PDE9 inhibitors cannot be ascribed to selective inhibition of PDE9 activity, and point to an off-target effect.

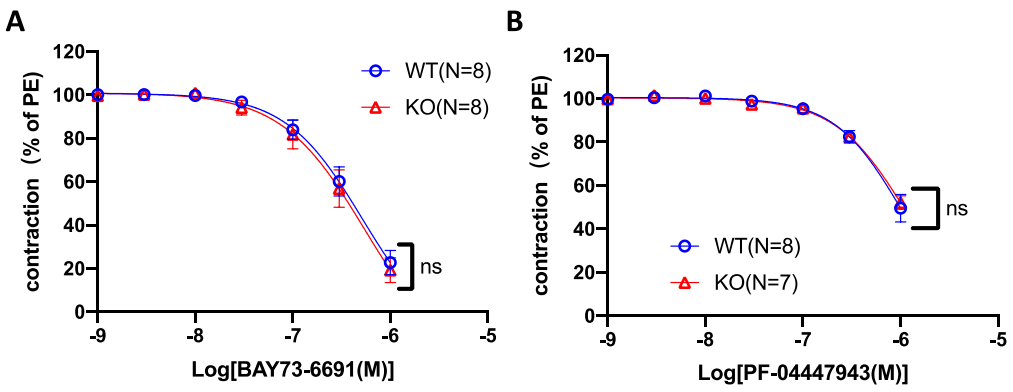

Figure 4. Concentration-relaxant responses to PDE9 inhibitors BAY73-6691 (A) and PF-04447943 (B) in pulmonary artery rings isolated from *Pde9*$^{+/+}$ (WT) and *Pde9*$^{-/-}$ (KO) mice. Data are expressed as mean ± SEM from N mice. Statistical analysis was performed using 2-way-ANOVA with repeated measures. NS, not significant.

In conclusion, despite displaying vasorelaxant properties, the pharmacological inhibitors tested could not discriminate both genotypes, and therefore show limited interest to pursue exploration

of PDE9 function in vasculature.

3.4 *Pde9a* genetic ablation did not have protective effect in chronic hypoxia induced pulmonary hypertension (CH-PH)

As PDE9 deficiency potentiated cGMP-related responses that are generally associated with beneficial effect in PAH, we hypothesized that *Pde9a*$^{-/-}$ would be protected against PAH induced by chronic exposure to hypoxia, a common experimental model of PAH. At baseline all parameters were similar between *Pde9a*$^{-/-}$ and *Pde9a*$^{+/+}$ mice, except body weight was smaller in knockout mice compared to age-matched wild-type littermates ($P<0.05$, Supplementary Table 2). Echocardiographic assessment confirmed that pulmonary artery acceleration time (PAAT) and PAAT / pulmonary ejection time (PET) ratio, a parameter of severity of PAH phenotype [41], were decreased by exposure to chronic hypoxia for 21 days (CHx) in *Pde9a*$^{+/+}$ mice compared to *Pde9a*$^{+/+}$ mice exposed to normoxia (Nx), indicating a decreased PA compliance (Figure 5, A and B). Accordingly, *Pde9a*$^{+/+}$ mice had significantly higher right ventricle systolic pressure in the CHx group than in the Nx group (Figure 5C). *Pde9a*$^{-/-}$ mice exposed to CHx displayed essentially similar changes as their wild-type littermates. TAPSE, an indicator for right ventricle systolic function[42], was reduced after hypoxia exposure ($P<0.01$, 2-WAY-ANOVA) but without any significant difference between genotypes (Supplementary figure 2B). Left ventricle ejection fraction was similar among all the groups and heart rate was increased by CHx in a similar fashion in both genotypes (Supplementary table 2).

Pde9a$^{+/+}$ and *Pde9a*$^{-/-}$ mice exposed to CHx both displayed a comparable increase in the Fulton index (Figure 5D) and in the right ventricle (RV) free wall thickness (Supplementary Figure 2) compared to Nx, indicating the presence of RV hypertrophy in CHx. The expressions of hypertrophy-related genes, such as *Nppb*, and *Myh-7*, in the RV were increased in the CHx group and did not differ between genotypes (Figure 6, A and B). *Nppa* mRNA expression in the RV was not significantly altered among four groups of mice (Figure 6C).

Overall, exposure to chronic hypoxia induced PAH characterized by elevated PA-related hemodynamics, RV hypertrophy and dysfunction, that was not influenced by the PDE9 deficiency.

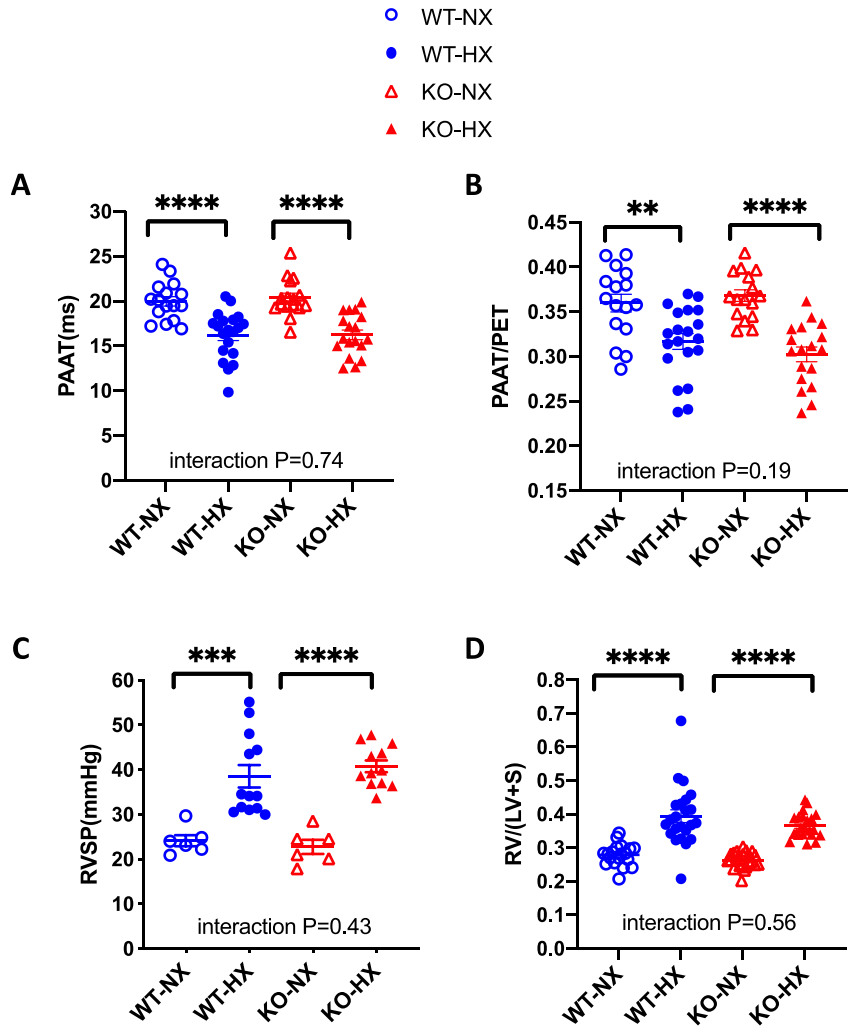

Figure 5. Phenotype of *Pde9*$^{+/+}$ (WT) and *Pde9*$^{-/-}$ (KO) mice submitted to chronic hypoxia (HX) or normoxia (NX) for 21 days. **A**: Pulmonary artery acceleration time (PAAT). **B**: PAAT over pulmonary ejection time (PET) ratio, PAAT/PET. **C**: Right ventricle systolic pressure (RVSP) **D**: Fulton index (right ventricle / (left ventricle + septum weight ratio, RV/(LV+S)). Data are expressed as mean ± SEM of N = 6-23mice. Statistical analysis was performed using 2-way-ANOVA followed by Holm-Sidak post test. **: P<0.01 ***: P<0.001, ****: P<0.0001.

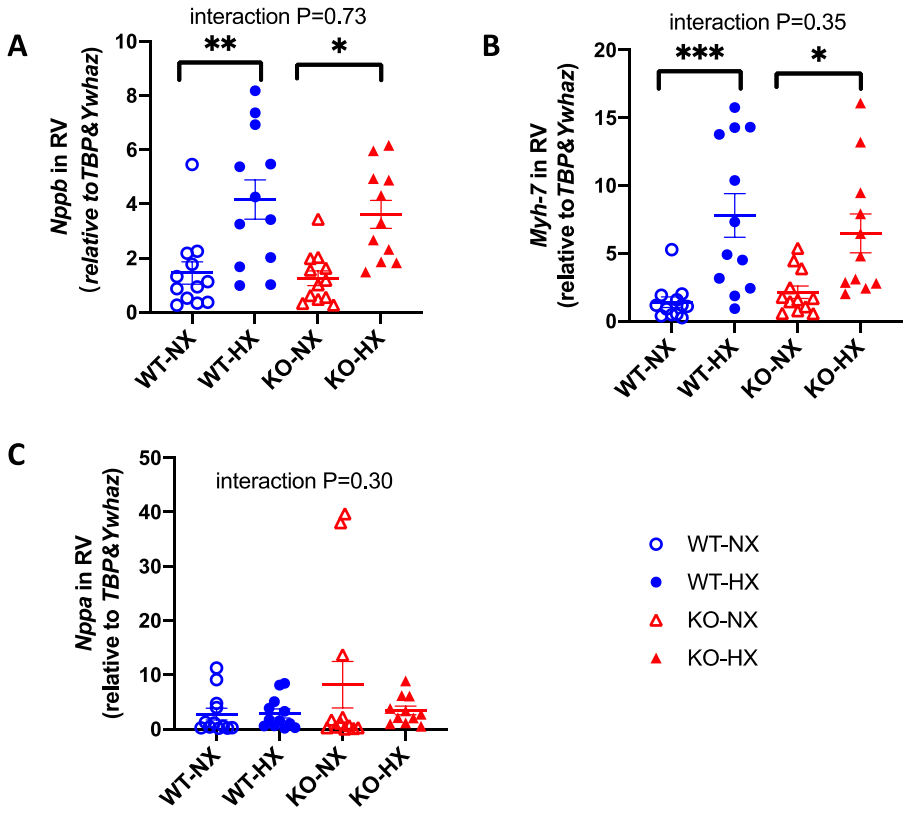

Figure 6. Transcript levels of *Nppa*, *Nppb* and *Myh-7* in right ventricle (RV) from *Pde9*$^{+/+}$ (WT) and *Pde9*$^{-/-}$ (KO) mice exposed 21 days to chronic-hypoxia (Hx) or normoxia (Nx). **A, B, C** represents the *Nppa, Nppb* and *Myh-7* transcript levels, respectively, in right ventricle homogenates (RV). Data are expressed as means ± SEM of N = 12 mice . Statistical analysis was performed using 2-way-ANOVA followed by Holm-Sidak post test. *P<0.05, **P<0.01, ***<0.001.

3.5 Effect of PDE9 deficiency on the expression of PDE9, PDE5 and VASP in RV and lung of CH-PH mice

Pde9a mRNA was significantly increased both in lung and RV from *Pde9*$^{+/+}$ mice submitted to CHx compared to Nx (Figure 7, A and B).

Because PDE5 is a quantitatively important cGMP-PDE in many tissues, we examined whether expression of this enzyme is modified in *Pde9a*$^{-/-}$, revealing a possible compensatory mechanism. In whole lung, amounts of *Pde5a* transcript or PDE5 protein were not influenced by CHx nor by the *Pde9a* deficiency (Figures 7C, 7E). In the RV, *Pde5a* mRNA was increased in *Pde9a*$^{-/-}$ (Figure 7D), which may indicate a compensation in *Pde9a* deficiency mouse RV.

Under CHx or at the protein level, however, expression of PDE5 did not show any difference between groups (Figure 7D, 7F).

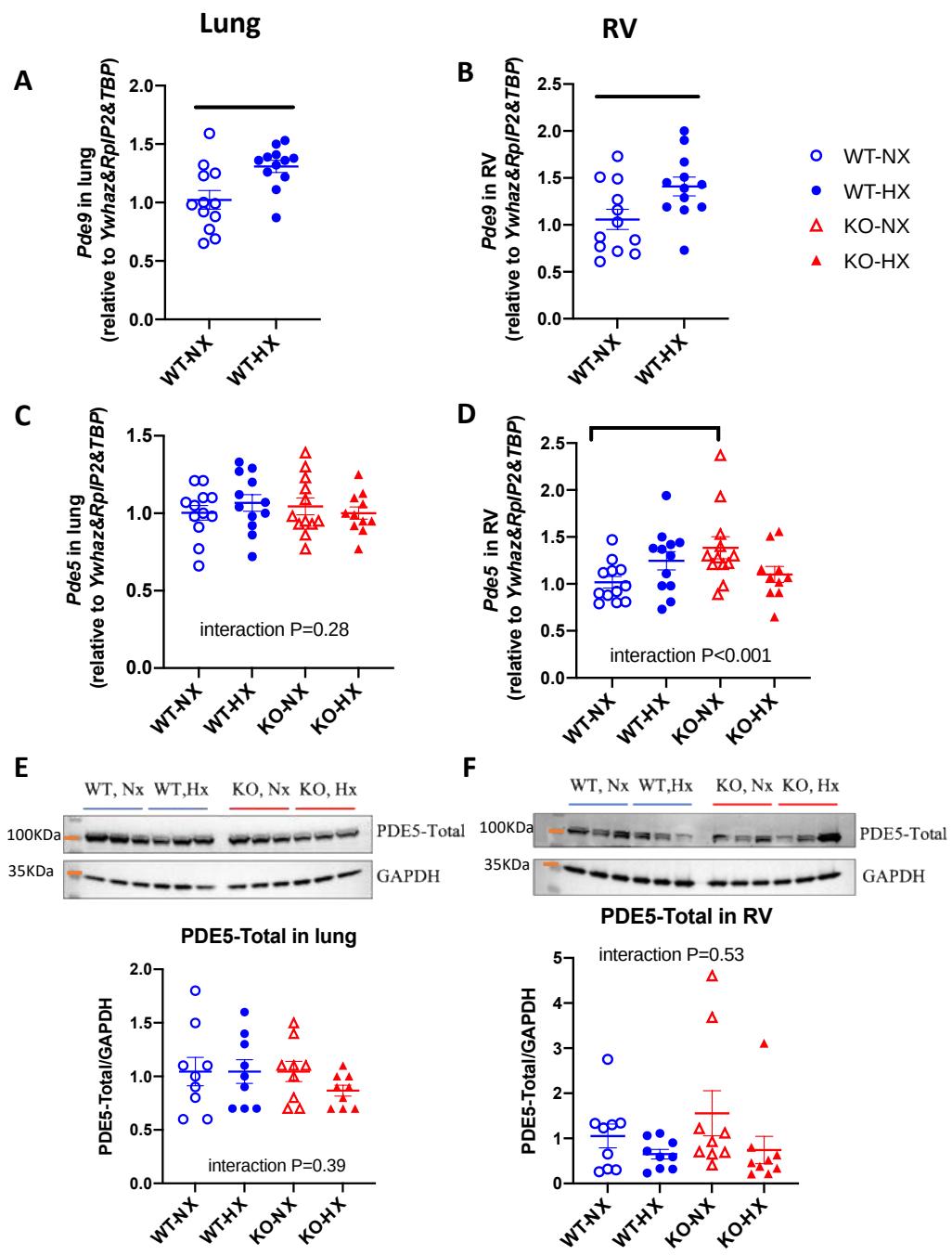

Figure 7. Expression of *Pde9a* transcripts, *Pde5a* transcripts and PDE5 protein in lung and right ventricle (RV) of chronic-hypoxia in *Pde9*$^{+/+}$ (WT) or *Pde9*$^{-/-}$ (KO) mice exposed 21 days to chronic-hypoxia (Hx) or normoxia (Nx). **A and B** show variation in *Pde9a* transcript level in lung and RV, respectively, by comparing WT-Hx mice with WT-Nx mice. **C and D,** show the transcript levels of *Pde5a* in lung and RV. **E and F** show PDE5 protein expression in lung and RV. Data are expressed as means ± SEM from N= 9-12 mice. Statistical analysis was performed using t-test for 2-group comparison and 2-way-ANOVA for 4 group-comparison. *P<0.05, **P<0.01.

Phosphorylation of downstream target VASP and PDE5 proteins can be used as readouts of the cGMP-PKG activation[39]. Phosphorylation of VASP-Ser239 in lungs and RV were not significantly altered in response to CHx and didnot differ between *Pde9*$^{+/+}$ and *Pde9a*$^{-/-}$ (Figure 8B, 8C). Similarly, phosphorylation of PDE5-Ser92 was similar in all groups (Figure 8A).

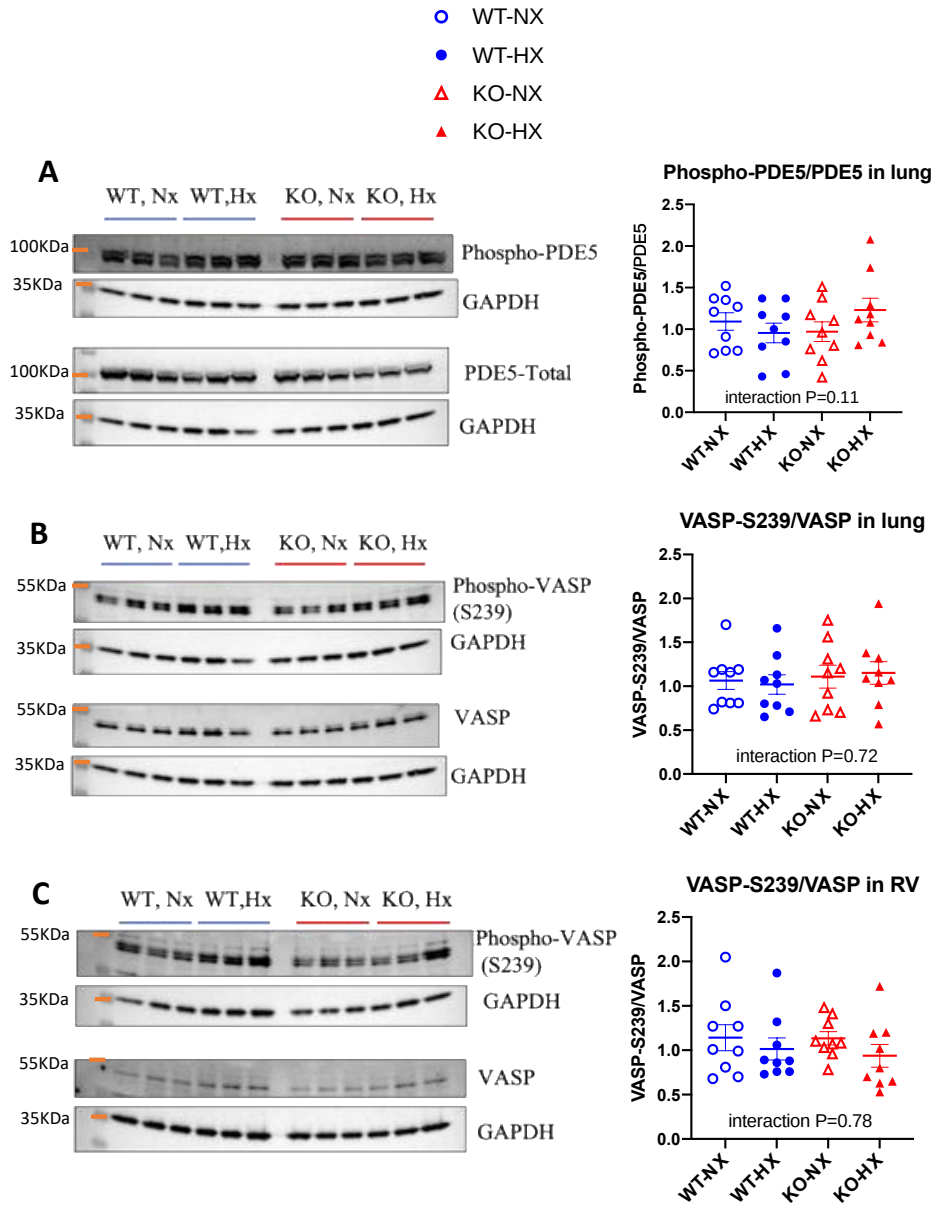

Figure 8. Phosphorylation of downstream substrates of cGMP-PKG pathway in lung and right ventricle (RV) from *Pde9*$^{+/+}$ (WT) and *Pde9*$^{-/-}$ (KO) exposed 21 days to chronic-hypoxia (Hx) or normoxia (Nx). **A:** phosphorylation of PDE5 in lung. **B, C:** phosphorylation of VASP-Ser239 in lung and RV, respectively. Data are expressed as means ± SEM from N = 9 mice. Statistical analysis was performed using 2-way-ANOVA.

Our findings suggest that, at the whole tissue scale, cGMP-PKG signaling levels may be not modified by the deficiency in PDE9.

4. Discussion

PDE9 has been emerging as a focus in diseases such as heart failure, sickle cell disease, and cognitive disordrs whereas the biology of PDE9 in pulmonary vasculature and right heart is less documented. Here, for the first time, we account that PDE9 is expressed in human and mouse pulmonary arteries. In addition, PDE9 was mostly abundant in lung tissues compared to other tissues including RV, LV and aorta. In this study, PDE9 regulated vascular reactivity of pulmonary arteries, not only by influencing the NO-cGMP-induced pathway, but also the NP-cGMP-mediated pathway. Even though an elevated PDE9 expression was observed in lung and RV from mice challenged by CHx, PDE9 deficiency fails to protect against pulmonary hypertension and RVH induced by chronic-hypoxia.

4.1 Contribution of PDE9 to PA vasomotricity

The genetically manipulated knockout mice provides a tool to study the role of PDE9 in regulating vascular reactivity. While PDE9 genetic ablation did not alter the contractile responses of isolated PA, it potentiated the relaxant effect evoked by either NO or NP.

By using similar knockout mice and pharmacological inhibitors (PF-04449613), it was previously reported that PDE9 preferentially controlled NP-mediated cGMP pathway in the cardiomyocyte[25]. By contrast, PDE9 was reported to regulate cGMP levels by NO-induced pathway in cultured rat aorta smooth muscle cells using pharmacological inhibitor (PF-04447943)[33]. However, we found that PDE9 regulated relaxation evoked via both NP and NO-stimulated pathways in pulmonary arteries. Here, although promising, pharmacological inhibitors of PDE9 (both BAY-73-6691 and PF-04447943) could not be used to further deciphering the role of the enzyme as they showed a relaxant effect that could not be ascribed to PDE9. Regarding these 3 PDE9 inhibitors, namely BAY-736691, PF-4447943 and PF-4449613, the IC50 for human recombinant PDE9A is 55 nM, 12 nM and 24 nM, respectively. All of 3 inhibitors show relative selectivity against PDE1C with IC50 ratio of 25, 78 and 35-

fold, respectively[32,30]. Considering that the observed relaxant effects were observed at relatively high concentrations of inhibitors compared to described in vitro potency, they may result from non-selective inhibition of PDE1C and other PDEs.

As expected, the PDE5 inhibitor sildenafil produced a highly potent relaxation of PA rings, confirming that reducing basal cGMP breakdown is sufficient to evoke complete relaxation. The observation that response to sildenafil, even at small concentration, is not potentiated in *Pde9a*$^{-/-}$ mice compared with WT mice, indicates that the hydrolysis efficacy of PDE5 exceeds that of PDE9 in smooth muscle. Zhang et al., reported that 0.2 μM sildenafil abolishes more that 50% of cGMP-PDE activity in rat aortic smooth muscle cells, while 5 μM PF-4447943 abolished 37% of activity. Despite this non-negligible activity, it is possible that concomitant stimulation of cGMP levels by, on the one side, by Ach, DEANO or ANP, and on the another side, inhibiting breakdown by PDE9, exert a synergistic effect on cGMP accumulation that translates into a significant potentiation of the relaxant effec[43, 44]. Possible segregation of PDE9 into discrete subcellular compartments, that is largely unknown, may explain differential contribution to basal versus stimulated cGMP balance. The existence of various splice variants targeted to specific locations has been suggested[38] and may be an interesting track to follow in order to further establish the function of PDE9 in vasculature.

4.2 Experimental PAH in *Pde9a*$^{-/-}$ mice

Pde9a$^{-/-}$ mice and their wild-type littermates were submitted to 21-day-hypoxia, a standard, well characterized PAH model[35]. Based on hemodynamics, non-invasive echocardiographic and biochemical readouts, we found that PDE9 deficiency failed to prevent the establishment of the disease. This result was in line with a very recent, parallel study by another group (Kolb et al.,[34]). Our study accounts for further morphometric and functional assessment, including PAAT, PAAT/PET, TAPSE and RVFWT were also examined to support our conclusion. These readouts were all confirmed to be similar in both genotypes. Also, measurement of the expression of gene associated with hypertrophy showed that PDE9 deficiency did not protect against remodeling of RV in this model. This is at odds with was reported in the myocardium in a hypertrophy model induced by pressure overload[25] where increase in *Myh7* expression was partially reduced in *Pde9a*$^{-/-}$ mice compared to wild-type. This suggests that PDE9 does not

have a role in regulating RV hypertrophy. Consistent with Kolb et al.[34], the *Nppa* mRNA expression in RV was unchanged in CHx, possibly pointing to a mild RV hypertrophy in this model.

In contrast to Kolb et al.[34], we found that the *Pde9a* mRNA was upregulated in lung and RV from hypoxic PAH mice compared to normoxic control mice. The difference between studies might lie in the animal sample size, age and gender. Moreover we did not observe any upregulation of PDE5 protein in lung after hypoxia. This is in line with another study reporting that PDE5 expression was stable upon CHx[45]..

As the downstream of cGMP-PKG, the phosphorylation of VASP on Ser-239 and PDE5 on Ser-92 was not changed by exposure to CHx. While this result is consistent with the study by Kolb et al.[34], it is at odds with other studies that reported an increase in Ser-239 phosphorylation[46]. The fact that this readout was unchanged by in tissues from *Pde9a*$^{-/-}$ mice suggest that the enzyme do not participate significantly in controlling the cGMP pathway at the whole-organ scale if the stimulation is limited.

4.3 Limitations to the study

There are several limitations to our study. First, the available antibody against PDE9 yield numerous non-specific signal[38], which made it difficult to obtain accurate quantification of PDE9 signal in mouse tissue and limit the detection of the enzyme in PA where small amount of material is available. Second, the PDE9 inhibition is reported to reduce obesity and cardiometabolic syndrome in male mice and ovariectomized female mice rather than non-ovariectomized female, which indicates a strong sexual dimorphism[47]. Thus female animals still need to be emphasized in exploring the role of PDE9 in future experiments. Third, the mouse model of CHx-induced PAH, even though reproducible and well-characterized, does not fully recapitulate the pulmonary vascular remodeling or inflammation observed in human PAH[48]. Besides, even though the phenotype of this model can be successfully established but not severe and typical PAH model. Therefore, our conclusions are only limited to this model and unable to reflect the role of PDE9 in human PAH.

5. Conclusion

Even though PDE9 deficiency did not prevent the development of PAH under hypoxic condition, our study highlight a functional role for PDE9 in hampering PA relaxations to cGMP-related dilators. While our study do not support a critical relevance of PDE9 in the pathophysiology of PAH, the discrepancy observed between right and left ventricle hypertrophy[25, 34] raises question about the role of this enzyme in the myocardium. Because hypertrophic response of the RV to CHx may be qualitatively different from the remodeling occurring upon pressure overload of the left ventricle, which stresses the need to further understand how cGMP-PDEs control the remodeling in both ventricles under comparable stimuli. Considering that PDE9 mRNA was upregulated in the RV and lung in our study, it may be speculated that treatment with PDE9 inhibition combined with another intervention that stimulates cGMP production may exert beneficial effect on PAH. Upon such association, systemic blood pressure should be monitored, since PDE9 inhibition was shown to decrease total peripheral vascular resistance in vivo in a heart failure model[26]. Also more severe and relevant animal models are needed to further explore the role of PDE9 in PAH and RV hypertrophy.

6. References

1. Simonneau G, Montani D, Celermajer DS, Denton CP, Gatzoulis MA, Krowka M, Williams PG and Souza R. Haemodynamic definitions and updated clinical classification of pulmonary hypertension. *Eur Respir J*. 2019;53.

2. Hassoun PM. Pulmonary Arterial Hypertension. *N Engl J Med*. 2021;385:2361-2376.

3. Yan Y, He YY, Jiang X, Wang Y, Chen JW, Zhao JH, Ye J, Lian TY, Zhang X, Zhang RJ, Lu D, Guo SS, Xu XQ, Sun K, Li SQ, Zhang LF, Zhang X, Zhang SY and Jing ZC. DNA methyltransferase 3B deficiency unveils a new pathological mechanism of pulmonary hypertension. *Sci Adv*. 2020;6.

4. Tonelli AR, Arelli V, Minai OA, Newman J, Bair N, Heresi GA and Dweik RA. Causes and circumstances of death in pulmonary arterial hypertension. *Am J Respir Crit Care Med*. 2013;188:365-9.

5. Vonk-Noordegraaf A, Haddad F, Chin KM, Forfia PR, Kawut SM, Lumens J, Naeije R, Newman J, Oudiz RJ, Provencher S, Torbicki A, Voelkel NF and Hassoun

PM. Right heart adaptation to pulmonary arterial hypertension: physiology and pathobiology. *J Am Coll Cardiol*. 2013;62:D22-33.

6. Guignabert C, Tu L, Girerd B, Ricard N, Huertas A, Montani D and Humbert M. New molecular targets of pulmonary vascular remodeling in pulmonary arterial hypertension: importance of endothelial communication. *Chest*. 2015;147:529-537.

7. Humbert M, Sitbon O, Chaouat A, Bertocchi M, Habib G, Gressin V, Yaici A, Weitzenblum E, Cordier JF, Chabot F, Dromer C, Pison C, Reynaud-Gaubert M, Haloun A, Laurent M, Hachulla E, Cottin V, Degano B, Jais X, Montani D, Souza R and Simonneau G. Survival in patients with idiopathic, familial, and anorexigen-associated pulmonary arterial hypertension in the modern management era. *Circulation*. 2010;122:156-63.

8. Benza RL, Miller DP, Barst RJ, Badesch DB, Frost AE and McGoon MD. An evaluation of long-term survival from time of diagnosis in pulmonary arterial hypertension from the REVEAL Registry. *Chest*. 2012;142:448-56.

9. Janssen W, Schermuly RT and Kojonazarov B. The role of cGMP in the physiological and molecular responses of the right ventricle to pressure overload. *Exp Physiol*. 2013;98:1274-8.

10. Baliga RS, MacAllister RJ and Hobbs AJ. New perspectives for the treatment of pulmonary hypertension. *Br J Pharmacol*. 2011;163:125-40.

11. Ghofrani HA, Galie N, Grimminger F, Grunig E, Humbert M, Jing ZC, Keogh AM, Langleben D, Kilama MO, Fritsch A, Neuser D, Rubin LJ and Group P-S. Riociguat for the treatment of pulmonary arterial hypertension. *N Engl J Med*. 2013;369:330-40.

12. Galie N, Ghofrani HA, Torbicki A, Barst RJ, Rubin LJ, Badesch D, Fleming T, Parpia T, Burgess G, Branzi A, Grimminger F, Kurzyna M, Simonneau G and Sildenafil Use in Pulmonary Arterial Hypertension Study G. Sildenafil citrate therapy for pulmonary arterial hypertension. *The New England journal of medicine*. 2005;353:2148-57.

13. Francis SH, Blount MA and Corbin JD. Mammalian cyclic nucleotide phosphodiesterases: molecular mechanisms and physiological functions. *Physiol Rev*. 2011;91:651-90.

14. Klein T, Eltze M, Grebe T, Hatzelmann A and Komhoff M. Celecoxib dilates guinea-pig coronaries and rat aortic rings and amplifies NO/cGMP signaling by PDE5 inhibition. *Cardiovasc Res*. 2007;75:390-7.

15. Maclean MR, Johnston ED, McCulloch KM, Pooley L, Houslay MD and Sweeney G. Phosphodiesterase isoforms in the pulmonary arterial circulation of the rat: changes in pulmonary hypertension. *The Journal of pharmacology and experimental therapeutics*. 1997;283:619-24.

16. Murray F, Patel HH, Suda RY, Zhang S, Thistlethwaite PA, Yuan JX and Insel PA. Expression and activity of cAMP phosphodiesterase isoforms in pulmonary artery smooth muscle cells from patients with pulmonary hypertension: role for PDE1. *Am J*

Physiol Lung Cell Mol Physiol. 2007;292:L294-303.

17. Tian X, Vroom C, Ghofrani HA, Weissmann N, Bieniek E, Grimminger F, Seeger W, Schermuly RT and Pullamsetti SS. Phosphodiesterase 10A upregulation contributes to pulmonary vascular remodeling. *PLoS One*. 2011;6:e18136.

18. Pauvert O, Lugnier C, Keravis T, Marthan R, Rousseau E and Savineau JP. Effect of sildenafil on cyclic nucleotide phosphodiesterase activity, vascular tone and calcium signaling in rat pulmonary artery. *Br J Pharmacol*. 2003;139:513-22.

19. Sebkhi A, Strange JW, Phillips SC, Wharton J and Wilkins MR. Phosphodiesterase type 5 as a target for the treatment of hypoxia-induced pulmonary hypertension. *Circulation*. 2003;107:3230-5.

20. Scott H. Soderling SJB, Joseph A. Beavo. Identification and Characterization of a Novel Family of Cyclic Nucleotide Phosphodiesterases. *The Journal of Biological Chemistry*. 1998;273:15553-15558.

21. Michel Guipponi HSS, Jun Kudoh, Kazuhiko Kawasaki, Kazunori Shibuya, Ai Shintani, Shuichi Asakawa, Haiming Chen, Maria D. Lalioti, Colette Rossier, Shinsei Minoshima, and Nobuyoshi Shimizu SEA. Identification and characterization of a novel cyclic nucleotide phosphodiesterase gene (PDE9A) that maps to 21q22.3: alternative splicing of mRNA transcripts, genomic structure and sequence. *Hum Genet*. 1998;103:386-392.

22. Douglas A. Fisher JFS, Joann S. Pillar, Suzanne H. St. Denis, John B. Cheng. Isolation and Characterization of PDE9A, a Novel Human cGMP-specific Phosphodiesterase. *The Journal of Biological Chemistry*. 1998;273:15559-15564.

23. Patel NS, Klett J, Pilarzyk K, Lee DI, Kass D, Menniti FS and Kelly MP. Identification of new PDE9A isoforms and how their expression and subcellular compartmentalization in the brain change across the life span. *Neurobiol Aging*. 2018;65:217-234.

24. Rentero C, Monfort A and Puigdomenech P. Identification and distribution of different mRNA variants produced by differential splicing in the human phosphodiesterase 9A gene. *Biochem Biophys Res Commun*. 2003;301:686-92.

25. Lee DI, Zhu G, Sasaki T, Cho GS, Hamdani N, Holewinski R, Jo SH, Danner T, Zhang M, Rainer PP, Bedja D, Kirk JA, Ranek MJ, Dostmann WR, Kwon C, Margulies KB, Van Eyk JE, Paulus WJ, Takimoto E and Kass DA. Phosphodiesterase 9A controls nitric-oxide-independent cGMP and hypertrophic heart disease. *Nature*. 2015;519:472-6.

26. Scott NJA, Rademaker MT, Charles CJ, Espiner EA and Richards AM. Hemodynamic, Hormonal, and Renal Actions of Phosphodiesterase-9 Inhibition in Experimental Heart Failure. *J Am Coll Cardiol*. 2019;74:889-901.

27. van der Horst IW, Morgan B, Eaton F, Reiss I, Tibboel D and Thebaud B. Expression and function of phosphodiesterases in nitrofen-induced congenital diaphragmatic hernia in rats. *Pediatr Pulmonol*. 2010;45:320-5.

28. Almeida CB, Scheiermann C, Jang JE, Prophete C, Costa FF, Conran N and Frenette PS. Hydroxyurea and a cGMP-amplifying agent have immediate benefits on acute vaso-occlusive events in sickle cell disease mice. *Blood*. 2012;120:2879-88.

29. Heckman PR, Wouters C and Prickaerts J. Phosphodiesterase inhibitors as a target for cognition enhancement in aging and Alzheimer's disease: a translational overview. *Curr Pharm Des*. 2015;21:317-31.

30. Kleiman RJ, Chapin DS, Christoffersen C, Freeman J, Fonseca KR, Geoghegan KF, Grimwood S, Guanowsky V, Hajos M, Harms JF, Helal CJ, Hoffmann WE, Kocan GP, Majchrzak MJ, McGinnis D, McLean S, Menniti FS, Nelson F, Roof R, Schmidt AW, Seymour PA, Stephenson DT, Tingley FD, Vanase-Frawley M, Verhoest PR and Schmidt CJ. Phosphodiesterase 9A regulates central cGMP and modulates responses to cholinergic and monoaminergic perturbation in vivo. *J Pharmacol Exp Ther*. 2012;341:396-409.

31. Hutson PH, Finger EN, Magliaro BC, Smith SM, Converso A, Sanderson PE, Mullins D, Hyde LA, Eschle BK, Turnbull Z, Sloan H, Guzzi M, Zhang X, Wang A, Rindgen D, Mazzola R, Vivian JA, Eddins D, Uslaner JM, Bednar R, Gambone C, Le-Mair W, Marino MJ, Sachs N, Xu G and Parmentier-Batteur S. The selective phosphodiesterase 9 (PDE9) inhibitor PF-04447943 (6-[(3S,4S)-4-methyl-1-(pyrimidin-2-ylmethyl)pyrrolidin-3-yl]-1-(tetrahydro-2H-py ran-4-yl)-1,5-dihydro-4H-pyrazolo[3,4-d]pyrimidin-4-one) enhances synaptic plasticity and cognitive function in rodents. *Neuropharmacology*. 2011;61:665-76.

32. Wunder F, Tersteegen A, Rebmann A, Erb C, Fahrig T and Hendrix M. Characterization of the first potent and selective PDE9 inhibitor using a cGMP reporter cell line. *Mol Pharmacol*. 2005;68:1775-81.

33. Zhang L, Bouadjel K, Manoury B, Vandecasteele G, Fischmeister R and Leblais V. Cyclic nucleotide signalling compartmentation by PDEs in cultured vascular smooth muscle cells. *Br J Pharmacol*. 2019;176:1780-1792.

34. Kolb TM, Johnston L, Damarla M, Kass DA and Hassoun PM. PDE9A deficiency does not prevent chronic-hypoxic pulmonary hypertension in mice. *Physiol Rep*. 2021;9:e15057.

35. Gomez-Arroyo J, Saleem SJ, Mizuno S, Syed AA, Bogaard HJ, Abbate A, Taraseviciene-Stewart L, Sung Y, Kraskauskas D, Farkas D, Conrad DH, Nicolls MR and Voelkel NF. A brief overview of mouse models of pulmonary arterial hypertension: problems and prospects. *Am J Physiol Lung Cell Mol Physiol*. 2012;302:L977-91.

36. Mulvany MJ and Halpern W. Contractile properties of small arterial resistance vessels in spontaneously hypertensive and normotensive rats. *Circ Res*. 1977;41:19-26.

37. Idres S, Perrin G, Domergue V, Lefebvre F, Gomez S, Varin A, Fischmeister R, Leblais V and Manoury B. Contribution of BKCa channels to vascular tone regulation by PDE3 and PDE4 is lost in heart failure. *Cardiovasc Res*. 2019;115:130-144.

38. Patel NS, Klett J, Pilarzyk K, Lee Di, Kass D, Menniti FS and Kelly MP.

Identification of new PDE9A isoforms and how their expression and subcellular compartmentalization in the brain change across the life span. *Neurobiology of Aging*. 2018;65:217-234.

39. Rybalkin SD, Rybalkina IG, Feil R, Hofmann F and Beavo JA. Regulation of cGMP-specific phosphodiesterase (PDE5) phosphorylation in smooth muscle cells. *J Biol Chem*. 2002;277:3310-7.

40. Nelson MT, Huang Y, Brayden JE, Hescheler J and Standen NB. Arterial dilations in response to calcitonin gene-related peptide involve activation of K+ channels. *Nature*. 1990;344:770-3.

41. Zhu Z, Godana D, Li A, Rodriguez B, Gu C, Tang H, Minshall RD, Huang W and Chen J. Echocardiographic assessment of right ventricular function in experimental pulmonary hypertension. *Pulm Circ*. 2019;9:2045894019841987.

42. Forfia PR, Fisher MR, Mathai SC, Housten-Harris T, Hemnes AR, Borlaug BA, Chamera E, Corretti MC, Champion HC, Abraham TP, Girgis RE and Hassoun PM. Tricuspid annular displacement predicts survival in pulmonary hypertension. *Am J Respir Crit Care Med*. 2006;174:1034-41.

43. Baliga RS, Zhao L, Madhani M, Lopez-Torondel B, Visintin C, Selwood D, Wilkins MR, MacAllister RJ and Hobbs AJ. Synergy between natriuretic peptides and phosphodiesterase 5 inhibitors ameliorates pulmonary arterial hypertension. *American journal of respiratory and critical care medicine*. 2008;178:861-9.

44. Wharton J, Strange JW, Moller GM, Growcott EJ, Ren X, Franklyn AP, Phillips SC and Wilkins MR. Antiproliferative effects of phosphodiesterase type 5 inhibition in human pulmonary artery cells. *Am J Respir Crit Care Med*. 2005;172:105-13.

45. Nozik-Grayck E, Woods C, Taylor JM, Benninger RK, Johnson RD, Villegas LR, Stenmark KR, Harrison DG, Majka SM, Irwin D and Farrow KN. Selective depletion of vascular EC-SOD augments chronic hypoxic pulmonary hypertension. *Am J Physiol Lung Cell Mol Physiol*. 2014;307:L868-76.

46. Patel D, Alhawaj R and Wolin MS. Exposure of mice to chronic hypoxia attenuates pulmonary arterial contractile responses to acute hypoxia by increases in extracellular hydrogen peroxide. *Am J Physiol Regul Integr Comp Physiol*. 2014;307:R426-33.

47. Mishra S, Sadagopan N, Dunkerly-Eyring B, Rodriguez S, Sarver DC, Ceddia RP, Murphy SA, Knutsdottir H, Jani VP, Ashok D, Oeing CU, O'Rourke B, Gangoiti JA, Sears DD, Wong GW, Collins S and Kass D. Inhibition of phosphodiesterase type 9 reduces obesity and cardiometabolic syndrome in mice. *J Clin Invest*. 2021.

48. Boucherat O, Agrawal V, Lawrie A and Bonnet S. The Latest in Animal Models of Pulmonary Hypertension and Right Ventricular Failure. *Circ Res*. 2022;130:1466-1486.

Supplementary Tables

Supplementary Table 1: sequence of primers used in this study.

Target	Forward 5'→3', Reverse 5'→3';	Product size (bp)	Annealing temperature (°C)	Accession number
mouse primers				
Pde1a	GCAGGGAGACAAAGAAGCTG	224	60,0°C 20s	NM_001355142.2
	CAATCATGGTGGACGAGCTG			
Pde1b	GTCCACAACTGTCTCAAGAACC	133	60,0°C 20s	NM_001357980.1
	TAAAGCGGCTGATGAGGCTAT			
Pde1c	CTGAACAAGGCACAACCAGC	155	60,0°C 20s	NM_001355475.1
	ACCGTCTTTCAAGTCACCGT			
Pde2a	TGGGGAACTCTTTGACTTGG	135	60,0°C 20s	NM_001243758.1
	ATGACCTTGCAGGAAAGCTG			
Pde3a	CAGCATAAAGCCGCACGAAG	81	60,0°C 20s	NM_018779.2
	GTGAGAGTCGTCAACCCTGG			
Pde3b	ATGTTCAGGAGACCGTCGTT	175	60,0°C 20s	NM_011055.2
	TTGGGTCAATCAGCAGGTCT			
Pde5a	ATCTGGAGACCCTTGCGTTG	177	60,0°C 20s	NM_153422.2
	GGTTGCCTGGGCTGTTTAGA			
Pde9a	CACAGATGATGTACAGTATGGTCTGG	294	60,0°C 20s	NM_001163748.1
	ATGTGATCATCCCCTGCCTG			
Nppa	AGGCCATATTGGAGCAAATC	88	60,0°C 20s	NM_008725.3
	CTCCTCCAGGTGGTCTAGCA			
Nppb	CTGGGAAGTCCTAGCCAGTC	132	60,0°C 20s	NM_013684.3
	TTTTCTCTTATCAGCTCCAGCA			
Myh7	AATGCACTCAATGCCAGGAT	153	60,0°C 20s	NM_080728.3
	GTCAGAGCGCAGCTTCTCC			
Ywhaz	AGACGGAAGGTGCTGAGAAA	127	60,0°C 20s	NM_001356569.1
	GAA GCATTGGGGATCAAGAA			
Tbp	AAAGACCATTGCACTTCGTG	132	60,0°C 20s	NM_013684.3
	GCTCCTGTGCACACCATTTT			
Rplp2	GCTGTGGCTGTTTCTGCTG	119	60,0°C 20s	NM_026020.7
	ATGTCGTCATCCGACTCCTC			
human primers				
PDE9A	ACATGGCAAGACATGCAGAA	200	60,0°C 20s	NM_001001580.1
	ACGGTCGCTCTGCATAAAAT			
Ywhaz	AGACGGAAGGTGCTGAGAAA	127	60,0°C 20s	NM_001356569.1
	GAA GCATTGGGGATCAAGAA			

Supplementary Table 2: The parameters of PDE9 WT and KO mice before and after establishment of CH-PH models.

	WT-NX	WT-HX	KO-NX	KO-HX	P(Hx)	P(Gnt)	P(inter)
			Day 0				
Age (weeks)	10.52± 0.37	10.52± 0.28	9.84± 0.38	10.36± 0.36	ns	ns	ns
Body weight (g)	26.07± 0.71	27.70± 0.50	24.88± 0.46	26.00± 0.66	*	*	ns
EF (%)	56.07± 1.78	55.20± 1.77	55.54± 1.76	55.52± 1.52	ns	ns	ns
HR (bpm)	422.7± 9.2	423.8± 5.0	420.9± 4.9	417.8± 7.9	ns	ns	ns
PAAT (ms)	20.09± 0.69	19.98± 0.59	20.62± 0.62	19.43± 0.35	ns	ns	ns
TAPSE (mm)	0.944± 0.031	0.945± 0.031	0.950± 0.031	0.967± 0.040	ns	ns	ns
RVFWT (mm)	0.244± 0.007	0.0248± 0.009	0.240± 0.008	0.240± 0.005	ns	ns	ns
PAAT/PET	0.358± 0.009	0.359± 0.008	0.369± 0.010	0.350± 0.007	ns	ns	ns
			Day 21				
Body weight (g)	27.11± 0.60	26.80± 0.33	26.04± 0.34	25.17± 0.44	ns	**	ns
RVSP (mmHg)	24.12± 1.24	38.54± 2.50	22.76± 1.56	40.75± 1.33	****	ns	ns
PAAT (ms)	19.96± 0.53	16.20± 0.60	20.37± 0.52	16.22± 0.55	****	ns	ns
RV/(LV+S)	0.279± 0.007	0.394± 0.018	0.264± 0.005	0.366± 0.008	****	ns	ns
TAPSE (mm)	0.885± 0.048	0.755± 0.039	0.861± 0.037	0.730± 0.032	**	ns	ns
RVFWT(mm)	0.240± 0.012	0.323± 0.013	0.246± 0.009	0.325± 0.012	****	ns	ns
PAAT/PET	0.360± 0.010	0.317± 0.009	0.368± 0.007	0.302± 0.008	****	ns	ns
EF(%)	55.84± 1.73	52.69± 2.37	50.83± 1.03	53.94± 1.28	ns	ns	ns
HR(bpm)	431.9± 11.2	455.4± 8.9	424.9± 5.2	443.8± 9.7	*	ns	ns
Tibia length(mm)	17.74± 0.11	17.80± 0.08	17.60± 0.12	17.45± 0.10	ns	*	ns

HR: heart rate; EF: ejection fraction; PAAT: pulmonary artery acceleration time; PET: pulmonary ejection time; TAPSE: tricuspid annular plane systolic excursion; RVFWT: right ventricular free wall thickness; RV: right ventricle; LV+S: left ventricle+septum; RVSP: right ventricular systolic pressure. P(Hx): P value for exposure to hypoxia; P(Gnt): P value for genotype; P(inter): P value for interaction; Statistical analysis was performed using 2-way-ANOVA followed by Holm-Sidak post test. N=6-23 mice in every group. *P<0.05, **P<0.01,****P<0.0001.

Supplementary Figures

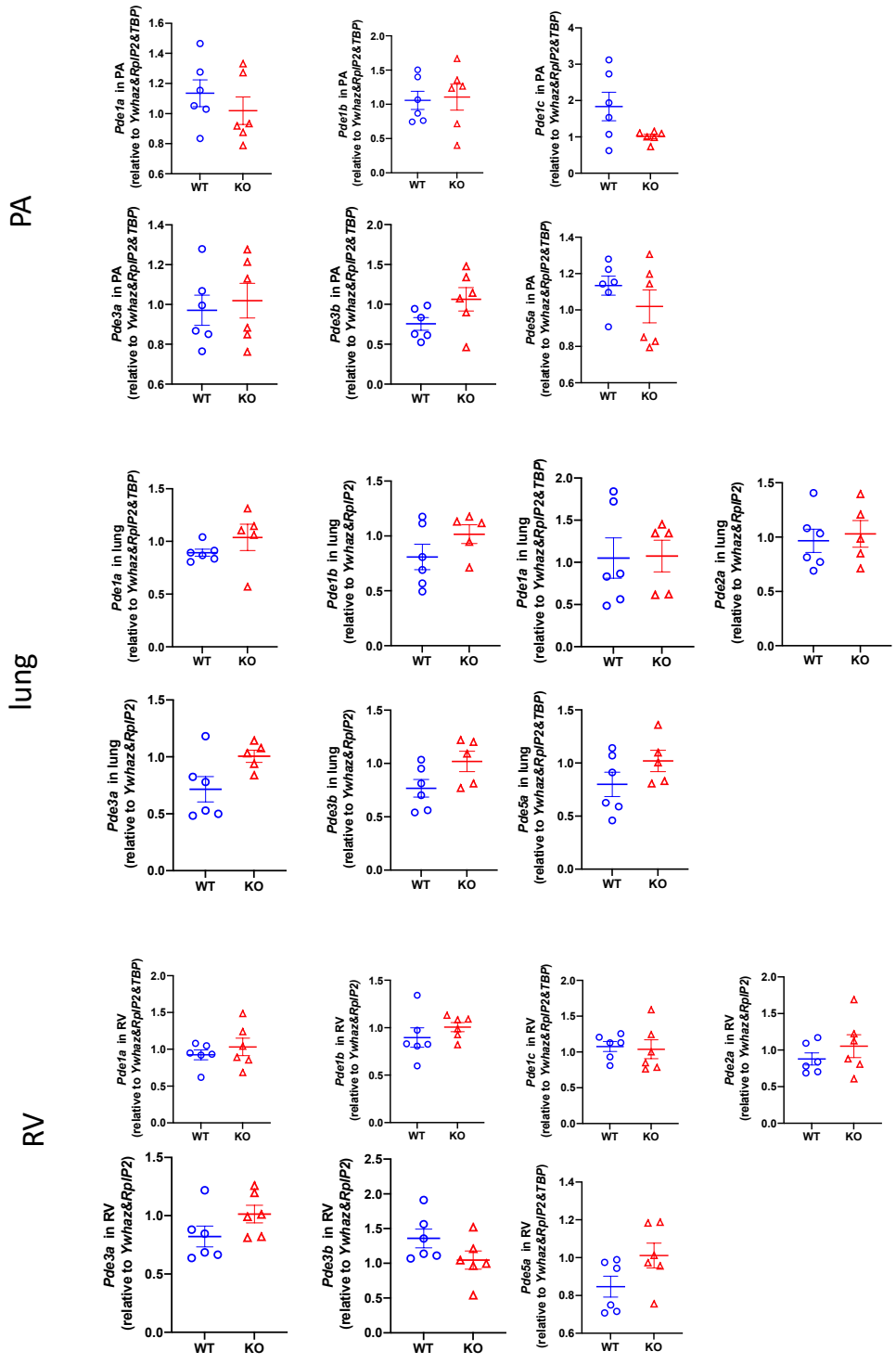

Supplementary Figure 1: The mRNA expression levels of cGMP-hydrolyzing related PDEs in pulmonary artery (PA), lung and right ventricle(RV) of both WT and KO mice.

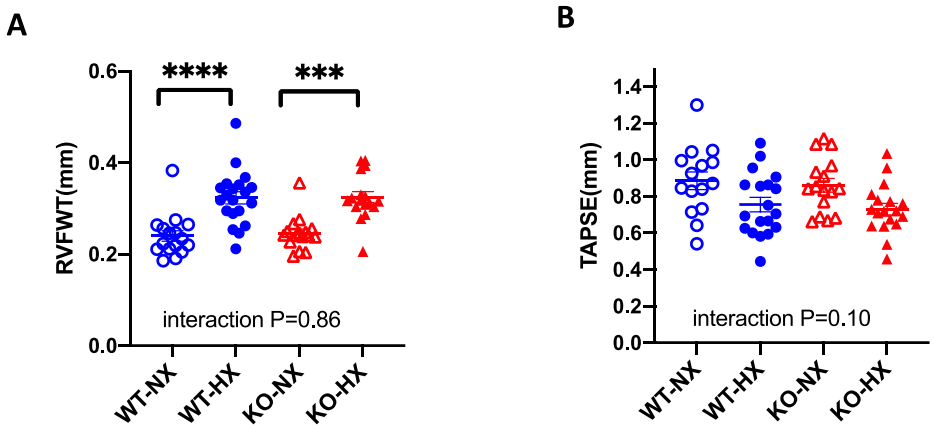

Supplementary Figure 2: Right ventricle free wall thickness (RVFWT, **A**) and tricuspid annular plane systolic excursion(TAPSE, **B**) from *Pde9*$^{+/+}$ (WT) and *Pde9*$^{-/-}$ (KO) mice exposed 21 days to chronic-hypoxia (Hx) or normoxia (Nx) and evaluated by TTE. Data are expressed as means ± SEM. Statistical analysis using 2-way ANOVA. B: P<0.01 for global effect of hypoxia. N=16-20 mice in every group. ***P<0.001,****P<0.0001.

4.1.2 Discussion and perspectives

PDE9 emerges as a promising therapeutic target in several disorders, such as Alzheimer's disease[358,456], sickle cell disease[357], left heart disease which includes hypertrophic heart disease[355,457], EFrHF[363], EFpHF[458] and diastolic dysfunction disease[459], as well as obesity and cardiometabolic syndrome[366]. Here, We fill gaps of its contribution in pulmonary hypertension and associated right heart failure induced by CHx in murine model.

The main findings of our work are that: 1) We examined that PDE9 was expressed in both human and murine pulmonary artery, murine lungs and right ventricle. This finding is a fundamental contribution urging for further exploring the role of PDE9 in pulmonary hypertension and/or right heart diseases in vivo in human or animal models. 2) PDE9 is involved in regulating pulmonary artery tone by modulating both NO-related and NP-dependent cGMP pathway, and thus PDE9 inhibition potentiate relaxant response of pulmonary artery to agents stimulating cGMP generation. This somewhat contrasts with what was observed in rat cultured aorta smooth muscle cells, where PDE9 pharmacological inhibition mainly potentiated NO-sGC-cGMP pathway[170] . Also, PDE9 is reported to control NP-pGC-cGMP pathway in the cardiomyocytes[355]. These discrepancies may indicate tissue-specific pattern of PDE9 localization and thus possibly resultant differential pathway. 3) PDE9 deficiency does not prevent the development of pulmonary hypertension in the mouse model of chronic-hypoxia, while upregulation of PDE9 mRNA levels in lung and right ventricle still encourages us to further validate its role in more typical animal models considering the mild phenotype of PAH model in mouse.

The detailed discussion of the figures has been inserted in the manuscript included in the Results section of the thesis, following a paper format. Here we will not redundantly repeat this aspect. Even though we found that the PDE9 genetic invalidation enhances vasorelaxant response to NPs and NO donors, it remains difficult for us to further explore the downstream signals since the mouse pulmonary artery is too small to get enough tissues for measurement of cGMP levels and PKG activity. Alternatively, we can isolate PASMCs and culture them,

infect them with the cGMP sensor and do real time FRET experiments to monitor the cGMP dynamics. In addition, we did not show direct evidence of cGMP levels for PDE9 abolition in lung and right ventricle of animal models, and ideally, in PA. Thus this important part of the work should be performed shortly. Although the protein level of PDE9 is difficult to test due to lack of specific antibody, the PDE9 enzymatic activity would provide a complementary method to evaluate the amount of PDE9 in this mouse models and to further check the alteration of PDE9 in hypoxia models. Since the subcellular distribution of PDE9 has been studied both in cardiomyocyte[355] and brain[353], we expected more specific antibody of PDE9 to help us better exploring cellular or subcellular localization of PDE9 in the future.

As presented in the discussion of the manuscript, a similar study by another group has been recently published[367], that account for mainly comparable results. In general, although the in vivo data of animal model seems a disappointing for us, we do believe this work is still instructive and meaningful to future work. Clinical studies about PDE9 pharmacological inhibitors are now ongoing in stable sickle cell disease[365] and neurocognitive disorders including schizophrenia and Alzheimer diseases[185] and human data supports safety and tolerability of multiple PDE9 inhibitors as well as negligible impact on arterial blood pressure or heart rate[460]. Therefore, given the considerable potential for the clinical benefit of PDE9A inhibition and our important preclinical work, further studies with more robust PH models and/or right heart failure models are needed to test the effect of PDE9 inhibition alone or combination with other approved treatments.

4.2 Project 2: The role of cAMP-related PDEs in mesentery artery from both normal and heart failure rats

4.2.1 Original Research Article

The results of this work will be presented as a "ready-to-submit" manuscript (**ARTICLE #2**), entitled:

"**Phosphodiesterases type 2, 3 and 4 influence vascular tone in mesenteric arteries from rats with heart failure**",

by the following authors:

Liting Wang*[1], Fabien Hubert*[1], Sarah Idres[1], Milia Belacel-Ouari[1], Valérie Domergue[2], Florence Lefebvre[1], Delphine Mika[1], Rodolphe Fischmeister[1], Véronique Leblais[1], Boris Manoury[1].

[1]Université Paris-Saclay, Inserm, UMR-S 1180, 91400, Orsay, France.

[2]Université Paris-Saclay, Inserm, Cnrs, Ingénierie et Plateformes au Service de l'Innovation Thérapeutique 91400, Orsay, France.

* Mrs Liting Wang and Dr Fabien Hubert contributed equally.

The following manuscript has been submitted to the European Journal of Pharmacology (manuscript # EJP-62301) on 27 July 2022.

European Journal of Pharmacology

Phosphodiesterases type 2, 3 and 4 influence vascular tone in mesenteric arteries from rats with heart failure

--Manuscript Draft--

Manuscript Number:	EJP-62301
Article Type:	Research Paper
Section/Category:	Cardiovascular pharmacology
Keywords:	phosphodiesterase inhibitor; vascular tone; mesenteric artery; heart failure; nitric oxide
Corresponding Author:	Boris Manoury, Ph.D Universite Paris-Saclay Orsay, FRANCE
First Author:	Liting Wang, M.D
Order of Authors:	Liting Wang, M.D
	Fabien Hubert, Ph.D
	Sarah Idres, Ph.D, Pharm.D
	Milia Belacel-Ouari, Ph.D, Pharm.D
	Valérie Domergue
	Florence Lefebvre
	Delphine Mika, Ph.D
	Rodolphe Fischmeister, Ph.D
	Véronique Leblais, Ph.D, Pharm.D
	Boris Manoury, Ph.D
Abstract:	PDE3 and PDE4 regulate arterial tone by hydrolysing cAMP in vasculature. Their respective contributions are jeopardized in large vessels from animals with heart failure (HF). However, data from a resistance vessel such as mesenteric artery (MAs) are needed. Additionally, as PDE2 emerges as regulator of failing myocardium, its possible vascular implication remains elusive. Here, the functions of PDE2, PDE3 and PDE4 in rat MAs were characterized in experimental HF. MAs were isolated from rats sacrificed 22 weeks after surgical stenosis of the ascending aorta (HF), or Sham surgery. PDE inhibitors were used to probe isoenzymes contributions in enzymatic and isometric tension assays. PDE2 and PDE4 activities, but not PDE3 activity, facilitate contraction produced by the thromboxane analogue U46619 in Sham arteries, while in HF all three isoenzymes contribute to this response. NOS inhibition by L-NAME abolishes the action of the PDE2 inhibitor. L-NAME also eliminates the contribution of PDE4 in HF, but unmasks a contribution for PDE3 in Sham. PDE3 and PDE4 activities attenuate β-adrenergic relaxant response in Sham and HF. PDE2 does not participate in any tested cAMP or cGMP-mediated relaxant response. PDE3 and PDE4 cAMP-hydrolyzing activities are smaller in lysates of HF MAs, while PDE2 activity is scarce in both groups. However, endothelial cells and arterial myocytes displayed PDE2 immunolabelling. We highlight that, by contrast with previous observations in aorta, PDE4 participates equally as PDE3 in controlling reactivity of MA in HF. PDE2 activity emerges as a discrete, NO-dependent promoter of contractile response that is preserved in HF.
Suggested Reviewers:	George Pak-Heng Leung The University of Hong Kong gphleung@hku.hk relevant expertise
	Long Chen Nanjing University of Chinese Medicine

	longchen@njucm.edu.cn relevant expertise

Phosphodiesterases type 2, 3 and 4 influence vascular tone in mesenteric arteries from rats with heart failure

Running title: Role of PDEs in a resistance vascular bed in heart failure

Authors: Liting Wang*[1], Fabien Hubert*[1], Sarah Idres[1], Milia Belacel-Ouari[1], Valérie Domergue[2], Florence Lefebvre[1], Delphine Mika[1], Rodolphe Fischmeister[1], Véronique Leblais[1], Boris Manoury[1].

[1]Université Paris-Saclay, Inserm, UMR-S 1180, 91400, Orsay, France.

[2]Université Paris-Saclay, Inserm, Cnrs, Ingénierie et Plateformes au Service de l'Innovation Thérapeutique 91400, Orsay, France.

* Mrs Liting Wang and Dr Fabien Hubert contributed equally.

Correspondence to: Boris Manoury, Université Paris-Saclay, Inserm UMR-S 1180, 17 Avenue des Sciences, 91400 Orsay, France.

E-mail: boris.manoury@universite-paris-saclay.fr; Tel: +33-1-80-00-62-90

Data availability statement

Data available on request from the authors. The data that support the findings of this study are available from the corresponding author upon reasonable request. Some data may not be made available because of privacy or ethical restrictions.

Acknowledgements

We thank the animal core facility for efficient animal care, Séverine Domenichini at the MIPSIT microscopy facility and the from ACTAGen transcriptomic facility for helpful technical assistance (IPSIT, Université Paris-Saclay, Châtenay-Malabry, France). This work was supported by the Fondation Leducq for the Transatlantic Network of Excellence cycAMP grant 06CVD02 (to R. F.), the University Paris-Sud (Bonus Attractivité Paris-Sud 2009–2013 to F. H., V. L and B. M.), the Ministère de l'Education Nationale, de l'Enseignement Supérieur et de la Recherche (including PhD fellowship to M. B. O., S. I.). This work was funded by the Grant ANR-10-LABX-33 as member of the Laboratory of Excellence LERMIT and ANR-16-

CE14-0014 (to D.M.) and Fédération Française de Cardiologie (to D.M.) and ANR13BSV10003-02. L.W was supported by the China Scholarship Council (PhD fellowship) and by a grant from Pr Zhi-Cheng Jing (Peking Union Medical College Hospital, Chinese Academy of Medical Sciences and Peking Union Medical College, Beijing, China).

Authors contributions

B.M., V.L., LW, F.H., and R.F. conceived and designed the study. L.W, F.H., S.I., M.B.O., V.D, F.L., D.M. and B.M. carried out the experiments. L.W., F.H., S.I., M.B.O., D.M., V.L. and B.M. collected and analysed the data. B.M., L.W., V.L, R.F. wrote up the manuscript. L.W. and F.H. and contributed equally.

Declaration of interest

None

Orcid ID

B.M.: 0000-0001-7305-5633

Abstract

PDE3 and PDE4 regulate arterial tone by hydrolysing cAMP in vasculature. Their respective contributions are jeopardized in large vessels from animals with heart failure (HF). However, data from a resistance vessel such as mesenteric artery (MAs) are needed. Additionally, as PDE2 emerges as regulator of failing myocardium, its possible vascular implication remains elusive. Here, the functions of PDE2, PDE3 and PDE4 in rat MAs were characterized in experimental HF.

MAs were isolated from rats sacrificed 22 weeks after surgical stenosis of the ascending aorta (HF), or Sham surgery. PDE inhibitors were used to probe isoenzymes contributions in enzymatic and isometric tension assays. PDE2 and PDE4 activities, but not PDE3 activity, facilitate contraction produced by the thromboxane analogue U46619 in Sham arteries, while in HF all three isoenzymes contribute to this response. NOS inhibition by L-NAME abolishes the action of the PDE2 inhibitor. L-NAME also eliminates the contribution of PDE4 in HF, but unmasks a contribution for PDE3 in Sham. PDE3 and PDE4 activities attenuate β-adrenergic relaxant response in Sham and HF. PDE2 does not participate in any tested cAMP or cGMP-mediated relaxant response. PDE3 and PDE4 cAMP-hydrolyzing activities are smaller in lysates of HF MAs, while PDE2 activity is scarce in both groups. However, endothelial cells and arterial myocytes displayed PDE2 immunolabelling.

We highlight that, by contrast with previous observations in aorta, PDE4 participates equally as PDE3 in controlling reactivity of MA in HF. PDE2 activity emerges as a discrete, NO-dependent promoter of contractile response that is preserved in HF.

KEY-WORDS

phosphodiesterase inhibitor, vascular tone; mesenteric artery; heart failure; nitric oxide

1. Introduction

Cyclic nucleotides (CN), namely cAMP and cGMP, are intracellular messengers that mediate transduction of various cellular stimuli. In blood vessels, they inhibit smooth muscle cell (SMC) contractility and proliferation, platelet activity and endothelial permeability (Bobin et al., 2016). Phosphodiesterases (PDEs) are enzymes responsible for CN degradation and as such influence CN dynamics and vascular function (Baillie et al., 2019; Bobin et al., 2016). PDEs encompass a large group of different families of enzymes displaying various catalytic properties, cell distribution and mechanisms of regulation.

Heart failure is a severe condition with altered functional, structural and metabolic features in the heart (McDonagh et al., 2021). This is associated with sustained, deleterious neurohormonal activation that increases vasomotor tone of small resistance arteries and thus resistance of the vascular tree (Hartupee & Mann, 2017). Because the cAMP and cGMP signalling pathways are primary targets of the drugs used to alleviate or treat heart failure (HF) (Ghionzoli et al., 2021), it is crucial to clarify how specific PDE families influence vascular tone in this particular pathological context. Abundant work from our laboratory and others has clarified the role of PDEs in the heart (recently reviewed by (Chen & Yan, 2021; Preedy, 2020)). However, the impact of HF on their ability to control the vascular tone has been much less explored. In the vascular smooth muscle, PDE3 and PDE4 families are regarded as the main contributors for cAMP hydrolytic activity, whereas cGMP is mainly degraded by PDE5 and PDE1 (Hubert et al., 2014; Lugnier et al., 1986). By using a pharmacological approach, reports suggested that PDE2 also opposes vasoconstriction (Baliga et al., 2018; Bubb et al., 2014; Haynes et al., 1996; Wang et al., 2021). Because expression of PDE2 in vascular smooth muscle cells is still elusive (Bubb et al., 2014; Komas, Lugnier, Andriantsitohaina, et al., 1991; Lugnier et al., 1986; Stephenson et al., 2009), how PDE2 may be a contributor to vasomotor tone in these vascular bed remains unclear. Moreover, because specific contribution of PDE2 in the cardiac function in HF has been controversial (Chen & Yan, 2021; Preedy, 2020; Sadek et al., 2020), it is of interest to clarify how PDE2 influence vascular tone in this pathological context.

We recently reported that PDE3 and PDE4 relative participations to tone regulation were altered, quantitatively or qualitatively, in aorta and coronary arteries isolated from rats with congestive heart failure (Hubert et al., 2014; Idres et al., 2019). Because increased in peripheral vascular resistance is a hallmark of HF in patients and experimental models (Hartupee & Mann, 2017; Hentschel et al., 2007), it is also crucial to address whether such modifications of PDE

contributions are also present in small vascular beds that directly impact cardiac afterload. Thus, in order to address these points, we set out to characterize PDE2, PDE3 and PDE4 contributions to arterial tone in mesenteric artery (MA), a typical resistance vascular bed (Falloon et al., 1993), in an experimental model of HF.

2. Material and Methods

2.1 Drugs and reagents

Chemicals and pharmacological reagents were purchased at standard manufacturers. Details on the suppliers can be found in the online supplement (1.1).

All PDE inhibitors were dissolved in dimethylsulfoxyde (DMSO). Final concentration of DMSO did not exceed 0.02%. For each given experiment, amounts of vehicle (water or DMSO) were matched in all groups studied.

2.2 Animals and surgical procedures

All animal care and experimental procedures conformed to the European Community guiding principles in the care and use of animals (Directive 2010/63/EU of the European Parliament) and authorizations to perform animal experiments according to application decrees were obtained from the French Ministry of Agriculture, Fisheries and Food (No. C92-019-01, 03 August 2016). All studies involving animals are reported in accordance with the ARRIVE 2.0 guidelines for reporting experiments involving animals (Percie du Sert et al., 2020).

Heart failure was induced in rats by following a surgical procedure mimicking aortic stenosis, as previously described (De Sousa et al., 1999). The surgery was carried out on 3-week-old rats, under anaesthesia with a ketamine-xylazine mix (75 mg/kg – 10 mg/kg, respectively, 0.3 mL/100 g, i.p.). Aortic stenosis was mimicked by placing a stainless steel hemoclip (0.6 mm-internal diameter) on the ascending aorta via thoracic incision, Also, age-matched control animals underwent the same procedure without placement of the clip (Sham group). Buprenorphine chlorhydrate (0.03 mg/kg, 0.2 mL/100 g, s.c.) was administered twice daily for 3 days beginning at the end of the surgery.

Animals were housed under standard conditions and were sacrificed 22 weeks after surgery according the following procedure. Rats were injected pentobarbital (150 mg/kg, i.p.) to obtain deep anaesthesia, demonstrated by the absence of reaction following toe pinch. The heart, lung,

kidneys, liver and gut associated with the mesenteric vascular bed were quickly isolated and placed in an ice-cold "Krebs" solution of following composition (in mM): NaCl 119, KCl 4.7, $CaCl_2$ 2.5, $MgSO_4$ 1.2, KH_2PO_4 1.2, glucose 11, $NaHCO_3$ 25, bubbled with 95% O_2 and 5% CO_2 to maintain pH at 7.4. Gut was used for isolation of mesenteric arteries. Heart, lung, kidneys and liver were used for gravimetric analysis.

In order to comply with the "Reduce" criteria mentioned in the guidelines, some data presented in this work were obtained using tissues sampled from rats shared with previous studies published by our group, that were focussing on other vascular beds (Hubert et al., 2014; Idres et al., 2019). All organs were sampled immediately following the sacrifice, kept in ice-cold Krebs solutions and frozen or used within 2 hours.

A total of 34 rats with HF sacrificed 22 weeks after surgical aortic stenosis and displaying obvious lung congestion were used (lung weight/tibia length ratio >600 mg/cm). 45 Sham rats were used. In addition, 6 standards, 8-12 week-old, male Wistar rats were used for immunolabelling experiments.

2.3 Mesenteric artery preparation

The gut was pinned on a Sylgard®-coated dish filled with cold Krebs solution so that mesenteric vasculature was apparent. Second and third order MA branches, displaying thick wall and longitudinal striation, were carefully cleaned from connective and fat tissue and dissected. Dissecting solution was renewed every 10-15 min with cold, bubbled solution. Collected tissue was then frozen in liquid nitrogen and stored at -80°C, or freshly processed, according to the following relevant protocols.

2.4 Isometric tension measurement

MA branches were cut into small segments (length 1,5-2 mm) and mounted in the chamber of a small vessel myograph (620 M, Danish Myo Technology A/S, Aarhus, Denmark) using 40 µm tungsten wire, as previously described (Idres et al., 2019). Briefly, Vessels underwent a normalization procedure by stretching the vessels stepwise to construct tension-circumference relationship. Rings were eventually set at an internal circumference corresponding to 90% of the circumference the vessel would have if submitted to a transmural pressure of 100 mmHg (13.3 kPa). Working internal diameters were ≈ 150-350 µm. Contractile capacity of the vessels was evaluated by a challenge with a modified Krebs solution containing 60 mM KCl with equimolar substitution of NaCl (K60). Vessels with response less than 2 mN/mm after 5 min

were excluded from analysis, unless otherwise indicated. Endothelial function was evaluated in all vessels by measurement of the relaxant effect induced by 10 µM acetylcholine (ACh) or 10 µM carbachol on K60-contracted rings. Vessels with poor response (<20%) were excluded. After washes with Krebs, the vessels were submitted to various pharmacological protocols:

(i) Concentration–response curves (CRC) to the thromboxane analogue U46619 (10^{-9} – 3.10^{-6} M) were performed by adding the drug in a stepwise, cumulative manner. The influence of specific PDE isoenzymes activity on the contractile response can be inferred by using selective PDE inhibitors used at relevant concentrations (Bobin et al., 2016; Hubert et al., 2014; Lugnier et al., 1986). Thus this protocol was performed in the presence of Bay-60-7550 (Bay-60, 0.1 µM), cilostamide (Cil, 1 µM) or Ro-20-1724 (Ro, 10 µM) inhibiting PDE2, PDE3 or PDE4, respectively. Selectivity ratio with relevant references are shown in Supplementary Table S1. Respective vehicle solution contained 0.02% DMSO. Contractile responses were expressed in mN/mm or in percent of the contraction evoked by K60.

(ii) In other experiments, CRC for vasorelaxant agents (ACh, isoprenaline (ISO), L-858051 (L85), rat atrial natriuretic peptide (ANP), diethylamine nonoate (DEA-NO), or Bay-60) were established on 10^{-6} M U46619-contracted vessels. ISO was added in the presence of the α-adrenergic receptor antagonist phentolamine (10^{-5} M). When relevant, Bay-60, Cil or Ro were added at least 10 min before contraction. In order to examine the influence of nitric oxide synthase (NOS) activity on responses, some experiments were performed in the presence of 300 µM L-NG-Nitroarginine methyl ester (L-NAME), added at least 20 min before contraction. Relaxant responses were expressed in %, relative to the amplitude of the contraction obtained with U46619.

2.5 cAMP-PDE activity assay

Cyclic AMP-PDE activity was measured by a two-step radioenzymatic assay as previously described (Hubert et al., 2014). Reactions were carried out with inhibitors of PDEs, namely 1 mM 3-isobutyl-1-methylxanthine (IBMX), as a non-selective PDE inhibitor, 0.1 µM Bay-60 as a selective PDE2 inhibitor, 1 µM Cil, as a selective PDE3 inhibitor and 10 µM Ro, as a selective PDE4 inhibitor (see Suppl. Table 2), or vehicle. IBMX-sensitive PDE activity, PDE2, PDE3 and PDE4 activities were defined as the activity that was sensitive to the corresponding inhibitor, compared to the total activity with vehicle in the same experiment. Each data point was obtained from one single animal and was the average of technical duplicates.

2.6 Analysis of PDE isoforms transcripts

Total RNA was extracted from rat MAs following previously described procedure used for rat aorta (Hubert et al., 2014). cDNA was synthesized from 1 µg total RNA using iSCRIPT (Bio-Rad, Marnes-la-Coquette, France). Negative RT controls were prepared by using RNA without addition of the reverse transcriptase. Real-time quantitative PCR (RT-qPCR) was performed using the SYBR-Green method on a CFX384 TouchTM Real-Time PCR Detection System (Bio-Rad). Detection of *Pde2a* and *Pde4c* were carried out using SYBR Premix (Takara Bio Europe, Saint-Germain-en-Laye, France) and SYBR Supermix (Bio-Rad) was used for *Pde3a*, *Pde3b*, *Pde4a*, *Pde4b* and *Pde4d* detection. For each target gene, a standard curve was constructed from the analysis of serial dilution of cDNA and was used to determine efficiency (E). For normalisation, threshold cycle (Ct) for target was subtracted from the mean of Ct for 3 reference genes (ΔCt) to calculate $(1+E)^{\Delta Ct}$ according to the ΔCt method. *Ywhaz*, *Rpl32* and *Rplp2* were generally used as reference genes, except for *Pde2a* and *Pde4c* where *Tbp* substituted for *Rplp2*. Relative expression was expressed as the ratio to the $(1+E)^{\Delta Ct}$ geometric average obtained for Sham samples. Each data point was obtained from one single animal and was the average of technical duplicates. Sequences of the primers used are provided in Supplementary Table S2.

2.7 Immunocytochemistry

Freshly isolated vascular cells were obtained using procedures previously described (Antigny et al., 2016; Idres et al., 2019) and detailed in the Supplementary material (1.2).

Single drops of suspended cell solutions were added on glass coverslips. The coverslips for ECs were incubated with Corning@ Cell-Tak adhesive (Sigma) to improve cell adhesion. Laminin was used for cardiac myocytes. Cells were fixed with 4% paraformaldehyde, washed with PBS, permeabilized with Triton X-100 0.3% in PBS, quenched with NH_4Cl 50 mM in PBS, and blocked with BSA 5% in PBS. Coverslips were then incubated overnight at 4°C with the following primary antibodies: rabbit anti-PDE2A-101AP (1:300, Fabgennix, Frisco, TX); rabbit anti-CD31 (1:50, Abcam, Paris, France); rabbit anti-Calponin (1:200, Santa Cruz Biotechnology, Inc., Dallas, TX), then with anti-rabbit secondary antibodies for 1 h at room temperature (1:500, Alexa Fluor 488- or Alexa Fluor 647-conjugated; Invitrogen, Thermofisher Scientific, Les Ulis, France). The cells were viewed under a fluorescent microscope in inverted confocal laser scanning microscope Leica TCS SP8 (Leica Microsystems, Germany) with an HC PL APO CS2 63x/1.40 oil immersion objective. Sections stained by immunofluorescence

were visualized using Leica SP8 LAS X software (Version 3.5.5; Leica Microsystems, Germany) and processed using the FIJI/ ImageJ software. Furthermore, bright field (BF) images were present to show relevant cell shape. Cells incubated with secondary antibody, without primary antibody, were included as negative controls.

2.8 Data analysis and statistics

CRC obtained for each vessel were fitted with the Hill equation using Prism 7 software (Graphpad Software, La Jolla, CA) and pharmacological parameters, namely pD_2 and maximal effect (E_{max}), were obtained. Data were expressed as mean ± SEM of N experiments, with N representing the number of rats. Where relevant (values normally distributed, equality of variance), group comparisons were performed using one-way ANOVA followed by Holm-Sidak multiple comparison post-test. When above assumptions could not be met, non-parametric Kruskal-Wallis test followed by Dunn's post-test was used. Similarly, either t-test, with or without Welch correction, or Mann-Whitney test were used for 2-group comparison, respectively. Two-group planned comparisons were performed using Mann-Whitney test with Holm correction. Comparisons of CRC were performed using 2-way ANOVA for repeated measures. Values of $P<0.05$ were considered for statistical significance.

3. Results

3.1 Characterization of the heart failure model

Twenty-two weeks after surgery, rats with aortic stenosis included in this study (HF group) displayed dramatic increases in heart weight and lung weight compared to Sham rats, indicating cardiac hypertrophy and lung congestion (Suppl. Figure 1). Kidney weight was significantly decreased in HF, without any change in liver weight or body weight. Because some of these rats were shared with other studies focussing on other vascular beds, echocardiographic and hemodynamic data from these series were published previously (Hubert et al., 2014; Idres et al., 2019). This model was characterized by an increase in left ventricle (LV) mass, LV enlargement, decreased ejection fraction and decreased blood pressure. Overall, these data confirm that all rats included in the HF groups displayed important signs of heart failure.

3.2 Basic vascular reactivity of arteries isolated from rats with HF

First, basic vascular reactivity of MA from Sham and HF rats was explored (Suppl. Figure 2). High potassium, depolarizing solution (K60) evoked robust contraction in rings from both HF and Sham rats, although response to K60 in HF was significantly smaller than in Sham rings (Suppl. Figure 2.A). The thromboxane A_2 mimetic U46619, a standard vasoconstrictor agonist, increased the tension in a concentration-dependent manner that was not significantly different between Sham and HF (Suppl. Figure 2.B, Suppl. Figure 4E-F).

Addition of cumulative concentrations of ACh on rings pre-contracted with U46619 revealed a slight but significant inhibition of the response in HF rats (Suppl. Figure 2.C). Relaxations evoked by DEA-NO were similar in Sham and HF rings (Suppl. Figure 2.D). Overall, these results indicate that MA rings from HF rats display minor alterations in contractile responses. In addition, there was a mild decrease in the relaxation to ACh without any change in the effect of the NO-donor, an observation compatible with endothelial dysfunction in HF.

3.3 Effect of PDE inhibitors on the response to the thromboxane analogue U46619 in HF and Sham MAs

The effects of PDE2, PDE3 and PDE4 inhibition were first assessed on the contractile response evoked by increasing concentrations of U46619 in rat MAs. Compared to vehicle, the selective PDE2 inhibitor Bay-60 (0.1 µM) significantly shifted the CRC to the right and significantly decreased pD_2 for U46619 in rings isolated from both Sham and HF rats (Figure 1.A, B, E, F). Consistently, Bay-60 produced a concentration-dependent relaxation of Sham and HF MAs contracted with U46619 (Figure 5.A, 5B). These data indicate that PDE2 activity influences the vascular tone induced by U46619 in Sham and HF rat MAs.

PDE3 inhibition with 1 µM Cil significantly hampered the response to U46619 by decreasing its pD_2 in HF, but not in Sham vessels (Figure 1.C, D, E, F). The PDE4 inhibitor Ro used at 10 µM strongly inhibited response to U46619 in both Sham and HF groups and this was associated with a significant decrease in its pD_2 values (Figure 1.C, D, E, F). Incubation with PDE inhibitors did not change E_{max} of the response to U46619 (Suppl. Figure 4.A, B). Overall, these

results show that PDE4 activity regulates contractile response to U46619 in both Sham and HF rat MAs, while PDE3 influence can only be demonstrated in HF.

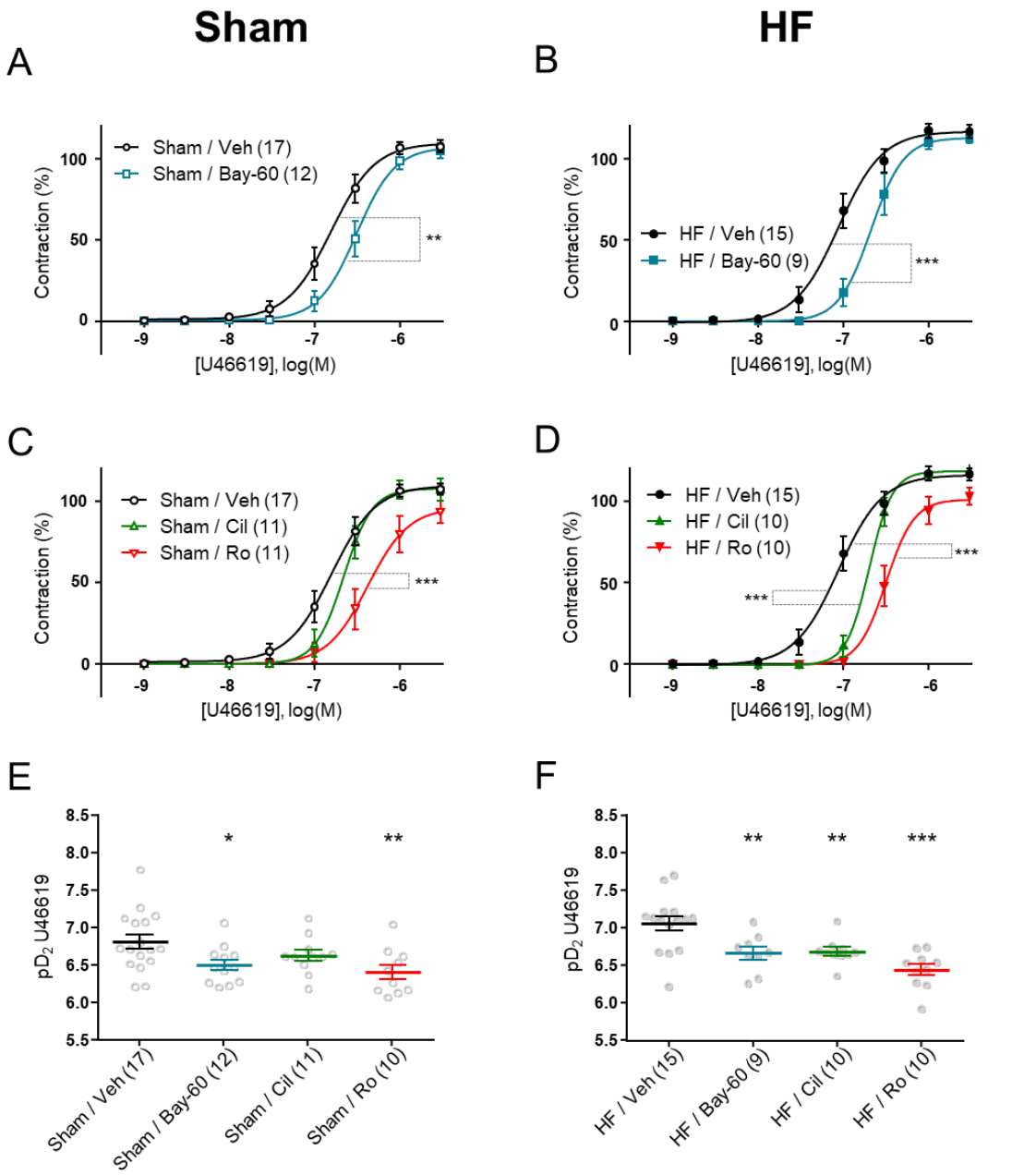

Figure 1: Effect of PDE2 inhibitor (Bay-60-7550, Bay-60, 100 nM), PDE3 inhibitor (cilostamide, Cil, 1 µM), PDE4 inhibitor (Ro-20-1724, Ro, 10 µM) or vehicle (Veh) on CRC to U46619 (10^{-9} – 3.10^{-6} M) in MA rings from rat with heart failure (HF) or Sham littermates. A-D: CRC present mean ± SEM of contractile response (% of K60 response) of rings from (N) animals. Sham-Veh and HF-Veh curves represent the same data for A and C, and for B and D, respectively. **: P< 0.01, ***: P< 0.001 (repeated measures, two-way ANOVA). E, F: Scatter plot and mean ± SEM of pD_2 calculated for (N) responses in Sham (E) and HF (F) groups. *: P< 0.05, **: P< 0.01,***: P< 0.001 compared to respective Veh group (One-way ANOVA followed by Holm-Sidak's post-test).

3.4 cAMP-PDE activity and expression of PDE isoforms in rat mesenteric artery

Cyclic AMP-PDE activity was measured in whole MA lysates. Total activity was reduced in HF MAs in comparison with Sham (Figure 2.A), and this was mainly due to a decrease in both Cil-sensitive and Ro-sensitive PDE activities (Figure 2.B). However, the relative contributions of Cil-sensitive and Ro-sensitive PDE activities were similar in Sham and HF MAs, with PDE3 activity accounting for 52 ± 4% and 52 ± 4% of total activity in Sham and HF, respectively, and PDE4 activity for 49 ± 2%, and 44 ± 4%, respectively (not significantly different, 2-way ANOVA). Bay-60 inhibited less than 10% of total activity and this effect was not different between Sham and HF (Figure 2.B).

Because HF may be associated with some modification in molecular expression of PDE isoforms, relative mRNA quantification was carried out from whole lysate rat MA samples. Figure 2.C shows that expressions of *Pde2a*, *Pde3a*, *Pde3b*, *Pde4a*, *Pde4b* and *Pde4d* were not different in the HF group compared to the Sham group. The *Pde4c* transcript was not detected.

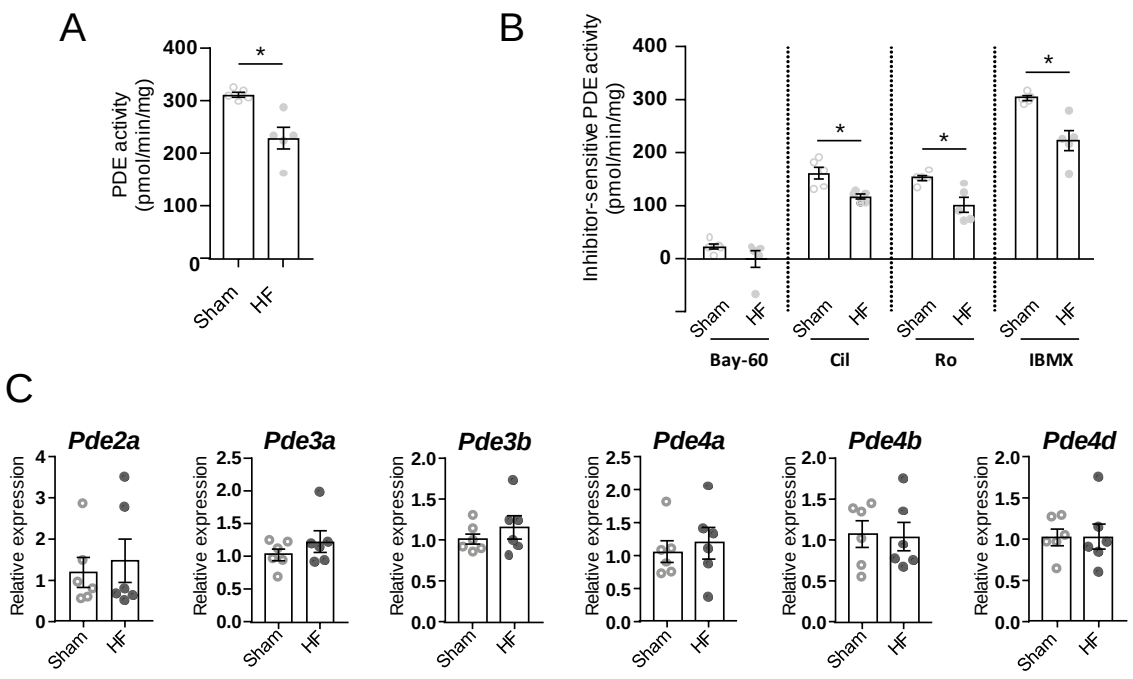

Figure 2: A, B: PDE activity in MA from rats with heart failure (HF) or Sham (Sh) littermates. A. Total PDE activity. *: P<0.05 (Welch's t-test). B. PDE activity sensitive to inhibitors of PDE2 (Bay-60-7550, Bay-60, 100 nM), PDE3 (cilostamide, Cil, 1 µM), PDE4 (Ro-201724, Ro, 10 µM) inhibitors and to the broad PDE inhibitor IBMX (1 mM). A-B: Scatter plot and mean ± SEM of N=5 experiments are shown. *: P<0.05 (Mann-Whitney t-tests with Holm-Sidak correction). C: Relative expression of rat *Pde2a*, *Pde3a*, *Pde3b*, *Pde4a*, *Pde4b*, and *Pde4d* mRNA transcripts in Sham and HF rat MA. Scatter plot and mean ± SEM are shown from N=6 rats.

3.5 Effect of PDE inhibitors on the response to U46619 in the absence of nitric oxide production

The vascular nitric oxide (NO)-cGMP pathway is known to influence some PDE activities: While cGMP stimulates PDE2, it inhibits PDE3-mediated cAMP hydrolysis (Bobin et al., 2016; Eckly & Lugnier, 1994; Lugnier & Schini, 1990). In addition, the NO-cGMP pathway is reported to be depressed in HF (Drexler & Lu, 1992; Hubert et al., 2014; Katz et al., 1992). Therefore, contraction protocols were repeated in the presence of the NOS inhibitor L-NAME (300 µM) in order to reveal a possible action of basal NO release in Sham and HF MAs. L-NAME did not produce any tone in MAs (data not shown). L-NAME significantly potentiated the response to U46619 in both Sham and HF arteries with pD_2 values being significantly increased in both groups (Figure 3.A, B, Suppl. Fig 3.E, F). These observations show that tonic production of NO impedes contractile response to U46619 in both Sham and HF arteries.

In the presence of L-NAME, Bay-60 had no effect on the response to U46619 in Sham nor in HF vessels (Figure 3.A, B, E, F). In similar conditions, both Cil and Ro inhibited significantly the response in the Sham group (Figure 3.C, E). By contrast, only Cil inhibited the response in HF vessels, while Ro had no effect (Figure 3.D, F). When comparing side-by-side these results obtained with (Figure 3) or without (Figure 1) L-NAME, it can be concluded that NOS inhibition: i) prevented the ability of PDE2 inhibition to blunt the U46619 response in both Sham and HF rings; ii) revealed an ability of PDE3 inhibition to impede the U46619 response in Sham arteries, while the effect of Cil in HF arteries was preserved; iii) did not affect the capacity of PDE4 inhibition to blunt the U46619 response in Sham, but dramatically abolished this effect in HF.

3.6 Effect of PDE inhibitors on the response to cAMP stimulation in HF and Sham MAs

PDE3 and PDE4 are important regulators of cAMP in the vascular smooth muscle from various vascular beds, including MA (Bobin et al., 2016; Keravis & Lugnier, 2012; Komas, Lugnier, Andriantsitohaina, et al., 1991; Komas, Lugnier, & Stoclet, 1991). Thus, relaxation to the β-adrenergic receptor agonist isoprenaline (ISO), a typical cAMP-mediated response (Schoeffter et al., 1987), was studied in Sham and HF MAs precontracted with U46619, in the absence or presence of PDE inhibition. The responses to ISO in HF did not differ significantly from that in Sham (Figure 4A, 4.B, see insert for comparison). In Sham, Bay-60 had no significant effect

on the β-adrenergic response, but cil and Ro significantly increased the pD_2 value of this response, indicating a potentiated relaxation (Figure 4.A, C). In HF, both Cil and Ro potentiated

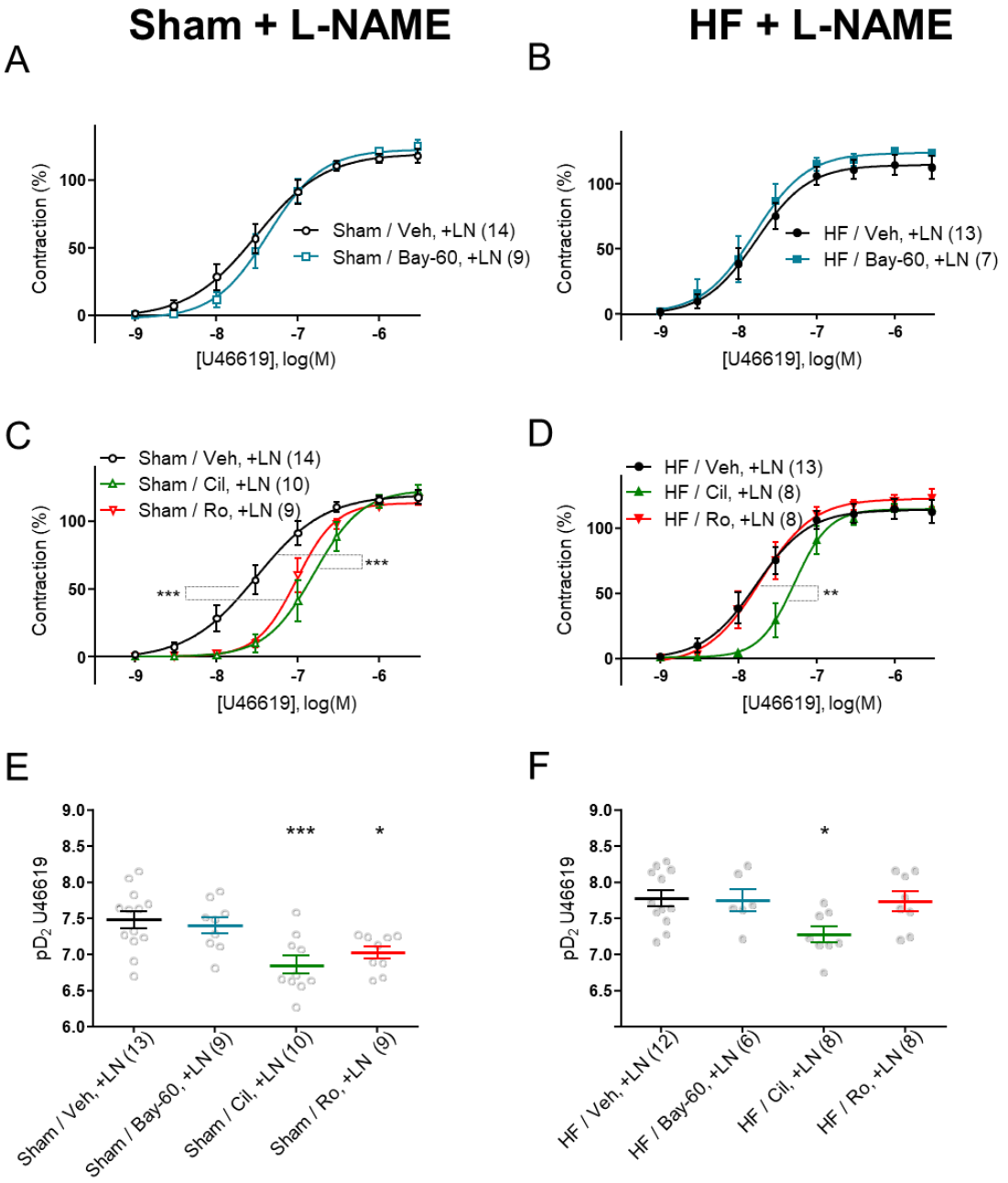

Figure 3: Effect of PDE2 inhibitor (Bay-60-7550, Bay-60, 100 nM), PDE3 inhibitor (cilostamide, Cil, 1 µM), PDE4 inhibitor (Ro-201724, Ro, 10 µM) or vehicle (Veh) on CRC to U46619 (10^{-9} – 3.10^{-6} M) in the presence of 300 µM L-NAME (+LN) in MA rings from rat with heart failure (HF) or Sham littermates. A-D: CRC present mean ± SEM of contractile response of rings from (N) animals. Sham-Veh and HF-Veh curves represent the same data for A and C, and for B and D, respectively. **: P< 0.01, ***: P< 0.001 (repeated measures, two-way ANOVA). E, F: Scatter plot and mean ± SEM of pD_2 calculated for (N) responses in Sham (E) and HF (F) groups. *: P< 0.05, ***: P< 0.001 compared to the respective Veh group (one-way ANOVA followed by Holm-Sidak's post-test).

the response to ISO, but Bay-60 had no effect (Figure 4.B, D). Cil and Ro increased E_{max} of the response to ISO, but not pD_2 (Figure 4.G, H).

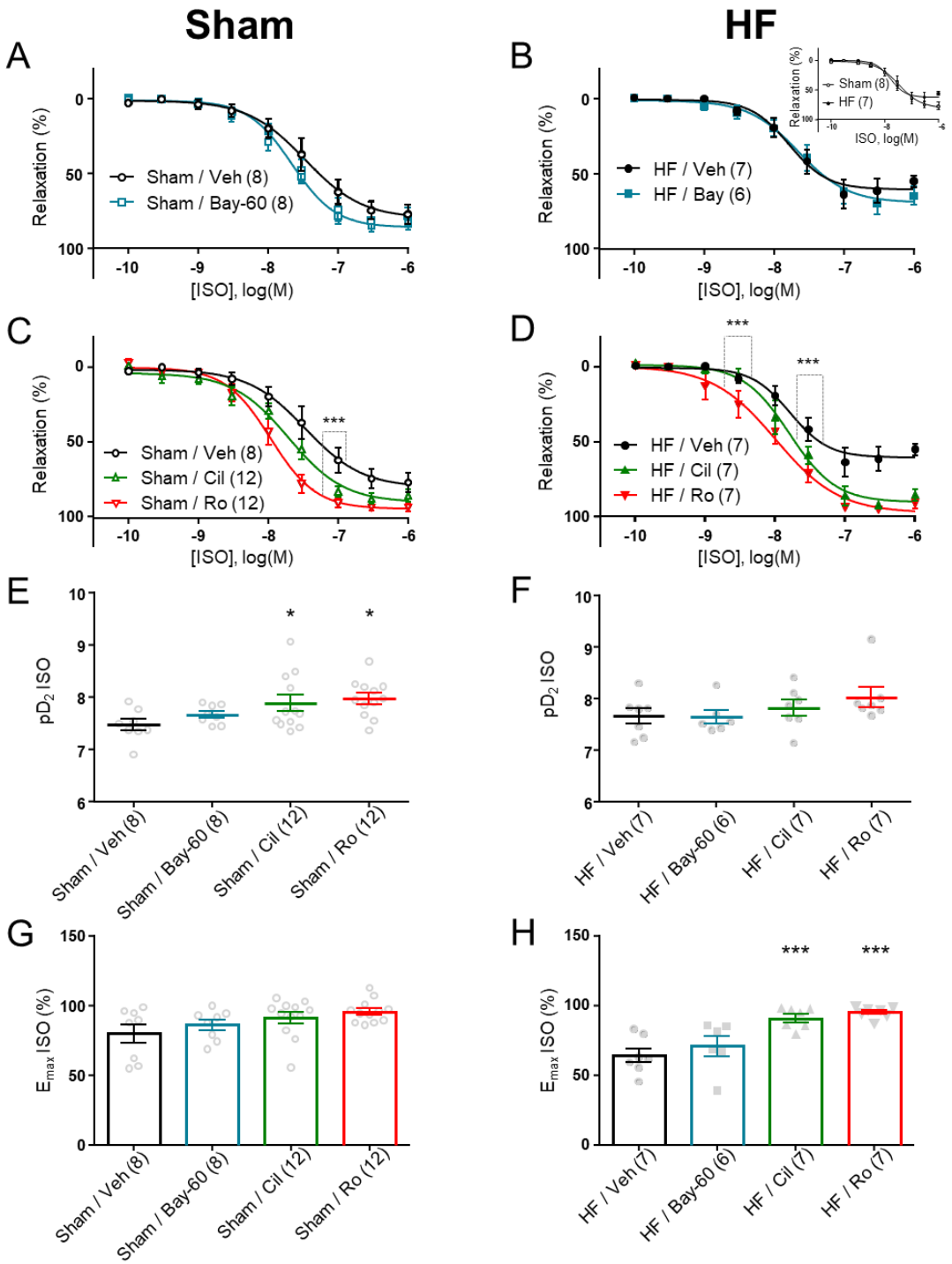

Figure 4: Effect of PDE2 inhibitor (Bay-60-7550, Bay-60, 100 nM), PDE3 inhibitor (cilostamide, Cil, 1 µM), PDE4 inhibitor (Ro-201724, Ro, 10 µM) or vehicle (Veh) on CRC to isoprenaline (ISO, 10^{-10} – 10^{-6} M) in MA rings from rat with heart failure (HF) or Sham littermates. A-D: CRC present mean ± SEM of relaxant response of rings from (N) animals. Insert in B compares responses with Veh in Sham and HF. Sham-Veh and HF-Veh curves represent the same data for A and C, and for B and D, respectively. ***: P< 0.001 (repeated measures, two-way ANOVA). E-H: Scatter plot or bar graph showing mean ± SEM of pD_2 (E, F) and E_{max} (G, H) calculated for (N) responses in Sham (E, G) and HF (F, H) groups. *: P< 0.05, compared to respective Veh group (one-way ANOVA followed by Holm-Sidak's post-test).

It can be concluded that PDE2 inhibition does not significantly modify the response to ISO in rat MAs. Influence of PDE3 and PDE4 activity is revealed in both Sham and HF rings where their respective inhibitors potentiate the β-adrenergic response to ISO.

Because the β-adrenergic receptor transduction pathway may be complex due to cAMP-independent pathways (Banquet et al., 2011), we investigated the effect of Bay-60 on a pure cAMP-mediated response, namely the relaxation to the forskolin analogue L-858051 (L85), a hydrosoluble direct activator of adenylyl cyclases. L85 produced a concentration-dependent relaxation which was similar in Sham and HF MA rings (Figure 5.C, 5.D, see insert for comparison). Pre-incubation with Bay-60 did not alter this response in Sham nor in HF arteries. Thus, taken together, these results show that PDE2 inhibition does not influence the relaxation evoked by stimulation of cAMP production in rat MA.

3.7 Effect of PDE2 inhibition in cGMP-mediated vasorelaxation in HF and Sham MA

An effect of Bay-60 in cGMP-mediated vasorelaxation had been previously characterized in rat pulmonary artery (Bubb et al., 2014). Thus, we set out experiments to examine whether inhibition of PDE2 could also improve the responses to soluble or particulate guanylate cyclase (GC) stimulation in MA rings from Sham and HF rats. Pre-incubation with Bay-60 did not alter the response to the NO donor, DEA-NO, in Sham nor HF arteries precontracted arteries (Figure 5.E, 5.F), showing that PDE2 inhibition does not influence relaxation evoked by stimulation with exogenous NO.

The addition of rat ANP (10^{-13} - 10^{-8} M) on U46619-precontracted MA did not produce any clear concentration-dependent relaxation (N=3), and Bay-60 had no effect on the tension in Sham nor in HF (Figure 5.G, 5.H).

3.8 Expression of PDE2 in SMCs and ECs freshly isolated from rat MA

In order to further address the cell type expressing PDE2 in rat MA, isolated EC and SMC preparations were processed for immunolabelling. Our two cell preparations were pure as shown by specific CD31 and calponin labelling (Figure 6.B, C, see Suppl. Figure 4 for negative controls). We then confirmed that our anti-PDE2 antibody stained the recombinant murine

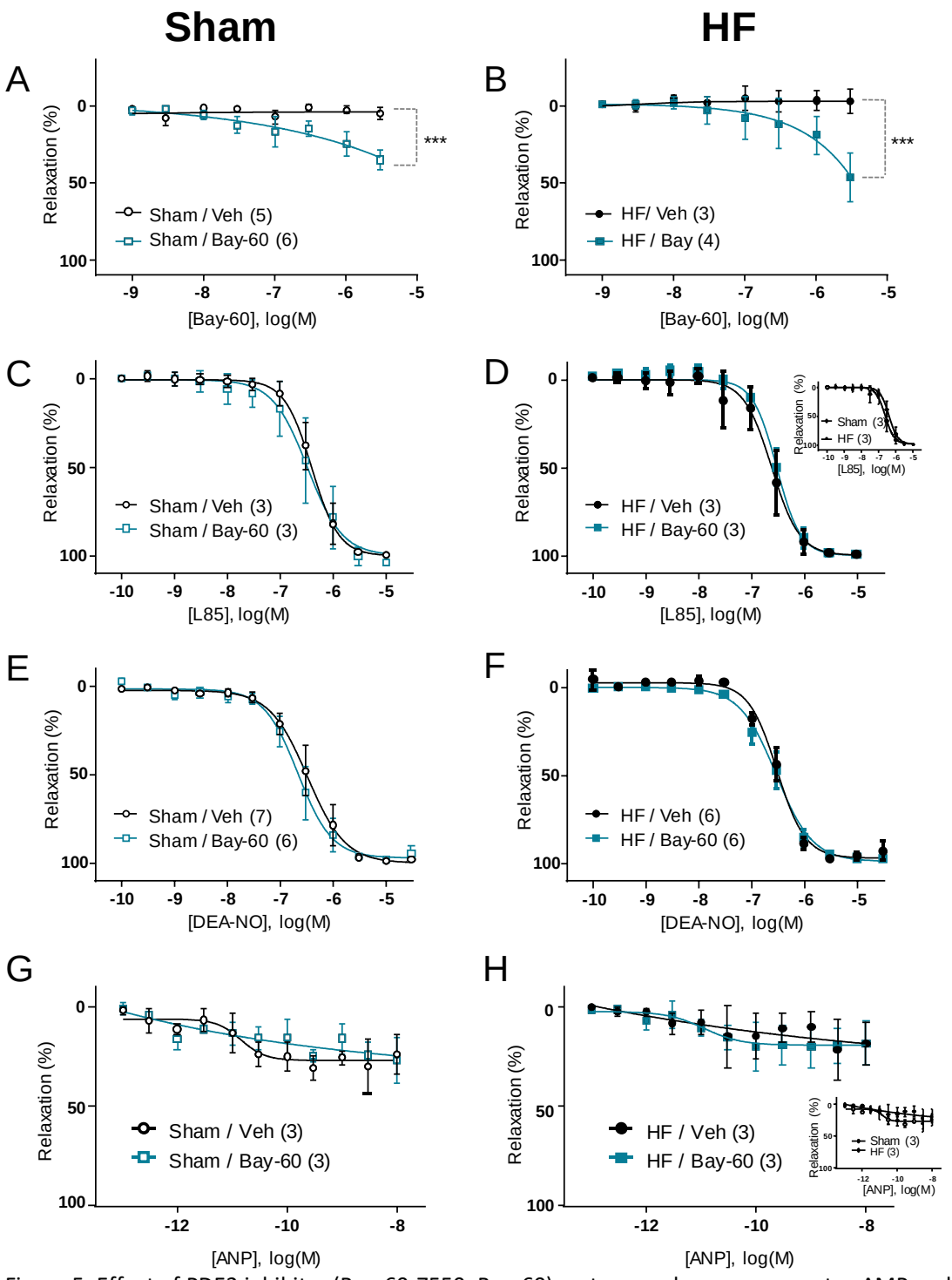

Figure 5: Effect of PDE2 inhibitor (Bay-60-7550, Bay-60) on tone and on responses to cAMP and cGMP stimulators in MAs from rat with heart failure (HF) or Sham littermates. A, B: Vasorelaxant action of Bay-60 (10^{-9} – 3.10^{-6} M) or Veh on rat MA rings precontracted with U46619 (1 µM). C-H: CRCs to the adenylyl cyclase stimulator L-858051 (C,D, L85, 10^{-10} – 10^{-5} M), the nitric oxide donor DEA-nonoate (E, F, DEA-NO, 10^{-10} – 3.10^{-5} M) or rat ANP (G, H, 10^{-13} – 10^{-8} M) in MA rings. CRC present mean ± SEM of relaxant response of rings from (N) animals. Inserts in D and H compare responses with Veh in Sham and HF. Responses to DEA-NO in Sham and HF are compared elsewhere in Figure 2.D. In A (Veh group) and D (Bay group), one ring contracted less than 2 mN/mm while the response to ACh was normal. ***: P< 0.001 vs. Veh (repeated measures, two-way ANOVA).

PDE2A3 overexpressed in mouse cardiomyocytes (Vettel et al., 2016) (Suppl. Figure 5). A similar protocol with the anti-PDE2 antibody yielded clear staining in ECs and SMCs isolated from rat MA, indicating PDE2 expression in both cell types (Figure 6.A). Negative controls showing no staining when omitting primary antibodies are shown in Suppl. Figure 4.

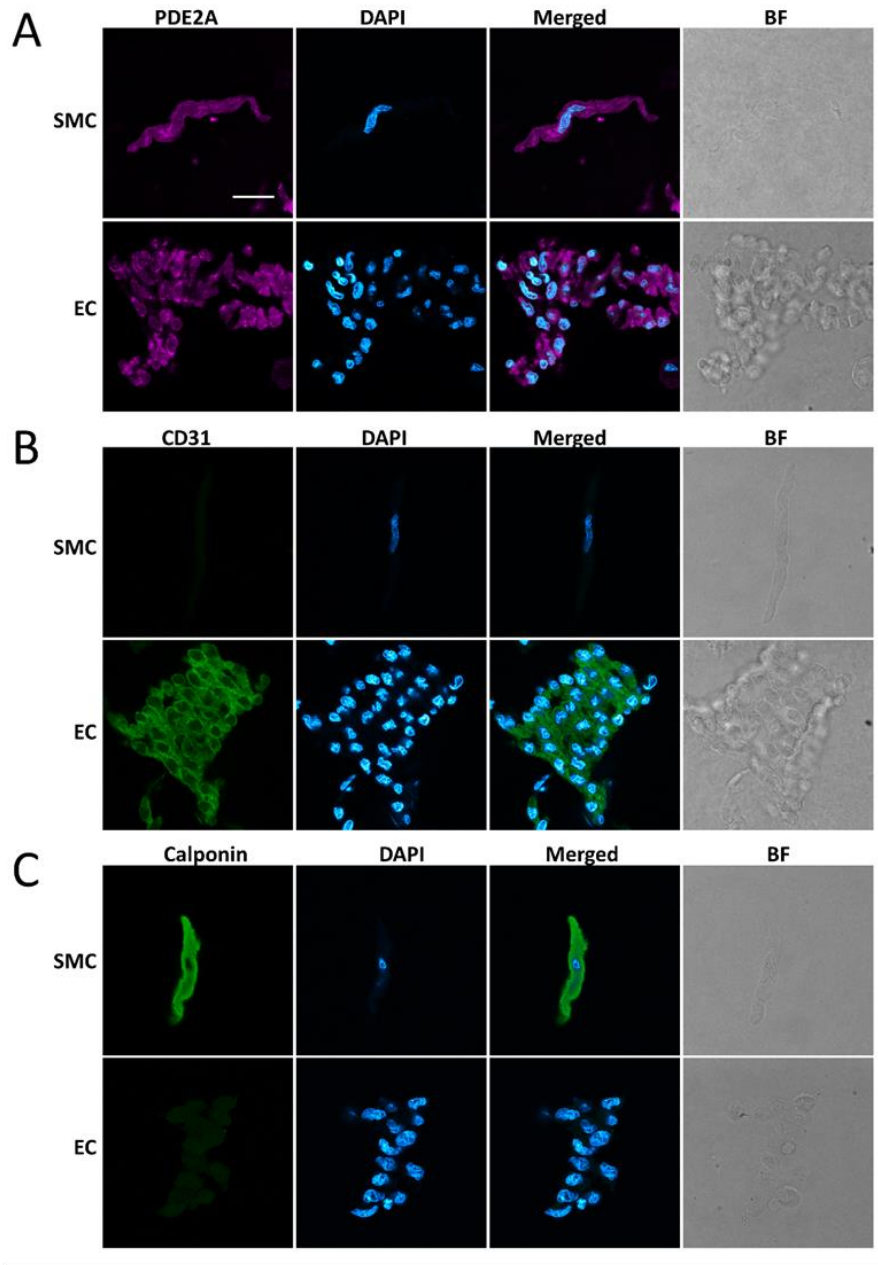

Figure 6: Immunolabelling of PDE2 in freshly isolated smooth muscle cells (SMC) and endothelial cells (EC) from rat MA. Confocal images of isolated SMC or EC sheets immunostained with primary antibodies against PDE2 (A), the EC marker CD31 (B) and the SMC marker calponin (C). All images were obtained at an identical level of laser illumination and have not been altered. DAPI staining indicates nuclei. "Merged" shows overlap of both images. BF: bright field. Scale bar: 20 µm is valid for all images. Representative pictures from N=6 independent experiments are shown.

4. Discussion

We report here novel findings on the control of vascular tone by cAMP-PDEs in experimental HF. While we previously focussed on isolated rat aorta as a model, we now address the effect of PDE2, PDE3 and PDE4 inhibitors in small resistance arteries. We observed that PDE4 contributes to the control of U46619-mediated contraction in Sham and, surprisingly, also in HF groups. PDE3 influence, however, was only obvious in HF. When cAMP signalling was stimulated with the β-adrenergic agonist ISO, both PDE3 and PDE4 influenced the relaxant response in Sham and HF MAs. Interestingly, PDE2 was shown to control U46619 contraction in both Sham and HF vessels. This action was dependent on NOS activity, but neither relaxation evoked by cGMP pathways stimulators nor by direct adenylyl cyclase activation was influenced by the PDE2 inhibitor. These results point to a possible role for endothelial PDE2 in fine tuning contractile response in a vascular bed.

The model of HF used in this study was severe, featured by dramatic LV hypertrophy, kidney atrophy and severe lung congestion. This was supported by echocardiographic data summarized in previous studies, showing LV systolic dysfunction, LV enlargement and decreased blood pressure (Hubert et al., 2014; Idres et al., 2019). The vasoreactivity of mesenteric vessels from animals with HF displayed mild reduction in contractile capacity together with slight endothelial dysfunction. Likewise, aorta and coronary arteries demonstrated impaired response to ACh in the same model of HF (Hubert et al., 2014; Idres et al., 2019). By contrast, other groups studying HF models following myocardial infarction in rat or mice reported no change in responses to K^+, U46619 nor ACh in MA (Bergdahl et al., 1999; Maupoint et al., 2016; Xu et al., 2007). The ability of L-NAME to strongly potentiate U46619 response reveals the existence of a constitutive production of NO that hampers contraction. This effect was maintained in the HF group, suggesting that NO production units are still functional in this vessels. Interestingly, Xu et al. previously observed that the endothelium-derived hyperpolarizing factor component was diminished in MAs from rat with chronic HF (Xu et al., 2007). Thus, alteration of a NO-independent component of the ACh response may explain the slight endothelial dysfunction that was observed in this study.

PDE3 and PDE4 are the main PDE families responsible for cAMP hydrolysis in arteries. Although responsible for more than 50% of total activity, PDE3 did not appear to contribute significantly to arterial tone in Sham, unless cAMP pathway was stimulated with ISO. Yet, Cil promoted relaxation in other vascular beds (Hubert et al., 2014; Idres et al., 2019; Pauvert et al.,

2002). This may be explained by a relatively large PDE4 activity in rat MAs, which would mask the effect of PDE3 inhibition in Sham. Our enzymatic data suggest that relative abundance of PDE4 activity in Sham vessels is higher in MA (49%) than in aorta (28%, (Hubert et al., 2014)), although other studies found equivalent values in both vascular beds (Tahseldar-Roumieh et al., 2009). Because cGMP can inhibit cAMP-hydrolysis by PDE3 (Bobin et al., 2016; Eckly & Lugnier, 1994; Lugnier & Schini, 1990), depressed contribution of PDE3 could also be caused by a strong constitutive NO release, causing sufficient cGMP production to repress PDE3 activity. Accordingly, Cil was able to relax rat MA contracted with phenylephrine in the presence of a NOS inhibitor (Matsumoto et al., 2004). This is consistent with our study showing that inhibition of NO-cGMP signalling with L-NAME clearly promoted PDE3 contribution in Sham arteries.

The main alteration in HF was the smaller PDE3 and PDE4 activities in HF whole MAs lysates. This is at odds with models for other pathologies such as pulmonary arterial hypertension and diabetes, where increases in PDE3 activity were reported in different vascular beds (Maclean et al., 1997; Matsumoto et al., 2003; Wagner et al., 1997), highlighting that PDE regulation undergoes specific changes in HF. Nevertheless, contribution of PDE3 and PDE4 to vascular tone was still robust in HF. This discrepancy suggests that attenuation of whole tissue PDE activity is not a limiting factor for these enzymes to control vasomotor responses. Recent literature underlines the relevance of subcellular molecular complexes including receptors, effectors, PDEs and scaffolding proteins for shaping CN signals at a nanometric scale and ensure tight control of cellular function (Bers et al., 2019). While characterization of compartmentalization in vasculature is only emerging (Lorigo et al., 2021), it may be hypothesized that such a molecular network is preserved in HF and salvages the fine tuning of cAMP pathways that influence vascular tone.

In aorta, the absence of cGMP exacerbates PDE3 activity contribution and masks the participation of PDE4 in the control of vascular tone (Eckly & Lugnier, 1994; Hubert et al., 2014). However, our data suggest that this mechanism is not relevant in Sham MA, because the effect of Ro was still observed in the presence of L-NAME. Moreover, in HF, PDE4 inhibition still hampered contraction and potentiated β-adrenergic response in MA. In the latter vessels, however, effect of Ro was still clearly NO-dependent, indicating that the cGMP signalling is still active in HF and influences PDE activities. Overall, our results suggest that no decrease in NO bioavailability occurs in MAs of HF rats, and thus does not influence the relative contribution of PDE3 and PDE4 in cAMP hydrolysis. The reason why PDE4 contribution is

more vulnerable to NO loss in HF is unclear. This may be caused by the absolute smaller PDE4 activity in tissue, making it more sensitive to competition with PDE3, which displays above 100-time higher affinity for the substrate (Omori & Kotera, 2007).

Altogether, our data suggest that PDE4 inhibition may still present a valid means to produce vasorelaxation in peripheral, resistance vessel in HF. This may emerge as a relevant clinical strategy to relieve the elevated postcharge burden on the left ventricle in this disease.

By using the selective inhibitor Bay-60 to probe PDE2 contribution to vasomotor tone, we observed that it inhibited contractile response to U46619 in both Sham and HF groups. This observation is in line with previous studies reporting that PDE2 opposes vasorelaxation in pulmonary and coronary circulation (Baliga et al., 2018; Bubb et al., 2014; Haynes et al., 1996). It also fits in vivo data where Bay-60 decreases arterial elastance, an indicator proportional to peripheral vascular resistance (Wang et al., 2021). Interestingly, NOS inhibition by L-NAME abolished the effect of Bay-60. Similarly, modest vasodilator effect of Bay-60 in perfused mouse heart was abolished in GC-1$\alpha^{-/-}$ animals (Baliga et al., 2018). Together, these results suggest that constitutive activity of the NO pathway is necessary to reveal PDE2 activity, enabling this enzyme to control CN signalling and tone in resistance arteries. Nevertheless, this may be explained by several underlying mechanisms, whether PDE2 is localized in vascular SMCs or in ECs. Both options are discussed in the following paragraphs.

Activity and expression of PDE2 were previously reported in vasculature (Bubb et al., 2014; Haynes et al., 1996; Pauvert et al., 2002; Sadhu et al., 1999; Saeki & Saito, 1993), whereas immunostaining revealed only weak expression in tunica media (Stephenson et al., 2009). We showed here that the PDE2 transcript and protein are present in whole MA and isolated SMCs, respectively. Such a SMC-located PDE2 may provide an obvious means to mitigate CN signalling and associated vasorelaxation. However, because Bay-60 did not facilitate such responses (L85, DEA-NO), we reasoned that the inhibiting influence on the U46619 response is unlikely to be explained by a potentiation of CN signalling in MA SMCs. PDE2 expression in the SMCs may not be sufficient to overcome PDE3 or PDE4 activities and influence tone. This is consistent with the very low contribution of PDE2 activity to cAMP hydrolysis in whole-MA homogenates.

Rather, we propose a model where an endothelial PDE2 would control paracrine regulation of smooth muscle contractility. PDE2 expression *in situ* and in primary cultured ECs is widely documented (Lugnier & Schini, 1990; Sadhu et al., 1999; Souness et al., 1990; Stephenson et

al., 2009). We confirmed PDE2 expression in freshly ECs isolated from rat MA. Besides, it was demonstrated that PDE inhibitors increase the basal production of NO in ECs (Hashimoto et al., 2006). Our results are compatible with the hypothesis that inhibiting PDE2 in endothelium enhances NOS activity, stimulating the NO - cGMP pathway and hampering SMC contraction. PDE inhibition may facilitate NOS stimulation by dowstream cAMP effectors in ECs such as PKA or EPAC (Garcia-Morales et al., 2017; Iring et al., 2019). Further studies are needed to establish the modalities of this mechanism in functional arteries.

As to a limitation of study, it cannot be absolutely ruled out that a non-selective, off-target effect of Bay-60 may be responsible for the observed inhibition of U46619 response. Nevertheless, Bay-60 was used at 0.1 µM which is reported to selectively inhibit PDE2 compared to other PDE families (Supplementary Table S2). The fact that Bay-60 produced effects that were distinct from inhibitors of other PDEs also supports that they can be ascribed to selective PDE2 inhibition.

5. Conclusion

This study extends the characterization of the effects of PDE2, PDE3 and PDE4 inhibitors on vascular tone in HF to an archetypical resistance vessel, namely MA. We show that relative contribution of these PDEs to contractile and β-adrenergic relaxant responses are in general less impacted by HF than what was observed in aorta (Hubert et al., 2014). While influence of PDE3 is more limited in Sham than in HF MA, the role of PDE4 is more prominent in both normal and pathological contexts, making this family of enzymes a potential target to obtain peripheral vasodilation in patients with HF. Our data also revealed a discrete influence of PDE2 on the contractile response to U46619, which depends on constitutive NO production but is preserved in HF. This opens new perspectives on how specific PDE activities fine tune the control of peripheral vascular beds by CNs.

6. References

Antigny, F., Hautefort, A., Meloche, J., Belacel-Ouari, M., Manoury, B., Rucker-Martin, C., . . . Perros, F. (2016). Potassium-Channel Subfamily K-Member 3 (KCNK3) Contributes to the Development of Pulmonary Arterial Hypertension. *Circulation*. doi:10.1161/CIRCULATIONAHA.115.020951

Baillie, G. S., Tejeda, G. S., & Kelly, M. P. (2019). Therapeutic targeting of 3',5'-cyclic nucleotide phosphodiesterases: inhibition and beyond. *Nat Rev Drug Discov, 18*(10), 770-796. doi:10.1038/s41573-019-0033-4

Baliga, R. S., Preedy, M. E. J., Dukinfield, M. S., Chu, S. M., Aubdool, A. A., Bubb, K. J., . . . Hobbs, A. J. (2018). Phosphodiesterase 2 inhibition preferentially promotes NO/guanylyl cyclase/cGMP signaling to reverse the development of heart failure. *Proc Natl Acad Sci U S A, 115*(31), E7428-E7437. doi:10.1073/pnas.1800996115

Banquet, S., Delannoy, E., Agouni, A., Dessy, C., Lacomme, S., Hubert, F., . . . Leblais, V. (2011). Role of G(i/o)-Src kinase-PI3K/Akt pathway and caveolin-1 in beta-adrenoceptor coupling to endothelial NO synthase in mouse pulmonary artery. *Cell Signal, 23*(7), 1136-1143.

Bergdahl, A., Valdemarsson, S., Nilsson, T., Sun, X. Y., Hedner, T., & Edvinsson, L. (1999). Dilatory responses to acetylcholine, calcitonin gene-related peptide and substance P in the congestive heart failure rat. *Acta Physiol Scand, 165*(1), 15-23. doi:10.1046/j.1365-201x.1999.00456.x

Bers, D. M., Xiang, Y. K., & Zaccolo, M. (2019). Whole-Cell cAMP and PKA Activity are Epiphenomena, Nanodomain Signaling Matters. *Physiology (Bethesda), 34*(4), 240-249. doi:10.1152/physiol.00002.2019

Bobin, P., Belacel-Ouari, M., Bedioune, I., Zhang, L., Leroy, J., Leblais, V., . . . Vandecasteele, G. (2016). Cyclic nucleotide phosphodiesterases in heart and vessels: A therapeutic perspective. *Arch Cardiovasc Dis, 109*(6-7), 431-443. doi:10.1016/j.acvd.2016.02.004

Bubb, K. J., Trinder, S. L., Baliga, R. S., Patel, J., Clapp, L. H., MacAllister, R. J., & Hobbs, A. J. (2014). Inhibition of Phosphodiesterase 2 Augments cGMP and cAMP Signaling to Ameliorate Pulmonary Hypertension. *Circulation, 130*(6), 496-507. doi:10.1161/CIRCULATIONAHA.114.009751

Chen, S., & Yan, C. (2021). An update of cyclic nucleotide phosphodiesterase as a target for cardiac diseases. *Expert Opin Drug Discov, 16*(2), 183-196. doi:10.1080/17460441.2020.1821643

De Sousa, E., Veksler, V., Minajeva, A., Kaasik, A., Mateo, P., Mayoux, E., . . . Ventura-Clapier, R. (1999). Subcellular creatine kinase alterations. Implications in heart failure. *Circ Res, 85*(1), 68-76.

Drexler, H., & Lu, W. (1992). Endothelial dysfunction of hindquarter resistance vessels in experimental heart failure. *Am J Physiol, 262*(6 Pt 2), H1640-1645. doi:10.1152/ajpheart.1992.262.6.H1640

Eckly, A. E., & Lugnier, C. (1994). Role of phosphodiesterases III and IV in the modulation of vascular cyclic AMP content by the NO/cyclic GMP pathway. *Br J Pharmacol, 113*(2), 445-450.

Falloon, B. J., Bund, S. J., Tulip, J. R., & Heagerty, A. M. (1993). In vitro perfusion studies of resistance artery function in genetic hypertension. *Hypertension, 22*(4), 486-495. doi:10.1161/01.hyp.22.4.486

Garcia-Morales, V., Luaces-Regueira, M., & Campos-Toimil, M. (2017). The cAMP effectors PKA and Epac activate endothelial NO synthase through PI3K/Akt pathway in human endothelial cells. *Biochem Pharmacol, 145*, 94-101. doi:10.1016/j.bcp.2017.09.004

Ghionzoli, N., Gentile, F., Del Franco, A. M., Castiglione, V., Aimo, A., Giannoni, A., . . . Vergaro, G. (2021). Current and emerging drug targets in heart failure treatment. *Heart Fail Rev*. doi:10.1007/s10741-021-10137-2

Hartupee, J., & Mann, D. L. (2017). Neurohormonal activation in heart failure with reduced ejection fraction. *Nat Rev Cardiol, 14*(1), 30-38. doi:10.1038/nrcardio.2016.163

Hashimoto, A., Miyakoda, G., Hirose, Y., & Mori, T. (2006). Activation of endothelial nitric oxide synthase by cilostazol via a cAMP/protein kinase A- and phosphatidylinositol 3-kinase/Akt-dependent mechanism. *Atherosclerosis, 189*(2), 350-357. doi:10.1016/j.atherosclerosis.2006.01.022

Haynes, J., Jr., Killilea, D. W., Peterson, P. D., & Thompson, W. J. (1996). Erythro-9-(2-hydroxy-3-nonyl)adenine inhibits cyclic-3',5'-guanosine monophosphate-stimulated phosphodiesterase to reverse hypoxic pulmonary vasoconstriction in the perfused rat lung. *J Pharmacol Exp Ther, 276*(2), 752-757.

Hentschel, T., Yin, N., Riad, A., Habbazettl, H., Weimann, J., Koster, A., . . . Kuebler, W. M. (2007). Inhalation of the phosphodiesterase-3 inhibitor milrinone attenuates pulmonary hypertension in a rat model of congestive heart failure. *Anesthesiology, 106*(1), 124-131. doi:10.1097/00000542-200701000-00021

Hubert, F., Belacel-Ouari, M., Manoury, B., Zhai, K., Domergue-Dupont, V., Mateo, P., . . . Leblais, V. (2014). Alteration of vascular reactivity in heart failure: role of phosphodiesterases 3 and 4. *Br J Pharmacol, 171*(23), 5361-5375. doi:10.1111/bph.12853

Idres, S., Perrin, G., Domergue, V., Lefebvre, F., Gomez, S., Varin, A., . . . Manoury, B. (2019). Contribution of BKCa channels to vascular tone regulation by PDE3 and PDE4 is lost in heart failure. *Cardiovasc Res, 115*(1), 130-144. doi:10.1093/cvr/cvy161

Iring, A., Jin, Y. J., Albarran-Juarez, J., Siragusa, M., Wang, S., Dancs, P. T., . . . Offermanns, S. (2019). Shear stress-induced endothelial adrenomedullin signaling regulates vascular tone and blood pressure. *J Clin Invest, 129*(7), 2775-2791. doi:10.1172/JCI123825

Katz, S. D., Biasucci, L., Sabba, C., Strom, J. A., Jondeau, G., Galvao, M., . . . LeJemtel, T. H. (1992). Impaired endothelium-mediated vasodilation in the peripheral vasculature of patients with congestive heart failure. *J Am Coll Cardiol, 19*(5), 918-925.

Keravis, T., & Lugnier, C. (2012). Cyclic nucleotide phosphodiesterase (PDE) isozymes as targets of the intracellular signalling network: benefits of PDE inhibitors in various diseases and perspectives for future therapeutic developments. *Br J Pharmacol, 165*(5), 1288-1305. doi:10.1111/j.1476-5381.2011.01729.x

Komas, N., Lugnier, C., Andriantsitohaina, R., & Stoclet, J. C. (1991). Characterisation of cyclic nucleotide phosphodiesterases from rat mesenteric artery. *Eur J Pharmacol, 208*(1), 85-87.

Komas, N., Lugnier, C., & Stoclet, J. C. (1991). Endothelium-dependent and independent relaxation of the rat aorta by cyclic nucleotide phosphodiesterase inhibitors. *Br J Pharmacol, 104*(2), 495-503.

Lorigo, M., Oliveira, N., & Cairrao, E. (2021). PDE-Mediated Cyclic Nucleotide Compartmentation in Vascular Smooth Muscle Cells: From Basic to a Clinical Perspective. *J Cardiovasc Dev Dis, 9*(1). doi:10.3390/jcdd9010004

Lugnier, C., & Schini, V. B. (1990). Characterization of cyclic nucleotide phosphodiesterases from cultured bovine aortic endothelial cells. *Biochem Pharmacol, 39*(1), 75-84.

Lugnier, C., Schoeffter, P., Le Bec, A., Strouthou, E., & Stoclet, J. C. (1986). Selective inhibition of cyclic nucleotide phosphodiesterases of human, bovine and rat aorta. *Biochem Pharmacol, 35*(10), 1743-1751.

Maclean, M. R., Johnston, E. D., McCulloch, K. M., Pooley, L., Houslay, M. D., & Sweeney, G. (1997). Phosphodiesterase isoforms in the pulmonary arterial circulation of the rat: changes in pulmonary hypertension. *J Pharmacol Exp Ther, 283*(2), 619-624.

Matsumoto, T., Kobayashi, T., & Kamata, K. (2003). Alterations in EDHF-type relaxation and phosphodiesterase activity in mesenteric arteries from diabetic rats. *Am J Physiol Heart Circ Physiol, 285*(1), H283-291. doi:10.1152/ajpheart.00954.2002

Matsumoto, T., Wakabayashi, K., Kobayashi, T., & Kamata, K. (2004). Diabetes-related changes in cAMP-dependent protein kinase activity and decrease in relaxation response in rat mesenteric artery. *Am J Physiol Heart Circ Physiol, 287*(3), H1064-1071. doi:10.1152/ajpheart.00069.2004

Maupoint, J., Besnier, M., Gomez, E., Bouhzam, N., Henry, J. P., Boyer, O., . . . Richard, V. (2016). Selective Vascular Endothelial Protection Reduces Cardiac Dysfunction in Chronic Heart Failure. *Circ Heart Fail, 9*(4), e002895. doi:10.1161/CIRCHEARTFAILURE.115.002895

McDonagh, T. A., Metra, M., Adamo, M., Gardner, R. S., Baumbach, A., Bohm, M., . . . Group, E. S. C. S. D. (2021). 2021 ESC Guidelines for the diagnosis and treatment of acute and chronic heart failure. *Eur Heart J, 42*(36), 3599-3726. doi:10.1093/eurheartj/ehab368

Omori, K., & Kotera, J. (2007). Overview of PDEs and their regulation. *Circ Res, 100*(3), 309-327. doi:10.1161/01.RES.0000256354.95791.f1

Pauvert, O., Salvail, D., Rousseau, E., Lugnier, C., Marthan, R., & Savineau, J. P. (2002). Characterisation of cyclic nucleotide phosphodiesterase isoforms in the media layer of the main pulmonary artery. *Biochem Pharmacol, 63*(9), 1763-1772.

Percie du Sert, N., Hurst, V., Ahluwalia, A., Alam, S., Avey, M. T., Baker, M., . . . Wurbel, H. (2020). The ARRIVE guidelines 2.0: Updated guidelines for reporting animal research. *PLoS Biol, 18*(7), e3000410. doi:10.1371/journal.pbio.3000410

Preedy, M. E. J. (2020). Cardiac Cyclic Nucleotide Phosphodiesterases: Roles and Therapeutic Potential in Heart Failure. *Cardiovasc Drugs Ther, 34*(3), 401-417. doi:10.1007/s10557-020-06959-1

Sadek, M. S., Cachorro, E., El-Armouche, A., & Kammerer, S. (2020). Therapeutic Implications for PDE2 and cGMP/cAMP Mediated Crosstalk in Cardiovascular Diseases. *Int J Mol Sci, 21*(20). doi:10.3390/ijms21207462

Sadhu, K., Hensley, K., Florio, V. A., & Wolda, S. L. (1999). Differential expression of the cyclic GMP-stimulated phosphodiesterase PDE2A in human venous and capillary endothelial cells. *J Histochem Cytochem, 47*(7), 895-906. doi:10.1177/002215549904700707

Saeki, T., & Saito, I. (1993). Isolation of cyclic nucleotide phosphodiesterase isozymes from pig aorta. *Biochem Pharmacol, 46*(5), 833-839.

Schoeffter, P., Lugnier, C., Demesy-Waeldele, F., & Stoclet, J. C. (1987). Role of cyclic AMP- and cyclic GMP-phosphodiesterases in the control of cyclic nucleotide levels and smooth muscle tone in rat isolated aorta. A study with selective inhibitors. *Biochem Pharmacol, 36*(22), 3965-3972.

Souness, J. E., Diocee, B. K., Martin, W., & Moodie, S. A. (1990). Pig aortic endothelial-cell cyclic nucleotide phosphodiesterases. Use of phosphodiesterase inhibitors to evaluate their roles in regulating cyclic nucleotide levels in intact cells. *Biochem J, 266*(1), 127-132. doi:10.1042/bj2660127

Stephenson, D. T., Coskran, T. M., Wilhelms, M. B., Adamowicz, W. O., O'Donnell, M. M., Muravnick, K. B., . . . Morton, D. (2009). Immunohistochemical localization of phosphodiesterase 2A in multiple mammalian species. *J Histochem Cytochem, 57*(10), 933-949. doi:10.1369/jhc.2009.953471

Vettel, C., Lindner, M., Dewenter, M., Lorenz, K., Schanbacher, C., Riedel, M., . . . El-Armouche, A. (2016). Phosphodiesterase 2 Protects Against Catecholamine-Induced

Arrhythmia and Preserves Contractile Function After Myocardial Infarction. *Circ Res*. doi:10.1161/CIRCRESAHA.116.310069

Wagner, R. S., Smith, C. J., Taylor, A. M., & Rhoades, R. A. (1997). Phosphodiesterase inhibition improves agonist-induced relaxation of hypertensive pulmonary arteries. *J Pharmacol Exp Ther, 282*(3), 1650-1657.

Wang, Y. W., Gao, Q. W., Xiao, Y. J., Zhu, X. J., Gao, L., Zhang, W. H., . . . Chen, L. (2021). Bay 60-7550, a PDE2 inhibitor, exerts positive inotropic effect of rat heart by increasing PKA-mediated phosphorylation of phospholamban. *Eur J Pharmacol, 901*, 174077. doi:10.1016/j.ejphar.2021.174077

Xu, Y., Henning, R. H., Lipsic, E., van Buiten, A., van Gilst, W. H., & Buikema, H. (2007). Acetylcholine stimulated dilatation and stretch induced myogenic constriction in mesenteric artery of rats with chronic heart failure. *Eur J Heart Fail, 9*(2), 144-151. doi:10.1016/j.ejheart.2006.05.003

7. Figure legends

Figure 1: Effect of PDE2 inhibitor (Bay-60-7550, Bay-60, 100 nM), PDE3 inhibitor (cilostamide, Cil, 1 µM), PDE4 inhibitor (Ro-20-1724, Ro, 10 µM) or vehicle (Veh) on CRC to U46619 (10^{-9} – 3.10^{-6} M) in MA rings from rat with heart failure (HF) or Sham littermates. A-D: CRC present mean ± SEM of contractile response (% of K60 response) of rings from (N) animals. Sham-Veh and HF-Veh curves represent the same data for A and C, and for B and D, respectively. **: P< 0.01, ***: P< 0.001 (repeated measures, two-way ANOVA). E, F: Scatter plot and mean ± SEM of pD_2 calculated for (N) responses in Sham (E) and HF (F) groups. *: P< 0.05, **: P< 0.01, ***: P< 0.001 compared to respective Veh group (One-way ANOVA followed by Holm-Sidak's post-test).

Figure 2: A, B: PDE activity in MA from rats with heart failure (HF) or Sham (Sh) littermates. A. Total PDE activity. *: P<0.05 (Welch's t-test). B. PDE activity sensitive to inhibitors of PDE2 (Bay-60-7550, Bay-60, 100 nM), PDE3 (cilostamide, Cil, 1 µM), PDE4 (Ro-201724, Ro, 10 µM) inhibitors and to the broad PDE inhibitor IBMX (1 mM). A-B: Scatter plot and mean ± SEM of N=5 experiments are shown. *: P<0.05 (Mann-Whitney t-tests with Holm-Sidak correction). C: Relative expression of rat *Pde2a*, *Pde3a*, *Pde3b*, *Pde4a*, *Pde4b*, and *Pde4d* mRNA transcripts in Sham and HF rat MA. Scatter plot and mean ± SEM are shown from N=6 rats.

Figure 3: Effect of PDE2 inhibitor (Bay-60-7550, Bay-60, 100 nM), PDE3 inhibitor (cilostamide, Cil, 1 µM), PDE4 inhibitor (Ro-201724, Ro, 10 µM) or vehicle (Veh) on CRC to U46619 (10^{-9} – 3.10^{-6} M) in the presence of 300 µM L-NAME (+LN) in MA rings from rat with heart failure (HF) or Sham littermates. A-D: CRC present mean ± SEM of contractile response of rings from (N) animals. Sham-Veh and HF-Veh curves represent the same data for A and C, and for B and D, respectively. **: P< 0.01, ***: P< 0.001 (repeated measures, two-way ANOVA). E, F: Scatter plot and mean ± SEM of pD_2 calculated for (N) responses in Sham (E) and HF (F) groups. *: P< 0.05, ***: P< 0.001 compared to the respective Veh group (one-way ANOVA followed by Holm-Sidak's post-test).

Figure 4: Effect of PDE2 inhibitor (Bay-60-7550, Bay-60, 100 nM), PDE3 inhibitor (cilostamide, Cil, 1 µM), PDE4 inhibitor (Ro-201724, Ro, 10 µM) or vehicle (Veh) on CRC to isoprenaline (ISO, 10^{-10} – 10^{-6} M) in MA rings from rat with heart failure (HF) or Sham

littermates. A-D: CRC present mean ± SEM of relaxant response of rings from (N) animals. Insert in B compares responses with Veh in Sham and HF. Sham-Veh and HF-Veh curves represent the same data for A and C, and for B and D, respectively. ***: P< 0.001 (repeated measures, two-way ANOVA). E-H: Scatter plot or bar graph showing mean ± SEM of pD_2 (E, F) and E_{max} (G, H) calculated for (N) responses in Sham (E, G) and HF (F, H) groups. *: P< 0.05, compared to respective Veh group (one-way ANOVA followed by Holm-Sidak's post-test).

Figure 5: Effect of PDE2 inhibitor (Bay-60-7550, Bay-60) on tone and on responses to cAMP and cGMP stimulators in MAs from rat with heart failure (HF) or Sham littermates. A, B: Vasorelaxant action of Bay-60 (10-9 – 3.10-6 M) or Veh on rat MA rings precontracted with U46619 (1 µM). C-H: CRCs to the adenylyl cyclase stimulator L-858051 (C,D, L85, 10-10 – 10-5 M), the nitric oxide donor DEA-nonoate (E, F, DEA-NO, 10-10 – 3.10-5 M) or rat ANP (G, H, 10-13 – 10-8 M) in MA rings. CRC present mean ± SEM of relaxant response of rings from (N) animals. Inserts in D and H compare responses with Veh in Sham and HF. Responses to DEA-NO in Sham and HF are compared elsewhere in Figure 2.D. In A (Veh group) and D (Bay group), one ring contracted less than 2 mN/mm while the response to ACh was normal. ***: P< 0.001 vs. Veh (repeated measures, two-way ANOVA).

Figure 6: Immunolabelling of PDE2 in freshly isolated smooth muscle cells (SMC) and endothelial cells (EC) from rat MA. Confocal images of isolated SMC or EC sheets immunostained with primary antibodies against PDE2 (A), the EC marker CD31 (B) and the SMC marker calponin (C). All images were obtained at an identical level of laser illumination and have not been altered. DAPI staining indicates nuclei. "Merged" shows overlap of both images. BF: bright field. Scale bar: 20 µm is valid for all images. Representative pictures from N=6 independent experiments are shown.

Supplementary material

1. Additional Material and Methods

1.1. Drugs and reagents

Cilostamide (Cil) was purchased from Tocris Bioscience (Bristol, UK) and Ro-20-1724 (Ro) from Calbiochem (Merck Chemicals Ltd, Nottingham, UK). 3-isobutyl-1-methylxanthine (IBMX), acetylcholine (ACh), carbamylcholine chloride (carbachol, CCh), isoprenaline (ISO), phentolamine, trypsin inhibitor, bovine serum albumin (BSA), dithiothreitol (DTT), rat atrial natriuretic peptide (ANP) and snake venom from Crotalus atrox were supplied by Sigma-Aldrich (Merck Millipore, Saint Quentin-Fallavier, France). U46619, Bay-60-7550 (Bay-60) were bought from Cayman (Interchim, Montluçon, France) and L-858051 (L85), diethylamine nonoate (DEA-NONOate), L-NG-Nitroarginine methyl ester (L-NAME), from Enzo Life Science (Villeurbanne, France).

1.2. Preparation of freshly isolated vascular cells

Rat MA EC sheets were isolated following enzymatic digestion at 37°C for 60 min with papain papain (0.2 mg/ml) and DTT (0.2 mg/ml) using a modified Hank's balanced salt solution (HBSS) solution of following composition (in mM): $CaCl_2$ 1.26, $MgCl_2$ 0.49, $MgSO_4$ 0.41, KCl 5.33, KH_2PO_4 0.44, $NaHCO_3$ 4.16, NaCl 137.9, Na_2HPO_4 0.34, D-glucose 5.55, pH=7.4 (Antigny et al., 2016). The SMCs were isolated as previously described (Idres et al., 2019) using serial bathing in dissociation medium (DM, in mM: NaCl 10, KCl 5, HEPES 10, KH_2PO_4 0.5, NaH_2PO_4 0.5, $NaHCO_3$ 10, Taurine 10, EDTA 0.5, D-glucose 10, $CaCl_2$ 0.16, $MgCl_2$ 2, Phenol Red 0.03) first containing papain (1.5 mg/mL) and DTT (1 mg/mL) (37 °C, 6 min) and then collagenase and 1.6 mg/ml trypsin inhibitor (37 °C, 4 min). Vessel segments were subsequently washed 3 times in DM containing 1 mg/mL BSA and gently triturated by pipette to release the SMCs. After smooth centrifugation, SMCs were resuspended in control DM for immunocytochemistry. Mouse adult cardiac myocytes (ACM) were isolated following a standard procedure described elsewhere by our laboratory (Vettel et al., 2016). Transgenic mice overexpressing the PDE2A3 variant under the control of αMHC promoter (line TG-4320), and their wild-type littermates were used (Vettel et al., 2016).

2. Supplementary Tables

2.1. Table S1: Reference supporting selectivity of pharmacological PDE inhibitors used.

Compound	Concentr. used (µM)	Target inhibited	IC50 (µM)	Selectivity ratio ($IC50_{PDEx}$ / $IC50_{target}$)	Reference
Bay 60-7550	0.1	PDE2	0.002 - 0.005	≈ 50 fold (PDE1) ≈ 150 fold (PDE5) ≈ 350 fold (PDE4B) ≈ 850 fold (PDE3B)	(Boess et al., 2004)
cilostamide	1	PDE3	0.027 - 0.050	≈ 250 fold (PDE2) ≈ 300 fold (PDE5) ≈ 400 fold (PDE7) ≈ 1700 fold (PDE4) ≈ 6000 fold (PDE1)	(Sudo et al., 2000)
Ro-20-1724	10	PDE4	1-2	≈ 26 fold (PDE3) > 50 fold (PDE2) ≈ 100 fold (PDE1) ≈ 125 fold (PDE5)	(Rich et al., 2001)

2.2. Table S2. Primers pairs used in RT-qPCR to quantify mRNA expression.

Target (rat)	Accession number	Forward 5'→3', Reverse 5'→3';	Product size (Bp)	Annealing temperature (°C)
Pde2a	NM_001143847	CTGTGCTGGCTGCACTCTAC GAGGATAGCAATGGCCTGAG	**77**	**60**
Pde3a	NM_017337	ACCTCCCTGCCCTGCATAC CCTCTCTTGTGGTCCCATTC	**65**	**60**
Pde3b	NM_017229	GTGGCTACAAATGCACCTCA CTGGGCGAGAAAGATACAGA	**100**	**60**
Pde4a	NM_ 013101	CGTCAGTGCTGCGACAGTC CCAGCGTACTCCGACACACA	**190**	**60**
Pde4b	NM_017031	GATGAGCAGATCAGGGAACC GATGGGATTTCCACATCGTT	**81**	**60**
Pde4c	XM_214325	GACCCTGTCCTTCCTGTTGA AACCGTCTCAGGATCACACC	**99**	**60**
Pde4d	NM_001113328	GCCAGCCTTCGAACTGTAAG ATGGATGGTTGGTTGCACAT	**98**	**60**
Ywhaz	NM_013011	AGA CGG AAG GTG CTG AGA AA GAA GCA TTG GGG ATC AAG AA	**127**	**60**
Tbp	NM_001004198	AAA GAC CAT TGC ACT TCG TG GCT CCT GTG CAC ACC ATT TT	**132**	**60**
Rpl32	NM_013226	GCT GCT GAT GTG CAA CAA A GGG ATT GGT GAC TCT GAT GG	**115**	**60**
Rplp2	NM_001030021	GCT GTG GCT GTT TCT GCT TC ATG TCG TCA TCC GAC TCC TC	**119**	**60**

3. Supplementary references

Antigny, F., Hautefort, A., Meloche, J., Belacel-Ouari, M., Manoury, B., Rucker-Martin, C., . . . Perros, F. (2016). Potassium-Channel Subfamily K-Member 3 (KCNK3) Contributes to the Development of Pulmonary Arterial Hypertension. *Circulation*. doi:10.1161/CIRCULATIONAHA.115.020951

Boess, F. G., Hendrix, M., van der Staay, F. J., Erb, C., Schreiber, R., van Staveren, W., . . . Koenig, G. (2004). Inhibition of phosphodiesterase 2 increases neuronal cGMP, synaptic plasticity and memory performance. *Neuropharmacology, 47*(7), 1081-1092. doi:10.1016/j.neuropharm.2004.07.040

Idres, S., Perrin, G., Domergue, V., Lefebvre, F., Gomez, S., Varin, A., . . . Manoury, B. (2019). Contribution of BKCa channels to vascular tone regulation by PDE3 and PDE4 is lost in heart failure. *Cardiovasc Res, 115*(1), 130-144. doi:10.1093/cvr/cvy161

Rich, T. C., Tse, T. E., Rohan, J. G., Schaack, J., & Karpen, J. W. (2001). In vivo assessment of local phosphodiesterase activity using tailored cyclic nucleotide-gated channels as cAMP sensors. *J Gen Physiol, 118*(1), 63-78.

Sudo, T., Tachibana, K., Toga, K., Tochizawa, S., Inoue, Y., Kimura, Y., & Hidaka, H. (2000). Potent effects of novel anti-platelet aggregatory cilostamide analogues on recombinant cyclic nucleotide phosphodiesterase isozyme activity. *Biochem Pharmacol, 59*(4), 347-356.

Vettel, C., Lindner, M., Dewenter, M., Lorenz, K., Schanbacher, C., Riedel, M., . . . El-Armouche, A. (2016). Phosphodiesterase 2 Protects Against Catecholamine-Induced Arrhythmia and Preserves Contractile Function After Myocardial Infarction. *Circ Res*. doi:10.1161/CIRCRESAHA.116.310069

Supplementary Figures

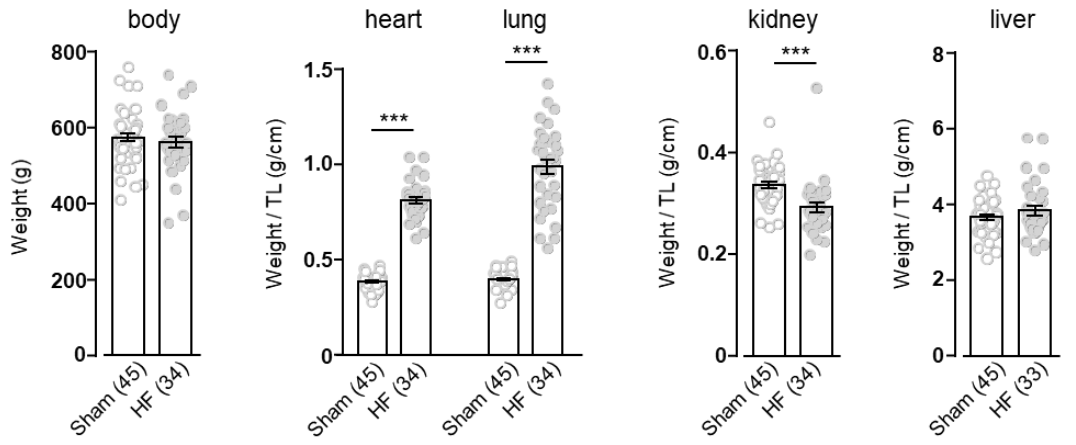

Suppl. Figure 1: Summary data of organ weight normalized to tibia length (TL) and body weight of Sham and HF rats used in this study. Scatter plots with bar indicating mean ± SEM from (N) animals are shown. ***: P< 0.001 (t-test, Welsh's t-test or Mann-Whitney test when relevant).

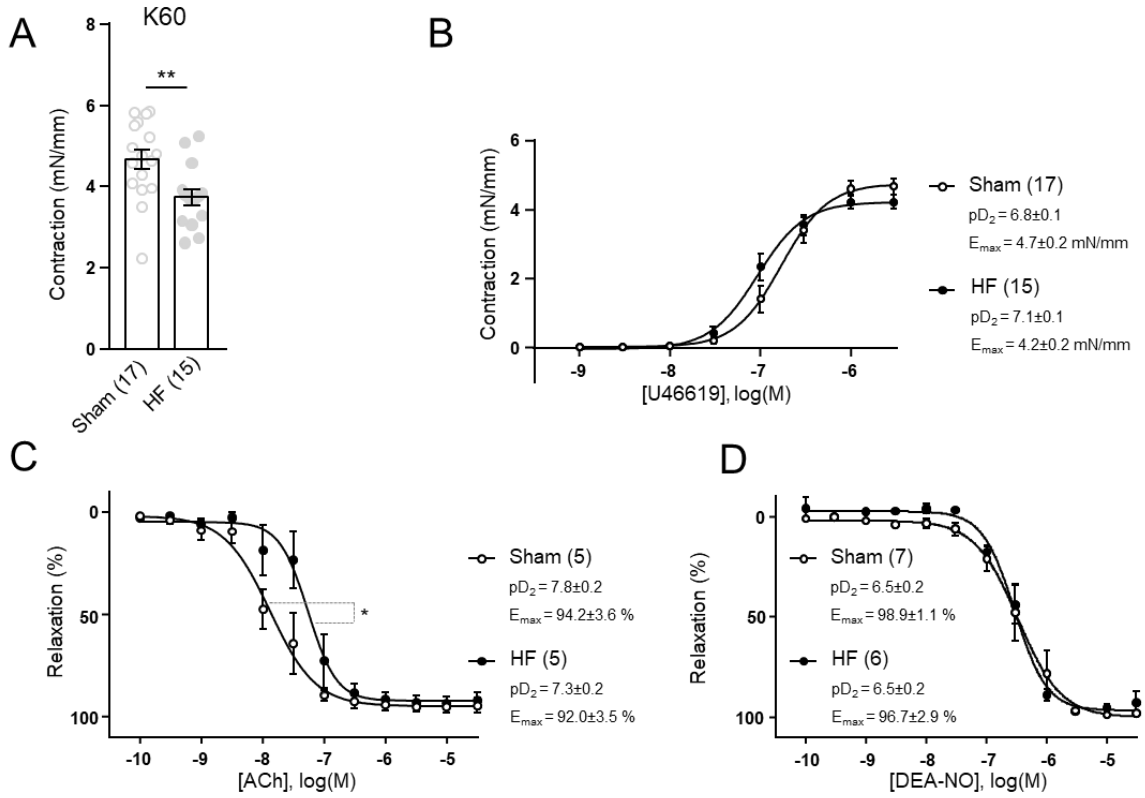

Suppl. Figure 2: Basic vascular reactivity of MA isolated from Sham and HF rats. A: Amplitude of response to K60 challenges in Sham and HF rings. **: P< 0.01 (t-test). Scatter plots with bar indicating mean ± SEM from (N) animals are shown. B: Amplitude of contractile response to U46619 (mN/mm) on Sham and HF rings. C, D: Effect of acetylcholine (C, ACh, 10^{-10} – 3.10^{-5} M) and DEA-NONOate (D, DEA-NO, 10^{-10} – 3.10^{-5} M) on Sham and HF rings precontracted with U46619 (1 µM). *: P< 0.05 (two-way ANOVA). B-D : All data present mean ± SEM response of rings from (N) animals. pD_2 and Emax data are shown with no significant difference between Sham and HF groups.

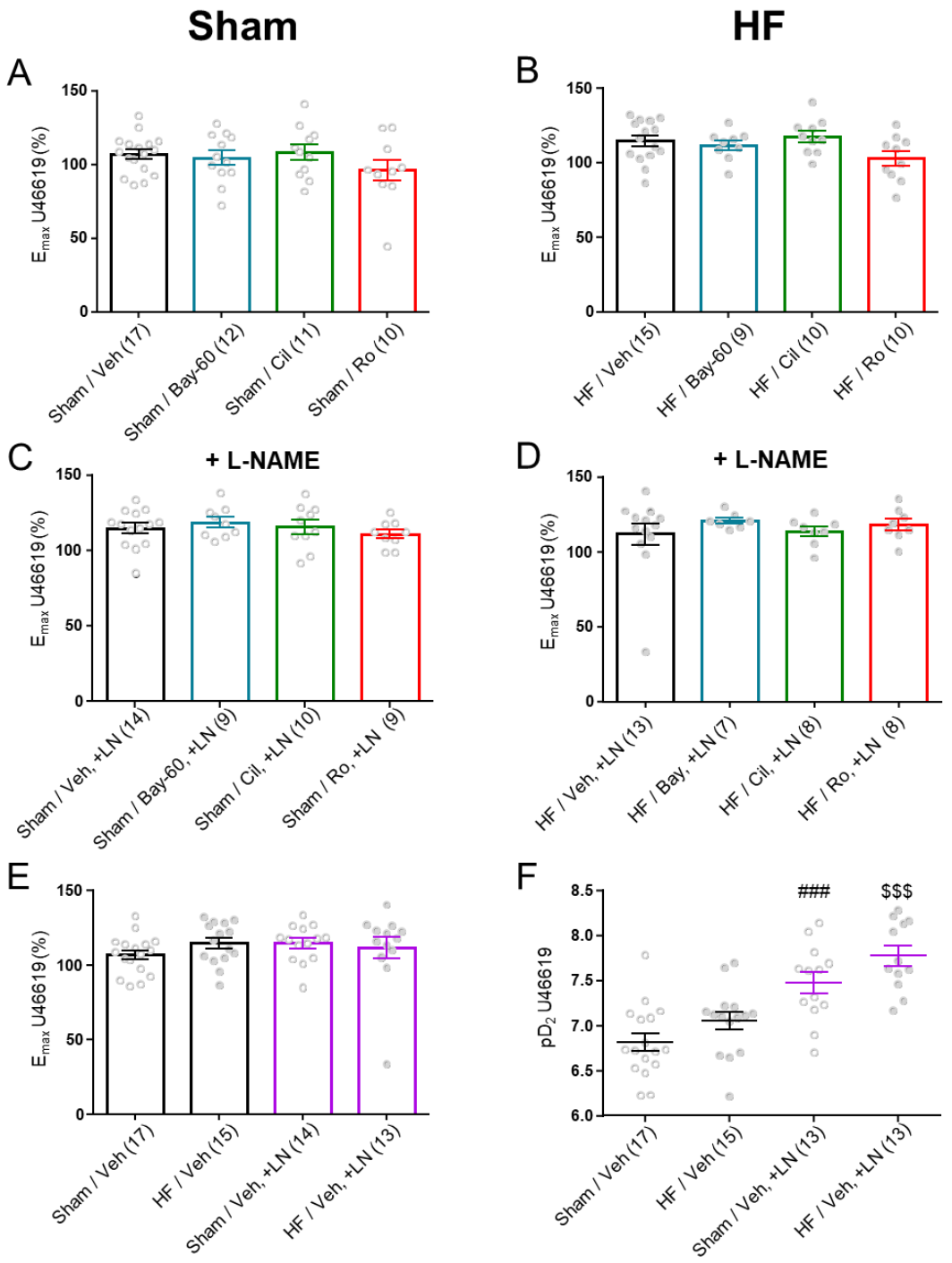

Suppl. Figure 3: Effect of PDE2 inhibitor (Bay-60-7550, Bay-60, 100 nM), PDE3 inhibitor (cilostamide, Cil, 1 µM), PDE4 inhibitor (Ro-201724, Ro, 10 µM) or vehicle (Veh), in the presence or absence of L-NAME (LN, 300 µM) on E_{max} and pD_2 of U46619 response in MA rings from rat with heart failure (HF) or Sham littermates. Graphs display scatter plot and mean ± SEM of E_{max} (A-E) or pD_2 (F) calculated for (N) responses in Sham and HF groups. $^{###}$: P< 0.001, compared to "Sham / Veh" group; $^{\$\$\$}$: P< 0.001, compared to "HF / Veh" group (one-way ANOVA followed by Holm-Sidak's post-test, F). Data in E represent the same data as Veh groups in A-D. Data in F represent the same data as Veh groups in Figure 1.E, 1.F and Figure 3.E, 3.F.

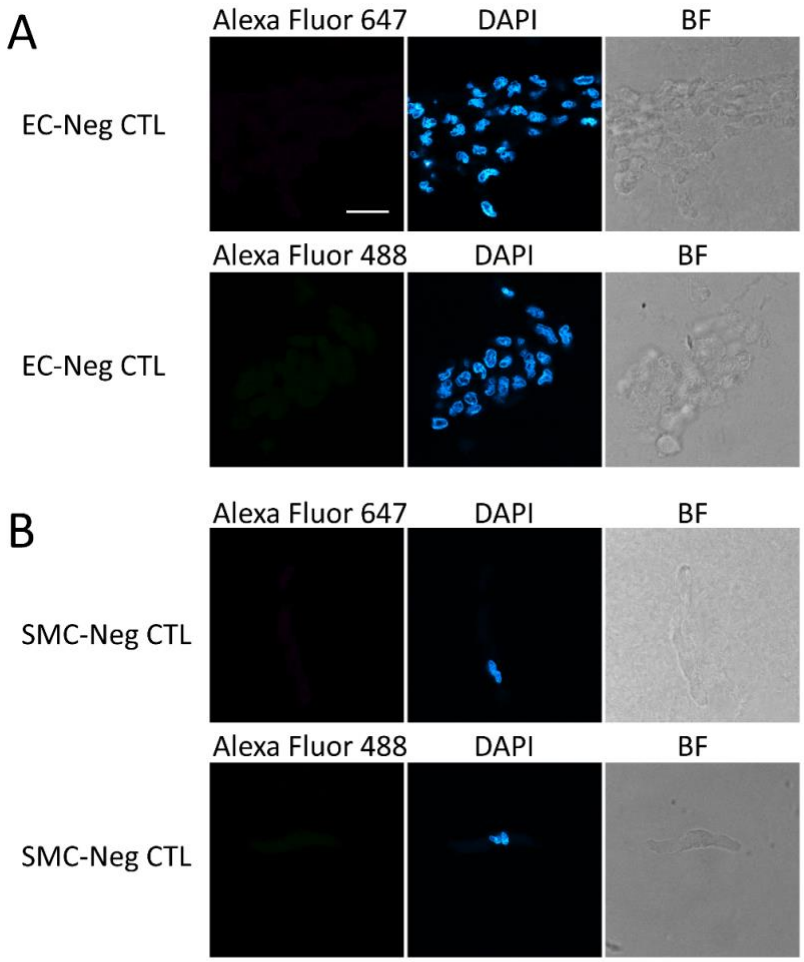

Suppl. Figure 4: Negative controls for the immunolabelling of PDE2 in freshly isolated endothelial cells (A, ECs) and smooth muscle cells (B, SMCs) from rat MA. Confocal images of ECs or SMC immunostained without primary antibodies, and with anti-rabbit secondary antibodies coupled with AlexaFluor 647 or 488. All images were obtained at an identical level of laser illumination and have not been altered. DAPI staining indicates nuclei. "Merged" shows overlap of both images. BF: bright field. Scale bar: 20 µm is valid for all images. Representative pictures from N= 6 independent experiments are shown.

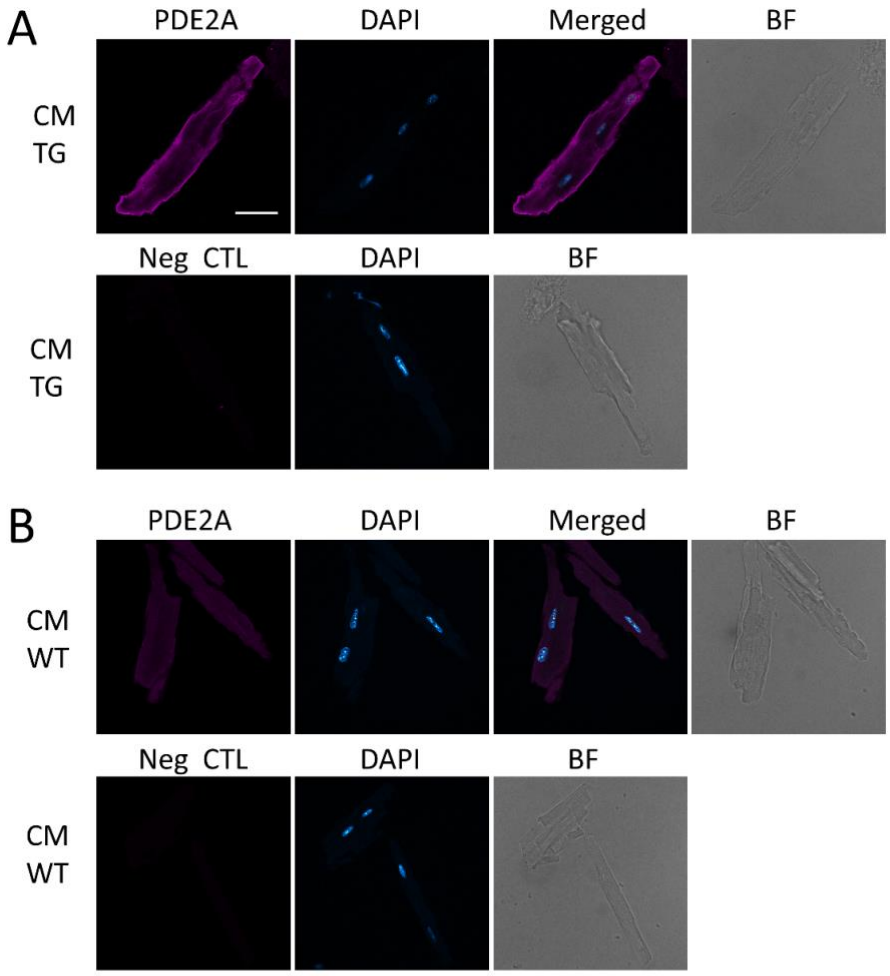

Suppl. Figure 5: Immunolabelling of PDE2 in freshly isolated cardiomyocytes (CM) from mice expressing the PDE2A3 enzyme under the control of alpha-myosin-heavy-chain gene promoter (A) and their WT littermates (B). Confocal images of cells labelled with a primary antibody against PDE2 are shown. All images were obtained at an identical level of laser illumination and have not been altered. DAPI staining indicates nuclei. "Merged" shows overlap of both images. BF: bright field. Scale bar: 20 µm is valid for all images.

4.2.2 Discussion and perspectives

In this second part of my work, we were interested in the functional role of PDE2, PDE3, PDE4 in the control of the vasomotion of MA, and their potential alteration in a pathological situation of HF models. The HF model was previously validated in my lab and were presented in a previous publication[162,163]. Even though the mRNA levels of each subfamily of PDE2, PDE3 and PDE4 were not altered in MA from HF compared to Sham rats, the total PDE activity and PDE3, PDE4 activity were decreased in HF. These findings were inconsistent with aorta from the same model which showed that PDE activity were not significantly altered in HF models[162]. This may indicate that PDE regulation undergoes specific changes in different vascular bed of HF. In MA, PDE3 and PDE4 showed majority and equivalent cAMP-related PDE activity both in Sham and HF model, whereas the PDE2 activity was hardly detectable in whole arterial lysate.

4.2.2.1 The role of PDE2 in rat MA from both HF and Sham models

The most interesting part of the work in this project is the description of the property of the PDE2 inhibitor, Bay-60-7550, to attenuate contractile response evoked by U46619, a common vasoconstrictor. We demonstrated that PDE2 is expressed in MA both in EC and SMCs which is verified by immunofluorescent experiment. Consistently, the activity and mRNA(Ct≈33)of PDE2 was detected in intact MA even though with relative lower levels. Besides, the PDE2 inhibitor, BAY 60-7550, exhibits a weak dose-dependent relaxant effect in MA from Sham rat. PDE2 inhibition also reduced U46619 contraction in the MA. Interestingly, this effect was abolished after pretreatment with NOS inhibitor, L-NAME. These results suggest the existence of a functional specificity of PDE2 in MA. Moreover , these results also indicate that PDE2 activity is rely on the ECs, and PDE2 inhibition indirectly enhances NOS activity thus generates more NO to oppose contraction induced by U46619. The underlying mechanism is unknown, maybe mediated by cAMP effectors in ECs such as PKA or EPAC which enhances the NOS activity[118,461,462]. Further studies are needed to decipher this mechanism in functional arteries. Since cAMP and cGMP are both substrates for PDE2, we then assessed the differential

involvement of this PDE in the relaxant pathways of these two cyclic nucleotides. Our experiments revealed that when stimulating the cAMP generation with the β-adrenergic agonist isoprenaline or the broad AC activator L858051, PDE2 inhibition did not modify the relaxant responses, neither in Sham nor in HF groups. Similarly, pretreatment by PDE2 inhibitor did not alter the NP nor the NO donor-stimulated cGMP relaxant responses. By contrast with our results, study by Bubb et al. reported that inhibition of PDE2 potentiates the vasorelaxant response to both ANP and NO donor in PA, and potentiates NO donor response in aorta, but does not affect relaxant effect of Treprostinil under normal condition[152]. This suggests that the role of PDE2 in the cGMP pathway depends on the vascular bed studied and the pathology associated with it. PDE2 has been extensively described in ECs[463]. We verified PDE2 expressed in both cell types, whereas we speculate that PDE2 maybe more predominant in ECs compared to SMCs. Even though the slight dysfunction of EC in MA of HF rats has been detected by weaker relaxant response to Ach, this change is not enough to disturb the distribution or function of PDE2 in MA from HF rats.

4.2.2.2 The role of PDE3 and PDE4 in rat MA from both HF and Sham models

We then evaluated the functional role of PDE3 and PDE4 in the MA from Sham and HF rats by using selective inhibitors. PDE3 and PDE4 were the main PDE families responsible for cAMP hydrolysis in arteries. Although responsible for more than 50% of total activity, PDE3 did not appear to contribute significantly to arterial tone in Sham rat, unless cAMP pathway was stimulated with Iso. In particular, the PDE3 inhibition failed to repress the contractile response to U46619 in MA of sham rats. However, it could compromise the contractile response to U46619 either in HF group or in both L-NAME pretreated groups. This may indicate that this reduced contribution of PDE3 in sham MA could also be caused by a strong constitutive NO release, causing sufficient cGMP production to repress PDE3 activity. Accordingly, it is reported that PDE3 inhibitor was able to relax rat MA contracted with phenylephrine in the presence of NOS inhibitor[104]. Moreover, PDE4 inhibition hampered contraction of U46619 and potentiated β-adrenergic mediated relaxant response in MA both from Sham and HF rats, which highlights the role of PDE4 in modulating vascular tone of MA. The effect of Ro was still

observed in the presence of L-NAME in Sham rats, which is inconsistent with what was found in aorta. It is reported that the absence of cGMP exacerbates PDE3 contribution and masks the participation of PDE4 in the control of vascular tone[162,464]. However, the effect of PDE4 inhibition to U46619 induced contraction was absent in HF rats with L-NAME pretreatment, which may partly due to the global decrease of PDE4 activity in MA of HF model. The underlying mechanism of this finding deserves further investigation. Overall, our data suggest that PDE4 inhibition may still present a valid means to produce vasorelaxation in peripheral, resistance vessel in HF.

Overall, our results suggest that no decrease in NO bioavailability occurs in MAs of HF rats, and thus does not influence the relative contribution of PDE3 and PDE4 in cAMP hydrolysis.

4.3 Project 3: The role of PKA RI in aorta

4.3.1 Introduction

The cAMP- PKA signalling pathway is a well-characterized signal transduction pathway in a number of cell types and organ systems, including vasculature[68]. The generation of cAMP results from many extracellular hormones and factors binding to their GPCR which activate Gs proteins and membrane AC to catalyze the substrate ATP into cAMP. Whereupon the cAMP diffuses and acts on downstream effector molecules to functionate, among which PKA is the most characterized one. The cAMP is degraded by a superfamily PDEs[122].

PKA holoenzyme exists as a dormant tetramer with two regulatory (R) subunits locking two catalytic(C) subunits in an inactive state. Upon binding of two cAMP molecules to each R subunit, PKA is activated by release of C subunits. The free C subunits then phosphorylate nearby target substrates on serine or threonine residues presented in a sequence context of Arg-Arg-X-Ser/Thr, Arg-Lys-X-Ser/Thr, Lys-Arg-X-Ser/Thr, or Lys-Lys-X- Ser/Thr[99]. Each R subunit has 2 cAMP binding sites, site A and site B respectively, and site A is inaccessible until cAMP occupies site B[95-97]. There are two forms of R subunits, type I and type II, and each type of R subunit has two subtypes, so called RIα and RIβ, RIIα and RIIβ respectively. As well as there are three C subunits, namely Cα, Cβ, Cγ (testis specific)[98]. It is generally claimed that α subunits (RIα, RIIα, and Cα) are expressed ubiquitously, while β subunits (RIβ, RIIβ, and Cβ) show a more restricted pattern of expression. The different PKA isoforms are functionally non-redundant. The type-I PKA is preferentially cytosolic, while type II PKA is mainly associated with the particulate fraction of cell lysates and compartmentalized to subcellular organelles via binding AKAPs at N-terminal dimerization and docking(D/D) domain[99]. The PKA RIα, coded by *PRKAR1A*, is the most abundant and ubiquitous R subunit [465], and presents a compensatory potential to cooperate with other PKA subunits to safeguard cells from unbound catalytic subunit activity[466,467].

The structure of PKA RIα is composed of dimerization domain, an "inhibitory sequence" that interacts with the catalytic subunit, cAMP-binding domain A, and cAMP-binding domain B from N-terminal to C-terminal[95]. Different mutations of PKA RIα exist and are related to different diseases. The inactivating mutations of *PRKAR1A* are recognized as a genetic cause of Carney complex, characterized by a multiple endocrine neoplasia syndrome and manifested by pigmented micronodular adrenal hyperplasia, cardiac myxoma, spotty skin pigmentation, pituitary tumors, and other abnormalities. Most of the mutations are frame shift, nonsense, splice-site or missense mutations, resulting in non-sense-mediated decay of the mRNA and thus absence of protein translation from mutant allele, so that the haploinsufficiency causes constitutive activation of PKA due to increased concentrations of free catalytic subunits[468]. Conversely, other kind of mutation affect cAMP-binding A or B domains, leading to a disease named Acrodysostosis type 1. It presents a phenotype of skeletal malformations, resistance to hormones and possible intellectual disability[469,470]. Functional characterization of this mutant RIα protein demonstrated that it normally associates with the catalytic subunits[471]. Nevertheless, a reduced affinity of the RIα mutant for cAMP binding leads to an alteration of the potency of the nucleotide to promote subunits dissociation[471]. Deletion of *PRKAR1A* caused embryonic lethality with severe development abnormalities[472]. However, overexpression of RIα in vitro experiments demonstrated total PKA activity is not affected[473].

The PKA subunits expression in vasculature is not well documented. It is reported that the RIα, RIIα/β, Cα/β forms are expressed in rat mesenteric artery[104], and RIα and RIIβ are predominant in cultured aortic VSMCs[105]. Even though it is well known that PKA functionally regulates vascular tone[68,474] and maintains mature phenotype in SMCs, it is difficult to ascribe these specific physiological functions to any given isoform of PKA subunits. Hence, here we want to use a mouse model harboring a *PRKAR1A* mutation, which results from an amino acid substitution, R368X in PKA RIα subunit (R368X knock-in mice)[454]. This mouse lineage represents a model of Acrodysostosis type-1 in human. We hypothesize that it may be useful to decipher the role and function of PKA type-1 in vascular system. In this study we focus on how R368X mutation in PKA RIα subunit impact the vascular tone of aorta.

4.3.2 Materials and methods

Material and methods for this study were already inserted in the **section 3.4** above.

4.3.3 Results

For this section the numbering of the figures was reset at "Figure 1".

4.3.3.1 Basic characteristics of the KI mouse compared to WT mouse

The mutant mice exhibited lower body weight (BW) and smaller tibia length (TB) compared to WT mice as shown in Figure 1, A and B. Consistently, the mutant mice harbored smaller vascular size, as the internal circumference (IC90) of aorta under a transmural pressure 100 mmHg in mutant mice is smaller (Figure 1C). These characteristics were in line with the previous reported data that this mouse model have features of chondrodysplasia and thus with smaller body size[454].

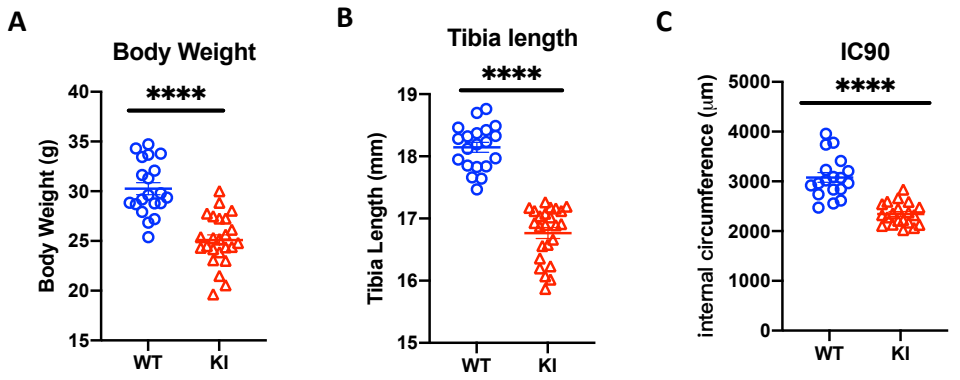

Figure 1. The basic characteristics of *Prkar1α* WT and KI mice. Body weight (**A**), tibia length (**B**) and 90% internal circumference (IC90, **C**) of mounted aorta under a transmural pressure of 100 mmHg of *Prkar1α* WT and KI mice. Data are expressed as means ± SEM. N=18-24 mice in every group. Statistical analysis by student-t test, ****P < 0.0001.

4.3.3.2 Expression of mRNAs and proteins for PKA subunits in mouse aorta

First, the mRNA level of PKA subunits was tested to examine the subunits expressed in mouse aorta. As presented in Figure 2, there were 4 R subunits and 2 C subunits expressed in aorta. The transcripts for the main subunits from both WT and KI mice were RIα, RIIα, Cα and Cβ

and all of these subunits were decreased in KI mice (Figure 2A, B, E, F). RIβ and RIIβ, which were less expressed in mouse aorta, were not significantly altered in KI mice (Figure 2C, D). Even though there was a general decrease of mRNA expression of PKA subunits in KI mice, the relative proportion of each subunit in aorta of WT mice and KI mice were quite close. In WT mouse aorta, the ratio of RIα: RIIα: RIβ: RIIβ: Cα: Cβ were 3.1: 1.8: 0: 0.1 : 0.1: 0.9 (Figure 2G), and in KI mice, the ratio of RIα: RIIα: RIβ: RIIβ: Cα: Cβ were 2.9: 1.9: 0: 0.1: 0.1: 0.9 (Figure 2H), respectively.

Subsequently, the protein expression of PKA subunits were further assessed by immunoblot assays. Data showed that the WT PKA RIα was expressed in aorta of both WT and heterozygous KI mice with a size of 49 kDa band as expected (Figure 3A). Since KI mice were carriers of a heterozygous mutation which introduce a premature a stop codon in the C-terminal portion and domain B of *PRKARIA*, thus generated truncated protein, which was present in aorta as a 47 kDa band. Interestingly, this mutant allele was the major form of RIα subunit in aorta of mutant mice, while the wide-type allele of RIα only occupied less than one third (Figure 3A, right). However, the total PKA RIα protein expression was similar in both groups (Figure 3A, left). Then the PKA RIIα was tested to be expressed in mouse aorta with equivalent levels (Figure 3B). At last, the catalytic subunit PKA Cα was expressed in mouse aorta, and was upregulated in KI mice (Figure 3C).

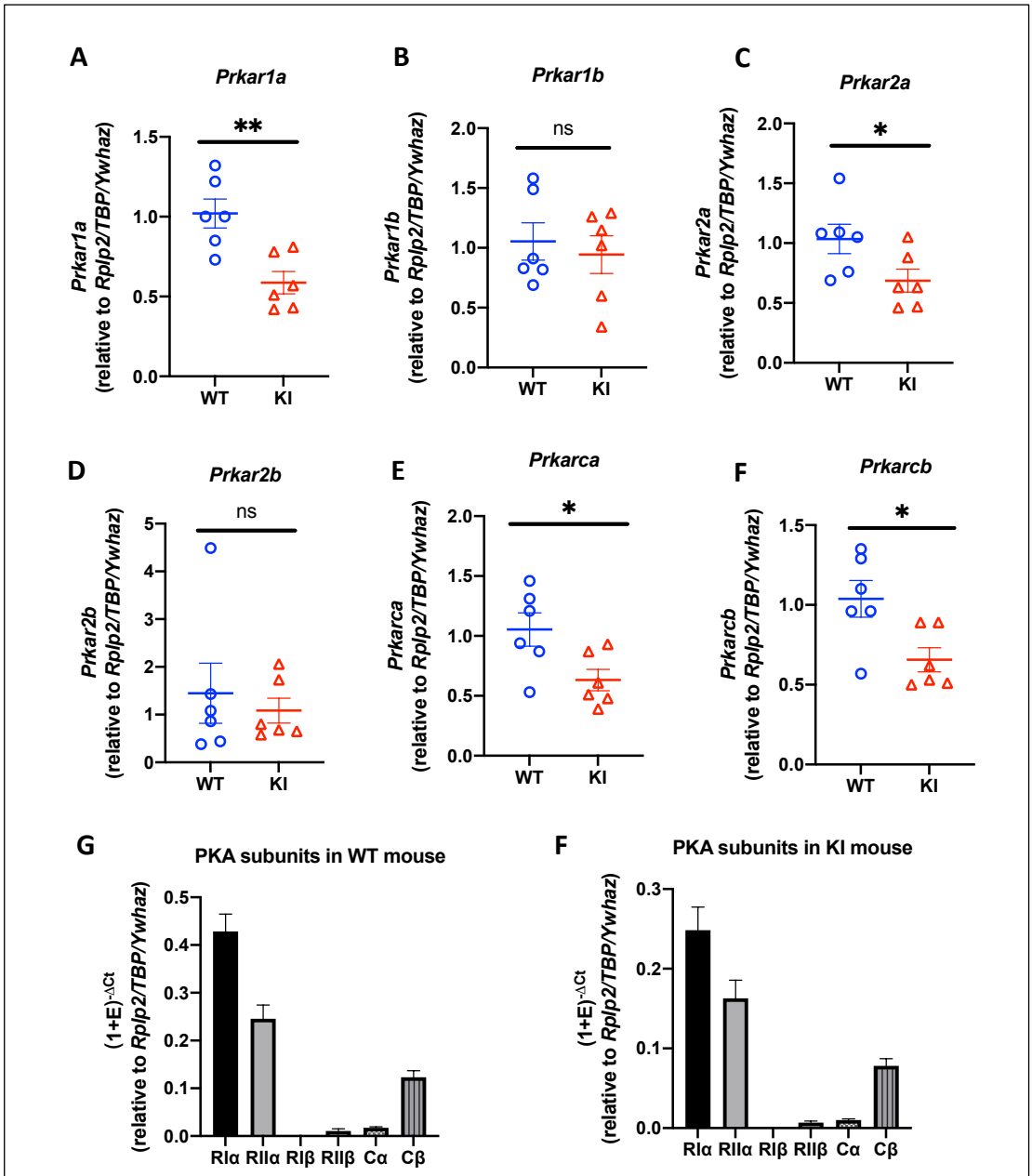

Figure 2. The transcripts of PKA subunits expressed in aorta from both WT and KI mice. The mRNA levels of RIα (A), RIIα (B), Cα(E) and Cβ (F) were significantly decreased in KI mice and RIβ (C), RIIβ (D) were not altered in KI mice. G and F show the relative levels of transcripts for PKA subunits in WT and KI mice, respectively. Data are expressed as means ± SEM. N=5-6 mice in every group. Statistical analysis by student-t test, NS, non-significant. * $P < 0.05$, ** $P < 0.01$.

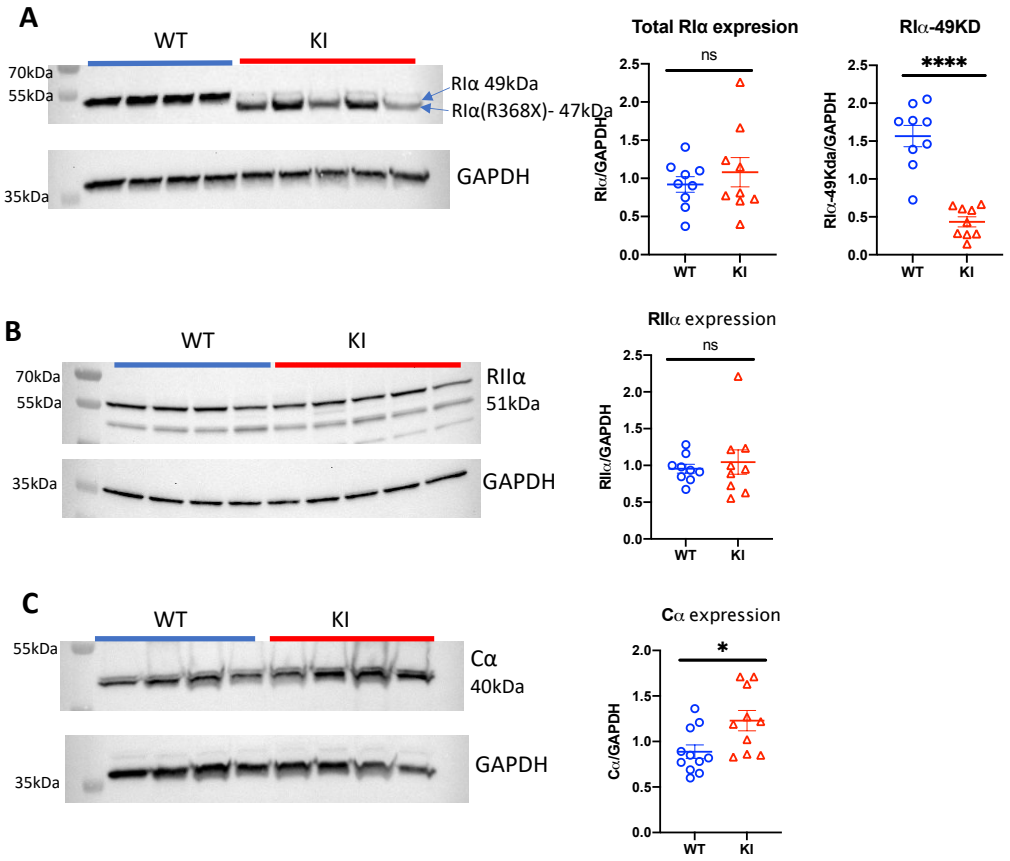

Figure 3. Immunoblots showing the subunits of PKA expressed in WT and KI mouse aorta. **A,** the PKA RIα was expressed in mouse aorta, as indicated by 49 kDa band both in WT and KI mice, and the mutant band was expressed in KI mice with a smaller size of 47 kDa. The total PKA RIα expression was similar in both groups (left), while the WT band of PKA RIα amounts for less than one third in mutant mice aorta (right). **B,** PKA RIIα was expressed in mice aorta, and showed no significant alteration in KI mice**; C,** Cα was expressed in mouse aorta, and displayed slightly higher level in KI mice. Data are expressed as means ± SEM. N= 9-10 mice in every group. Statistical analysis by student-t test,NS, non-significant. * $P < 0.05$, ****$P < 0.0001$.

4.3.3.3 Aorta from KI mouse contain higher PKA activity under basal state than WT, but less potent stimulation by a R1-selective cAMP analog

To further clarify the influence of the heterozygous R368X RIα mutation in the whole PKA activity in aortic tissue, an in vitro enzymatic assay was performed. Under basal state (i.e. in absence of exogenous PKA stimulation and in the presence of IBMX 300μM), PKA activity was clearly higher in tissues from KI mice compared to WT mice (Figure 4A). Then PKA activity was measured under different concentration of 8-AHA-2-Cl-cAMP stimulation, which

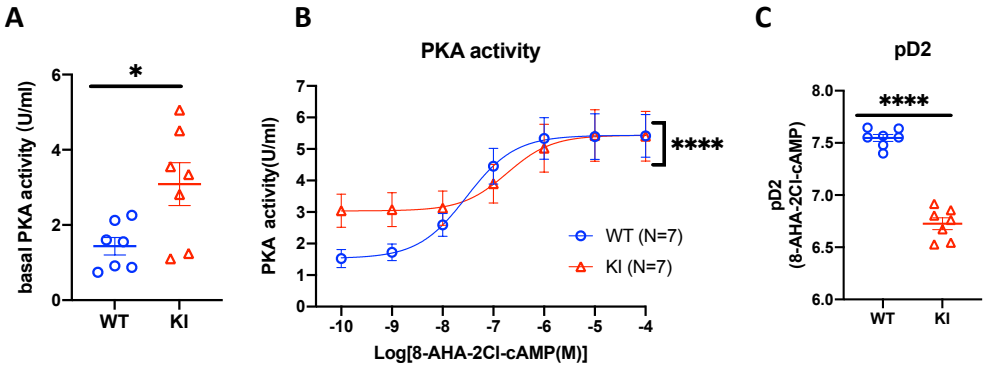

Figure 4. The KI mice displayed higher PKA activity under basal state and relatively reduced sensitivity to 8-AHA-2-Cl-cAMP stimulation compared to WT mice. **A,** The basal PKA activity without exogenous 8-AHA-2-Cl-cAMP stimulation was higher in KI mice aorta. **B,** PKA activity of aorta stimulated by 8-AHA-2-Cl-cAMP showed smaller pD2 in KI mice (**C**). Data are expressed as means ± SEM. Statistical analysis using 2-way ANOVA with repeated measurements for concentration response curves and student-t test or Welch's t-test for 2-group comparison. N= 7 mice in every group. * $P < 0.05$, ****$P < 0.0001$.

dose-dependently activated the endogenous enzyme. As expected, response to the analogue was more potent in WT samples compared to KI (Figure 4B). Hence, the pD2 was lower in WT mice (Figure 4C), which indicated an impaired ability of 8-AHA-2-Cl-cAMP to activate PKA holoenzyme. Besides, PKI peptide, which is a synthetic and selective inhibitor of PKA, was added together with highest concentration of 8-AHA-2-Cl-cAMP(100μM) both in WT and KI, the results showed that the PKA activity was completely abolished.

Activity of the endogenous enzyme present in aorta was assessed by biochemical indicator of phosphorylation-VASP at ser-157 which is a downstream substrate of PKA. It showed that the phosphorylation levels of VASP-S157 was not significantly altered in KI mouse under basal condition without cAMP analog stimulation (Figure 5).

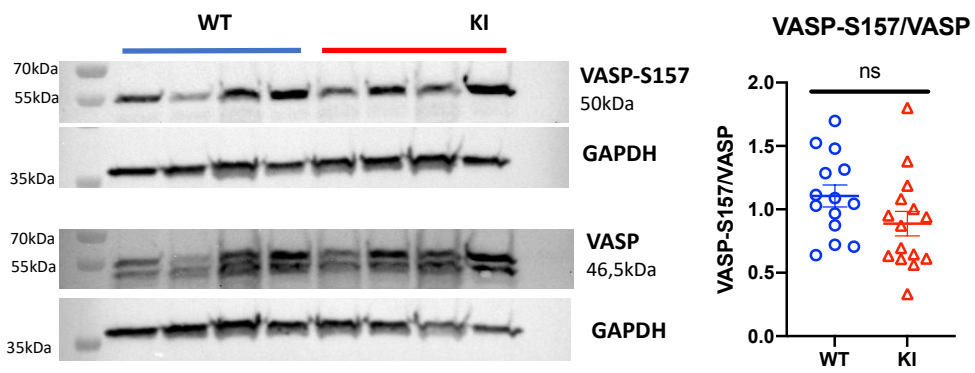

Figure 5. Phosphorylation of VASP at residue S157, as a substrate of PKA, was not altered in KI mice under basal state. Data are expressed as means ± SEM. Statistical analysis by student-t test. N=14-15 mice in every group.

4.3.3.4 Isolated aorta from KI mouse show alteration of vascular reactivity.

Isometric tension experiments were carried out to see whether RIα $^{R368X/+}$ genotype translates into dysfunctional manifestation of vascular reactivity of aorta. The absolute contractile capacity (in mN/mm) to a depolarizing solution, K60, was significantly smaller in KI mice even though both could evoke robust contraction (Figure 6A). Amplitude of the K60 response is used as an indicator of the contractile capacity of the smooth muscle layer on the studied vascular segment. Thus this difference was in line with the smaller circumference observed in aorta rings from KI mice.

Since the different vascular size between two strains, the tension of vessel was normalized to K60 to offset the divergence owing to the vascular size, so the contractile response curves were present as % of K60. The relative relaxant response to Ach (10 µM) applied on K60-contracted vessels was small between 3-4%, but similar in both genotypes (Figure 6B). The gradual increase in bath K^+ concentration evoked a contractile response curve, while there was no significant difference between WT and KI mice (Figure 6C). Then contractile response to PE, an α1-adrenergic receptor agonist, showed a concentration-dependent contraction, although maximal response were weak in both genotypes, reaching around 40% of K60. There was no significant difference between WT and KI groups (Figure 6D). At last, the thromboxane A2 mimetic U46619, a standard vasoconstrictor agonist, evoked strong vasocontraction in both

genotypes (Figure 6E), whereas the maximum effect was stronger in KI mice compared with WT mice (Figure 6F).

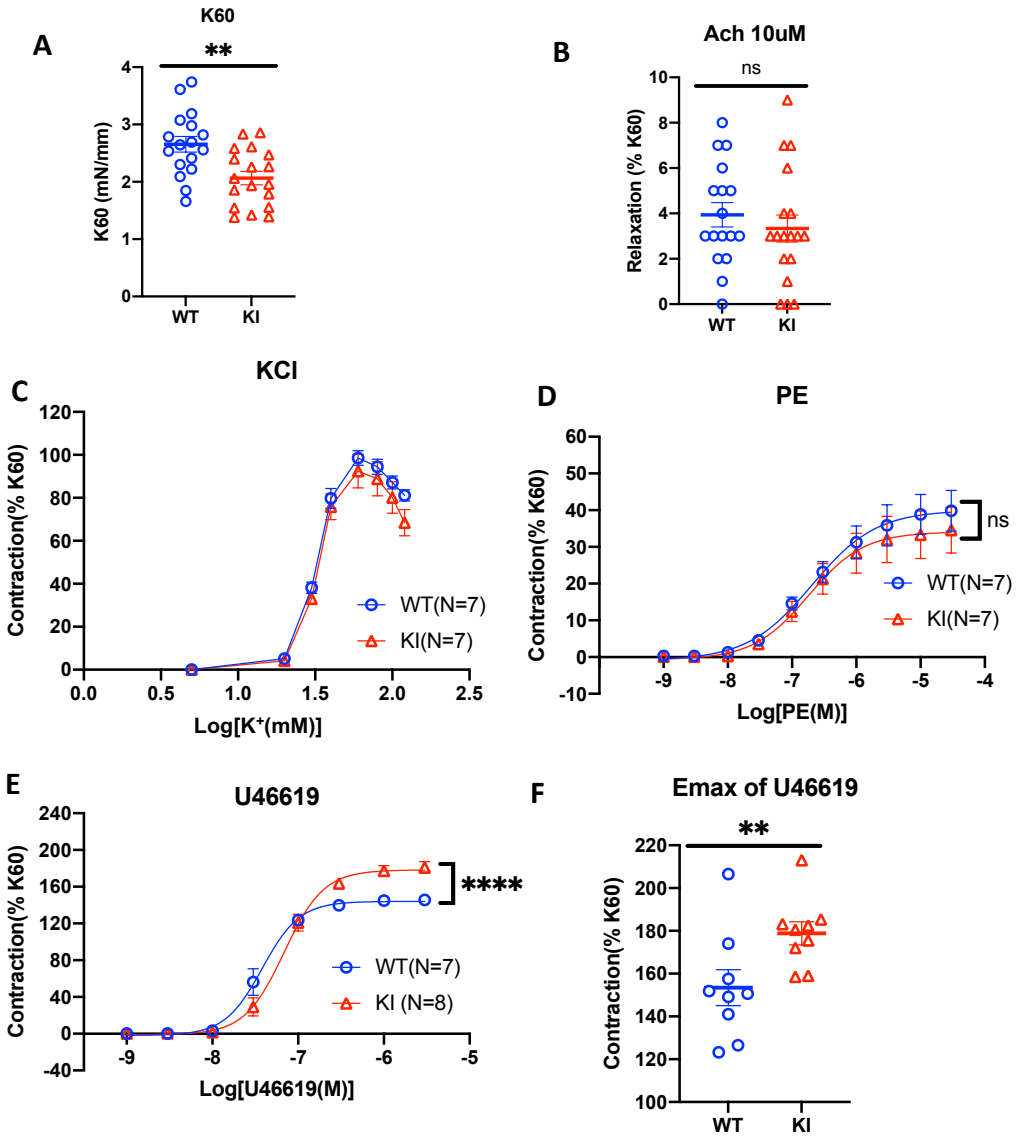

Figure 6. Evaluation of basic vascular reactivity and contractile concentration response in aorta from WT and KI mice. **A,** The contractile response to K60; **B,** the relaxant response to acetylcholine (Ach) 10 µM after K60 contraction; **C, D, E:** Contractile-response curves to KCl (KCl 60mM, a depolarizing solution), phenylephrine (PE, α_1-adrenergic receptor agonist), and U46619 (thromboxane A2 mimetic) in PA from in WT and KI mice. **F,** the maximum effect (Emax) of U46619 in WT and KI mice. Data are expressed as means ± SEM. N, number of animals. Statistical analysis using student-t test for 2-group comparison and using 2-way ANOVA with repeated measures for concentration-response curves. NS, non-significant. ** P < 0.01, ****P < 0.0001.

Then the relaxant dose response to Ach was further tested in vessels precontracted by PE. While Ach produced robust dose-dependent relaxations in aorta, there was no difference between two groups (Figure 7A). Because RIα $^{R368X/+}$ genotype may affect the cAMP-PKA related relaxant pathways, the response to β-adrenergic receptor agonist ISO was tested and appeared similar in both WT and KI groups (Figure 7B). The relaxant effect to L858051, a broad AC activator, was however slightly less potent in KI mice, showing a right-shift of the curve (Figure 7C), translating in a significant decrease in pD2 (Figure 7D).

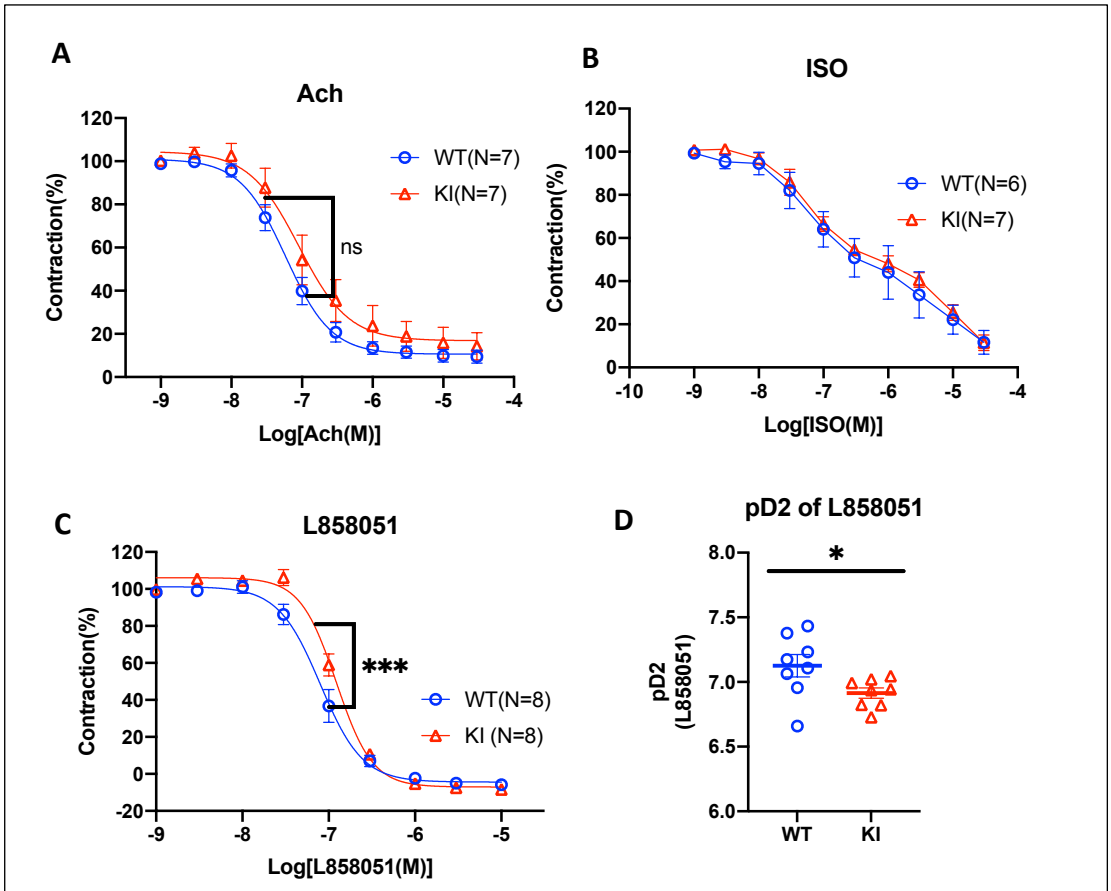

Figure 7. Relaxant concentration-response of aorta from WT and KI mice. The relaxant-response curves to acetylcholine (Ach) **(A)**, isoprenaline (ISO) **(B)** and L858051 **(C)** in WT and KI mice aorta, respectively. **D,** the pD2 of L858051 response in WT and KI mice. Data are expressed as means ± SEM. N, number of animals. Statistical analysis using student-t test or Welch's t-test for 2-group comparison and using 2-way ANOVA with repeated measures for concentration response curves. N, number of animals. NS, non-significant. NS, non-significant. * $P < 0.05$, ***$P < 0.001$.

On the whole, these experiments demonstrate that the contractile response to U46619 is specifically increased in KI aorta. Also, these vessels displayed a less potent relaxant ability to global cAMP stimulation, while the β-adrenergic receptor-mediated response was not influenced.

4.3.4 Discussion

In the present study, our main findings are we made three findings which are (1) the abnormal pattern of mRNA expression of PKA subunits in aorta from mutant mouse; (2) the abnormal PKA activity with higher basal activity (PKI-sensitive) and impairment of RI selective cAMP analogue-stimulated PKA activity in mutant mouse; (3) some discrete alteration of vascular reactivity in response to U46619 and L858051.

The phenotype of R368X mutation of *PRKAR1A* has been carefully described in Linglart's[469] and Stunff's[454] report in human and mouse, respectively. Both indicated that this mutation mainly results in chondrodysplasia associated with resistance to several hormones. Thus, the shorter stature or size and resultant lower mass and smaller vessel circumference in our data are consistent with the characteristics of this mutation of both mouse model and patients.

The transcripts expression of PKA subunits in aorta was checked for first time in our study, which represents the generation levels of PKA subunits. Even though all of the subunits we examined were expressed in aorta, the RIβ was the lowest expressed one. Expression of RIα, RIIα, RIIβ, Cα and Cβ in mouse aorta is consistent with mouse mesenteric artery as reported[104]. The reason of general decreasing expression of 4 main subunits (RIα, RIIα, Cα and Cβ) in mutant aorta is elusive for us. It is possibly due to the different proportions of each type of cells in aorta from mutant and WT mice, for example, the less proportion of SMCs occupied in intact aorta tissue from mutant mice. Since we observed that, no matter target genes or reference genes, all of them obtained a lower Ct value inKI mice when using 10 ng of cDNA for real-time quantitative PCR. However, the relative ratio of each subunit was conserved between WT and KI mice. The quantity of PKA subunits existing in tissue not only depends on their generation, but also their degradation. It is reported that the free R and C subunits are

susceptible to proteolytic degradation in the cell, whereas holoenzymes are resistant[95]. The property of RIα, no matter wide-type or mutant, has been explored in vitro experiment. It indicates that the mutations present in Acrocytososis-1 are all relevant to the mutation in cAMP binding domain A or B, and the identical mechanism of this disease is impaired ability of cAMP to disaggregate catalytic subunits from regulatory subunits, thus causing the reduction of cAMP-induced PKA activation[471]. Hence, it is reasonable that there are more mutant allele of RIα in mutant mice compared with wide-type allele, since less free mutant RIα is released and degraded. In fact, all mRNA levels of subunits were reduced in mutant mice aorta, yet the protein levels were equivalent or even increased, which may indicate general slow degradation of subunits protein in mutant mice. Besides, the higher expression of Cα subunits in aorta of mutant mice is to some extent surprising, since it is reported that Cα is decreased in kidney, and not altered in liver and bone in same mouse model[454]. This may indicate that the expression of PKA subunits follow a tissue-specific pattern. And it requires deeper exploration to see whether this upregulation is functionally meaningful, as we are not clear how much proportion is free and active Cα. And as the majority of catalytic subunit, the protein level of Cβ hasn't been tested yet, so we need to further examined it. Similar PKA activity at maximal activation (Emax) in PKA assay indicates that total C levels are likely similar in both groups.

In the present study, PKA activity is increased in mutant aorta under the basal conditions which is not observed in in vitro experiment[469,471]. The concentration-response curve revealed an impaired of PKA activity in response to 8-AHA-2-Cl-cAMP in mutant mouse due to a lower pD2 was found in WT mice, which is consistent with previous in vitro experiment by Le Stunff et al.[469]. This result indicates that RIα is present and functional in the vascular sample. Performing the same experiment with natural ligand cAMP would further inform about the balance of the RI/RII PKA in this tissue. The endogenous cAMP levels in tissues would be an interesting data to collect. In human serum and mouse urine, the cAMP level were both reported to be increased in mutated subjects[454,469]. Thus, the increased basal PKA activity may partly attributable to increased cAMP levels. Besides, since it is in vitro data and the sample (and possible endogenous cAMP) is much diluted in the reaction mix. On the other hand, the

influence of increased Cα expression in mutant aorta is possibly involved, and the Cβ is still need to be tested. The property of PKA holoenzyme determined in vitro may not correlate directly with the responses observed in vivo, since there are more complicated internal milieu in vivo. However, the augmentation of PKA activity at basal state did not affect the phosphorylation levels of VASP-S157, which is a substrate of PKA in vasculature. The underlying mechanism of this observation may be due to the distinct compartments of different PKA isoforms participates in, since it is reported that stimulation of PKA type I or II phosphorylate different downstream targets in cardiomyocytes[475]. Therefore, it cannot be ruled out that VASP is a selective substrate of PKA type II.

PKA represents a key component in the in cAMP-mediated physiological effects in a variety of cells[476]. Activation of PKA by an elevated cytoplasmic cAMP results in relaxation of vascular smooth muscle cells via phosphorylating downstream substrates such as MLCP and MLCK, and MLCK is a more known substrate than MLCP[68]. Therefore, the impairment of PKA activity in response to cAMP stimuli logically may render relaxation of vessels less prominent. The contractile concentration-response to KCl and PE were not altered in mutant mice, while the contractile response to U46619 was enhanced in mutant mice. This is not consistent with increased basal activity observed in vitro. However, the activation status of PKA in non-stimulated condition and in vivo is unknown, and there may be endogenous, basal cAMP that is enough to stimulate PKA and interfere with the U46619 response. Moreover, the stronger contraction of U46619 in mutant mouse may indicate that PKA RIα phosphorylate MLCP rather than MLCK, since U46619 is reported mainly involved in Ca^{2+}-sensitization induced constriction via Rho Kinase-MLCP pathway in comparation with K^+ and PE [477]. So the phosphorylation of MLCP is required to further support this hypothesis. At last, the relaxant concentration response to AC activator, L858051, was weaker in mutant mice, which is in line with the impaired PKA activation curve in mutant mice. However, this abnormality of PKA RIα does not influence the relaxant dose response to ISO, which would mean the PKA RI is not involved in β-adrenergic involved compartmentalization. Consistently, it is reported that PKA type I and type II define distinct intracellular signaling compartments in cardiac myocytes.

And specifically, catecholamines generate restricted pools of cAMP that selectively engage PKA type II, and activation of the PGE1 leads to the generation of a restricted cAMP pool affecting PKA type I[475]. So further experiments are need to do to check the potential compartments of PKA RI in vascular smooth muscle cells by using this gene-modified mouse.

4.3.5 Perspectives

As discussed above, we should do more to better understand the role of PKA RI in aorta. First, we should continue to finish the immunoblot of other PKA subunits expression in aorta, especially Cβ which is important for us to understanding the alteration of PKA activity. Second, we need to measure cAMP levels in aorta tissue and blood from two strains of mice to see the real cAMP levels and its possible effect. Besides, it's necessary for us to check the phospho-PKA substrate by using specific antibody with and without cAMP analog stimulation to detect the effect of PKA basal activity and maximum activity. Alternatively, we can perform FRET experiments by using AKAR probe to test aorta SMC responses to either FSK, or various cAMP analogues. At last, we can try other agonists of GPCRs to explore the possible compartmentalization or pathway mediated by PKA RIα by myography experiments.

5. General discussion

Our three projects were focused on CNs, where we studied either their effector, such as PKA, or their elimination by PDEs. We carried out these studies in different vascular beds, i.e., pulmonary artery, a large conductance artery (aorta) and resistance artery. Noteworthy, the observed effects in one given vascular bed may give hint to another and thus may provide with a better understanding of the general role of these targets. Alternatively, organ- or diameter-specific organisations may provide variety in the results obtained with different vascular beds, which may reflect different facet and mechanisms, but also be caused by specific experimental conditions.

There are some common limitations in our projects. First, we detected mRNA or protein in tissues rather than in specific cell type, such as ECs and SMCs. This give us an information in a broad view, but not accurate. Thus this represent a hurdle in our understanding of the intracellular mechanisms or possibly underlying compartmentalization. For example, in the PDE9 project, even though we discovered that PDE9 inhibition potentiates both NO and NP-related cGMP relaxant effects in PA, we did not further explored the subcellular localization of PDE9 in SMC. This kind of study has been done in rat neonatal myocytes in Lee et al,'s study (2015). They showed PDE9 co-localization with T-tubular membranes (identified with labelling of SERCA2a) of cardiomyocyte by using confocal immunohistochemistry method with specific antibody[355], thus distilling some clues about the compartments existing in the heart. Additionally, Zhang et al. found that PDE9 regulates rat aorta SMCs through the NO-cGMP pathway by using a FRET experiment to monitor cGMP dynamics in response to PDE9 inhibitor[170]. This method provides more direct evidence about the way PDE9 handles cGMP.

Similarly, in PKA RIα project, we still have a general expression levels of PKA RIα whereas the subcellular localization is totally unknown in vascular SMCs. Even though PKA type 1 is classically recognized to be biochemically soluble and mainly cytoplasmic, several RI-specific AKAPs have also been characterized[99,100], which indicates that a potential by PKA type 1-mediated compartmentalization does exist. The discrete differences in the response to U46619 between both genotypes may indicate that PKA RIα is involved in MLCP pathway. In addition, weaker relaxant response to L858051 but not to ISO further indicates that PKA RIα induces

other signalling pathway which may be cAMP dependent (mediated by EPAC or a different balance between PKA R1 and R2 for instance) or cAMP-independent (mediated by interactions with G-proteins, as described in airways [478]). So there remains interesting challenges and a lot of work that will lead to uncover the exact roles of PKA RI in VSMCs.

There are two pathological models in my projects. Both these two projects in some extent exhibit mild impairment of vascular bed. For PDE9 project, we used the CHx-induced PAH model, which always regarded as non-typical model for human PAH disease and the mildest PAH phenotype compared to other classical models. Even though this model is always used in transgenic mouse to check genetic susceptibility, it may be easier to see a modified gene that triggers PAH, so forming a double hit together with chronic hypoxia to induce PAH. We speculate that, a gene modification expected to result in beneficial effect (such as *Pde9a* invalidation) may only yield a mild phenotype if studied in a less severe animal model. Thus, more severe animal models or combination treatment are needed. Similarly, in the rat model of HF, even though HF is well established in this project, our data indicates that MA is affected mildly, with a slight impairment of Ach relaxant effect. And this maybe one of reasons that some data are inconsistent with what we found in aorta. However, the data from pharmacological experiment in normal rat MA also reveals some overlooked, but important effect of cAMP-PDEs in MA, such as the importance of NOS for PDE2 activity.

However, studying different targets in different vascular bed supply interesting insights about interactions between cAMP-PKA or cAMP-PDEs. For example, it is reported that cAMP level is increased in PKA RIα (domain B) mutant patients and animals[454,469], and our data showed a basal higher PKA activity in the aorta from mutant mice. This lead to the question about how do the cAMP-PDEs change in this vessel? Another study in STZ-induced diabetic rats showed an increased phosphodiesterase (PDE 3) activity in MA and resultant reduced cAMP levels, but together with decreased PKA activity and imbalance between PKA catalytic and regulatory subunit expressions[104,447], whereas the exact mechanism is unknown. Thus, in our PKA project, the activity of PDEs may be needed to check.

Eventually, our data in the PDE9 project, do not support the hypothesis that PDE9 pharmacological inhibitor could represent a new promising means to treat PAH. However, in Scott et al.'s study[363], the PDE9 inhibitor (PF-04749982) also produced progressive falls in arterial pressure and peripheral resistance, pointing to a possible systemic hypotensive effect of targeting PDE9. This reminds us, on the one hand, to pay attention to blood pressure in using this pharmacological class to treat PAH or other diseases in clinics. On the another side, the role of PDE9 in systemic arteries remains to be explored.

6. Conclusions

6.1 PDE9 controls pulmonary arterial tone but does not influence chronic hypoxia-induced pulmonary hypertension in mouse.

PDE9 is expressed in human and mouse PA. In mouse, PDE9 deficiency potentiates mouse PA vasorelaxation to typical cGMP elevating agents via both NP- and NO-stimulated pathways. However, PDE9 cannot prevent chronic-hypoxia induced pulmonary hypertension and associated right ventricle hypertrophy. However, considering that PDE9 mRNA was upregulated in the RV and lung in our study, it may be speculated that treatment with PDE9 inhibition combined with another intervention that stimulates cGMP production may exert beneficial effect on PAH. Also more severe and relevant animal models are needed to further explore the role of PDE9 in PAH and RV hypertrophy.

6.2 Phosphodiesterases-type 2, 3 and 4 orchestrate vascular tone in mesenteric arteries from rats with heart failure.

Our study extends the characterization of the effect of PDE2, PDE3 and PDE4 inhibitors on vascular tone to an archetypical resistance vessel, namely MA, both in Sham and HF rats. We show that relative contribution of these PDEs to contractile and β-adrenergic relaxant responses are in general less impacted by HF than what was observed in aorta. While influence of PDE3 is smaller in Sham than in HF MA, the role of PDE4 is more prominent in both normal and pathological contexts, making this family of enzymes a potential target to obtain peripheral vasodilation in patients with HF. Our data also revealed a discrete influence of PDE2 on the contractile response to U46619, which depends on constitutive NO production but is preserved

in HF. This opens new perspectives on how specific PDE activities fine tune the control of peripheral vascular beds by CNs.

6.3 Role of PKA RIα in aorta

These preliminary data show PKA RIα is expressed and functional in mouse aorta. The smaller contractile capacity in mutant mice is consistent with smaller aorta circumference and body size.

Even though there is general decreased mRNA expression of PKA subunits in aorta from mutant mouse, the protein expression does not show decrease. Conversely, Cα expression is increased. PKA activity assay shows higher basal activity (PKI-sensitive) and impairment of RI selective cAMP analogue-stimulated PKA activity in mutant mouse. Vascular reactivity is altered in response to U46619 and L858051. Overall, this suggests that PKA type I is an important contributor to vascular tone in mouse aorta.

7. References

1 Simonneau, G. *et al.* Haemodynamic definitions and updated clinical classification of pulmonary hypertension. *Eur Respir J* **53**, doi:10.1183/13993003.01913-2018 (2019).
2 Widrich, J. & Shetty, M. in *StatPearls* (2022).
3 Delong, C. & Sharma, S. in *StatPearls* (2022).
4 Lindner, V. & Maciag, T. The putative convergent and divergent natures of angiogenesis and arteriogenesis. *Circ Res* **89**, 747-749 (2001).
5 Li, S. *et al.* Innate diversity of adult human arterial smooth muscle cells: cloning of distinct subtypes from the internal thoracic artery. *Circ Res* **89**, 517-525, doi:10.1161/hh1801.097165 (2001).
6 Sturtzel, C. Endothelial Cells. *Adv Exp Med Biol* **1003**, 71-91, doi:10.1007/978-3-319-57613-8_4 (2017).
7 Kruger-Genge, A., Blocki, A., Franke, R. P. & Jung, F. Vascular Endothelial Cell Biology: An Update. *Int J Mol Sci* **20**, doi:10.3390/ijms20184411 (2019).
8 Humbert, M. *et al.* Endothelial cell dysfunction and cross talk between endothelium and smooth muscle cells in pulmonary arterial hypertension. *Vascul Pharmacol* **49**, 113-118, doi:10.1016/j.vph.2008.06.003 (2008).
9 Li, S., Sims, S., Jiao, Y., Chow, L. H. & Pickering, J. G. Evidence from a novel human cell clone that adult vascular smooth muscle cells can convert reversibly between noncontractile and contractile phenotypes. *Circ Res* **85**, 338-348, doi:10.1161/01.res.85.4.338 (1999).
10 Rensen, S. S., Doevendans, P. A. & van Eys, G. J. Regulation and characteristics of vascular smooth muscle cell phenotypic diversity. *Neth Heart J* **15**, 100-108, doi:10.1007/BF03085963 (2007).
11 Sweeney, H. L. & Hammers, D. W. Muscle Contraction. *Cold Spring Harb Perspect Biol* **10**, doi:10.1101/cshperspect.a023200 (2018).
12 Uehata, M. *et al.* Calcium sensitization of smooth muscle mediated by a Rho-associated protein kinase in hypertension. *Nature* **389**, 990-994, doi:10.1038/40187 (1997).
13 Cole, W. C. & Welsh, D. G. Role of myosin light chain kinase and myosin light chain phosphatase in the resistance arterial myogenic response to intravascular pressure. *Arch Biochem Biophys* **510**, 160-173, doi:10.1016/j.abb.2011.02.024 (2011).
14 Ratz, P. H., Berg, K. M., Urban, N. H. & Miner, A. S. Regulation of smooth muscle calcium sensitivity: KCl as a calcium-sensitizing stimulus. *Am J Physiol Cell Physiol* **288**, C769-783, doi:10.1152/ajpcell.00529.2004 (2005).
15 Johnson, R. P. *et al.* Ca2+ sensitization via phosphorylation of myosin phosphatase targeting subunit at threonine-855 by Rho kinase contributes to the arterial myogenic response. *J Physiol* **587**, 2537-2553, doi:10.1113/jphysiol.2008.168252 (2009).
16 El-Yazbi, A. F. *et al.* Pressure-dependent contribution of Rho kinase-mediated calcium sensitization in serotonin-evoked vasoconstriction of rat cerebral arteries. *J Physiol* **588**, 1747-1762, doi:10.1113/jphysiol.2010.187146 (2010).
17 Rockman, H. A., Koch, W. J. & Lefkowitz, R. J. Seven-transmembrane-spanning receptors and heart function. *Nature* **415**, 206-212, doi:10.1038/415206a (2002).
18 Neves, S. R., Ram, P. T. & Iyengar, R. G protein pathways. *Science* **296**, 1636-1639, doi:10.1126/science.1071550 (2002).

19 Somlyo, A. P. & Somlyo, A. V. From pharmacomechanical coupling to G-proteins and myosin phosphatase. *Acta Physiol Scand* **164**, 437-448, doi:10.1046/j.1365-201X.1998.00454.x (1998).

20 Hayashi, Y., Senba, S., Yazawa, M., Brautigan, D. L. & Eto, M. Defining the structural determinants and a potential mechanism for inhibition of myosin phosphatase by the protein kinase C-potentiated inhibitor protein of 17 kDa. *J Biol Chem* **276**, 39858-39863, doi:10.1074/jbc.M107302200 (2001).

21 Ohki, S. *et al.* Solution NMR structure of the myosin phosphatase inhibitor protein CPI-17 shows phosphorylation-induced conformational changes responsible for activation. *J Mol Biol* **314**, 839-849, doi:10.1006/jmbi.2001.5200 (2001).

22 Kitazawa, T., Takizawa, N., Ikebe, M. & Eto, M. Reconstitution of protein kinase C-induced contractile Ca2+ sensitization in triton X-100-demembranated rabbit arterial smooth muscle. *J Physiol* **520 Pt 1**, 139-152, doi:10.1111/j.1469-7793.1999.00139.x (1999).

23 Kitazawa, T., Eto, M., Woodsome, T. P. & Brautigan, D. L. Agonists trigger G protein-mediated activation of the CPI-17 inhibitor phosphoprotein of myosin light chain phosphatase to enhance vascular smooth muscle contractility. *J Biol Chem* **275**, 9897-9900, doi:10.1074/jbc.275.14.9897 (2000).

24 Brozovich, F. V. *et al.* Mechanisms of Vascular Smooth Muscle Contraction and the Basis for Pharmacologic Treatment of Smooth Muscle Disorders. *Pharmacol Rev* **68**, 476-532, doi:10.1124/pr.115.010652 (2016).

25 Orallo, F. Regulation of cytosolic calcium levels in vascular smooth muscle. *Pharmacol Ther* **69**, 153-171, doi:10.1016/0163-7258(95)02042-x (1996).

26 Francis, S. H., Busch, J. L., Corbin, J. D. & Sibley, D. cGMP-dependent protein kinases and cGMP phosphodiesterases in nitric oxide and cGMP action. *Pharmacological reviews* **62**, 525-563, doi:10.1124/pr.110.002907 (2010).

27 Koyama, H., Bornfeldt, K. E., Fukumoto, S. & Nishizawa, Y. Molecular pathways of cyclic nucleotide-induced inhibition of arterial smooth muscle cell proliferation. *Journal of cellular physiology* **186**, 1-10, doi:10.1002/1097-4652(200101)186:1<1::AID-JCP1012>3.0.CO;2-D (2001).

28 Morgado, M., Cairrao, E., Santos-Silva, A. J. & Verde, I. Cyclic nucleotide-dependent relaxation pathways in vascular smooth muscle. *Cell Mol Life Sci* **69**, 247-266, doi:10.1007/s00018-011-0815-2 (2012).

29 Surapisitchat, J. & Beavo, J. A. Regulation of endothelial barrier function by cyclic nucleotides: the role of phosphodiesterases. *Handb Exp Pharmacol*, 193-210, doi:10.1007/978-3-642-17969-3_8 (2011).

30 Lugnier, C., Schoeffter, P., Le Bec, A., Strouthou, E. & Stoclet, J. C. Selective inhibition of cyclic nucleotide phosphodiesterases of human, bovine and rat aorta. *Biochem Pharmacol* **35**, 1743-1751, doi:10.1016/0006-2952(86)90333-3 (1986).

31 Kuhn, M. Molecular Physiology of Membrane Guanylyl Cyclase Receptors. *Physiological reviews* **96**, 751-804, doi:10.1152/physrev.00022.2015 (2016).

32 Zhao, Y., Vanhoutte, P. M. & Leung, S. W. Vascular nitric oxide: Beyond eNOS. *J Pharmacol Sci* **129**, 83-94, doi:10.1016/j.jphs.2015.09.002 (2015).

33 Lowenstein, C. J., Dinerman, J. L. & Snyder, S. H. Nitric oxide: a physiologic messenger. *Ann Intern Med* **120**, 227-237, doi:10.7326/0003-4819-120-3-199402010-00009 (1994).

34 Moncada, S. & Higgs, A. The L-arginine-nitric oxide pathway. *N Engl J Med* **329**, 2002-2012, doi:10.1056/NEJM199312303292706 (1993).

35 Goshi, E., Zhou, G. & He, Q. Nitric oxide detection methods in vitro and in vivo. *Med Gas Res* **9**, 192-207, doi:10.4103/2045-9912.273957 (2019).

36 Papadaki, M., Tilton, R. G., Eskin, S. G. & McIntire, L. V. Nitric oxide production by cultured human aortic smooth muscle cells: stimulation by fluid flow. *Am J Physiol* **274**, H616-626, doi:10.1152/ajpheart.1998.274.2.h616 (1998).

37 Andrew, P. J. & Mayer, B. Enzymatic function of nitric oxide synthases. *Cardiovasc Res* **43**, 521-531, doi:10.1016/s0008-6363(99)00115-7 (1999).

38 Yamada, T. *et al.* Thromboxane A2 regulates vascular tone via its inhibitory effect on the expression of inducible nitric oxide synthase. *Circulation* **108**, 2381-2386, doi:10.1161/01.CIR.0000093194.21109.EC (2003).

39 Huang, P. L. *et al.* Hypertension in mice lacking the gene for endothelial nitric oxide synthase. *Nature* **377**, 239-242, doi:10.1038/377239a0 (1995).

40 Moncada, S., Rees, D. D., Schulz, R. & Palmer, R. M. Development and mechanism of a specific supersensitivity to nitrovasodilators after inhibition of vascular nitric oxide synthesis in vivo. *Proceedings of the National Academy of Sciences of the United States of America* **88**, 2166-2170, doi:10.1073/pnas.88.6.2166 (1991).

41 Walch, L., Brink, C. & Norel, X. The muscarinic receptor subtypes in human blood vessels. *Therapie* **56**, 223-226 (2001).

42 Sessa, W. C. eNOS at a glance. *J Cell Sci* **117**, 2427-2429, doi:10.1242/jcs.01165 (2004).

43 Epstein, F. H. The L-arginine-Nitric Oxide Pathway. *The New England Journal of Medicine* **329**, 2002-2012 (1993).

44 Sandner, P. *et al.* Soluble Guanylate Cyclase Stimulators and Activators. *Handb Exp Pharmacol* **264**, 355-394, doi:10.1007/164_2018_197 (2021).

45 Stasch, J. P. & Hobbs, A. J. NO-independent, haem-dependent soluble guanylate cyclase stimulators. *Handb Exp Pharmacol*, 277-308, doi:10.1007/978-3-540-68964-5_13 (2009).

46 Schmidt, H. H., Schmidt, P. M. & Stasch, J. P. NO- and haem-independent soluble guanylate cyclase activators. *Handb Exp Pharmacol*, 309-339, doi:10.1007/978-3-540-68964-5_14 (2009).

47 Ghofrani, H. A. *et al.* Riociguat for the treatment of pulmonary arterial hypertension. *N Engl J Med* **369**, 330-340, doi:10.1056/NEJMoa1209655 (2013).

48 Ghofrani, H. A. *et al.* Riociguat for the treatment of chronic thromboembolic pulmonary hypertension. *N Engl J Med* **369**, 319-329, doi:10.1056/NEJMoa1209657 (2013).

49 Olschewski, A. & Weir, E. K. Redox regulation of ion channels in the pulmonary circulation. *Antioxid Redox Signal* **22**, 465-485, doi:10.1089/ars.2014.5899 (2015).

50 de Bold, A. J. Atrial natriuretic factor: a hormone produced by the heart. *Science* **230**,

767-770, doi:10.1126/science.2932797 (1985).
51 Mukoyama, M. *et al.* Human brain natriuretic peptide, a novel cardiac hormone. *Lancet* **335**, 801-802, doi:10.1016/0140-6736(90)90925-u (1990).
52 Mukoyama, M. *et al.* Brain natriuretic peptide as a novel cardiac hormone in humans. Evidence for an exquisite dual natriuretic peptide system, atrial natriuretic peptide and brain natriuretic peptide. *J Clin Invest* **87**, 1402-1412, doi:10.1172/JCI115146 (1991).
53 Edwards, B. S., Zimmerman, R. S., Schwab, T. R., Heublein, D. M. & Burnett, J. C., Jr. Atrial stretch, not pressure, is the principal determinant controlling the acute release of atrial natriuretic factor. *Circ Res* **62**, 191-195, doi:10.1161/01.res.62.2.191 (1988).
54 Kinnunen, P., Vuolteenaho, O. & Ruskoaho, H. Mechanisms of atrial and brain natriuretic peptide release from rat ventricular myocardium: effect of stretching. *Endocrinology* **132**, 1961-1970, doi:10.1210/endo.132.5.8477647 (1993).
55 Potter, L. R., Yoder, A. R., Flora, D. R., Antos, L. K. & Dickey, D. M. Natriuretic peptides: their structures, receptors, physiologic functions and therapeutic applications. *Handb Exp Pharmacol*, 341-366, doi:10.1007/978-3-540-68964-5_15 (2009).
56 Stingo, A. J. *et al.* Presence of C-type natriuretic peptide in cultured human endothelial cells and plasma. *Am J Physiol* **263**, H1318-1321, doi:10.1152/ajpheart.1992.263.4.H1318 (1992).
57 Suga, S. *et al.* Endothelial production of C-type natriuretic peptide and its marked augmentation by transforming growth factor-beta. Possible existence of "vascular natriuretic peptide system". *J Clin Invest* **90**, 1145-1149, doi:10.1172/JCI115933 (1992).
58 Del Ry, S. *et al.* Expression of C-type natriuretic peptide and its receptor NPR-B in cardiomyocytes. *Peptides* **32**, 1713-1718, doi:10.1016/j.peptides.2011.06.014 (2011).
59 Horio, T. *et al.* Gene expression, secretion, and autocrine action of C-type natriuretic peptide in cultured adult rat cardiac fibroblasts. *Endocrinology* **144**, 2279-2284, doi:10.1210/en.2003-0128 (2003).
60 Lorigo, M., Oliveira, N. & Cairrao, E. PDE-Mediated Cyclic Nucleotide Compartmentation in Vascular Smooth Muscle Cells: From Basic to a Clinical Perspective. *J Cardiovasc Dev Dis* **9**, doi:10.3390/jcdd9010004 (2021).
61 Hofmann, F., Feil, R., Kleppisch, T. & Schlossmann, J. Function of cGMP-dependent protein kinases as revealed by gene deletion. *Physiol Rev* **86**, 1-23, doi:10.1152/physrev.00015.2005 (2006).
62 Feil, R. *et al.* Functional reconstitution of vascular smooth muscle cells with cGMP-dependent protein kinase I isoforms. *Circ Res* **90**, 1080-1086, doi:10.1161/01.res.0000019586.95768.40 (2002).
63 Wolfe, L., Corbin, J. D. & Francis, S. H. Characterization of a novel isozyme of cGMP-dependent protein kinase from bovine aorta. *J Biol Chem* **264**, 7734-7741 (1989).
64 Kim, C. & Sharma, R. Cyclic nucleotide selectivity of protein kinase G isozymes. *Protein Sci* **30**, 316-327, doi:10.1002/pro.4008 (2021).
65 Scott, J. D. Cyclic nucleotide-dependent protein kinases. *Pharmacol Ther* **50**, 123-145, doi:10.1016/0163-7258(91)90075-w (1991).
66 Francis, S. H. & Corbin, J. D. Structure and function of cyclic nucleotide-dependent

protein kinases. *Annu Rev Physiol* **56**, 237-272, doi:10.1146/annurev.ph.56.030194.001321 (1994).

67 Pfeifer, A. *et al.* Defective smooth muscle regulation in cGMP kinase I-deficient mice. *EMBO J* **17**, 3045-3051, doi:10.1093/emboj/17.11.3045 (1998).

68 Manoury, B., Idres, S., Leblais, V. & Fischmeister, R. Ion channels as effectors of cyclic nucleotide pathways: Functional relevance for arterial tone regulation. *Pharmacol Ther*, 107499, doi:10.1016/j.pharmthera.2020.107499 (2020).

69 Komalavilas, P. & Lincoln, T. M. Phosphorylation of the inositol 1,4,5-trisphosphate receptor. Cyclic GMP-dependent protein kinase mediates cAMP and cGMP dependent phosphorylation in the intact rat aorta. *J Biol Chem* **271**, 21933-21938, doi:10.1074/jbc.271.36.21933 (1996).

70 Schlossmann, J. *et al.* Regulation of intracellular calcium by a signalling complex of IRAG, IP3 receptor and cGMP kinase Ibeta. *Nature* **404**, 197-201, doi:10.1038/35004606 (2000).

71 Desch, M. *et al.* IRAG determines nitric oxide- and atrial natriuretic peptide-mediated smooth muscle relaxation. *Cardiovasc Res* **86**, 496-505, doi:10.1093/cvr/cvq008 (2010).

72 Geiselhoringer, A. *et al.* IRAG is essential for relaxation of receptor-triggered smooth muscle contraction by cGMP kinase. *EMBO J* **23**, 4222-4231, doi:10.1038/sj.emboj.7600440 (2004).

73 Andriantsitohaina, R., Lagaud, G. J., Andre, A., Muller, B. & Stoclet, J. C. Effects of cGMP on calcium handling in ATP-stimulated rat resistance arteries. *Am J Physiol* **268**, H1223-1231, doi:10.1152/ajpheart.1995.268.3.H1223 (1995).

74 Cohen, R. A. *et al.* Mechanism of nitric oxide-induced vasodilatation: refilling of intracellular stores by sarcoplasmic reticulum Ca2+ ATPase and inhibition of store-operated Ca2+ influx. *Circ Res* **84**, 210-219, doi:10.1161/01.res.84.2.210 (1999).

75 Low, A. M., Darby, P. J., Kwan, C. Y. & Daniel, E. E. Effects of thapsigargin and ryanodine on vascular contractility: cross-talk between sarcoplasmic reticulum and plasmalemma. *Eur J Pharmacol* **230**, 53-62, doi:10.1016/0014-2999(93)90409-b (1993).

76 Baltensperger, K., Carafoli, E. & Chiesi, M. The Ca2+-pumping ATPase and the major substrates of the cGMP-dependent protein kinase in smooth muscle sarcolemma are distinct entities. *Eur J Biochem* **172**, 7-16, doi:10.1111/j.1432-1033.1988.tb13848.x (1988).

77 Furukawa, K. & Nakamura, H. Cyclic GMP regulation of the plasma membrane (Ca2+-Mg2+)ATPase in vascular smooth muscle. *J Biochem* **101**, 287-290, doi:10.1093/oxfordjournals.jbchem.a121904 (1987).

78 Furukawa, K., Tawada, Y. & Shigekawa, M. Regulation of the plasma membrane Ca2+ pump by cyclic nucleotides in cultured vascular smooth muscle cells. *J Biol Chem* **263**, 8058-8065 (1988).

79 Rashatwar, S. S., Cornwell, T. L. & Lincoln, T. M. Effects of 8-bromo-cGMP on Ca2+ levels in vascular smooth muscle cells: possible regulation of Ca2+-ATPase by cGMP-dependent protein kinase. *Proceedings of the National Academy of Sciences of the*

United States of America **84**, 5685-5689, doi:10.1073/pnas.84.16.5685 (1987).

80 Vrolix, M., Raeymaekers, L., Wuytack, F., Hofmann, F. & Casteels, R. Cyclic GMP-dependent protein kinase stimulates the plasmalemmal Ca2+ pump of smooth muscle via phosphorylation of phosphatidylinositol. *Biochem J* **255**, 855-863, doi:10.1042/bj2550855 (1988).

81 Yoshida, Y., Cai, J. Q. & Imai, S. Plasma membrane Ca(2+)-pump ATPase is not a substrate for cGMP-dependent protein kinase. *J Biochem* **111**, 559-562, doi:10.1093/oxfordjournals.jbchem.a123796 (1992).

82 Popescu, L. M., Panoiu, C., Hinescu, M. & Nutu, O. The mechanism of cGMP-induced relaxation in vascular smooth muscle. *Eur J Pharmacol* **107**, 393-394, doi:10.1016/0014-2999(85)90269-9 (1985).

83 Furukawa, K., Ohshima, N., Tawada-Iwata, Y. & Shigekawa, M. Cyclic GMP stimulates Na+/Ca2+ exchange in vascular smooth muscle cells in primary culture. *J Biol Chem* **266**, 12337-12341 (1991).

84 Nakamura, K., Koga, Y., Sakai, H., Homma, K. & Ikebe, M. cGMP-dependent relaxation of smooth muscle is coupled with the change in the phosphorylation of myosin phosphatase. *Circ Res* **101**, 712-722, doi:10.1161/CIRCRESAHA.107.153981 (2007).

85 Wooldridge, A. A. *et al.* Smooth muscle phosphatase is regulated in vivo by exclusion of phosphorylation of threonine 696 of MYPT1 by phosphorylation of Serine 695 in response to cyclic nucleotides. *The Journal of biological chemistry* **279**, 34496-34504, doi:10.1074/jbc.M405957200 (2004).

86 Surks, H. K. *et al.* Regulation of myosin phosphatase by a specific interaction with cGMP- dependent protein kinase Ialpha. *Science* **286**, 1583-1587 (1999).

87 Sauzeau, V. *et al.* Cyclic GMP-dependent protein kinase signaling pathway inhibits RhoA-induced Ca2+ sensitization of contraction in vascular smooth muscle. *The Journal of biological chemistry* **275**, 21722-21729, doi:10.1074/jbc.M000753200 (2000).

88 Willoughby, D. & Cooper, D. M. Organization and Ca2+ regulation of adenylyl cyclases in cAMP microdomains. *Physiol Rev* **87**, 965-1010, doi:10.1152/physrev.00049.2006 (2007).

89 Ostrom, R. S. *et al.* Localization of adenylyl cyclase isoforms and G protein-coupled receptors in vascular smooth muscle cells: expression in caveolin-rich and noncaveolin domains. *Mol Pharmacol* **62**, 983-992, doi:10.1124/mol.62.5.983 (2002).

90 Webb, J. G., Yates, P. W., Yang, Q., Mukhin, Y. V. & Lanier, S. M. Adenylyl cyclase isoforms and signal integration in models of vascular smooth muscle cells. *Am J Physiol Heart Circ Physiol* **281**, H1545-1552, doi:10.1152/ajpheart.2001.281.4.H1545 (2001).

91 Nelson, C. P. *et al.* Principal role of adenylyl cyclase 6 in K(+) channel regulation and vasodilator signalling in vascular smooth muscle cells. *Cardiovasc Res* **91**, 694-702, doi:10.1093/cvr/cvr137 (2011).

92 Clement, N., Glorian, M., Raymondjean, M., Andreani, M. & Limon, I. PGE2 amplifies the effects of IL-1beta on vascular smooth muscle cell de-differentiation: a

consequence of the versatility of PGE2 receptors 3 due to the emerging expression of adenylyl cyclase 8. *Journal of cellular physiology* **208**, 495-505, doi:10.1002/jcp.20673 (2006).

93 Gueguen, M. *et al.* Implication of adenylyl cyclase 8 in pathological smooth muscle cell migration occurring in rat and human vascular remodelling. *J Pathol* **221**, 331-342, doi:10.1002/path.2716 (2010).

94 Alexander, S. P., Mathie, A. & Peters, J. A. Guide to Receptors and Channels (GRAC), 5th edition. *Br J Pharmacol* **164 Suppl 1**, S1-324, doi:10.1111/j.1476-5381.2011.01649_1.x (2011).

95 Spaulding, S. W. The ways in which hormones change cyclic adenosine 3',5'-monophosphate-dependent protein kinase subunits, and how such changes affect cell behavior. *Endocr Rev* **14**, 632-650, doi:10.1210/edrv-14-5-632 (1993).

96 Kim, C., Cheng, C. Y., Saldanha, S. A. & Taylor, S. S. PKA-I holoenzyme structure reveals a mechanism for cAMP-dependent activation. *Cell* **130**, 1032-1043, doi:10.1016/j.cell.2007.07.018 (2007).

97 Su, Y. *et al.* Regulatory subunit of protein kinase A: structure of deletion mutant with cAMP binding domains. *Science* **269**, 807-813, doi:10.1126/science.7638597 (1995).

98 Turnham, R. E. & Scott, J. D. Protein kinase A catalytic subunit isoform PRKACA; History, function and physiology. *Gene* **577**, 101-108, doi:10.1016/j.gene.2015.11.052 (2016).

99 Pidoux, G. & Tasken, K. Specificity and spatial dynamics of protein kinase A signaling organized by A-kinase-anchoring proteins. *J Mol Endocrinol* **44**, 271-284, doi:10.1677/JME-10-0010 (2010).

100 Colombe, A. S. & Pidoux, G. Cardiac cAMP-PKA Signaling Compartmentalization in Myocardial Infarction. *Cells* **10**, doi:10.3390/cells10040922 (2021).

101 Maurice, D. H. *et al.* Advances in targeting cyclic nucleotide phosphodiesterases. *Nat Rev Drug Discov* **13**, 290-314, doi:10.1038/nrd4228 (2014).

102 Bobin, P. *et al.* Cyclic nucleotide phosphodiesterases in heart and vessels: A therapeutic perspective. *Arch Cardiovasc Dis* **109**, 431-443, doi:10.1016/j.acvd.2016.02.004 (2016).

103 Mika, D., Leroy, J., Vandecasteele, G. & Fischmeister, R. PDEs create local domains of cAMP signaling. *J Mol Cell Cardiol* **52**, 323-329, doi:10.1016/j.yjmcc.2011.08.016 (2012).

104 Matsumoto, T., Wakabayashi, K., Kobayashi, T. & Kamata, K. Diabetes-related changes in cAMP-dependent protein kinase activity and decrease in relaxation response in rat mesenteric artery. *Am J Physiol Heart Circ Physiol* **287**, H1064-1071, doi:10.1152/ajpheart.00069.2004 (2004).

105 Indolfi, C. *et al.* 8-chloro-cAMP inhibits smooth muscle cell proliferation in vitro and neointima formation induced by balloon injury in vivo. *J Am Coll Cardiol* **36**, 288-293, doi:10.1016/s0735-1097(00)00679-3 (2000).

106 Yu, X., Li, F., Klussmann, E., Stallone, J. N. & Han, G. G protein-coupled estrogen receptor 1 mediates relaxation of coronary arteries via cAMP/PKA-dependent activation of MLCP. *Am J Physiol Endocrinol Metab* **307**, E398-407,

doi:10.1152/ajpendo.00534.2013 (2014).

107 Adelstein, R. S., Conti, M. A., Hathaway, D. R. & Klee, C. B. Phosphorylation of smooth muscle myosin light chain kinase by the catalytic subunit of adenosine 3': 5'-monophosphate-dependent protein kinase. *J Biol Chem* **253**, 8347-8350 (1978).

108 Conti, M. A. & Adelstein, R. S. The relationship between calmodulin binding and phosphorylation of smooth muscle myosin kinase by the catalytic subunit of 3':5' cAMP-dependent protein kinase. *J Biol Chem* **256**, 3178-3181 (1981).

109 de Lanerolle, P., Nishikawa, M., Yost, D. A. & Adelstein, R. S. Increased phosphorylation of myosin light chain kinase after an increase in cyclic AMP in intact smooth muscle. *Science* **223**, 1415-1417, doi:10.1126/science.6322302 (1984).

110 Raina, H., Zacharia, J., Li, M. & Wier, W. G. Activation by Ca2+/calmodulin of an exogenous myosin light chain kinase in mouse arteries. *J Physiol* **587**, 2599-2612, doi:10.1113/jphysiol.2008.165258 (2009).

111 White, R. E., Kryman, J. P., El-Mowafy, A. M., Han, G. & Carrier, G. O. cAMP-dependent vasodilators cross-activate the cGMP-dependent protein kinase to stimulate BK(Ca) channel activity in coronary artery smooth muscle cells. *Circ Res* **86**, 897-905, doi:10.1161/01.res.86.8.897 (2000).

112 Dao, K. K. *et al.* Epac1 and cAMP-dependent protein kinase holoenzyme have similar cAMP affinity, but their cAMP domains have distinct structural features and cyclic nucleotide recognition. *The Journal of biological chemistry* **281**, 21500-21511, doi:10.1074/jbc.M603116200 (2006).

113 de Rooij, J. *et al.* Epac is a Rap1 guanine-nucleotide-exchange factor directly activated by cyclic AMP. *Nature* **396**, 474-477, doi:10.1038/24884 (1998).

114 Zieba, B. J. *et al.* The cAMP-responsive Rap1 guanine nucleotide exchange factor, Epac, induces smooth muscle relaxation by down-regulation of RhoA activity. *J Biol Chem* **286**, 16681-16692, doi:10.1074/jbc.M110.205062 (2011).

115 Roberts, O. L., Kamishima, T., Barrett-Jolley, R., Quayle, J. M. & Dart, C. Exchange protein activated by cAMP (Epac) induces vascular relaxation by activating Ca2+-sensitive K+ channels in rat mesenteric artery. *J Physiol* **591**, 5107-5123, doi:10.1113/jphysiol.2013.262006 (2013).

116 Purves, G. I., Kamishima, T., Davies, L. M., Quayle, J. M. & Dart, C. Exchange protein activated by cAMP (Epac) mediates cAMP-dependent but protein kinase A-insensitive modulation of vascular ATP-sensitive potassium channels. *J Physiol* **587**, 3639-3650, doi:10.1113/jphysiol.2009.173534 (2009).

117 Jeyaraj, S. C. *et al.* Cyclic AMP-Rap1A signaling activates RhoA to induce alpha(2c)-adrenoceptor translocation to the cell surface of microvascular smooth muscle cells. *Am J Physiol Cell Physiol* **303**, C499-511, doi:10.1152/ajpcell.00461.2011 (2012).

118 Garcia-Morales, V., Luaces-Regueira, M. & Campos-Toimil, M. The cAMP effectors PKA and Epac activate endothelial NO synthase through PI3K/Akt pathway in human endothelial cells. *Biochemical pharmacology* **145**, 94-101, doi:10.1016/j.bcp.2017.09.004 (2017).

119 Garcia-Morales, V., Cuinas, A., Elies, J. & Campos-Toimil, M. PKA and Epac activation mediates cAMP-induced vasorelaxation by increasing endothelial NO

production. *Vascul Pharmacol* **60**, 95-101, doi:10.1016/j.vph.2014.01.004 (2014).

120 Lakshmikanthan, S. *et al.* Rap1b in smooth muscle and endothelium is required for maintenance of vascular tone and normal blood pressure. *Arterioscler Thromb Vasc Biol* **34**, 1486-1494, doi:10.1161/ATVBAHA.114.303678 (2014).

121 Wehbe, N. *et al.* EPAC in Vascular Smooth Muscle Cells. *Int J Mol Sci* **21**, doi:10.3390/ijms21145160 (2020).

122 Omori, K. & Kotera, J. Overview of PDEs and their regulation. *Circ Res* **100**, 309-327, doi:10.1161/01.RES.0000256354.95791.f1 (2007).

123 Francis, S. H., Blount, M. A. & Corbin, J. D. Mammalian cyclic nucleotide phosphodiesterases: molecular mechanisms and physiological functions. *Physiol Rev* **91**, 651-690, doi:10.1152/physrev.00030.2010 (2011).

124 Keravis, T. & Lugnier, C. Cyclic nucleotide phosphodiesterase (PDE) isozymes as targets of the intracellular signalling network: benefits of PDE inhibitors in various diseases and perspectives for future therapeutic developments. *British journal of pharmacology* **165**, 1288-1305, doi:10.1111/j.1476-5381.2011.01729.x (2012).

125 Heikaus, C. C., Pandit, J. & Klevit, R. E. Cyclic nucleotide binding GAF domains from phosphodiesterases: structural and mechanistic insights. *Structure* **17**, 1551-1557, doi:10.1016/j.str.2009.07.019 (2009).

126 Turko, I. V., Francis, S. H. & Corbin, J. D. Binding of cGMP to both allosteric sites of cGMP-binding cGMP-specific phosphodiesterase (PDE5) is required for its phosphorylation. *Biochem J* **329 (Pt 3)**, 505-510, doi:10.1042/bj3290505 (1998).

127 Martinez, S. E. *et al.* The two GAF domains in phosphodiesterase 2A have distinct roles in dimerization and in cGMP binding. *Proceedings of the National Academy of Sciences of the United States of America* **99**, 13260-13265, doi:10.1073/pnas.192374899 (2002).

128 Gross-Langenhoff, M., Hofbauer, K., Weber, J., Schultz, A. & Schultz, J. E. cAMP is a ligand for the tandem GAF domain of human phosphodiesterase 10 and cGMP for the tandem GAF domain of phosphodiesterase 11. *J Biol Chem* **281**, 2841-2846, doi:10.1074/jbc.M511468200 (2006).

129 Biel, M. & Michalakis, S. Cyclic nucleotide-gated channels. *Handb Exp Pharmacol*, 111-136, doi:10.1007/978-3-540-68964-5_7 (2009).

130 Yao, X., Leung, P. S., Kwan, H. Y., Wong, T. P. & Fong, M. W. Rod-type cyclic nucleotide-gated cation channel is expressed in vascular endothelium and vascular smooth muscle cells. *Cardiovasc Res* **41**, 282-290, doi:10.1016/s0008-6363(98)00158-8 (1999).

131 Cheng, K. T., Chan, F. L., Huang, Y., Chan, W. Y. & Yao, X. Expression of olfactory-type cyclic nucleotide-gated channel (CNGA2) in vascular tissues. *Histochem Cell Biol* **120**, 475-481, doi:10.1007/s00418-003-0596-2 (2003).

132 Leung, Y. K., Du, J., Huang, Y. & Yao, X. Cyclic nucleotide-gated channels contribute to thromboxane A2-induced contraction of rat small mesenteric arteries. *PLoS One* **5**, e11098, doi:10.1371/journal.pone.0011098 (2010).

133 Shen, B. *et al.* Epinephrine-induced Ca2+ influx in vascular endothelial cells is mediated by CNGA2 channels. *J Mol Cell Cardiol* **45**, 437-445,

doi:10.1016/j.yjmcc.2008.06.005 (2008).

134 Kwan, H. Y. *et al.* CNGA2 contributes to ATP-induced noncapacitative Ca2+ influx in vascular endothelial cells. *J Vasc Res* **47**, 148-156, doi:10.1159/000235969 (2010).

135 Cheng, K. T. *et al.* CNGA2 channels mediate adenosine-induced Ca2+ influx in vascular endothelial cells. *Arterioscler Thromb Vasc Biol* **28**, 913-918, doi:10.1161/ATVBAHA.107.148338 (2008).

136 Wu, S. *et al.* Cyclic nucleotide-gated channels mediate membrane depolarization following activation of store-operated calcium entry in endothelial cells. *J Biol Chem* **275**, 18887-18896, doi:10.1074/jbc.M002795200 (2000).

137 Ahmad, F. *et al.* Cyclic Nucleotide Phosphodiesterases: important signaling modulators and therapeutic targets. *Oral Diseases* **21**, e25-e50, doi:10.1111/odi.12275 (2015).

138 Wang, P., Wu, P., Egan, R. W. & Billah, M. M. Identification and characterization of a new human type 9 cGMP-specific phosphodiesterase splice variant (PDE9A5). *Gene* **314**, 15-27, doi:10.1016/s0378-1119(03)00733-9 (2003).

139 Maclean, M. R. *et al.* Phosphodiesterase isoforms in the pulmonary arterial circulation of the rat: changes in pulmonary hypertension. *The Journal of pharmacology and experimental therapeutics* **283**, 619-624 (1997).

140 Rabe, K. F., H. Tenor, G. Dent, C. Schudt, M. Na- kashima, H. Magnussen. . Identification of PDE isozymes in human pulmonary artery and effect of selective PDE inhibitors. *American Journal of Physiology* **266**, 536-543 (1994).

141 Crosswhite, P. & Sun, Z. Inhibition of phosphodiesterase-1 attenuates cold-induced pulmonary hypertension. *Hypertension* **61**, 585-592, doi:10.1161/HYPERTENSIONAHA.111.00676 (2013).

142 Pauvert, O. *et al.* Characterisation of cyclic nucleotide phosphodiesterase isoforms in the media layer of the main pulmonary artery. *Biochemical pharmacology* **63**, 1763-1772 (2002).

143 Schermuly, R. T. *et al.* Phosphodiesterase 1 upregulation in pulmonary arterial hypertension: target for reverse-remodeling therapy. *Circulation* **115**, 2331-2339, doi:10.1161/CIRCULATIONAHA.106.676809 (2007).

144 Mai Kimura, Y. T., Christophe Guignabert, Makoto Takei, Kenjiro Kosaki, Nobuhiro Tanabe, Koichiro Tatsumi, Tsutomu Saji, Toru Satoh, Masaharu Kataoka, Shigeo Kamitsuji, Naoyuki Kamatani, Raphaël Thuillet, Ly Tu, Marc Humbert, Keiichi Fukuda, Motoaki Sano. A genome-wide association analysis identi es PDE1A|DNAJC10 locus on chromosome 2 associated with idiopathic pulmonary arterial hypertension in a Japanese population. *Oncotarget* **8**, 74917-74926 (2017).

145 Growcott, E. J. *et al.* Phosphodiesterase type 4 expression and anti-proliferative effects in human pulmonary artery smooth muscle cells. *Respir Res* **7**, 9, doi:10.1186/1465-9921-7-9 (2006).

146 Komas, N., Lugnier, C., Andriantsitohaina, R. & Stoclet, J. C. Characterisation of cyclic nucleotide phosphodiesterases from rat mesenteric artery. *European journal of pharmacology* **208**, 85-87, doi:10.1016/0922-4106(91)90056-n (1991).

147 Komas, N., Lugnier, C. & Stoclet, J. C. Endothelium-dependent and independent

relaxation of the rat aorta by cyclic nucleotide phosphodiesterase inhibitors. *Br J Pharmacol* **104**, 495-503, doi:10.1111/j.1476-5381.1991.tb12457.x (1991).

148 Khammy, M. M. *et al.* PDE1A inhibition elicits cGMP-dependent relaxation of rat mesenteric arteries. *British journal of pharmacology* **174**, 4186-4198, doi:10.1111/bph.14034 (2017).

149 Rybalkin, S. D. *et al.* Calmodulin-stimulated cyclic nucleotide phosphodiesterase (PDE1C) is induced in human arterial smooth muscle cells of the synthetic, proliferative phenotype. *J Clin Invest* **100**, 2611-2621, doi:10.1172/JCI119805 (1997).

150 Netherton, S. J. & Maurice, D. H. Vascular endothelial cell cyclic nucleotide phosphodiesterases and regulated cell migration: implications in angiogenesis. *Molecular pharmacology* **67**, 263-272, doi:10.1124/mol.104.004853 (2005).

151 Haynes, J., Jr., Killilea, D. W., Peterson, P. D. & Thompson, W. J. Erythro-9-(2-hydroxy-3-nonyl)adenine inhibits cyclic-3',5'-guanosine monophosphate-stimulated phosphodiesterase to reverse hypoxic pulmonary vasoconstriction in the perfused rat lung. *The Journal of pharmacology and experimental therapeutics* **276**, 752-757 (1996).

152 Bubb, K. J. *et al.* Inhibition of phosphodiesterase 2 augments cGMP and cAMP signaling to ameliorate pulmonary hypertension. *Circulation* **130**, 496-507, doi:10.1161/CIRCULATIONAHA.114.009751 (2014).

153 Suttorp, N., Weber, U., Welsch, T. & Schudt, C. Role of phosphodiesterases in the regulation of endothelial permeability in vitro. *J Clin Invest* **91**, 1421-1428, doi:10.1172/JCI116346 (1993).

154 Stephenson, D. T. *et al.* Immunohistochemical localization of phosphodiesterase 2A in multiple mammalian species. *J Histochem Cytochem* **57**, 933-949, doi:10.1369/jhc.2009.953471 (2009).

155 Zhai, K. *et al.* beta-Adrenergic cAMP signals are predominantly regulated by phosphodiesterase type 4 in cultured adult rat aortic smooth muscle cells. *PLoS One* **7**, e47826, doi:10.1371/journal.pone.0047826 (2012).

156 Lugnier, C. & Schini, V. B. Characterization of cyclic nucleotide phosphodiesterases from cultured bovine aortic endothelial cells. *Biochem Pharmacol* **39**, 75-84, doi:10.1016/0006-2952(90)90650-a (1990).

157 Favot, L., Keravis, T., Holl, V., Le Bec, A. & Lugnier, C. VEGF-induced HUVEC migration and proliferation are decreased by PDE2 and PDE4 inhibitors. *Thromb Haemost* **90**, 334-343, doi:10.1160/TH03-02-0084 (2003).

158 Souness, J. E., Diocee, B. K., Martin, W. & Moodie, S. A. Pig aortic endothelial-cell cyclic nucleotide phosphodiesterases. Use of phosphodiesterase inhibitors to evaluate their roles in regulating cyclic nucleotide levels in intact cells. *Biochem J* **266**, 127-132, doi:10.1042/bj2660127 (1990).

159 Surapisitchat, J., Jeon, K. I., Yan, C. & Beavo, J. A. Differential regulation of endothelial cell permeability by cGMP via phosphodiesterases 2 and 3. *Circulation research* **101**, 811-818, doi:10.1161/CIRCRESAHA.107.154229 (2007).

160 Sadhu, K., Hensley, K., Florio, V. A. & Wolda, S. L. Differential expression of the cyclic GMP-stimulated phosphodiesterase PDE2A in human venous and capillary

endothelial cells. *J Histochem Cytochem* **47**, 895-906, doi:10.1177/002215549904700707 (1999).

161 Murray, F., MacLean, M. R. & Pyne, N. J. Increased expression of the cGMP-inhibited cAMP-specific (PDE3) and cGMP binding cGMP-specific (PDE5) phosphodiesterases in models of pulmonary hypertension. *British journal of pharmacology* **137**, 1187-1194, doi:10.1038/sj.bjp.0704984 (2002).

162 Hubert, F. *et al.* Alteration of vascular reactivity in heart failure: role of phosphodiesterases 3 and 4. *Br J Pharmacol* **171**, 5361-5375, doi:10.1111/bph.12853 (2014).

163 Idres, S. *et al.* Contribution of BKCa channels to vascular tone regulation by PDE3 and PDE4 is lost in heart failure. *Cardiovasc Res* **115**, 130-144, doi:10.1093/cvr/cvy161 (2019).

164 Ercu, M. *et al.* Phosphodiesterase 3A and Arterial Hypertension. *Circulation* **142**, 133-149, doi:10.1161/CIRCULATIONAHA.119.043061 (2020).

165 Dunkerley, H. A. *et al.* Reduced phosphodiesterase 3 activity and phosphodiesterase 3A level in synthetic vascular smooth muscle cells: implications for use of phosphodiesterase 3 inhibitors in cardiovascular tissues. *Mol Pharmacol* **61**, 1033-1040, doi:10.1124/mol.61.5.1033 (2002).

166 Wilson, L. S. *et al.* A phosphodiesterase 3B-based signaling complex integrates exchange protein activated by cAMP 1 and phosphatidylinositol 3-kinase signals in human arterial endothelial cells. *J Biol Chem* **286**, 16285-16296, doi:10.1074/jbc.M110.217026 (2011).

167 Houslay, M. D., Baillie, G. S. & Maurice, D. H. cAMP-Specific phosphodiesterase-4 enzymes in the cardiovascular system: a molecular toolbox for generating compartmentalized cAMP signaling. *Circ Res* **100**, 950-966, doi:10.1161/01.RES.0000261934.56938.38 (2007).

168 Rampersad, S. N. *et al.* Cyclic AMP phosphodiesterase 4D (PDE4D) Tethers EPAC1 in a vascular endothelial cadherin (VE-Cad)-based signaling complex and controls cAMP-mediated vascular permeability. *J Biol Chem* **285**, 33614-33622, doi:10.1074/jbc.M110.140004 (2010).

169 Sebkhi, A., Strange, J. W., Phillips, S. C., Wharton, J. & Wilkins, M. R. Phosphodiesterase type 5 as a target for the treatment of hypoxia-induced pulmonary hypertension. *Circulation* **107**, 3230-3235, doi:10.1161/01.CIR.0000074226.20466.B1 (2003).

170 Zhang, L. *et al.* Cyclic nucleotide signalling compartmentation by PDEs in cultured vascular smooth muscle cells. *Br J Pharmacol* **176**, 1780-1792, doi:10.1111/bph.14651 (2019).

171 Ashikaga, T., Strada, S. J. & Thompson, W. J. Altered expression of cyclic nucleotide phosphodiesterase isozymes during culture of aortic endothelial cells. *Biochem Pharmacol* **54**, 1071-1079, doi:10.1016/s0006-2952(97)00287-6 (1997).

172 Phillips, P. G., Long, L., Wilkins, M. R. & Morrell, N. W. cAMP phosphodiesterase inhibitors potentiate effects of prostacyclin analogs in hypoxic pulmonary vascular remodeling. *Am J Physiol Lung Cell Mol Physiol* **288**, L103-115,

doi:10.1152/ajplung.00095.2004 (2005).

173 Murray, F. *et al.* Expression and activity of cAMP phosphodiesterase isoforms in pulmonary artery smooth muscle cells from patients with pulmonary hypertension: role for PDE1. *Am J Physiol Lung Cell Mol Physiol* **292**, L294-303, doi:10.1152/ajplung.00190.2006 (2007).

174 Tian, X. *et al.* Phosphodiesterase 10A upregulation contributes to pulmonary vascular remodeling. *PLoS One* **6**, e18136, doi:10.1371/journal.pone.0018136 (2011).

175 Zhu, J., Yang, Q., Dai, D. & Huang, Q. X-ray crystal structure of phosphodiesterase 2 in complex with a highly selective, nanomolar inhibitor reveals a binding-induced pocket important for selectivity. *J Am Chem Soc* **135**, 11708-11711, doi:10.1021/ja404449g (2013).

176 Hidaka, H. *et al.* Selective inhibitor of platelet cyclic adenosine monophosphate phosphodiesterase, cilostamide, inhibits platelet aggregation. *J Pharmacol Exp Ther* **211**, 26-30 (1979).

177 Lugnier, C. *et al.* Tissue and substrate specificity of inhibition by alkoxy-aryl-lactams of platelet and arterial smooth muscle cyclic nucleotide phosphodiesterases relationship to pharmacological activity. *Biochem Biophys Res Commun* **113**, 954-959, doi:10.1016/0006-291x(83)91091-4 (1983).

178 Komas, N. *et al.* Differential sensitivity to cardiotonic drugs of cyclic AMP phosphodiesterases isolated from canine ventricular and sinoatrial-enriched tissues. *J Cardiovasc Pharmacol* **14**, 213-220, doi:10.1097/00005344-198908000-00005 (1989).

179 Wallis, R. M. The pharmacology of sildenafil, a novel and selective inhibitor of phosphodiesterase (PDE) type 5. *Nihon Yakurigaku Zasshi* **114 Suppl 1**, 22P-26P, doi:10.1254/fpj.114.supplement_22 (1999).

180 Rybalkin, S. D., Rybalkina, I., Beavo, J. A. & Bornfeldt, K. E. Cyclic nucleotide phosphodiesterase 1C promotes human arterial smooth muscle cell proliferation. *Circ Res* **90**, 151-157, doi:10.1161/hh0202.104108 (2002).

181 Le, M. L., Jiang, M. Y., Han, C., Yang, Y. Y. & Wu, Y. PDE1 inhibitors: a review of the recent patent literature (2008-present). *Expert Opin Ther Pat*, 1-17, doi:10.1080/13543776.2022.2027910 (2022).

182 Laursen, M. *et al.* Novel selective PDE type 1 inhibitors cause vasodilatation and lower blood pressure in rats. *British journal of pharmacology* **174**, 2563-2575, doi:10.1111/bph.13868 (2017).

183 Campos-Toimil, M., Keravis, T., Orallo, F., Takeda, K. & Lugnier, C. Short-term or long-term treatments with a phosphodiesterase-4 (PDE4) inhibitor result in opposing agonist-induced Ca(2+) responses in endothelial cells. *Br J Pharmacol* **154**, 82-92, doi:10.1038/bjp.2008.56 (2008).

184 Favot, L., Keravis, T. & Lugnier, C. Modulation of VEGF-induced endothelial cell cycle protein expression through cyclic AMP hydrolysis by PDE2 and PDE4. *Thromb Haemost* **92**, 634-645, doi:10.1160/TH03-12-0768 (2004).

185 Baillie, G. S., Tejeda, G. S. & Kelly, M. P. Therapeutic targeting of 3',5'-cyclic nucleotide phosphodiesterases: inhibition and beyond. *Nature reviews. Drug discovery* **18**, 770-796, doi:10.1038/s41573-019-0033-4 (2019).

186 Donnelly, R. Evidence-based symptom relief of intermittent claudication: efficacy and safety of cilostazol. *Diabetes Obes Metab* **4 Suppl 2**, S20-25, doi:10.1046/j.1463-1326.2002.0040s2s20.x (2002).

187 Cuffe, M. S. *et al.* Short-term intravenous milrinone for acute exacerbation of chronic heart failure: a randomized controlled trial. *JAMA* **287**, 1541-1547, doi:10.1001/jama.287.12.1541 (2002).

188 Martinez, F. J. *et al.* Effect of roflumilast on exacerbations in patients with severe chronic obstructive pulmonary disease uncontrolled by combination therapy (REACT): a multicentre randomised controlled trial. *Lancet* **385**, 857-866, doi:10.1016/S0140-6736(14)62410-7 (2015).

189 Galie, N. *et al.* Tadalafil therapy for pulmonary arterial hypertension. *Circulation* **119**, 2894-2903, doi:10.1161/CIRCULATIONAHA.108.839274 (2009).

190 Barnes, H., Brown, Z., Burns, A. & Williams, T. Phosphodiesterase 5 inhibitors for pulmonary hypertension. *Cochrane Database Syst Rev* **1**, CD012621, doi:10.1002/14651858.CD012621.pub2 (2019).

191 Montani, D. *et al.* Phosphodiesterase type 5 inhibitors in pulmonary arterial hypertension. *Adv Ther* **26**, 813-825, doi:10.1007/s12325-009-0064-z (2009).

192 Andersson, K. E. PDE5 inhibitors - pharmacology and clinical applications 20 years after sildenafil discovery. *British Journal of Pharmacology* **175**, 2554-2565, doi:10.1111/bph.14205 (2018).

193 Humbert, M. *et al.* Pulmonary arterial hypertension in France: results from a national registry. *American journal of respiratory and critical care medicine* **173**, 1023-1030, doi:10.1164/rccm.200510-1668OC (2006).

194 Peacock, A. J., Murphy, N. F., McMurray, J. J., Caballero, L. & Stewart, S. An epidemiological study of pulmonary arterial hypertension. *Eur Respir J* **30**, 104-109, doi:10.1183/09031936.00092306 (2007).

195 Ling, Y. *et al.* Changing demographics, epidemiology, and survival of incident pulmonary arterial hypertension: results from the pulmonary hypertension registry of the United Kingdom and Ireland. *Am J Respir Crit Care Med* **186**, 790-796, doi:10.1164/rccm.201203-0383OC (2012).

196 Strange, G. *et al.* Pulmonary hypertension: prevalence and mortality in the Armadale echocardiography cohort. *Heart* **98**, 1805-1811, doi:10.1136/heartjnl-2012-301992 (2012).

197 Thenappan, T., Shah, S. J., Rich, S. & Gomberg-Maitland, M. A USA-based registry for pulmonary arterial hypertension: 1982-2006. *Eur Respir J* **30**, 1103-1110, doi:10.1183/09031936.00042107 (2007).

198 Badesch, D. B. *et al.* Pulmonary arterial hypertension: baseline characteristics from the REVEAL Registry. *Chest* **137**, 376-387, doi:10.1378/chest.09-1140 (2010).

199 Wu, W., He, J. & Shao, X. Incidence and mortality trend of congenital heart disease at the global, regional, and national level, 1990-2017. *Medicine (Baltimore)* **99**, e20593, doi:10.1097/MD.0000000000020593 (2020).

200 Deol, A. K. *et al.* Schistosomiasis - Assessing Progress toward the 2020 and 2025 Global Goals. *N Engl J Med* **381**, 2519-2528, doi:10.1056/NEJMoa1812165 (2019).

201 collaborators, G. H. Global, regional, and national incidence, prevalence, and mortality of HIV, 1980-2017, and forecasts to 2030, for 195 countries and territories: a systematic analysis for the Global Burden of Diseases, Injuries, and Risk Factors Study 2017. *Lancet HIV* **6**, e831-e859, doi:10.1016/S2352-3018(19)30196-1 (2019).

202 Rich, S. *et al.* Primary pulmonary hypertension. A national prospective study. *Ann Intern Med* **107**, 216-223, doi:10.7326/0003-4819-107-2-216 (1987).

203 Hoeper, M. M. *et al.* Elderly patients diagnosed with idiopathic pulmonary arterial hypertension: results from the COMPERA registry. *Int J Cardiol* **168**, 871-880, doi:10.1016/j.ijcard.2012.10.026 (2013).

204 Benza, R. L. *et al.* The REVEAL Registry risk score calculator in patients newly diagnosed with pulmonary arterial hypertension. *Chest* **141**, 354-362, doi:10.1378/chest.11-0676 (2012).

205 Humbert, M. *et al.* Survival in patients with idiopathic, familial, and anorexigen-associated pulmonary arterial hypertension in the modern management era. *Circulation* **122**, 156-163, doi:10.1161/CIRCULATIONAHA.109.911818 (2010).

206 McGoon, M. D. *et al.* Pulmonary arterial hypertension: epidemiology and registries. *J Am Coll Cardiol* **62**, D51-59, doi:10.1016/j.jacc.2013.10.023 (2013).

207 Hoeper, M. M. & Simon, R. G. J. The changing landscape of pulmonary arterial hypertension and implications for patient care. *Eur Respir Rev* **23**, 450-457, doi:10.1183/09059180.00007814 (2014).

208 D'Alonzo, G. E. *et al.* Survival in patients with primary pulmonary hypertension. Results from a national prospective registry. *Ann Intern Med* **115**, 343-349, doi:10.7326/0003-4819-115-5-343 (1991).

209 Benza, R. L. *et al.* An evaluation of long-term survival from time of diagnosis in pulmonary arterial hypertension from the REVEAL Registry. *Chest* **142**, 448-456, doi:10.1378/chest.11-1460 (2012).

210 Sitbon, O. *et al.* Initial dual oral combination therapy in pulmonary arterial hypertension. *Eur Respir J* **47**, 1727-1736, doi:10.1183/13993003.02043-2015 (2016).

211 Humbert, M. *et al.* Cellular and molecular pathobiology of pulmonary arterial hypertension. *J Am Coll Cardiol* **43**, 13S-24S, doi:10.1016/j.jacc.2004.02.029 (2004).

212 Guignabert, C. *et al.* New molecular targets of pulmonary vascular remodeling in pulmonary arterial hypertension: importance of endothelial communication. *Chest* **147**, 529-537, doi:10.1378/chest.14-0862 (2015).

213 Tuder, R. M. *et al.* Development and pathology of pulmonary hypertension. *J Am Coll Cardiol* **54**, S3-S9, doi:10.1016/j.jacc.2009.04.009 (2009).

214 Hassoun, P. M. Pulmonary Arterial Hypertension. *N Engl J Med* **385**, 2361-2376, doi:10.1056/NEJMra2000348 (2021).

215 Evans, C. E., Cober, N. D., Dai, Z., Stewart, D. J. & Zhao, Y.-Y. Endothelial Cells in the Pathogenesis of Pulmonary Arterial Hypertension. *European Respiratory Journal*, doi:10.1183/13993003.03957-2020 (2021).

216 Budhiraja, R., Tuder, R. M. & Hassoun, P. M. Endothelial dysfunction in pulmonary hypertension. *Circulation* **109**, 159-165, doi:10.1161/01.CIR.0000102381.57477.50 (2004).

217 Guignabert, C. *et al.* Pathogenesis of pulmonary arterial hypertension: lessons from cancer. *Eur Respir Rev* **22**, 543-551, doi:10.1183/09059180.00007513 (2013).
218 Humbert, M. *et al.* Sotatercept for the Treatment of Pulmonary Arterial Hypertension. *N Engl J Med* **384**, 1204-1215, doi:10.1056/NEJMoa2024277 (2021).
219 Perros, F. *et al.* Pulmonary lymphoid neogenesis in idiopathic pulmonary arterial hypertension. *Am J Respir Crit Care Med* **185**, 311-321, doi:10.1164/rccm.201105-0927OC (2012).
220 Soon, E. *et al.* Elevated levels of inflammatory cytokines predict survival in idiopathic and familial pulmonary arterial hypertension. *Circulation* **122**, 920-927, doi:10.1161/CIRCULATIONAHA.109.933762 (2010).
221 Price, L. C. *et al.* Inflammation in pulmonary arterial hypertension. *Chest* **141**, 210-221, doi:10.1378/chest.11-0793 (2012).
222 Hassoun, P. M. *et al.* Inflammation, growth factors, and pulmonary vascular remodeling. *J Am Coll Cardiol* **54**, S10-S19, doi:10.1016/j.jacc.2009.04.006 (2009).
223 Zolty, R. Pulmonary arterial hypertension specific therapy: The old and the new. *Pharmacol Ther* **214**, 107576, doi:10.1016/j.pharmthera.2020.107576 (2020).
224 Dunham-Snary, K. J. *et al.* Hypoxic Pulmonary Vasoconstriction: From Molecular Mechanisms to Medicine. *Chest* **151**, 181-192, doi:10.1016/j.chest.2016.09.001 (2017).
225 Boucherat, O., Agrawal, V., Lawrie, A. & Bonnet, S. The Latest in Animal Models of Pulmonary Hypertension and Right Ventricular Failure. *Circ Res* **130**, 1466-1486, doi:10.1161/CIRCRESAHA.121.319971 (2022).
226 Stenmark, K. R. *et al.* Severe pulmonary hypertension and arterial adventitial changes in newborn calves at 4,300 m. *J Appl Physiol (1985)* **62**, 821-830, doi:10.1152/jappl.1987.62.2.821 (1987).
227 Bonnet, S. *et al.* An abnormal mitochondrial-hypoxia inducible factor-1alpha-Kv channel pathway disrupts oxygen sensing and triggers pulmonary arterial hypertension in fawn hooded rats: similarities to human pulmonary arterial hypertension. *Circulation* **113**, 2630-2641, doi:10.1161/CIRCULATIONAHA.105.609008 (2006).
228 Hoshikawa, Y. *et al.* Hypoxia induces different genes in the lungs of rats compared with mice. *Physiol Genomics* **12**, 209-219, doi:10.1152/physiolgenomics.00081.2001 (2003).
229 Stenmark, K. R., Fagan, K. A. & Frid, M. G. Hypoxia-induced pulmonary vascular remodeling: cellular and molecular mechanisms. *Circ Res* **99**, 675-691, doi:10.1161/01.RES.0000243584.45145.3f (2006).
230 Burke, D. L. *et al.* Sustained hypoxia promotes the development of a pulmonary artery-specific chronic inflammatory microenvironment. *Am J Physiol Lung Cell Mol Physiol* **297**, L238-250, doi:10.1152/ajplung.90591.2008 (2009).
231 Bigham, A. W. & Lee, F. S. Human high-altitude adaptation: forward genetics meets the HIF pathway. *Genes Dev* **28**, 2189-2204, doi:10.1101/gad.250167.114 (2014).
232 Dai, Z., Li, M., Wharton, J., Zhu, M. M. & Zhao, Y. Y. Prolyl-4 Hydroxylase 2 (PHD2) Deficiency in Endothelial Cells and Hematopoietic Cells Induces Obliterative Vascular Remodeling and Severe Pulmonary Arterial Hypertension in Mice and Humans Through Hypoxia-Inducible Factor-2alpha. *Circulation* **133**, 2447-2458,

doi:10.1161/CIRCULATIONAHA.116.021494 (2016).

233 Jiang, Y., Dai, A., Li, Q. & Hu, R. Hypoxia induces transforming growth factor-beta1 gene expression in the pulmonary artery of rats via hypoxia-inducible factor-1alpha. *Acta Biochim Biophys Sin (Shanghai)* **39**, 73-80, doi:10.1111/j.1745-7270.2007.00249.x (2007).

234 Pullamsetti, S. S. *et al.* Inhibition of microRNA-17 improves lung and heart function in experimental pulmonary hypertension. *Am J Respir Crit Care Med* **185**, 409-419, doi:10.1164/rccm.201106-1093OC (2012).

235 Brock, M. *et al.* AntagomiR directed against miR-20a restores functional BMPR2 signalling and prevents vascular remodelling in hypoxia-induced pulmonary hypertension. *Eur Heart J* **35**, 3203-3211, doi:10.1093/eurheartj/ehs060 (2014).

236 Stenmark, K. R., Meyrick, B., Galie, N., Mooi, W. J. & McMurtry, I. F. Animal models of pulmonary arterial hypertension: the hope for etiological discovery and pharmacological cure. *Am J Physiol Lung Cell Mol Physiol* **297**, L1013-1032, doi:10.1152/ajplung.00217.2009 (2009).

237 Zhu, Z. *et al.* Echocardiographic assessment of right ventricular function in experimental pulmonary hypertension. *Pulm Circ* **9**, 2045894019841987, doi:10.1177/2045894019841987 (2019).

238 Taraseviciene-Stewart, L. *et al.* Inhibition of the VEGF receptor 2 combined with chronic hypoxia causes cell death-dependent pulmonary endothelial cell proliferation and severe pulmonary hypertension. *FASEB J* **15**, 427-438, doi:10.1096/fj.00-0343com (2001).

239 Abe, K. *et al.* Formation of plexiform lesions in experimental severe pulmonary arterial hypertension. *Circulation* **121**, 2747-2754, doi:10.1161/CIRCULATIONAHA.109.927681 (2010).

240 Moreno-Vinasco, L. *et al.* Genomic assessment of a multikinase inhibitor, sorafenib, in a rodent model of pulmonary hypertension. *Physiol Genomics* **33**, 278-291, doi:10.1152/physiolgenomics.00169.2007 (2008).

241 Oka, M. *et al.* Rho kinase-mediated vasoconstriction is important in severe occlusive pulmonary arterial hypertension in rats. *Circ Res* **100**, 923-929, doi:10.1161/01.RES.0000261658.12024.18 (2007).

242 Toba, M. *et al.* Temporal hemodynamic and histological progression in Sugen5416/hypoxia/normoxia-exposed pulmonary arterial hypertensive rats. *Am J Physiol Heart Circ Physiol* **306**, H243-250, doi:10.1152/ajpheart.00728.2013 (2014).

243 de Raaf, M. A. *et al.* SuHx rat model: partly reversible pulmonary hypertension and progressive intima obstruction. *Eur Respir J* **44**, 160-168, doi:10.1183/09031936.00204813 (2014).

244 Vitali, S. H. *et al.* The Sugen 5416/hypoxia mouse model of pulmonary hypertension revisited: long-term follow-up. *Pulm Circ* **4**, 619-629, doi:10.1086/678508 (2014).

245 Gomez-Arroyo, J. *et al.* A brief overview of mouse models of pulmonary arterial hypertension: problems and prospects. *Am J Physiol Lung Cell Mol Physiol* **302**, L977-991, doi:10.1152/ajplung.00362.2011 (2012).

246 Ye, C. *et al.* Distribution, metabolism, and excretion of the anti-angiogenic compound

SU5416. *Toxicol In Vitro* **20**, 154-162, doi:10.1016/j.tiv.2005.06.047 (2006).

247 Wilson, D. W., Segall, H. J., Pan, L. C. & Dunston, S. K. Progressive inflammatory and structural changes in the pulmonary vasculature of monocrotaline-treated rats. *Microvasc Res* **38**, 57-80, doi:10.1016/0026-2862(89)90017-4 (1989).

248 Meyrick, B. O. & Reid, L. M. Crotalaria-induced pulmonary hypertension. Uptake of 3H-thymidine by the cells of the pulmonary circulation and alveolar walls. *Am J Pathol* **106**, 84-94 (1982).

249 Omura, J. *et al.* Identification of Long Noncoding RNA H19 as a New Biomarker and Therapeutic Target in Right Ventricular Failure in Pulmonary Arterial Hypertension. *Circulation* **142**, 1464-1484, doi:10.1161/CIRCULATIONAHA.120.047626 (2020).

250 Gomez-Arroyo, J. G. *et al.* The monocrotaline model of pulmonary hypertension in perspective. *American journal of physiology. Lung cellular and molecular physiology* **302**, L363-369, doi:10.1152/ajplung.00212.2011 (2012).

251 Sztuka, K. & Jasinska-Stroschein, M. Animal models of pulmonary arterial hypertension: A systematic review and meta-analysis of data from 6126 animals. *Pharmacol Res* **125**, 201-214, doi:10.1016/j.phrs.2017.08.003 (2017).

252 Rafikova, O. *et al.* Metabolic Changes Precede the Development of Pulmonary Hypertension in the Monocrotaline Exposed Rat Lung. *PLoS One* **11**, e0150480, doi:10.1371/journal.pone.0150480 (2016).

253 McMurtry, M. S. *et al.* Dichloroacetate prevents and reverses pulmonary hypertension by inducing pulmonary artery smooth muscle cell apoptosis. *Circ Res* **95**, 830-840, doi:10.1161/01.RES.0000145360.16770.9f (2004).

254 Morty, R. E. *et al.* Dysregulated bone morphogenetic protein signaling in monocrotaline-induced pulmonary arterial hypertension. *Arterioscler Thromb Vasc Biol* **27**, 1072-1078, doi:10.1161/ATVBAHA.107.141200 (2007).

255 Schermuly, R. T. *et al.* Reversal of experimental pulmonary hypertension by PDGF inhibition. *J Clin Invest* **115**, 2811-2821, doi:10.1172/JCI24838 (2005).

256 Yung, L. M. *et al.* A Selective Transforming Growth Factor-beta Ligand Trap Attenuates Pulmonary Hypertension. *Am J Respir Crit Care Med* **194**, 1140-1151, doi:10.1164/rccm.201510-1955OC (2016).

257 Vitry, G. *et al.* Oxidized DNA Precursors Cleanup by NUDT1 Contributes to Vascular Remodeling in Pulmonary Arterial Hypertension. *Am J Respir Crit Care Med* **203**, 614-627, doi:10.1164/rccm.202003-0627OC (2021).

258 Meloche, J. *et al.* Role for DNA damage signaling in pulmonary arterial hypertension. *Circulation* **129**, 786-797, doi:10.1161/CIRCULATIONAHA.113.006167 (2014).

259 Hong, J. *et al.* Single-Cell Study of Two Rat Models of Pulmonary Arterial Hypertension Reveals Connections to Human Pathobiology and Drug Repositioning. *Am J Respir Crit Care Med* **203**, 1006-1022, doi:10.1164/rccm.202006-2169OC (2021).

260 Morimatsu, Y. *et al.* Development and characterization of an animal model of severe pulmonary arterial hypertension. *J Vasc Res* **49**, 33-42, doi:10.1159/000329594 (2012).

261 White, R. J. *et al.* Plexiform-like lesions and increased tissue factor expression in a rat model of severe pulmonary arterial hypertension. *Am J Physiol Lung Cell Mol Physiol* **293**, L583-590, doi:10.1152/ajplung.00321.2006 (2007).

262 Okada, K. *et al.* Pulmonary hemodynamics modify the rat pulmonary artery response to injury. A neointimal model of pulmonary hypertension. *Am J Pathol* **151**, 1019-1025 (1997).

263 Nelson, D. R. *et al.* Comparison of cytochrome P450 (CYP) genes from the mouse and human genomes, including nomenclature recommendations for genes, pseudogenes and alternative-splice variants. *Pharmacogenetics* **14**, 1-18, doi:10.1097/00008571-200401000-00001 (2004).

264 Hasegawa, M. *et al.* Quantitative prediction of human pregnane X receptor and cytochrome P450 3A4 mediated drug-drug interaction in a novel multiple humanized mouse line. *Mol Pharmacol* **80**, 518-528, doi:10.1124/mol.111.071845 (2011).

265 Dumitrascu, R. *et al.* Characterization of a murine model of monocrotaline pyrrole-induced acute lung injury. *BMC Pulm Med* **8**, 25, doi:10.1186/1471-2466-8-25 (2008).

266 Aldred, M. A., Morrell, N. W. & Guignabert, C. New Mutations and Pathogenesis of Pulmonary Hypertension: Progress and Puzzles in Disease Pathogenesis. *Circ Res* **130**, 1365-1381, doi:10.1161/CIRCRESAHA.122.320084 (2022).

267 Beppu, H. *et al.* BMP type II receptor is required for gastrulation and early development of mouse embryos. *Developmental biology* **221**, 249-258, doi:10.1006/dbio.2000.9670 (2000).

268 Song, Y. *et al.* Increased susceptibility to pulmonary hypertension in heterozygous BMPR2-mutant mice. *Circulation* **112**, 553-562, doi:10.1161/CIRCULATIONAHA.104.492488 (2005).

269 Beppu, H. *et al.* BMPR-II heterozygous mice have mild pulmonary hypertension and an impaired pulmonary vascular remodeling response to prolonged hypoxia. *Am J Physiol Lung Cell Mol Physiol* **287**, L1241-1247, doi:10.1152/ajplung.00239.2004 (2004).

270 Frank, D. B. *et al.* Increased susceptibility to hypoxic pulmonary hypertension in Bmpr2 mutant mice is associated with endothelial dysfunction in the pulmonary vasculature. *American journal of physiology. Lung cellular and molecular physiology* **294**, L98-109, doi:10.1152/ajplung.00034.2007 (2008).

271 Long, L. *et al.* Serotonin increases susceptibility to pulmonary hypertension in BMPR2-deficient mice. *Circ Res* **98**, 818-827, doi:10.1161/01.RES.0000215809.47923.fd (2006).

272 Pickworth, J. *et al.* Differential IL-1 signaling induced by BMPR2 deficiency drives pulmonary vascular remodeling. *Pulm Circ* **7**, 768-776, doi:10.1177/2045893217729096 (2017).

273 Soon, E. *et al.* Bone morphogenetic protein receptor type II deficiency and increased inflammatory cytokine production. A gateway to pulmonary arterial hypertension. *American journal of respiratory and critical care medicine* **192**, 859-872, doi:10.1164/rccm.201408-1509OC (2015).

274 West, J. *et al.* Pulmonary hypertension in transgenic mice expressing a dominant-negative BMPRII gene in smooth muscle. *Circ Res* **94**, 1109-1114, doi:10.1161/01.RES.0000126047.82846.20 (2004).

275 West, J. *et al.* Mice expressing BMPR2R899X transgene in smooth muscle develop

pulmonary vascular lesions. *Am J Physiol Lung Cell Mol Physiol* **295**, L744-755, doi:10.1152/ajplung.90255.2008 (2008).

276 Hong, K. H. *et al.* Genetic ablation of the BMPR2 gene in pulmonary endothelium is sufficient to predispose to pulmonary arterial hypertension. *Circulation* **118**, 722-730, doi:10.1161/CIRCULATIONAHA.107.736801 (2008).

277 Hautefort, A. *et al.* Bmpr2 Mutant Rats Develop Pulmonary and Cardiac Characteristics of Pulmonary Arterial Hypertension. *Circulation* **139**, 932-948, doi:10.1161/CIRCULATIONAHA.118.033744 (2019).

278 Tian, W. *et al.* Phenotypically Silent Bone Morphogenetic Protein Receptor 2 Mutations Predispose Rats to Inflammation-Induced Pulmonary Arterial Hypertension by Enhancing the Risk for Neointimal Transformation. *Circulation* **140**, 1409-1425, doi:10.1161/CIRCULATIONAHA.119.040629 (2019).

279 Jerkic, M. *et al.* Pulmonary hypertension in adult Alk1 heterozygous mice due to oxidative stress. *Cardiovasc Res* **92**, 375-384, doi:10.1093/cvr/cvr232 (2011).

280 Toporsian, M. *et al.* Spontaneous adult-onset pulmonary arterial hypertension attributable to increased endothelial oxidative stress in a murine model of hereditary hemorrhagic telangiectasia. *Arterioscler Thromb Vasc Biol* **30**, 509-517, doi:10.1161/ATVBAHA.109.200121 (2010).

281 Zhao, Y. Y. *et al.* Defects in caveolin-1 cause dilated cardiomyopathy and pulmonary hypertension in knockout mice. *Proceedings of the National Academy of Sciences of the United States of America* **99**, 11375-11380, doi:10.1073/pnas.172360799 (2002).

282 Lambert, M. *et al.* Characterization of Kcnk3-Mutated Rat, a Novel Model of Pulmonary Hypertension. *Circ Res* **125**, 678-695, doi:10.1161/CIRCRESAHA.119.314793 (2019).

283 Steiner, M. K. *et al.* Interleukin-6 overexpression induces pulmonary hypertension. *Circ Res* **104**, 236-244, 228p following 244, doi:10.1161/CIRCRESAHA.108.182014 (2009).

284 Patel, M. *et al.* Modulation of Intersectin-1s Lung Expression Induces Obliterative Remodeling and Severe Plexiform Arteriopathy in the Murine Pulmonary Vascular Bed. *Am J Pathol* **187**, 528-542, doi:10.1016/j.ajpath.2016.11.012 (2017).

285 Humbert, M. & Ghofrani, H. A. The molecular targets of approved treatments for pulmonary arterial hypertension. *Thorax* **71**, 73-83, doi:10.1136/thoraxjnl-2015-207170 (2016).

286 Chen, C. N., Watson, G. & Zhao, L. Cyclic guanosine monophosphate signalling pathway in pulmonary arterial hypertension. *Vascul Pharmacol* **58**, 211-218, doi:10.1016/j.vph.2012.09.001 (2013).

287 Sassi, Y. & Hulot, J. S. Pulmonary hypertension: novel pathways and emerging therapies inhibitors of cGMP and cAMP metabolism. *Handb Exp Pharmacol* **218**, 513-529, doi:10.1007/978-3-642-38664-0_20 (2013).

288 Sayner, S. L. Emerging themes of cAMP regulation of the pulmonary endothelial barrier. *American journal of physiology. Lung cellular and molecular physiology* **300**, L667-678, doi:10.1152/ajplung.00433.2010 (2011).

289 MacLean, M. R. *et al.* 5-Hydroxytryptamine receptors mediating vasoconstriction in

pulmonary arteries from control and pulmonary hypertensive rats. *Br J Pharmacol* **119**, 917-930, doi:10.1111/j.1476-5381.1996.tb15760.x (1996).

290 Baliga, R. S. *et al.* Synergy between natriuretic peptides and phosphodiesterase 5 inhibitors ameliorates pulmonary arterial hypertension. *American journal of respiratory and critical care medicine* **178**, 861-869, doi:10.1164/rccm.200801-121OC (2008).

291 O'Connell, C. *et al.* Comparative Safety and Tolerability of Prostacyclins in Pulmonary Hypertension. *Drug Saf* **39**, 287-294, doi:10.1007/s40264-015-0365-x (2016).

292 Murray, F., Maclean, M. R. & Insel, P. A. Role of phosphodiesterases in adult-onset pulmonary arterial hypertension. *Handb Exp Pharmacol*, 279-305, doi:10.1007/978-3-642-17969-3_12 (2011).

293 Wharton, J. *et al.* Antiproliferative effects of phosphodiesterase type 5 inhibition in human pulmonary artery cells. *Am J Respir Crit Care Med* **172**, 105-113, doi:10.1164/rccm.200411-1587OC (2005).

294 Izikki, M. *et al.* Effects of roflumilast, a phosphodiesterase-4 inhibitor, on hypoxia- and monocrotaline-induced pulmonary hypertension in rats. *J Pharmacol Exp Ther* **330**, 54-62, doi:10.1124/jpet.108.148742 (2009).

295 Schermuly, R. T. *et al.* Chronic sildenafil treatment inhibits monocrotaline-induced pulmonary hypertension in rats. *Am J Respir Crit Care Med* **169**, 39-45, doi:10.1164/rccm.200302-282OC (2004).

296 Zhao, L. *et al.* Sildenafil inhibits hypoxia-induced pulmonary hypertension. *Circulation* **104**, 424-428, doi:10.1161/hc2901.093117 (2001).

297 Zhao, L., Mason, N. A., Strange, J. W., Walker, H. & Wilkins, M. R. Beneficial Effects of Phosphodiesterase 5 Inhibition in Pulmonary Hypertension Are Influenced by Natriuretic Peptide Activity. *Circulation* **107**, 234-237, doi:10.1161/01.Cir.0000050653.10758.6b (2003).

298 Murray, F., MacLean, M. R. & Pyne, N. J. An assessment of the role of the inhibitory gamma subunit of the retinal cyclic GMP phosphodiesterase and its effect on the p42/p44 mitogen-activated protein kinase pathway in animal and cellular models of pulmonary hypertension. *Br J Pharmacol* **138**, 1313-1319, doi:10.1038/sj.bjp.0705190 (2003).

299 Bender, A. T. & Beavo, J. A. Cyclic nucleotide phosphodiesterases: molecular regulation to clinical use. *Pharmacol Rev* **58**, 488-520, doi:10.1124/pr.58.3.5 (2006).

300 M. R. Maclean, E. D. J., K. M. Mcculluch, L. Pooley, M. D. Houslay, G. Sweeney. Phosphodiesterase Isoforms in the Pulmonary Arterial Circulation of the Rat: Changes in Pulmonary Hypertension. *The Journal of Pharmacology and experimental therapeutics* **283**, 619-624 (1997).

301 Evgenov, O. V. *et al.* Inhibition of phosphodiesterase 1 augments the pulmonary vasodilator response to inhaled nitric oxide in awake lambs with acute pulmonary hypertension. *Am J Physiol Lung Cell Mol Physiol* **290**, L723-L729, doi:10.1152/ajplung.00485.2004 (2006).

302 Ahn, H. S., Crim, W., Romano, M., Sybertz, E. & Pitts, B. Effects of selective inhibitors on cyclic nucleotide phosphodiesterases of rabbit aorta. *Biochem Pharmacol* **38**, 3331-

3339, doi:10.1016/0006-2952(89)90631-x (1989).

303 Wells, J. N. & Miller, J. R. Methylxanthine inhibitors of phosphodiesterases. *Methods Enzymol* **159**, 489-496, doi:10.1016/0076-6879(88)59048-1 (1988).

304 Bonoczk, P. *et al.* Role of sodium channel inhibition in neuroprotection: effect of vinpocetine. *Brain Res Bull* **53**, 245-254, doi:10.1016/s0361-9230(00)00354-3 (2000).

305 Jeon, K. I. *et al.* Vinpocetine inhibits NF-kappaB-dependent inflammation via an IKK-dependent but PDE-independent mechanism. *Proceedings of the National Academy of Sciences of the United States of America* **107**, 9795-9800, doi:10.1073/pnas.0914414107 (2010).

306 Nadur, N. F. *et al.* The long and winding road of designing phosphodiesterase inhibitors for the treatment of heart failure. *Eur J Med Chem* **212**, 113123, doi:10.1016/j.ejmech.2020.113123 (2020).

307 Wu, A. Y., Tang, X. B., Martinez, S. E., Ikeda, K. & Beavo, J. A. Molecular determinants for cyclic nucleotide binding to the regulatory domains of phosphodiesterase 2A. *J Biol Chem* **279**, 37928-37938, doi:10.1074/jbc.M404287200 (2004).

308 Boess, F. G. *et al.* Inhibition of phosphodiesterase 2 increases neuronal cGMP, synaptic plasticity and memory performance. *Neuropharmacology* **47**, 1081-1092, doi:10.1016/j.neuropharm.2004.07.040 (2004).

309 Degerman, E., Belfrage, P. & Manganiello, V. C. Structure, localization, and regulation of cGMP-inhibited phosphodiesterase (PDE3). *J Biol Chem* **272**, 6823-6826, doi:10.1074/jbc.272.11.6823 (1997).

310 Wagner, R. S., Smith, C. J., Taylor, A. M. & Rhoades, R. A. Phosphodiesterase inhibition improves agonist-induced relaxation of hypertensive pulmonary arteries. *J Pharmacol Exp Ther* **282**, 1650-1657 (1997).

311 Ito, T. *et al.* Model difference in the effect of cilostazol on the development of experimental pulmonary hypertension in rats. *BMC Pulm Med* **21**, 377, doi:10.1186/s12890-021-01710-4 (2021).

312 Chang, L. T. *et al.* Cilostazol therapy attenuates monocrotaline-induced pulmonary arterial hypertension in rat model. *Circ J* **72**, 825-831, doi:10.1253/circj.72.825 (2008).

313 Schermuly, R. T. *et al.* Low-dose systemic phosphodiesterase inhibitors amplify the pulmonary vasodilatory response to inhaled prostacyclin in experimental pulmonary hypertension. *Am J Respir Crit Care Med* **160**, 1500-1506, doi:10.1164/ajrccm.160.5.9901102 (1999).

314 Clarke, W. R., Uezono, S., Chambers, A. & Doepfner, P. The type III phosphodiesterase inhibitor milrinone and type V PDE inhibitor dipyridamole individually and synergistically reduce elevated pulmonary vascular resistance. *Pulm Pharmacol* **7**, 81-89, doi:10.1006/pulp.1994.1009 (1994).

315 Matot, I. & Gozal, Y. Pulmonary responses to selective phosphodiesterase-5 and phosphodiesterase-3 inhibitors. *Chest* **125**, 644-651, doi:10.1378/chest.125.2.644 (2004).

316 Packer, M. *et al.* Effect of oral milrinone on mortality in severe chronic heart failure. The PROMISE Study Research Group. *N Engl J Med* **325**, 1468-1475,

doi:10.1056/NEJM199111213252103 (1991).

317 Mathew, R. *et al.* Milrinone as Compared with Dobutamine in the Treatment of Cardiogenic Shock. *N Engl J Med* **385**, 516-525, doi:10.1056/NEJMoa2026845 (2021).

318 Chi, Y. W., Lavie, C. J., Milani, R. V. & White, C. J. Safety and efficacy of cilostazol in the management of intermittent claudication. *Vasc Health Risk Manag* **4**, 1197-1203, doi:10.2147/vhrm.s3160 (2008).

319 Fertig, B. A. & Baillie, G. S. PDE4-Mediated cAMP Signalling. *J Cardiovasc Dev Dis* **5**, doi:10.3390/jcdd5010008 (2018).

320 Beard, M. B. *et al.* UCR1 and UCR2 domains unique to the cAMP-specific phosphodiesterase family form a discrete module via electrostatic interactions. *J Biol Chem* **275**, 10349-10358, doi:10.1074/jbc.275.14.10349 (2000).

321 Baillie, G. S., MacKenzie, S. J., McPhee, I. & Houslay, M. D. Sub-family selective actions in the ability of Erk2 MAP kinase to phosphorylate and regulate the activity of PDE4 cyclic AMP-specific phosphodiesterases. *Br J Pharmacol* **131**, 811-819, doi:10.1038/sj.bjp.0703636 (2000).

322 Richter, W. & Conti, M. The oligomerization state determines regulatory properties and inhibitor sensitivity of type 4 cAMP-specific phosphodiesterases. *J Biol Chem* **279**, 30338-30348, doi:10.1074/jbc.M312687200 (2004).

323 Rich, T. C., Tse, T. E., Rohan, J. G., Schaack, J. & Karpen, J. W. In vivo assessment of local phosphodiesterase activity using tailored cyclic nucleotide-gated channels as cAMP sensors. *J Gen Physiol* **118**, 63-78, doi:10.1085/jgp.118.1.63 (2001).

324 Schermuly, R. T. *et al.* Antiremodeling effects of iloprost and the dual-selective phosphodiesterase 3/4 inhibitor tolafentrine in chronic experimental pulmonary hypertension. *Circ Res* **94**, 1101-1108, doi:10.1161/01.RES.0000126050.41296.8E (2004).

325 Corbin, J. D., Turko, I. V., Beasley, A. & Francis, S. H. Phosphorylation of phosphodiesterase-5 by cyclic nucleotide-dependent protein kinase alters its catalytic and allosteric cGMP-binding activities. *Eur J Biochem* **267**, 2760-2767, doi:10.1046/j.1432-1327.2000.01297.x (2000).

326 Francis, S. H. *et al.* Phosphorylation of isolated human phosphodiesterase-5 regulatory domain induces an apparent conformational change and increases cGMP binding affinity. *J Biol Chem* **277**, 47581-47587, doi:10.1074/jbc.M206088200 (2002).

327 Zoraghi, R., Bessay, E. P., Corbin, J. D. & Francis, S. H. Structural and functional features in human PDE5A1 regulatory domain that provide for allosteric cGMP binding, dimerization, and regulation. *J Biol Chem* **280**, 12051-12063, doi:10.1074/jbc.M413611200 (2005).

328 Corbin, J. D., Beasley, A., Blount, M. A. & Francis, S. H. High lung PDE5: a strong basis for treating pulmonary hypertension with PDE5 inhibitors. *Biochem Biophys Res Commun* **334**, 930-938, doi:10.1016/j.bbrc.2005.06.183 (2005).

329 Pauvert, O. *et al.* Effect of sildenafil on cyclic nucleotide phosphodiesterase activity, vascular tone and calcium signaling in rat pulmonary artery. *Br J Pharmacol* **139**, 513-522, doi:10.1038/sj.bjp.0705277 (2003).

330 Mauricio, M. D. *et al.* Relaxation and cyclic GMP levels in response to sildenafil in

human pulmonary arteries from donors. *Eur J Pharmacol* **530**, 259-262, doi:10.1016/j.ejphar.2005.11.042 (2006).

331 Alan H. Cohen, K. H., Ken Morris, Brian Fouty, Ivan F. McMurtry, William Clarke, David M. Rodman. Inhibition of Cyclic 3 -5 -Guanosine Monophosphate-specific Phosphodiesterase Selectively Vasodilates the Pulmonary Circulation in Chronically Hypoxic Rats. *American Journal of Respiritory Critical Care Medicine* **97**, 172-179 (1995).

332 Kang, K. K., Ahn, G. J., Sohn, Y. S., Ahn, B. O. & Kim, W. B. DA-8159, a new PDE5 inhibitor, attenuates the development of compensatory right ventricular hypertrophy in a rat model of pulmonary hypertension. *J Int Med Res* **31**, 517-528, doi:10.1177/147323000303100608 (2003).

333 Liu, H., Liu, Z. Y. & Guan, Q. Oral sildenafil prevents and reverses the development of pulmonary hypertension in monocrotaline-treated rats. *Interact Cardiovasc Thorac Surg* **6**, 608-613, doi:10.1510/icvts.2006.147033 (2007).

334 Sauzeau, V., Rolli-Derkinderen, M., Lehoux, S., Loirand, G. & Pacaud, P. Sildenafil prevents change in RhoA expression induced by chronic hypoxia in rat pulmonary artery. *Circ Res* **93**, 630-637, doi:10.1161/01.RES.0000093220.90027.D9 (2003).

335 Nagendran, J. *et al.* Phosphodiesterase type 5 is highly expressed in the hypertrophied human right ventricle, and acute inhibition of phosphodiesterase type 5 improves contractility. *Circulation* **116**, 238-248, doi:10.1161/CIRCULATIONAHA.106.655266 (2007).

336 Michelakis, E. D. *et al.* Long-term treatment with oral sildenafil is safe and improves functional capacity and hemodynamics in patients with pulmonary arterial hypertension. *Circulation* **108**, 2066-2069, doi:10.1161/01.CIR.0000099502.17776.C2 (2003).

337 Galie, N. *et al.* Sildenafil citrate therapy for pulmonary arterial hypertension. *The New England journal of medicine* **353**, 2148-2157, doi:10.1056/NEJMoa050010 (2005).

338 Jing, Z. C. *et al.* Vardenafil in pulmonary arterial hypertension: a randomized, double-blind, placebo-controlled study. *Am J Respir Crit Care Med* **183**, 1723-1729, doi:10.1164/rccm.201101-0093OC (2011).

339 Bischoff, E. Potency, selectivity, and consequences of nonselectivity of PDE inhibition. *International journal of impotence research* **16 Suppl 1**, S11-14, doi:10.1038/sj.ijir.3901208 (2004).

340 Souza, R. & Kawut, S. M. What is new about Rio? *Eur Respir J* **45**, 1211-1213, doi:10.1183/09031936.00032715 (2015).

341 Lau, E. M., Tamura, Y., McGoon, M. D. & Sitbon, O. The 2015 ESC/ERS Guidelines for the diagnosis and treatment of pulmonary hypertension: a practical chronicle of progress. *Eur Respir J* **46**, 879-882, doi:10.1183/13993003.01177-2015 (2015).

342 Jager, R. *et al.* Activation of PDE10 and PDE11 phosphodiesterases. *J Biol Chem* **287**, 1210-1219, doi:10.1074/jbc.M111.263806 (2012).

343 Yang, Y. *et al.* Discovery of highly selective and orally available benzimidazole-based phosphodiesterase 10 inhibitors with improved solubility and pharmacokinetic properties for treatment of pulmonary arterial hypertension. *Acta Pharm Sin B* **10**,

2339-2347, doi:10.1016/j.apsb.2020.04.003 (2020).

344 Huang, Y. Y. *et al.* Validation of Phosphodiesterase-10 as a Novel Target for Pulmonary Arterial Hypertension via Highly Selective and Subnanomolar Inhibitors. *J Med Chem* **62**, 3707-3721, doi:10.1021/acs.jmedchem.9b00224 (2019).

345 Chen, S. *et al.* A Novel Role of Cyclic Nucleotide Phosphodiesterase 10A in Pathological Cardiac Remodeling and Dysfunction. *Circulation* **141**, 217-233, doi:10.1161/CIRCULATIONAHA.119.042178 (2020).

346 Schmidt, C. J. *et al.* Preclinical characterization of selective phosphodiesterase 10A inhibitors: a new therapeutic approach to the treatment of schizophrenia. *J Pharmacol Exp Ther* **325**, 681-690, doi:10.1124/jpet.107.132910 (2008).

347 Tate, R. J., Arshavsky, V. Y. & Pyne, N. J. The identification of the inhibitory gamma-subunits of the type 6 retinal cyclic guanosine monophosphate phosphodiesterase in non-retinal tissues: differential processing of mRNA transcripts. *Genomics* **79**, 582-586, doi:10.1006/geno.2002.6740 (2002).

348 Tate, R. J., Lochhead, A., Brzeski, H., Arshavsky, V. & Pyne, N. J. The gamma-subunit of the rod photoreceptor cGMP-binding cGMP-specific PDE is expressed in mouse lung. *Cell Biochem Biophys* **29**, 133-144, doi:10.1007/BF02737832 (1998).

349 Wan, K. F., Sambi, B. S., Frame, M., Tate, R. & Pyne, N. J. The inhibitory gamma subunit of the type 6 retinal cyclic guanosine monophosphate phosphodiesterase is a novel intermediate regulating p42/p44 mitogen-activated protein kinase signaling in human embryonic kidney 293 cells. *J Biol Chem* **276**, 37802-37808, doi:10.1074/jbc.M105087200 (2001).

350 Scott H. Soderling, S. J. B., Joseph A. Beavo. Identification and Characterization of a Novel Family of Cyclic Nucleotide Phosphodiesterases. *The Journal of Biological Chemistry* **273**, 15553-15558 (1998).

351 Michel Guipponi, H. S. S., Jun Kudoh, Kazuhiko Kawasaki, Kazunori Shibuya, Ai Shintani, Shuichi Asakawa, Haiming Chen, Maria D. Lalioti, Colette Rossier, Shinsei Minoshima, & Nobuyoshi Shimizu, S. E. A. Identification and characterization of a novel cyclic nucleotide phosphodiesterase gene (PDE9A) that maps to 21q22.3: alternative splicing of mRNA transcripts, genomic structure and sequence. *Hum Genet* **103**, 386-392 (1998).

352 Douglas A. Fisher, J. F. S., Joann S. Pillar, Suzanne H. St. Denis, John B. Cheng. Isolation and Characterization of PDE9A, a Novel Human cGMP-specific Phosphodiesterase. *The Journal of Biological Chemistry* **273**, 15559-15564 (1998).

353 Patel, N. S. *et al.* Identification of new PDE9A isoforms and how their expression and subcellular compartmentalization in the brain change across the life span. *Neurobiol Aging* **65**, 217-234, doi:10.1016/j.neurobiolaging.2018.01.019 (2018).

354 Rentero, C., Monfort, A. & Puigdomenech, P. Identification and distribution of different mRNA variants produced by differential splicing in the human phosphodiesterase 9A gene. *Biochem Biophys Res Commun* **301**, 686-692, doi:10.1016/s0006-291x(03)00021-4 (2003).

355 Lee, D. I. *et al.* Phosphodiesterase 9A controls nitric-oxide-independent cGMP and hypertrophic heart disease. *Nature* **519**, 472-476, doi:10.1038/nature14332 (2015).

356 van der Horst, I. W. *et al.* Expression and function of phosphodiesterases in nitrofen-induced congenital diaphragmatic hernia in rats. *Pediatr Pulmonol* **45**, 320-325, doi:10.1002/ppul.21181 (2010).

357 Almeida, C. B. *et al.* Hydroxyurea and a cGMP-amplifying agent have immediate benefits on acute vaso-occlusive events in sickle cell disease mice. *Blood* **120**, 2879-2888, doi:10.1182/blood-2012-02-409524 (2012).

358 Heckman, P. R., Wouters, C. & Prickaerts, J. Phosphodiesterase inhibitors as a target for cognition enhancement in aging and Alzheimer's disease: a translational overview. *Curr Pharm Des* **21**, 317-331, doi:10.2174/1381612820666140826114601 (2015).

359 Kleiman, R. J. *et al.* Phosphodiesterase 9A regulates central cGMP and modulates responses to cholinergic and monoaminergic perturbation in vivo. *The Journal of pharmacology and experimental therapeutics* **341**, 396-409, doi:10.1124/jpet.111.191353 (2012).

360 Hutson, P. H. *et al.* The selective phosphodiesterase 9 (PDE9) inhibitor PF-04447943 (6-[(3S,4S)-4-methyl-1-(pyrimidin-2-ylmethyl)pyrrolidin-3-yl]-1-(tetrahydro-2H-py ran-4-yl)-1,5-dihydro-4H-pyrazolo[3,4-d]pyrimidin-4-one) enhances synaptic plasticity and cognitive function in rodents. *Neuropharmacology* **61**, 665-676, doi:10.1016/j.neuropharm.2011.05.009 (2011).

361 Wunder, F. *et al.* Characterization of the first potent and selective PDE9 inhibitor using a cGMP reporter cell line. *Mol Pharmacol* **68**, 1775-1781, doi:10.1124/mol.105.017608 (2005).

362 Richards, D. A. *et al.* CRD-733, a Novel PDE9 (Phosphodiesterase 9) Inhibitor, Reverses Pressure Overload-Induced Heart Failure. *Circ Heart Fail* **14**, e007300, doi:10.1161/CIRCHEARTFAILURE.120.007300 (2021).

363 Scott, N. J. A., Rademaker, M. T., Charles, C. J., Espiner, E. A. & Richards, A. M. Hemodynamic, Hormonal, and Renal Actions of Phosphodiesterase-9 Inhibition in Experimental Heart Failure. *J Am Coll Cardiol* **74**, 889-901, doi:10.1016/j.jacc.2019.05.067 (2019).

364 Almeida, C. B. *et al.* High expression of the cGMP-specific phosphodiesterase, PDE9A, in sickle cell disease (SCD) and the effects of its inhibition in erythroid cells and SCD neutrophils. *Br J Haematol* **142**, 836-844, doi:10.1111/j.1365-2141.2008.07264.x (2008).

365 Charnigo, R. J. *et al.* PF-04447943, a Phosphodiesterase 9A Inhibitor, in Stable Sickle Cell Disease Patients: A Phase Ib Randomized, Placebo-Controlled Study. *Clin Transl Sci* **12**, 180-188, doi:10.1111/cts.12604 (2019).

366 Mishra, S. *et al.* Inhibition of phosphodiesterase type 9 reduces obesity and cardiometabolic syndrome in mice. *J Clin Invest*, doi:10.1172/JCI148798 (2021).

367 Kolb, T. M., Johnston, L., Damarla, M., Kass, D. A. & Hassoun, P. M. PDE9A deficiency does not prevent chronic-hypoxic pulmonary hypertension in mice. *Physiol Rep* **9**, e15057, doi:10.14814/phy2.15057 (2021).

368 Kroker, K. S. *et al.* PDE9A inhibition rescues amyloid beta-induced deficits in synaptic plasticity and cognition. *Neurobiol Aging* **35**, 2072-2078, doi:10.1016/j.neurobiolaging.2014.03.023 (2014).

369 Claffey, M. M. *et al.* Application of structure-based drug design and parallel chemistry to identify selective, brain penetrant, in vivo active phosphodiesterase 9A inhibitors. *J Med Chem* **55**, 9055-9068, doi:10.1021/jm3009635 (2012).

370 Moschetti, V. *et al.* First-in-human study assessing safety, tolerability and pharmacokinetics of BI 409306, a selective phosphodiesterase 9A inhibitor, in healthy males. *Br J Clin Pharmacol* **82**, 1315-1324, doi:10.1111/bcp.13060 (2016).

371 Rosenbrock, H. *et al.* The Novel Phosphodiesterase 9A Inhibitor BI 409306 Increases Cyclic Guanosine Monophosphate Levels in the Brain, Promotes Synaptic Plasticity, and Enhances Memory Function in Rodents. *J Pharmacol Exp Ther* **371**, 633-641, doi:10.1124/jpet.119.260059 (2019).

372 Schwinger, R. H. G. Pathophysiology of heart failure. *Cardiovasc Diagn Ther* **11**, 263-276, doi:10.21037/cdt-20-302 (2021).

373 McDonagh, T. A. *et al.* 2021 ESC Guidelines for the diagnosis and treatment of acute and chronic heart failure. *Eur Heart J* **42**, 3599-3726, doi:10.1093/eurheartj/ehab368 (2021).

374 Ponikowski, P. *et al.* 2016 ESC Guidelines for the diagnosis and treatment of acute and chronic heart failure: The Task Force for the diagnosis and treatment of acute and chronic heart failure of the European Society of Cardiology (ESC)Developed with the special contribution of the Heart Failure Association (HFA) of the ESC. *Eur Heart J* **37**, 2129-2200, doi:10.1093/eurheartj/ehw128 (2016).

375 Borlaug, B. A. The pathophysiology of heart failure with preserved ejection fraction. *Nat Rev Cardiol* **11**, 507-515, doi:10.1038/nrcardio.2014.83 (2014).

376 Henkel, D. M., Redfield, M. M., Weston, S. A., Gerber, Y. & Roger, V. L. Death in heart failure: a community perspective. *Circ Heart Fail* **1**, 91-97, doi:10.1161/CIRCHEARTFAILURE.107.743146 (2008).

377 Ather, S. *et al.* Impact of noncardiac comorbidities on morbidity and mortality in a predominantly male population with heart failure and preserved versus reduced ejection fraction. *J Am Coll Cardiol* **59**, 998-1005, doi:10.1016/j.jacc.2011.11.040 (2012).

378 Hartupee, J. & Mann, D. L. Neurohormonal activation in heart failure with reduced ejection fraction. *Nature reviews. Cardiology* **14**, 30-38, doi:10.1038/nrcardio.2016.163 (2017).

379 Jacob, R., Dierberger, B. & Kissling, G. Functional significance of the Frank-Starling mechanism under physiological and pathophysiological conditions. *Eur Heart J* **13 Suppl E**, 7-14, doi:10.1093/eurheartj/13.suppl_e.7 (1992).

380 van Berlo, J. H., Maillet, M. & Molkentin, J. D. Signaling effectors underlying pathologic growth and remodeling of the heart. *The Journal of clinical investigation* **123**, 37-45, doi:10.1172/JCI62839 (2013).

381 Strulovici, B., Cerione, R. A., Kilpatrick, B. F., Caron, M. G. & Lefkowitz, R. J. Direct demonstration of impaired functionality of a purified desensitized beta-adrenergic receptor in a reconstituted system. *Science* **225**, 837-840, doi:10.1126/science.6089331 (1984).

382 Neef, S. & Maier, L. S. Novel aspects of excitation-contraction coupling in heart failure.

Basic Res Cardiol **108**, 360, doi:10.1007/s00395-013-0360-2 (2013).

383 Azevedo, P. S., Minicucci, M. F., Santos, P. P., Paiva, S. A. & Zornoff, L. A. Energy metabolism in cardiac remodeling and heart failure. *Cardiol Rev* **21**, 135-140, doi:10.1097/CRD.0b013e318274956d (2013).

384 Kostin, S., Hein, S., Arnon, E., Scholz, D. & Schaper, J. The cytoskeleton and related proteins in the human failing heart. *Heart Fail Rev* **5**, 271-280, doi:10.1023/A:1009813621103 (2000).

385 Schaper, J., Elsasser, A. & Kostin, S. The role of cell death in heart failure. *Circ Res* **85**, 867-869, doi:10.1161/01.res.85.9.867 (1999).

386 McMurray, J. J. V. *et al.* Dapagliflozin in Patients with Heart Failure and Reduced Ejection Fraction. *N Engl J Med* **381**, 1995-2008, doi:10.1056/NEJMoa1911303 (2019).

387 Packer, M. *et al.* Cardiovascular and Renal Outcomes with Empagliflozin in Heart Failure. *N Engl J Med* **383**, 1413-1424, doi:10.1056/NEJMoa2022190 (2020).

388 Armstrong, P. W. *et al.* Vericiguat in Patients with Heart Failure and Reduced Ejection Fraction. *N Engl J Med* **382**, 1883-1893, doi:10.1056/NEJMoa1915928 (2020).

389 Ziaeian, B. & Fonarow, G. C. Epidemiology and aetiology of heart failure. *Nat Rev Cardiol* **13**, 368-378, doi:10.1038/nrcardio.2016.25 (2016).

390 Maggioni, A. P. *et al.* EURObservational Research Programme: regional differences and 1-year follow-up results of the Heart Failure Pilot Survey (ESC-HF Pilot). *Eur J Heart Fail* **15**, 808-817, doi:10.1093/eurjhf/hft050 (2013).

391 Zarrinkoub, R. *et al.* The epidemiology of heart failure, based on data for 2.1 million inhabitants in Sweden. *Eur J Heart Fail* **15**, 995-1002, doi:10.1093/eurjhf/hft064 (2013).

392 Volpe, M., Carnovali, M. & Mastromarino, V. The natriuretic peptides system in the pathophysiology of heart failure: from molecular basis to treatment. *Clin Sci (Lond)* **130**, 57-77, doi:10.1042/CS20150469 (2016).

393 The Cardiac Insufficiency Bisoprolol Study II (CIBIS-II): a randomised trial. *Lancet* **353**, 9-13 (1999).

394 Hjalmarson, A. *et al.* Effects of controlled-release metoprolol on total mortality, hospitalizations, and well-being in patients with heart failure: the Metoprolol CR/XL Randomized Intervention Trial in congestive heart failure (MERIT-HF). MERIT-HF Study Group. *JAMA* **283**, 1295-1302, doi:10.1001/jama.283.10.1295 (2000).

395 Packer, M. *et al.* The effect of carvedilol on morbidity and mortality in patients with chronic heart failure. U.S. Carvedilol Heart Failure Study Group. *N Engl J Med* **334**, 1349-1355, doi:10.1056/NEJM199605233342101 (1996).

396 Calderone, A., Thaik, C. M., Takahashi, N., Chang, D. L. & Colucci, W. S. Nitric oxide, atrial natriuretic peptide, and cyclic GMP inhibit the growth-promoting effects of norepinephrine in cardiac myocytes and fibroblasts. *J Clin Invest* **101**, 812-818, doi:10.1172/JCI119883 (1998).

397 Chabrier, P. E., Roubert, P., Lonchampt, M. O., Plas, P. & Braquet, P. Regulation of atrial natriuretic factor receptors by angiotensin II in rat vascular smooth muscle cells. *J Biol Chem* **263**, 13199-13202 (1988).

398 Gopi, V., Parthasarathy, A., Umadevi, S. & Vellaichamy, E. Angiotensin-II down-regulates cardiac natriuretic peptide receptor-A mediated anti-hypertrophic signaling in experimental rat hearts. *Indian J Exp Biol* **51**, 48-55 (2013).

399 Hirooka, Y. *et al.* Attenuated forearm vasodilative response to intra-arterial atrial natriuretic peptide in patients with heart failure. *Circulation* **82**, 147-153, doi:10.1161/01.cir.82.1.147 (1990).

400 Fischer, D. *et al.* Endothelial dysfunction in patients with chronic heart failure is independently associated with increased incidence of hospitalization, cardiac transplantation, or death. *Eur Heart J* **26**, 65-69, doi:10.1093/eurheartj/ehi001 (2005).

401 Sarah Karam, J. P. M., Aurélia Bourcier, Delphine Mika, Audrey Varin, Ibrahim Bedioune, Marta Lindner, Kaouter Bouadjel, Matthieu Dessillons, Françoise Gaudin, Florence Lefebvre, Philippe Mateo, Patrick Lechène, Susana Gomez, Valérie Domergue, Pauline Robert, Charlène Coquard, Vincent Algalarrondo, Jane-Lise Samuel, Jean-Baptiste Michel, Flavien Charpentier, Alessandra Ghigo, Emilio Hirsch, Rodolphe Fischmeister, Jérôme Leroy, Grégoire Vandecasteele. Cardiac overexpression of PDE4B blunts β-adrenergic response and maladaptive remodeling in heart failure. *Circulation* **142(2)**, 161-174, doi:10.1161/CIRCULATIONAHA.119.042573 (2020).

402 Burke, R. M., Lighthouse, J. K., Mickelsen, D. M. & Small, E. M. Sacubitril/Valsartan Decreases Cardiac Fibrosis in Left Ventricle Pressure Overload by Restoring PKG Signaling in Cardiac Fibroblasts. *Circ Heart Fail* **12**, e005565, doi:10.1161/CIRCHEARTFAILURE.118.005565 (2019).

403 von Lueder, T. G. *et al.* Angiotensin receptor neprilysin inhibitor LCZ696 attenuates cardiac remodeling and dysfunction after myocardial infarction by reducing cardiac fibrosis and hypertrophy. *Circ Heart Fail* **8**, 71-78, doi:10.1161/CIRCHEARTFAILURE.114.001785 (2015).

404 Takimoto, E. *et al.* Chronic inhibition of cyclic GMP phosphodiesterase 5A prevents and reverses cardiac hypertrophy. *Nat Med* **11**, 214-222, doi:10.1038/nm1175 (2005).

405 Baliga, R. S. *et al.* Phosphodiesterase 2 inhibition preferentially promotes NO/guanylyl cyclase/cGMP signaling to reverse the development of heart failure. *Proceedings of the National Academy of Sciences of the United States of America* **115**, E7428-E7437, doi:10.1073/pnas.1800996115 (2018).

406 Wu, M. P. *et al.* Vinpocetine Attenuates Pathological Cardiac Remodeling by Inhibiting Cardiac Hypertrophy and Fibrosis. *Cardiovasc Drugs Ther* **31**, 157-166, doi:10.1007/s10557-017-6719-0 (2017).

407 Redfield, M. M. *et al.* Effect of phosphodiesterase-5 inhibition on exercise capacity and clinical status in heart failure with preserved ejection fraction: a randomized clinical trial. *JAMA* **309**, 1268-1277, doi:10.1001/jama.2013.2024 (2013).

408 Francis, G. S. & Cohn, J. N. Heart failure: mechanisms of cardiac and vascular dysfunction and the rationale for pharmacologic intervention. *FASEB J* **4**, 3068-3075, doi:10.1096/fasebj.4.13.2210153 (1990).

409 Negrao, C. E. *et al.* Impaired endothelium-mediated vasodilation is not the principal cause of vasoconstriction in heart failure. *American journal of physiology. Heart and*

circulatory physiology **278**, H168-174 (2000).

410 Zuchi, C. *et al.* Role of endothelial dysfunction in heart failure. *Heart Fail Rev* **25**, 21-30, doi:10.1007/s10741-019-09881-3 (2020).

411 Daiber, A. *et al.* Targeting vascular (endothelial) dysfunction. *Br J Pharmacol* **174**, 1591-1619, doi:10.1111/bph.13517 (2017).

412 Katz, S. D. *et al.* Vascular endothelial dysfunction and mortality risk in patients with chronic heart failure. *Circulation* **111**, 310-314, doi:10.1161/01.CIR.0000153349.77489.CF (2005).

413 Premer, C., Kanelidis, A. J., Hare, J. M. & Schulman, I. H. Rethinking Endothelial Dysfunction as a Crucial Target in Fighting Heart Failure. *Mayo Clin Proc Innov Qual Outcomes* **3**, 1-13, doi:10.1016/j.mayocpiqo.2018.12.006 (2019).

414 Richard, V., Vercauteren, M., Gomez, E. & Thuillez, C. [New pharmacological approaches in heart failure: should we treat the endothelium?]. *Therapie* **64**, 93-100, doi:10.2515/therapie/2009014 (2009).

415 Marti, C. N. *et al.* Endothelial dysfunction, arterial stiffness, and heart failure. *J Am Coll Cardiol* **60**, 1455-1469, doi:10.1016/j.jacc.2011.11.082 (2012).

416 Forstermann, U., Mugge, A., Alheid, U., Haverich, A. & Frolich, J. C. Selective attenuation of endothelium-mediated vasodilation in atherosclerotic human coronary arteries. *Circ Res* **62**, 185-190, doi:10.1161/01.res.62.2.185 (1988).

417 Treasure, C. B. *et al.* Endothelium-dependent dilation of the coronary microvasculature is impaired in dilated cardiomyopathy. *Circulation* **81**, 772-779, doi:10.1161/01.cir.81.3.772 (1990).

418 Drexler, H. *et al.* Endothelial function in chronic congestive heart failure. *Am J Cardiol* **69**, 1596-1601, doi:10.1016/0002-9149(92)90710-g (1992).

419 Katz, S. D. *et al.* Impaired endothelium-mediated vasodilation in the peripheral vasculature of patients with congestive heart failure. *Journal of the American College of Cardiology* **19**, 918-925 (1992).

420 Kubo, S. H., Rector, T. S., Bank, A. J., Williams, R. E. & Heifetz, S. M. Endothelium-dependent vasodilation is attenuated in patients with heart failure. *Circulation* **84**, 1589-1596 (1991).

421 Hirooka, Y. *et al.* Effects of L-arginine on impaired acetylcholine-induced and ischemic vasodilation of the forearm in patients with heart failure. *Circulation* **90**, 658-668 (1994).

422 Drexler, H. & Lu, W. Endothelial dysfunction of hindquarter resistance vessels in experimental heart failure. *Am J Physiol* **262**, H1640-1645, doi:10.1152/ajpheart.1992.262.6.H1640 (1992).

423 Bauersachs, J. & Widder, J. D. Endothelial dysfunction in heart failure. *Pharmacol Rep* **60**, 119-126 (2008).

424 McGoldrick, R. B., Kingsbury, M., Turner, M. A., Sheridan, D. J. & Hughes, A. D. Left ventricular hypertrophy induced by aortic banding impairs relaxation of isolated coronary arteries. *Clin Sci (Lond)* **113**, 473-478, doi:10.1042/CS20070136 (2007).

425 Baggia, S., Perkins, K. & Greenberg, B. Endothelium-dependent relaxation is not uniformly impaired in chronic heart failure. *J Cardiovasc Pharmacol* **29**, 389-396,

doi:10.1097/00005344-199703000-00013 (1997).

426 Mulder, P. *et al.* Peripheral artery structure and endothelial function in heart failure: effect of ACE inhibition. *Am J Physiol* **271**, H469-477, doi:10.1152/ajpheart.1996.271.2.H469 (1996).

427 Angus, J. A., Ferrier, C. P., Sudhir, K., Kaye, D. M. & Jennings, G. L. Impaired contraction and relaxation in skin resistance arteries from patients with congestive heart failure. *Cardiovascular research* **27**, 204-210 (1993).

428 Creager, M. A., Quigg, R. J., Ren, C. J., Roddy, M. A. & Colucci, W. S. Limb vascular responsiveness to beta-adrenergic receptor stimulation in patients with congestive heart failure. *Circulation* **83**, 1873-1879 (1991).

429 Katz, S. D., Schwarz, M., Yuen, J. & LeJemtel, T. H. Impaired acetylcholine-mediated vasodilation in patients with congestive heart failure. Role of endothelium-derived vasodilating and vasoconstricting factors. *Circulation* **88**, 55-61, doi:10.1161/01.cir.88.1.55 (1993).

430 Knecht, M. *et al.* Coronary endothelial dysfunction precedes heart failure and reduction of coronary reserve in awake dogs. *Journal of molecular and cellular cardiology* **29**, 217-227, doi:10.1006/jmcc.1996.0266 (1997).

431 Kiuchi, K. *et al.* Depressed beta-adrenergic receptor- and endothelium-mediated vasodilation in conscious dogs with heart failure. *Circ Res* **73**, 1013-1023, doi:10.1161/01.res.73.6.1013 (1993).

432 Gaballa, M. A., Eckhart, A., Koch, W. J. & Goldman, S. Vascular beta-adrenergic receptor system is dysfunctional after myocardial infarction. *Am J Physiol Heart Circ Physiol* **280**, H1129-1135, doi:10.1152/ajpheart.2001.280.3.H1129 (2001).

433 Nasa, Y. *et al.* Impairment of cGMP- and cAMP-mediated vasorelaxations in rats with chronic heart failure. *Am J Physiol* **271**, H2228-2237, doi:10.1152/ajpheart.1996.271.6.H2228 (1996).

434 Mathew, R., Wang, J., Gewitz, M. H., Hintze, T. H. & Wolin, M. S. Congestive heart failure alters receptor-dependent cAMP-mediated relaxation of canine pulmonary arteries. *Circulation* **87**, 1722-1728, doi:10.1161/01.cir.87.5.1722 (1993).

435 Inoue, T. *et al.* Vasodilatory capacity of coronary resistance vessels in dilated cardiomyopathy. *Am Heart J* **127**, 376-381, doi:10.1016/0002-8703(94)90127-9 (1994).

436 Gschwend, S. *et al.* Myogenic constriction is increased in mesenteric resistance arteries from rats with chronic heart failure: instantaneous counteraction by acute AT1 receptor blockade. *Br J Pharmacol* **139**, 1317-1325, doi:10.1038/sj.bjp.0705367 (2003).

437 Xu, Y. *et al.* Acetylcholine stimulated dilatation and stretch induced myogenic constriction in mesenteric artery of rats with chronic heart failure. *Eur J Heart Fail* **9**, 144-151, doi:10.1016/j.ejheart.2006.05.003 (2007).

438 Xu, Y. *et al.* Enhanced myogenic constriction of mesenteric artery in heart failure relates to decreased smooth muscle cell caveolae numbers and altered AT1- and epidermal growth factor-receptor function. *Eur J Heart Fail* **11**, 246-255, doi:10.1093/eurjhf/hfn027 (2009).

439 Blanco-Rivero, J., Couto, G. K., Paula, S. M., Fontes, M. T. & Rossoni, L. V. Enhanced

sympathetic neurotransduction in the superior mesenteric artery in a rat model of heart failure: role of noradrenaline and ATP. *Am J Physiol Heart Circ Physiol* **320**, H563-H574, doi:10.1152/ajpheart.00444.2020 (2021).

440 Jugdutt, B. I., Menon, V., Kumar, D. & Idikio, H. Vascular remodeling during healing after myocardial infarction in the dog model: effects of reperfusion, amlodipine and enalapril. *J Am Coll Cardiol* **39**, 1538-1545, doi:10.1016/s0735-1097(02)01805-3 (2002).

441 Longhurst, J., Capone, R. J. & Zelis, R. Evaluation of skeletal muscle capillary basement membrane thickness in congestive heart failure. *Chest* **67**, 195-198, doi:10.1378/chest.67.2.195 (1975).

442 Lindsay, D. C. *et al.* Ultrastructural analysis of skeletal muscle. Microvascular dimensions and basement membrane thickness in chronic heart failure. *Eur Heart J* **15**, 1470-1476, doi:10.1093/oxfordjournals.eurheartj.a060416 (1994).

443 Wroblewski, H., Kastrup, J., Norgaard, T., Mortensen, S. A. & Haunso, S. Evidence of increased microvascular resistance and arteriolar hyalinosis in skin in congestive heart failure secondary to idiopathic dilated cardiomyopathy. *Am J Cardiol* **69**, 769-774, doi:10.1016/0002-9149(92)90503-q (1992).

444 Dey, A. B. *et al.* Selective Phosphodiesterase 1 Inhibitor BTTQ Reduces Blood Pressure in Spontaneously Hypertensive and Dahl Salt Sensitive Rats: Role of Peripheral Vasodilation. *Front Physiol* **11**, 543727, doi:10.3389/fphys.2020.543727 (2020).

445 Wallis, R. M., Corbin, J. D., Francis, S. H. & Ellis, P. Tissue distribution of phosphodiesterase families and the effects of sildenafil on tissue cyclic nucleotides, platelet function, and the contractile responses of trabeculae carneae and aortic rings in vitro. *Am J Cardiol* **83**, 3C-12C, doi:10.1016/s0002-9149(99)00042-9 (1999).

446 Giachini, F. R., Lima, V. V., Carneiro, F. S., Tostes, R. C. & Webb, R. C. Decreased cGMP level contributes to increased contraction in arteries from hypertensive rats: role of phosphodiesterase 1. *Hypertension* **57**, 655-663, doi:10.1161/HYPERTENSIONAHA.110.164327 (2011).

447 Matsumoto, T., Kobayashi, T. & Kamata, K. Alterations in EDHF-type relaxation and phosphodiesterase activity in mesenteric arteries from diabetic rats. *American journal of physiology. Heart and circulatory physiology* **285**, H283-291, doi:10.1152/ajpheart.00954.2002 (2003).

448 Moreira, H. S. *et al.* Phosphodiesterase-3 inhibitor cilostazol reverses endothelial dysfunction with ageing in rat mesenteric resistance arteries. *Eur J Pharmacol* **822**, 59-68, doi:10.1016/j.ejphar.2018.01.019 (2018).

449 Lindgren, S., Andersson, K. E., Belfrage, P., Degerman, E. & Manganiello, V. C. Relaxant effects of the selective phosphodiesterase inhibitors milrinone and OPC 3911 on isolated human mesenteric vessels. *Pharmacol Toxicol* **64**, 440-445, doi:10.1111/j.1600-0773.1989.tb00683.x (1989).

450 Hamilton, T. C. The effects of some phosphodiesterase inhibitors on the conductance of the perfused vascular beds of the chloralosed cat. *Br J Pharmacol* **46**, 386-394, doi:10.1111/j.1476-5381.1972.tb08135.x (1972).

451 Kruse, L. S. *et al.* PDE9A, PDE10A, and PDE11A expression in rat trigeminovascular pain signalling system. *Brain Res* **1281**, 25-34, doi:10.1016/j.brainres.2009.05.012 (2009).

452 Mulvany, M. J. & Halpern, W. Contractile properties of small arterial resistance vessels in spontaneously hypertensive and normotensive rats. *Circ Res* **41**, 19-26, doi:10.1161/01.res.41.1.19 (1977).

453 Thompson, W. J. & Appleman, M. M. Multiple cyclic nucleotide phosphodiesterase activities from rat brain. *Biochemistry* **10**, 311-316 (1971).

454 Le Stunff, C. *et al.* Knock-In of the Recurrent R368X Mutation of PRKAR1A that Represses cAMP-Dependent Protein Kinase A Activation: A Model of Type 1 Acrodysostosis. *J Bone Miner Res* **32**, 333-346, doi:10.1002/jbmr.2987 (2017).

455 Huseby, S. *et al.* Cyclic AMP induces IPC leukemia cell apoptosis via CRE-and CDK-dependent Bim transcription. *Cell Death Dis* **2**, e237, doi:10.1038/cddis.2011.124 (2011).

456 van der Staay, F. J. *et al.* The novel selective PDE9 inhibitor BAY 73-6691 improves learning and memory in rodents. *Neuropharmacology* **55**, 908-918, doi:10.1016/j.neuropharm.2008.07.005 (2008).

457 Wang, P. X. *et al.* C33(S), a novel PDE9A inhibitor, protects against rat cardiac hypertrophy through upregulating cGMP signaling. *Acta Pharmacol Sin* **38**, 1257-1268, doi:10.1038/aps.2017.38 (2017).

458 Besler, C. *et al.* Evaluation of phosphodiesterase 9A as a novel biomarker in heart failure with preserved ejection fraction. *ESC Heart Fail*, doi:10.1002/ehf2.13327 (2021).

459 Methawasin, M. *et al.* Phosphodiesterase 9a Inhibition in Mouse Models of Diastolic Dysfunction. *Circ Heart Fail* **13**, e006609, doi:10.1161/CIRCHEARTFAILURE.119.006609 (2020).

460 Schwam, E. M. *et al.* A multicenter, double-blind, placebo-controlled trial of the PDE9A inhibitor, PF-04447943, in Alzheimer's disease. *Curr Alzheimer Res* **11**, 413-421, doi:10.2174/1567205011666140505100858 (2014).

461 Iring, A. *et al.* Shear stress-induced endothelial adrenomedullin signaling regulates vascular tone and blood pressure. *J Clin Invest* **129**, 2775-2791, doi:10.1172/JCI123825 (2019).

462 Hashimoto, A., Miyakoda, G., Hirose, Y. & Mori, T. Activation of endothelial nitric oxide synthase by cilostazol via a cAMP/protein kinase A- and phosphatidylinositol 3-kinase/Akt-dependent mechanism. *Atherosclerosis* **189**, 350-357, doi:10.1016/j.atherosclerosis.2006.01.022 (2006).

463 Krishna Sadhu, K. H., Vince A. Florio, Sharon L. Wolda. Differential expression of the cyclic GMP-stimulated phosphodiesterase PDE2A in human venous and capillary endothelial cells. *J Histochem Cytochem* **47(7)**, 895-905, doi:10.1177/002215549904700707 (1999).

464 Eckly, A. E. & Lugnier, C. Role of phosphodiesterases III and IV in the modulation of vascular cyclic AMP content by the NO/cyclic GMP pathway. *British journal of pharmacology* **113**, 445-450 (1994).

465 Uhler, M. D. *et al.* Isolation of cDNA clones coding for the catalytic subunit of mouse cAMP-dependent protein kinase. *Proceedings of the National Academy of Sciences of the United States of America* **83**, 1300-1304, doi:10.1073/pnas.83.5.1300 (1986).

466 Brandon, E. P., Idzerda, R. L. & McKnight, G. S. PKA isoforms, neural pathways, and behaviour: making the connection. *Curr Opin Neurobiol* **7**, 397-403, doi:10.1016/s0959-4388(97)80069-4 (1997).

467 Amieux, P. S. *et al.* Compensatory regulation of RIalpha protein levels in protein kinase A mutant mice. *J Biol Chem* **272**, 3993-3998, doi:10.1074/jbc.272.7.3993 (1997).

468 Bertherat, J. *et al.* Mutations in regulatory subunit type 1A of cyclic adenosine 5'-monophosphate-dependent protein kinase (PRKAR1A): phenotype analysis in 353 patients and 80 different genotypes. *J Clin Endocrinol Metab* **94**, 2085-2091, doi:10.1210/jc.2008-2333 (2009).

469 Linglart, A. *et al.* Recurrent PRKAR1A mutation in acrodysostosis with hormone resistance. *N Engl J Med* **364**, 2218-2226, doi:10.1056/NEJMoa1012717 (2011).

470 Linglart, A. *et al.* PRKAR1A and PDE4D mutations cause acrodysostosis but two distinct syndromes with or without GPCR-signaling hormone resistance. *J Clin Endocrinol Metab* **97**, E2328-2338, doi:10.1210/jc.2012-2326 (2012).

471 Rhayem, Y. *et al.* Functional Characterization of PRKAR1A Mutations Reveals a Unique Molecular Mechanism Causing Acrodysostosis but Multiple Mechanisms Causing Carney Complex. *J Biol Chem* **290**, 27816-27828, doi:10.1074/jbc.M115.656553 (2015).

472 Bossis, I. & Stratakis, C. A. Minireview: PRKAR1A: normal and abnormal functions. *Endocrinology* **145**, 5452-5458, doi:10.1210/en.2004-0900 (2004).

473 Pilz, R. B., Eigenthaler, M. & Boss, G. R. Chemically induced murine erythroleukemia cell differentiation is severely impaired when cAMP-dependent protein kinase activity is repressed by transfected genes. *J Biol Chem* **267**, 16161-16167 (1992).

474 Murray, K. J. Cyclic AMP and mechanisms of vasodilation. *Pharmacol Ther* **47**, 329-345, doi:10.1016/0163-7258(90)90060-f (1990).

475 Di Benedetto, G. *et al.* Protein kinase A type I and type II define distinct intracellular signaling compartments. *Circ Res* **103**, 836-844, doi:10.1161/CIRCRESAHA.108.174813 (2008).

476 Skalhegg, B. S. & Tasken, K. Specificity in the cAMP/PKA signaling pathway. Differential expression,regulation, and subcellular localization of subunits of PKA. *Front Biosci* **5**, D678-693, doi:10.2741/skalhegg (2000).

477 Shaw, L., O'Neill, S., Jones, C. J., Austin, C. & Taggart, M. J. Comparison of U46619-, endothelin-1- or phenylephrine-induced changes in cellular Ca2+ profiles and Ca2+ sensitisation of constriction of pressurised rat resistance arteries. *Br J Pharmacol* **141**, 678-688, doi:10.1038/sj.bjp.0705647 (2004).

478 Kume, H., Hall, I. P., Washabau, R. J., Takagi, K. & Kotlikoff, M. I. Beta-adrenergic agonists regulate KCa channels in airway smooth muscle by cAMP-dependent and -independent mechanisms. *The Journal of clinical investigation* **93**, 371-379 (1994).

ÉCOLE DOCTORALE
Innovation thérapeutique
du fondamental à l'appliqué
(ITFA)

Title : New aspects of vascular cyclic nucleotides signalling in pulmonary arterial hypertension and heart failure.

Key words : phosphodiesterases, pulmonary arterial hypertension, arterial tone, heart failure

Abstract: Phosphodiesterases (PDEs) are enzymes responsible for the degradation of cAMP and cGMP, intracellular messengers particularly involved in cardiovascular homeostasis. Important challenges remain as to define the respective roles of the various PDE isoforms, especially in the context of cardiovascular diseases.

The main objective of my work was to elucidate the role of PDE9, a cGMP-selective PDE, in pulmonary circulation and in experimental pulmonary hypertension. Our results revealed that PDE9 was expressed in human and mouse pulmonary arteries. By using a PDE9-deficient or wild-type mouse lineage, we conclude that PDE9 regulates vascular reactivity of pulmonary arteries, by hampering both the NO- and the natriuretic peptide-mediated cGMP pathways. Despite PDE9 expression was increased in lung and right ventricle from mice challenged by chronic hypoxia, PDE9 deficiency failed to protect against pulmonary hypertension and right ventricle hypertrophy in this model.

Besides, I completed a study addressing the contributions of cAMP-PDEs in arteries from rats submitted to a chronic heart failure (HF) model. We focussed on mesenteric artery (MA), an example of resistance vascular bed that directly impact cardiac afterload. We showed that PDE2, PDE3 and PDE4 contributions to contractility in rat MAs undergoes subtle alterations in HF compared to sham animals. By contrast with previous observations in aorta, PDE4 participates equally as PDE3 in controlling reactivity of MA in HF, making this family of enzymes as a potential target in patients with HF. PDE2 activity emerges as a discrete, NO-dependent promoter of contractile response that is preserved in HF.

Eventually, as part of a side project, I studied the protein-kinase A regulatory subunit type 1α (PKA-R1α) in mouse aorta.

This work contributes in the general understanding on how important elements of CN signalling, namely, PDE and PKA isoforms, distribute in the vasculature and contribute to the control of vascular tone in health and diseases.

Titre : Nouveaux aspects de la signalisation des nucléotides cycliques vasculaires dans l'hypertension artérielle pulmonaire et l'insuffisance cardiaque.

Mots clés : phosphodiestérases, hypertension artérielle pulmonaire, tonus artériel, insuffisance cardiaque

Résumé : Les phosphodiestérases (PDE) sont des enzymes responsables de la dégradation de l'AMPc et du GMPc, messagers intracellulaires particulièrement impliqués dans l'homéostasie cardiovasculaire. Des défis importants demeurent quant à la définition des rôles respectifs des isoformes de PDE dans le contexte pathologique.

J'ai exploré le rôle de la PDE9, sélective du GMPc, dans la circulation pulmonaire. Nous montrons que la PDE9 est exprimée dans les artères pulmonaires humaines et murines et que la PDE9 influence la réactivité vasculaire pulmonaires, en s'opposant aux effets du NO et des peptides natriurétiques. Bien que l'expression de la PDE9 était augmentée dans les poumons et le ventricule droit (VD) de souris exposées à une hypoxie chronique, la déficience de cette enzyme n'a pas prévenu le développement de l'HTAP ni de l'hypertrophie du VD associée.

J'ai aussi étudié les contributions des PDE2, PDE3 et PDE4 dans de petites artères isolées de rats soumis à un modèle expérimental d'insuffisance cardiaque. L'activité PDE2 apparaît en particulier comme un nouveau promoteur de la réponse contractile préservé dans l'IC et agissant de manière dépendante du NO.

Enfin, j'ai étudié le rôle de la PKA de type 1 dans la vasomotricité de l'aorte de souris.

Ce travail contribue à l'élargissement des connaissances sur la participation des PDEs et de la PKA au fonctionnement du système cardiovasculaire normal et pathologique.